CATALYTIC ROLE OF IMMOBILIZED VANADIUM COMPLEXES IN OXIDATION REACTIONS

Ph. D. THESIS

by

NIKITA CHAUDHARY

DEPARTMENT OF CHEMISTRY
INDIAN INSTITUTE OF TECHNOLOGY ROORKEE
ROORKEE 247 667 (INDIA)

JULY, 2014

CATALYTIC ROLE OF IMMOBILIZED VANADIUM COMPLEXES IN OXIDATION REACTIONS

A THESIS

Submitted in partial fulfilment of the requirements for the award of the degree

of

DOCTOR OF PHILOSOPHY

in

CHEMISTRY

by

NIKITA CHAUDHARY

DEPARTMENT OF CHEMISTRY
INDIAN INSTITUTE OF TECHNOLOGY ROORKEE
ROORKEE 247 667 (INDIA)

JULY, 2014

INDIAN INSTITUTE OF TECHNOLOGY ROORKEE
ROORKEE

CANDIDATE'S DECLARATION

I hereby certify that the work which is being presented in the thesis entitled "**CATALYTIC ROLE OF IMMOBILIZED VANADIUM COMPLEXES IN OXIDATION REACTIONS"** in partial fulfilment of the requirements for the award of the Degree of Doctor of Philosophy and submitted in the Department of Chemistry of the Indian Institute of Technology Roorkee is an authentic record of my own work carried out during a period from December, 2010 to July, 2014 under the supervision of Dr. Mannar R. Maurya, Professor, Department of Chemistry, Indian Institute of Technology Roorkee.

The matter presented in the thesis has not been submitted by me for the award of any other degree of this or any other Institute.

(Nikita Chaudhary)

This is to certify that the above statement made by the candidate is correct to the best of my knowledge.

Date: (Mannar R. Maurya)
Supervisor

The Ph.D. Viva Voice Examination of **Nikita Chaudhary**, Research Scholar, has been made on October 20 2014.

Chairman, SRC Signature of External Examiner

This is to certify that the student has made all the corrections in the thesis.

Signature of the Supervisor Head of the Department

ABSTRACT

A growing interest in the chemistry of vanadium is based on the recognition of its importance from the biological and pharmacological perspective. The potential therapeutic use of vanadium compounds in the treatment of parasitic diseases, diabetes and cancer as well as capability of cleaving DNA in visible light and cellular proteins on irradiation with light additionally stimulated the coordination chemistry of vanadium. Vanadium compounds have also been found to act as catalyst precursor for the oxidation of organic substrates. Basic chemistry and potential applications of vanadium complexes in diverse fields have been discussed time to time in International Vanadium Chemistry symposium held biannually. Several research papers and review articles have appeared in the literature in recent years on the catalytic applications of vanadium complexes.

The functionalized polymers (cross-linked as well as non-cross-linked) have widely been used as support to immobilize metal complexes through covalent bonding. These polymer-supported transition metal complexes have widely been used as catalyst for many organic transformations due to their additional advantages over simple transition metal complexes like operational flexibility due to their insolubility, recycle ability, better product selectivity and activity due to active site isolation and high surface area. Polymer-supported vanadium complexes have shown better results not only in modeling oxidative halogenations reactions but in other vanadium mediated oxygen transfer reactions as well. In view of the above it was considered desirable to study catalytic role of polymer-supported vanadium complexes in oxidation reactions.

For convenience, the work embodied in the thesis has been divided into following chapters:

First chapter is introductory one and presents general remarks on supported complexes and in particular polymer-supported vanadium complexes. Updated literature survey has also been included here.

Second chapter is based on polymer supported vanadium complexes with 1-(2-pyridylazo)-2-naphthol (Hpan) and their catalytic activities. Monobasic tridentate ONN donor ligand, 1-(2-pyridylazo)-2-naphthol [Hpan (**2.I**)] reacts with $[V^{IV}O(acac)_2]$ in dry

methanol to yield the oxidovanadium(IV) complex [$V^{IV}O$(acac)(pan)] (**2.1**). The dioxidovanadium(V) complex [{$V^{V}O$(pan)}$_2$(μ-O)$_2$] (**2.2**) is obtained by aerial oxidation of **2.1** in methanol. Complex **2.2** can also be prepared directly by reacting [$V^{IV}O(acac)_2$] with **2.I** followed by aerial oxidation in methanol. Treatment of **2.1** or **2.2** in methanol with H_2O_2 yields the oxidomonoperoxidovanadium(V) complex [$V^{V}O(O_2)$(pan)(MeOH)] (**2.3**). Reaction of imidazolomethylpolystyrene cross-linked with 5 % divinylbenzene (PS–im) with **2.2** in DMF resulted in the formation of polymer-grafted dioxidovanadium(V) complex, PS–im[$V^{V}O_2$(pan)] **(2.4)**. All these complexes are characterized by various spectroscopic techniques (IR, electronic, NMR (^{1}H and ^{51}V), and electron paramagnetic resonance (EPR)), thermal, field-emission scanning electron micrographs (FE–SEM) as well as Energy dispersive X-ray (EDX) studies. The crystal and molecular structure of **2.3** has been determined, confirming the *ONN* binding mode of **2.I**. The polymer-grafted complex **2.4** has been used for the oxidative bromination of styrene, salicylaldehyde and *trans*–stilbene. Various parameters, such as amounts of catalyst, oxidant (aqueous 30 % H_2O_2), KBr and aqueous 70 % $HClO_4$ have been optimized to obtain the maximum oxidative bromination of substrates. Under the optimized reaction conditions, styrene gave a maximum of 99 % conversion after 2 h of reaction with the main products having a selectivity order of: 1-phenylethane-1,2-diol (75 %) > 2-bromo-1-phenylethane-1-ol (20 %) > 1,2-dibromo-1-phenylethane (1.2 %). With nearly same conversion in same time, oxidative bromination of salicylaldehyde gave three products with the selectivity order: 5-bromosalicylaldehyde > 2,4,6-tribromophenol > 3,5-dibromosalicylaldehyde. A maximum of 91 % conversion of *trans*–stilbene has been obtained in 2 h of reaction time where selectivity of the obtained reaction products varied in the order: 2,3-diphenyloxirane (*trans*–stilbene oxide) > 1,2-dibromo-1,2-diphenylethane > 2-bromo-1,2-diphenylethanol. Catalytic activity of nonpolymer grafted complex **2.2** is lower than that of the polymer-grafted one. In addition, the recycle ability of grafted complex makes it better over neat one.

Three neat complexes [$V^{V}O_2$(acpy-bhz)] (**3.1**) [$V^{V}O_2$(acpy-inh)] (**3.2**) and [$V^{V}O_2$(acpy-nah] (**3.3**) and the corresponding polymer-supported (PS) dioxidovanadium(V) complexes having monobasic tridentate ONN donor ligands,

abbreviated herein as PS-im[$V^{V}O_2$(acpy-bhz)] (**3.4**) PS-im[$V^{V}O_2$(acpy-inh)] (**3.5**) and PS-im[$V^{V}O_2$(acpy-nah] (**3.6**) have been isolated through covalent bonding of imidazolomethylpolystyrene, obtained by reacting chloromethylated polystyrene cross-linked with 5 % divinylbenzene with imidazole, with the corresponding neat complexes **3.1**, **3.2** and **3.3**. All compounds are characterized in solid state and in solution, namely by spectroscopic techniques (IR, UV-Vis, ^{51}V NMR, thermal and scanning electron micrograph studies) and whole studies are reported in **Chapter 3**. The monomeric form {[VO_2(acpy-nah)]·DMSO (**3.3**·DMSO)} (**3.3a**) of complex **3.3** has also been isolated from its solution in DMSO and its molecular structure is confirmed by single crystal X-ray diffraction. Polymer-supported as well neat complexes have been used as catalyst precursors for the oxidative bromination of styrene and *trans*-stilbene using 30 % aqueous H_2O_2 as an oxidant, the compounds acting as functional models of vanadium dependent haloperoxidases. 1-phenylethane-1,2-diol, 2-bromo-1-phenylethane-1-ol (bromohydrin) and 1,2-dibromo-1-phenylethane are the reaction products of styrene after 1 h of reaction, while those of *trans*-stilbene are: 2,3-diphenyloxirane (trans-stilbene oxide), 2-bromo-1,2-diphenylethanol and 1,2-dibromo-1,2-diphenylethane. It has also been shown that all these compounds are catalyst precursors for the catalytic oxidation of benzoin by peroxide, the products being benzil, methylbenzoate, benzoic acid and benzaldehyde-dimethylacetal. An outline of the mechanism has been proposed and plausible intermediates involved in the catalytic processes are proposed/ established by UV-Vis and ^{51}V NMR studies.

Fourth chapter deals with polymer supported as well as neat vanadium complexes of 2-benzoylpyridine based ONN donor ligands. Reaction between monobasic tridentate ONN donor ligands, Hbzpy-tch (**4.I**) and Hbzpy-inh (**4.II**) with [$V^{IV}O(acac)_2$] in dry methanol gives two different types of complexes, [VO^{IV}(acac)(bzpy-tch)] (**4.1**) and [VO^{IV}(OMe)(bzpy-inh)] (**4.2**), respectively. Irrespective of their nature both complexes upon aerial oxidation in methanol give dimeric [{$V^{V}O$(bzpy-tch)}$_2$(μ-O_2)] (**4.3**) and [{$V^{V}O$(bzpy-inh)}$_2$(μ-O_2)] (**4.4**). These complexes can also be prepared directly by reacting [$V^{IV}O(acac)_2$] with these ligands followed by aerial oxidation in methanol. Treatment of **4.1** or **4.2** in methanol with H_2O_2 yields the oxidomonoperoxidovanadium(V) complexes [$V^{V}O(O_2)$(bzpy-

tch)(MeOH)] (**4.5**) and [$V^{V}O(O_2)$(bzpy-inh)(MeOH)] (**4.6**). Reaction of **4.3** and **4.4** with imidazolomethylpolystyrene cross-linked with 5 % divinylbenzene (PS–im) in DMF gives polymer-supported dioxidovanadium(V) complex, PS–im[$V^{V}O_2$(bzpy-inh)] (**4.7**) and PS–im[$V^{V}O_2$(bzpy-tch)] (**4.8**). The complexes have been characterized by various spectroscopic techniques (IR, electronic, NMR (^{1}H and ^{51}V), and electron paramagnetic resonance (EPR)), ESI-MS, thermal, atomic force microscopy (AFM), field-emission scanning electron micrographs (FE–SEM) as well as energy dispersive X-ray (EDAX) studies. The crystal and molecular structures of **4.3** and **4.4** have been determined confirming the μ-bis(O) and *ONN* binding mode of **4.II** in dimeric structure. The polymer-grafted complexes **4.7** and **4.8** have been used for the oxidation of isoeugenol. Intermediate peroxide species involved during catalytic action have also been isolated in the solid state as well as generated in solution and studied. Catalytic activity of non-polymer supported complexes has also been carried out which show lower conversion than that of the polymer-grafted one. The recycle ability of grafted complex makes them better over neat ones.

Chapter 5 describes peroxidase mimicking property of polymer-supported complex PS-[$V^{IV}O$(sal-dahp)] at pH 7 in aqueous medium. Polymeric complex [$V^{IV}O$(Hsal-dahp)]$_n$ has been prepared by the reaction of $VOSO_4$ or [$V^{IV}O(acac)_2$] with dibasic pentadentate ligand H_3sal-dahp (sal = salicylaldehyde and dahp = 1,3-diamino-2-hydroxypropane) in methanol. The polymeric complex upon dissolving in hot DMSO yields the monomeric complex [$V^{IV}O$(Hsal-dahp)(dmso)] (**5.1**); single crystal X-ray analysis of which confirms the coordination of two phenolic oxygen and two imine nitrogen atoms of the ligand to the vanadium center while hydroxyl group of the ligand does not participate in coordination. Reaction of **5.1** with chloromethylated polystyrene crosslinked with 5 % divinylbenzene (abbreviated as PS-Cl) in DMF in the presence of triethylamine and K_2CO_3 gives stable polymer-supported oxidovanadium(IV) complex PS-[$V^{IV}O$(sal-dahp)] (**5.2**). Both complexes have been characterized by IR, electronic and EPR spectral studies, thermogravimetric analysis, field-emission scanning electron micrographs (FE-SEM) and energy dispersive X-ray (EDAX) as well as atomic force microscopy (AFM) studies. The polymer-supported complex **5.2** has been successfully used for the peroxidase-like oxidation of pyrogallol. The plausible intermediate species

formed during peroxidase mimicking activity has been established in solution electronic absorption spectrophotometrically. A good peroxidase mimicking property of polymer-supported complex **5.2** at pH 7 in aqueous medium, its stability in a wide range of pHs, easy separation from the reaction medium and reusability without considerable decrease in activity i.e. maintaining its heterogeneity makes it better over its natural counterparts i.e. biological systems in terms of its greener application in industry.

Finally, summary and over all conclusions based on the achievements are presented.

ACKNOWLEDGEMENTS

First of all, I would like to thank the almighty God, who made everything possible by giving me strength and courage to complete the most significant and scientific accomplishment in my life.

I would like to express my sincere gratitude to my advisor Dr. M. R. Maurya, Professor, Department of Chemistry, Indian Institute of Technology Roorkee for the continuous support of my Ph.D. study and research, for his patience, motivation, enthusiasm, and immense knowledge. His guidance helped me in all the time of research and writing of this thesis. I could not have imagined having a better advisor and mentor for my Ph.D. study. I also wish to express my gratitude to Mrs. Usha Maurya, for her caring and loving gestures and giving a homely environment. I will always seek their devout blessings in my life.

I would like to gratefully acknowledge Prof. & Head Anil Kumar and former Heads, Department of Chemistry, Indian Institute of Technology Roorkee, for providing me essential infrastructural facilities to carry out this research work.

I am thankful to the Head, Institute Instrumentation Centre of our institute for providing me necessary instrumentation facilities for my research work. My sincere thanks also go to Mr. A. Haque and Mr. Madan Pal, who helped me from time to time during my research work. I am grateful to all the members of Chemistry Department for their cooperation in countless ways.

I am obliged to Prof. Joao Costa-Pessoa and Dr. Amit Kumar, Instituto Superior Tecnico, Portugal for carrying out the EPR and ^{51}V NMR studies of my samples. I would also like to thank Prof. Fernando Avecilla, Departamento de Química Fundamental, Facultad de Ciencias, Universidade da Coruña, Spain for carrying out Single crystal X-ray analyses of my samples.

A special word of thanks is also due to my seniors and laboratory colleagues, Dr. Manisha Bisht, Dr. Priyanka saini, Dr. Chanchal Haldar, Ms. Ruchi Singh, and my juniors Ms. Sarita Dhaka, Mr. Naveen Kumar, Ms. Bhawna

Uprety, Ms. Lata Rana, Ms. Bithika Sarkar, Mr. Neeraj Saini and Ms. Rachana Sharma for their lively company and motivation for the completion of my work.

I thank my friends, Kshama Ojha, Jyoti Sharma and Chetna Mangal, in my home town for their lovely friendship, and sweet memories which I will cherish in my life. My special thanks go to my friend Ms. Praveen Chandra. I greatly value her friendship and I deeply appreciate her belief in me.

I made some good friends here, during my stay at IIT Roorkee. I gratefully acknowledge Ms. Mridula Thakur, Ms. Sweety Rathi and Ms. Rajni Sharma. Their support and care helped me overcome setbacks and stay focused on my research.

I would have not finished this thesis without the support of my family who has always been there for me whenever I needed them. Their encouragements help me to keep going and their love empower me to always strive for success. I would like to express my eternal gratitude to my parents for their everlasting love and support. I am indebted to my father, Mr. Ramniwas Chaudhary, for his care, love and guidance. No words can define my gratitude for my mother, Mrs. Kamala Chaudhary. She has been my pillar of strength and I owe all my success to her. I also want to thank my sister, Dr. Priyanka Chaudhary and my brother, Mr. Jaideep Chaudhary for their love, fights, concern, laughter, and motivation.

I would like to acknowledge the Council of scientific and Industrial Research, New Delhi for the necessary financial support for this research.

Finally, I wish to acknowledge all those, whose names have not figured above, but have helped me in any form during the entire period of my research work.

(Nikita Chaudhary)

LIST OF PUBLICATIONS

Papers published/ accepted/ communicated for publication

From Ph.D. thesis:

1. M. R. Maurya, **N. Chaudhary**, A. Kumar, F. Avecilla and J. Costa Pessoa, Polystyrene bound dioxidovanadium(V) complexes of 2-acetylpyridine derived ligands for catalytic oxidations, *Inorg. Chim. Acta*, **420** (2014) 24–38.

2. M. R. Maurya, **N. Chaudhary** and F. Avecilla, Polymer-grafted and neat vanadium(V) complexes as functional mimics of haloperoxidases, *Polyhedron*, **67** (2014) 436–448.

3. M. R. Maurya, **N. Chaudhary**, F. Avecilla, P. Adão, and J. Costa Pessoa, Oxidovanadium(IV) and dioxidovanadium(V) complexes of hydrazones of 2-benzoylpyridine and their catalytic applications, Submitted after revision to *Dalton Trans.*

Other than Ph.D. thesis:

1. M. R. Maurya, M. Bisht, **N. Chaudhary**, A. Kumar, F. Avecilla and J. Costa Pessoa, Spectroscopic and Structural Characterization of Non-innocent Oxidovanadium(V) mixed ligand complexes, *Eur. J. Inorg. Chem.*, 2012, 4846–4855.

2. M. R. Maurya, M. Bisht, **N. Chaudhary**, F. Avecilla, Synthesis, structural characterization, encapsulation in zeolite-Y and catalytic activity of oxidovanadium(V) complex with tribasic pentadentate ligand, *Polyhedron*, **54** (2013) 180–188.

Papers presented in Symposia / Conferences

1. M. R. Maurya, M. Bisht and **N. Chaudhary**, Spectroscopic and structural characterization of oxovanadium(IV) and oxovanadium (V) complexes, *48th Annual Convention of Chemists*, Allahabad University, December 03–07, 2011.

2. M. R. Maurya, **N. Chaudhary** and M. Bisht, Spectroscopic and structural characterization of non-innocent oxidovanadium(V) mixed ligand complexes, *National Conference on Global Challenges: New Frontiers in Chemical Sciencess (GC: NFCS-2012)*, Kurukshetra University, September 22–23 2012.

3. M. R. Maurya and **N. Chaudhary**, Polystyrene bound dioxidovanadium(V) complexes of 2-acetylpyridine derived ligands for catalytic oxidations, *50th Annual Convention of Chemists*, Punjab University, December 04–07, 2013.

4. M. R. Maurya and **N. Chaudhary**, Oxidovanadium(IV) and dioxidovanadium(V) complexes of hydrazones of 2-benzoylpyridine and their catalytic applications, 2nd International Conference on Global Trends in Pure & Applied Chemical Sciences 2014, Hong Kong, October 03–04, 2014.

CONTENTS

CHAPTER 3

Polystyrene bound dioxidovanadium(V) complexes of 2-acetylpyridine derived ligands for catalytic oxidations

CHAPTER 4

Oxidovanadium(IV) and dioxidovanadium(V) complexes of hydrazones of 2-benzoylpyridine and their catalytic applications

CHAPTER 5

Polymer supported oxidovanadium (IV) complexes of Schiff base derived from salicylaldehyde and 1,3-diamino-2-hydroxypropane as peroxidase mimetic catalyst towards oxidation of pyrogallol

Chapter 1

General introduction and literature survey

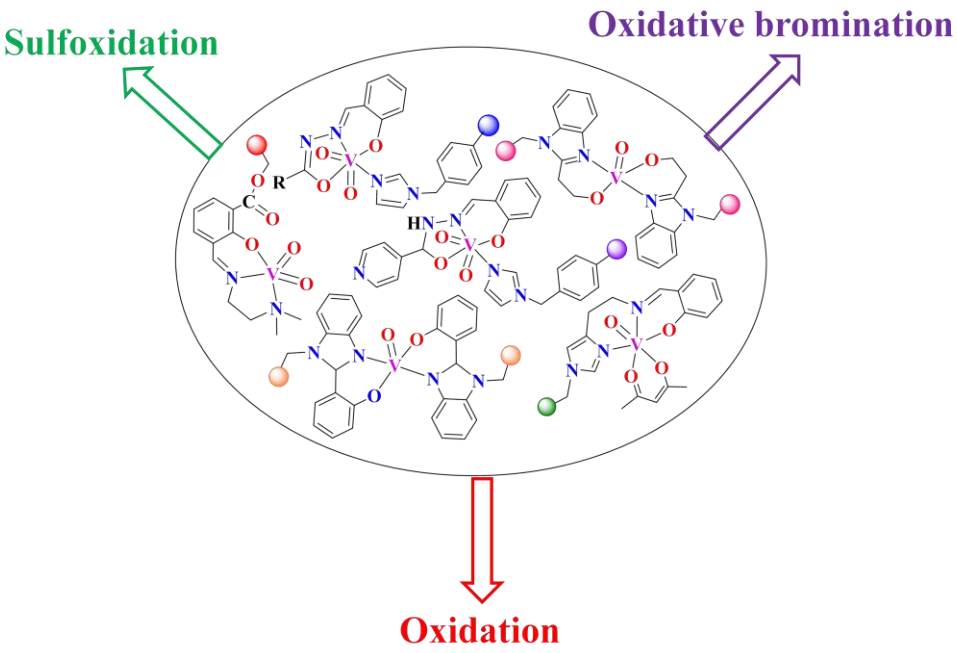

1.1. Historical

The word catalysis was introduced first by Berzelius in 1835 while first application of catalyst at industrial scale was reported in 1875 in the production of sulfuric acid using platinum catalyst by Contact process. Well known Ostwald process reported in 1903 also used platinum as catalyst for the production of nitric acid. Catalytic reaction generally proceeds through the bonding of reactant molecules to the catalyst forming an intermediate species and finally products detach from the catalyst leaving the catalyst for the next cycle. Researchers have worked day and night and one can see the continuous development of catalysts and their vital role in the economic growth of countries and quality of human life. In fact, more than 90 % processes in fields such as petrochemicals, fine chemicals, pharmaceuticals, fertilizers, food industries etc. involve the use of catalyst based technologies.

1.2. Vanadium complexes as catalyst

Transition metal complexes, particularly of manganese and molybdenum find special attention in past decades as catalysts for oxidation reactions [1–15] while metal complexes e.g. of palladium, ruthenium, rhodium etc. as catalysts for other catalytic reactions [16–18]. Research on the catalytic applications of vanadium complexes has been stimulated considerably due to the discovery of various biological catalytic processes shown by enzymes vanadate-dependent haloperoxidases having vanadium in their active center [19,20]. In fact, several research papers and review articles have appeared in the literature in recent years on the catalytic applications of vanadium complexes [21–40]. We do not intend to present here details of literature survey on the catalytic applications of vanadium complexes but some of the vanadium complexes used for catalytic studies are presented in Figure 1.1. Book written by Dieter Rehder “Bioinorganic Vanadium Chemistry” also deals with catalytic and several other aspects of vanadium complexes [41].

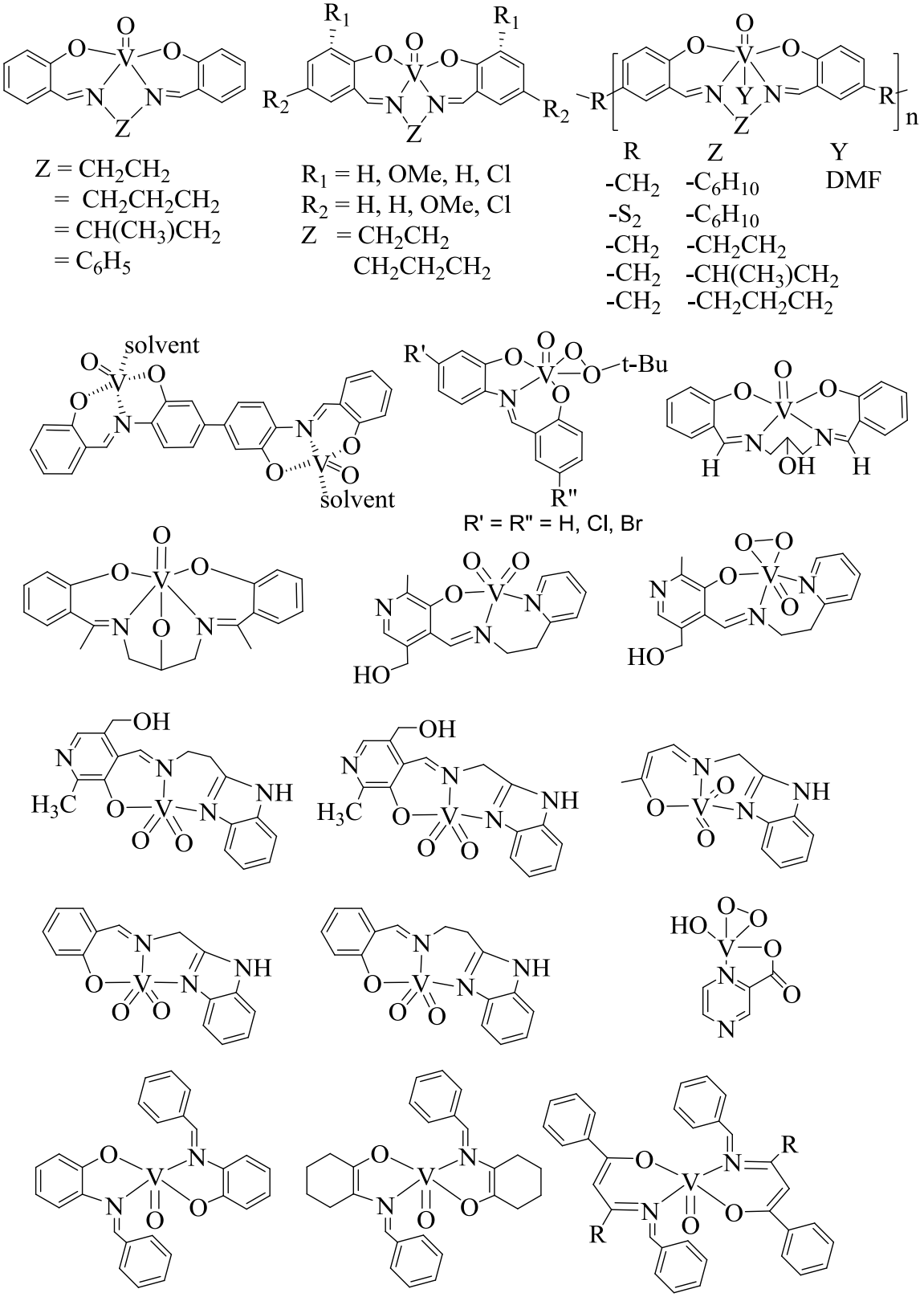

Figure 1.1. Examples of vanadium complexes having catalytic potentials.

1.3. Solid supports used for catalysts

All thermally stable materials having suitable functional group(s) or that can be functionalized easily may be used as support for catalyst. However, they should be chemically inert after immobilization of catalysts. Amongst various supports, alumina and silica are readily available inorganic compounds and can be modified to immobilize various catalysts by direct reaction of surface hydroxyl groups with reactive species. Immobilization of homogeneous catalysts (i.e. neat complexes) on such materials facilitates easy product separation, catalysts recovery and recycle ability; Figure 1.2 [43,44].

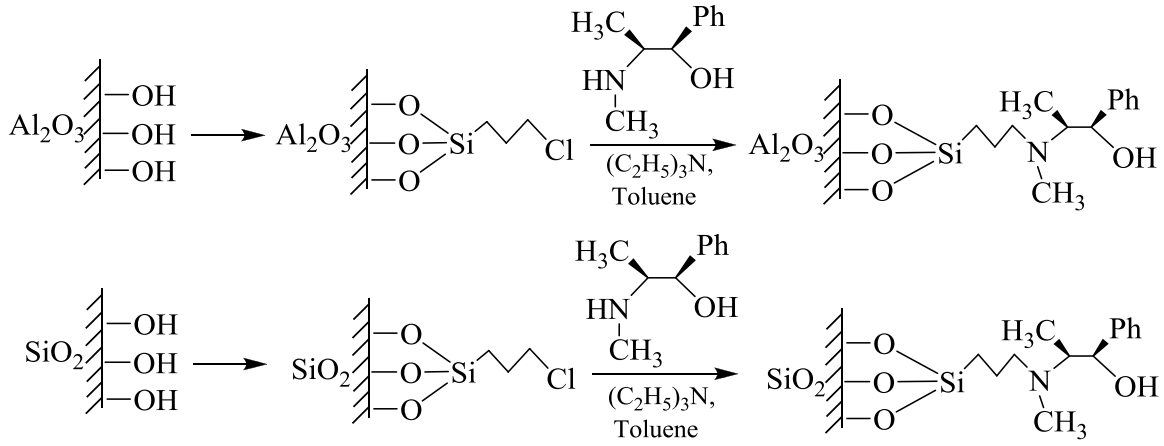

Figure 1.2. Schemes for the immobilization of ligands on modified alumina or silica.

Some other examples of catalysts immobilized on modified silica are given in Figure 1.3 [43,44].

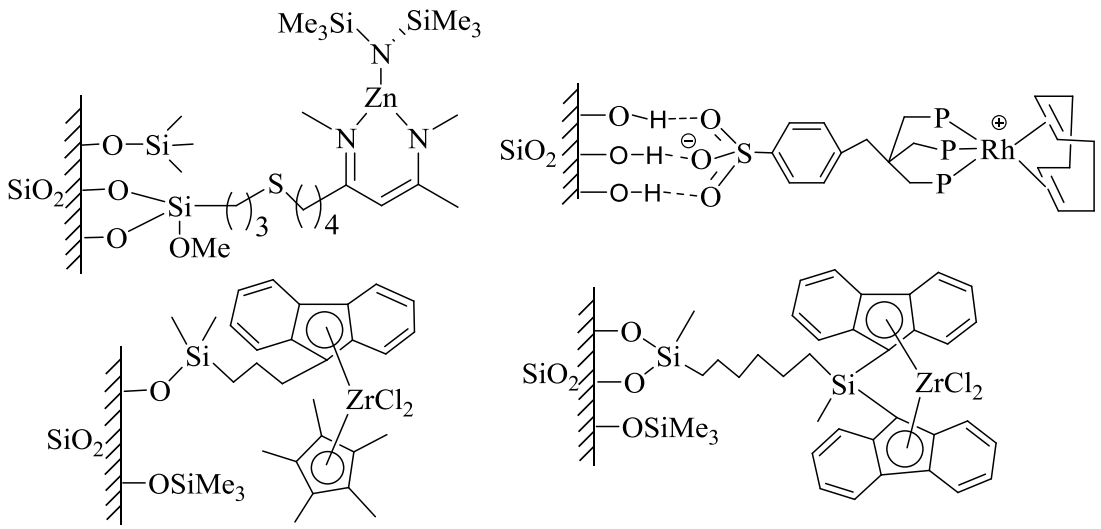

Figure 1.3. Catalysts immobilized on modified alumina or silica.

Similar to silica and alumina, mesoporous molecular sieves, Si-MCM-41 and Si-SBA-15 having hydroxyl groups present on the surface have been modified and used as support for the immobilization of catalysts. Immobilization of titanocene has been achieved according to the procedure shown in Figure 1.4 [45].

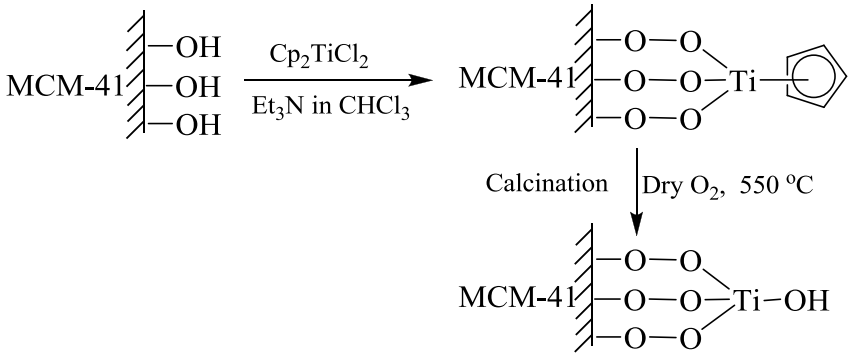

Figure 1.4. Scheme for the immobilization of catalysts on modified MCM-41, a mesoporous molecular sieve.

Joseph *et al.* have modified MCM-41/ SBA-15 as shown in Figure 1.5 to immobilize $[RuH(CO)(PPh_3)_3Cl]$ and $[V^{IV}O(saldien)]$ [H_2saldien = N,N′-bis(salicylidene)diethylenetriamine] [46,47]. Mesoporous SBA-15 and silica have also been functionalized by Jain *et al.* to immobilize oxidovanadium(IV) complexes [48].

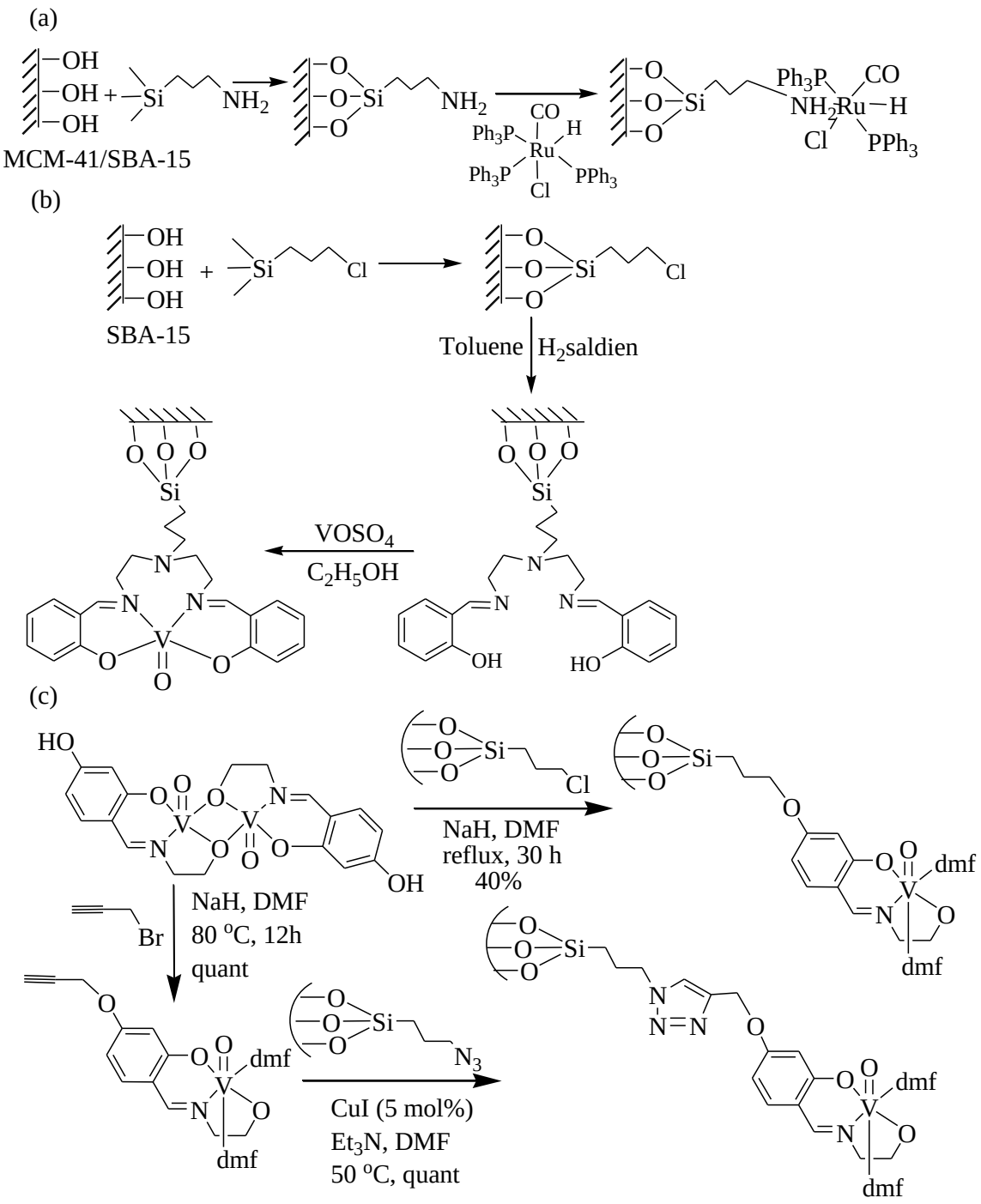

Figure 1.5. Schemes for the immobilization of catalysts on modified MCM-41/ SBA-15.

1.4. Functionalized polymers and their uses as support to homogeneous catalysts

Polymers e.g. polystyrene, polyvinylchloride, polyvinylpyridine, polyaniline, polyallyl, polyaminoacid, acrylic polymer, cellulose etc. are generally non-reactive and thermally stable materials. However, some of them can be modified with suitable functional groups to immobilize homogeneous catalysts [49–51]. Using co-polymerization method, the synthesis of chloromethylated polystyrene cross-linked with divinylbenzene is shown in Figure 1.6.

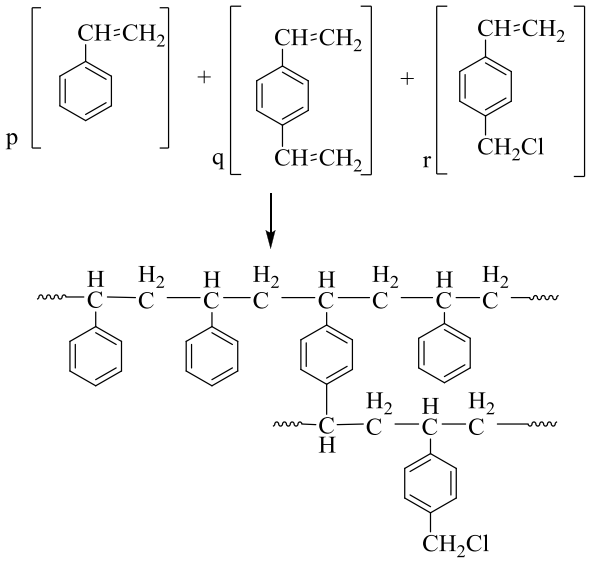

Figure 1.6. Synthetic scheme for chloromethylated polystyrene cross-linked with divinylbenzene

The functionalized polymers (cross-linked as well as non-cross-linked) have widely been used as support to immobilize metal complexes through covalent bonding. Metal complexes are immobilized onto polymer support via (i) covalent bonding to the central metal ion of the complex through suitable coordinating donor atom appended to the polymer, (ii) covalent bonding of organic molecule having suitable coordinating site(s) (e.g. ligand) with functionalized polymer followed by its coordination with metal ion, and (iii) direct covalent bonding of functionalized polymer to the ligand of the metal complex

[52–55]. The polymer-bound organic ligands are also called polymer-anchored ligands and their complexes are called polymer-anchored complexes.

Chloromethylated polystyrene cross-linked with divinylbenzene has been the most widely used polymer for immobilization of ligand and metal complexes. Ligands having functional groups like carboxylic acids, sulfonic acids, hydroxyl group etc. can be attached to the chloromethylated polystyrene as Shown in Figure 1.7 [56–59].

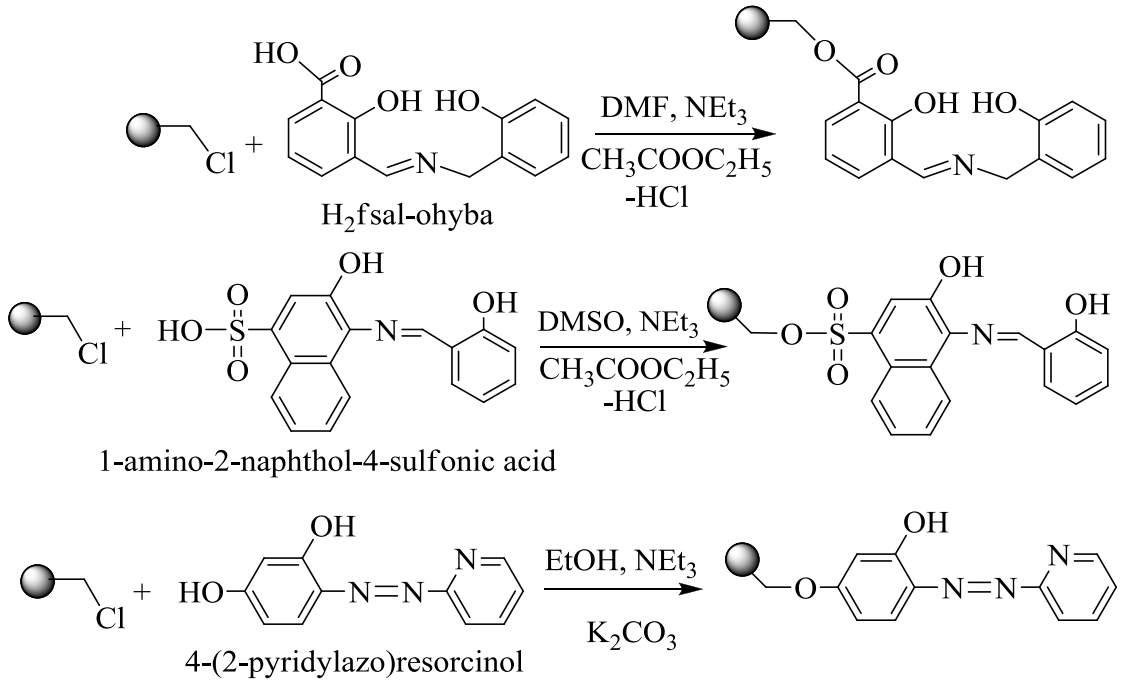

Figure 1.7. Schemes for the immobilization of catalysts on modified chloromethylated polystyrene.

Chloromethylated polystyrene also reacts with –NH group present on the ring under the reaction conditions prescribed for carboxylic acid group to give polymer-supported ligand; Figure 1.8 [60,61].

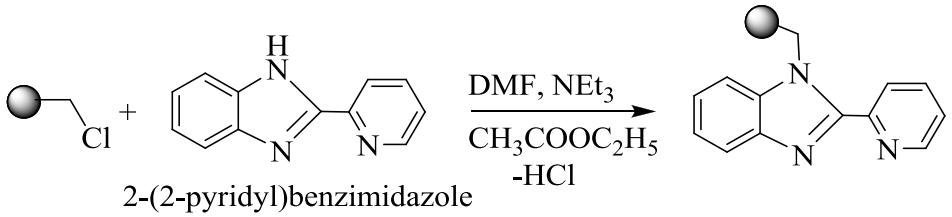

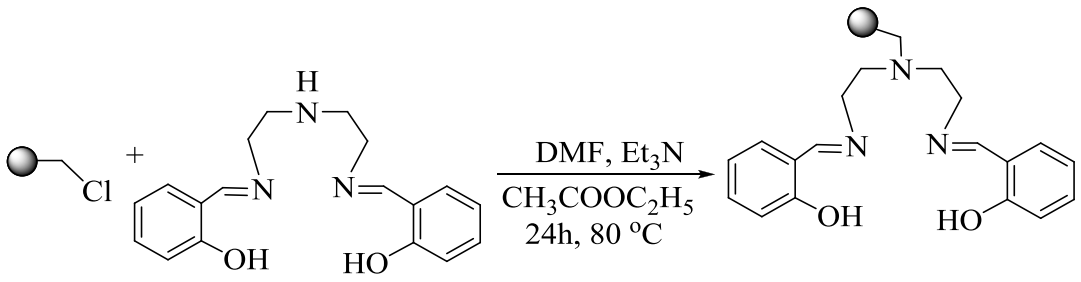

Figure 1.8. Schemes for the immobilization of catalysts on modified chloromethylated polystyrene.

The syntheses of the polymer-supported ligand, PS-H_2fsal-β-ala [62] and chiral "non-symmetrical" polymer-anchored dibasic tetradentate ligand [63] were achieved in two steps as represented in Figure 1.9.

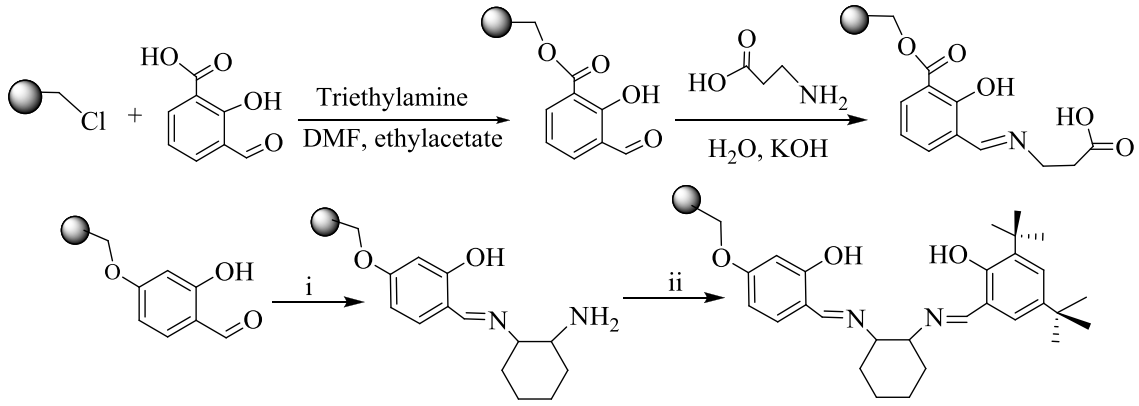

(i) (S, S)-1, 2-diaminocyclohexane, dioxane, 18-Crown-6, K_2CO_3, 85°C, 3 days.

(ii) Salicylaldehyde derivatives, 18-Crown-6, K_2CO_3, 85 °C, 3 days.

Figure 1.9. Reaction schemes for the synthesis of polymer-supported ligands starting from salicylaldehyde or its derivative.

Other similar ligands (Figure 1.10) were prepared similarly [64].

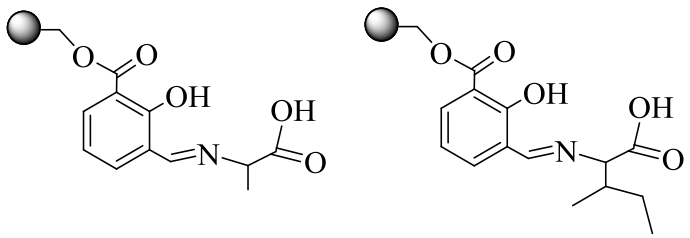

Figure 1.10. Examples of polymer-supported lignads.

Phenolic hydroxyl group generally reacts with chloromethylated polystyrene in the presence of alkali carbonate along with triethylamine [65] in solvent. This method is also applicable to immobilize porphyrins such as 5,10,15-tris(4-R-phenyl)-20-(4-hydroxyphenyl)porphyrins (Figure 1.11) bearing peripheral hydroxyl group onto chloromethylated polystyrene in DMF [66].

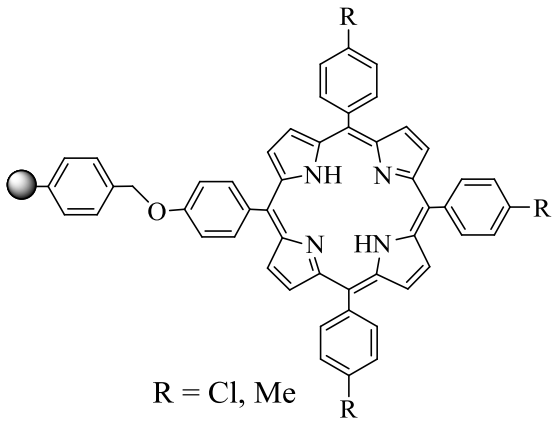

Figure 1.11. Example of polymer-anchored porphyrin.

Polymer-anchored metal complexes may also be obtained by reacting metal complexes having suitable binding site on ligand with polymeric resin; Figure 1.12 [67].

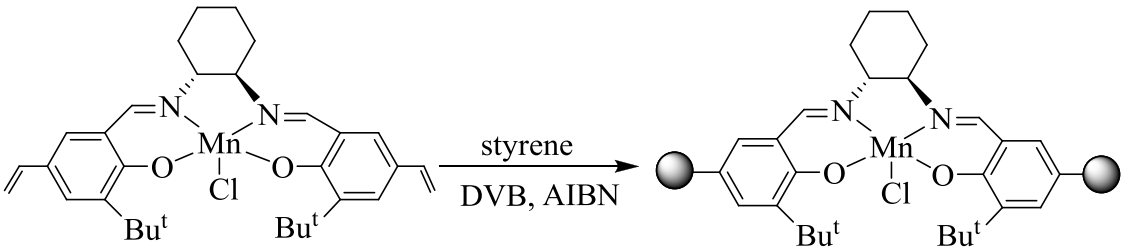

Figure 1.12. Route to prepare polymer-supported complex. DVB = divinyl benzene, AIBN = aizobisisobutyronitrile.

Direct covalent bonding of functionalized polymer to the metal complexes has also been reported in the literature; Fig. 1.13 [68].

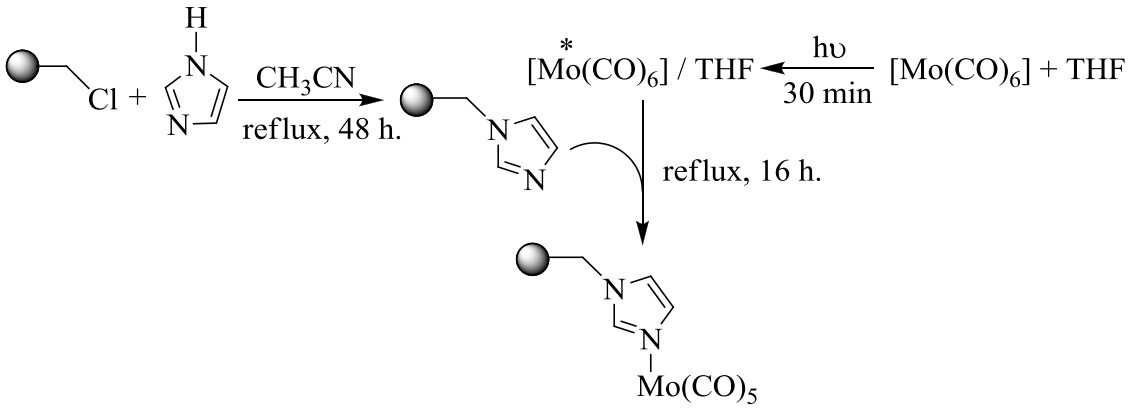

Figure 1.13. Reaction scheme for the synthesis of polymer-supported complex.

Similarly dioxidovanadium(V) complexes K[V^VO_2(sal-inh)(H_2O)] and K[V^VO_2(sal-bhz)(H_2O)] react with imidazolomethylpolystyrene (PS-im) in DMF to give the imidazolomethylpolystyrene bound complexes PS-K[V^VO_2(sal-inh)(im)] and PS-K[V^VO_2(sal-bhz)(im)], respectively; Figure 1.14 [69].

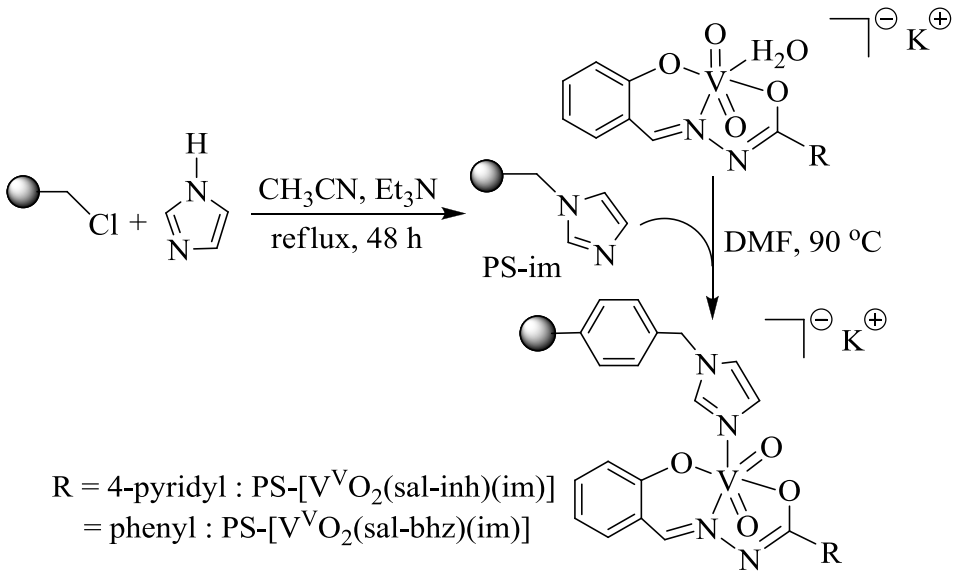

Figure 1.14. Formation of PS-K[$V^{V}O_2$(sal-inh)(im)] and PS-K[$V^{V}O_2$(sal-bhz)(im)].

1.5. Advantage using polymer-supported metal complexes as catalysts

Polymer-supported transition metal complexes have widely been used as catalyst [52–54,70–75] for many organic transformations due to their additional advantages over simple transition metal complexes like operational flexibility due to their insolubility, recycle ability, better product selectivity and activity due to active site isolation and high surface area. Moreover, expensive transition metal complexes on immobilization over polymer-support become materials of commercial advantage as they enjoy the advantageous features of heterogeneous catalyst while retain the nature of homogeneous catalyst.

1.6. Polymer-supported vanadium complexes and their catalytic applications: a literature survey

Vanadium-dependent haloperoxidases are able to activate hydrogen peroxide for the oxidation of halides that results in the production of halogenated compounds. Very similar to model vanadium complexes, polymer-supported complexes also model the catalytic activity shown by these enzymes. In fact, polymer-supported vanadium complexes have shown better results not only in model oxidative halogenations reactions but in other

vanadium mediated oxygen transfer reactions as well due to reasons mentioned in previous section. Important advances in polymer-supported vanadium complexes have recently been reviewed by Maurya *et al*. [53,54]. A brief advances in catalytic applications of polymer-supported vanadium complexes are summarized below:

Oxidative bromination of salicylaldehyde catalyzed by polymer-supported complexes PS-K[$V^{V}O_2$(sal-inh)(im)] and PS-K[$V^{V}O_2$(sal-bhz)(im)] using H_2O_2/KBr and $HClO_4$ in water has been reported by Maurya *et al.* [69]. Under the optimized reaction conditions, a maximum of 85 % conversion of salicylaldehyde by K[$V^{V}O_2$(sal-inh)(im)] and 82 % by PS-K[$V^{V}O_2$(sal-bhz)(im)] with *ca.* 90 % selectivity of 5-bromosalicylaldehdye (Scheme 1.15) was obtained. Addition of more $HClO_4$ improved the conversion but poor selectivity of 5-bromosalicylaldehdye as well as decomposition of catalysts both was observed. Addition of $HClO_4$ in four equal portions was suggested to avoid decomposition of catalysts [69]. Complex PS–[$VO(hmbmz)_2$] [Hhmbmz = 2-(α-hydroxymethyl)benzimidazole] gives 5-bromosalicylaldehdye selectively in quantitative yield upon oxidation of salicylaldehyde.

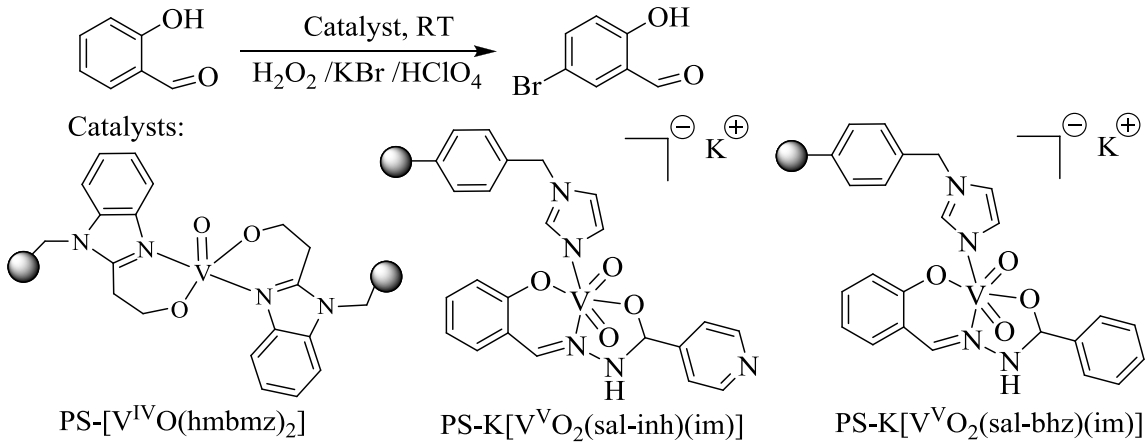

Figure 1.15. Oxidative bromination of salicylaldehyde and catalysts used for this reaction.

Complexes PS-K[$V^{V}O_2$(sal-inh)(im)] and PS-K[$V^{V}O_2$(sal-bhz)(im)] also catalyze the oxidation of methyl phenyl sulfide (mps) in the presence of H_2O_2 as oxidant with 97–100 % selectivity towards sulfoxide along with high turn-over frequency (TOF) [69] in 2 h of reaction time. Complexes PS-[*mer*-$V^{IV}O$(salae)], PS-[*mer*-$V^{IV}O$(salpheol)], PS-[*mer*-

$V^{IV}O$(salhisol)] and PS-[*mer*-$V^{IV}O$(salphe)] give 81–91 % conversion of methyl phenyl sulfide to sulfoxide with TBHP in 1.5 h. Enantiomeric excess of mps was as high as 40 % with PS-[*mer*-VO(salhisol)] [65]. Polymer-supported complexes [$V^{IV}O$(sal-hist)(acac)], PS-[$V^{V}O_2$(sal-hist)] [76] and PS-[$V^{IV}O(hpbmz)_2$] [77] (Figure 1.16) are also excellent catalysts for the oxidation of sulfides (methyl phenyl sulfide and diphenyl sulfide) with high turn-over frequency. Solvent plays an important role in that using impure solvent (e.g. acetonitrile) may alter the conversion of sulfides as well as selectivity of the reaction products.

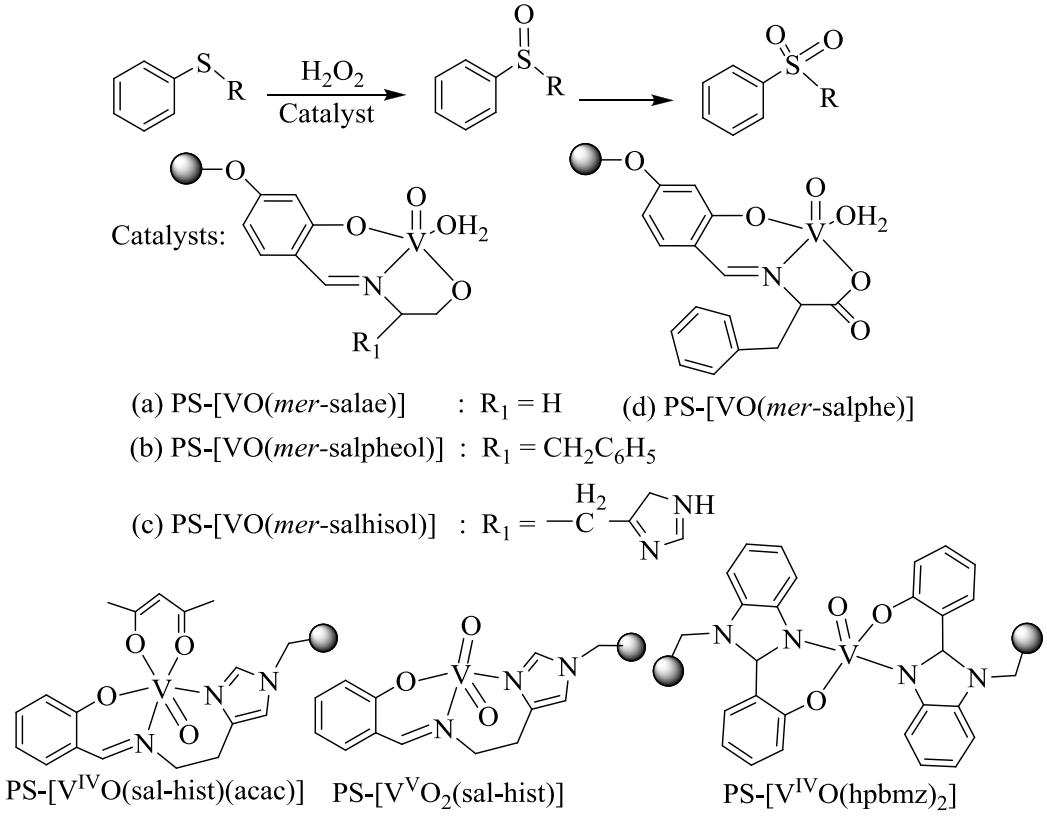

Figure 1.16. Catalysts used for the oxidation of sulfides. R = CH_3- : methyl phenyl sulfide = mps, R = C_6H_5-: diphenyl sulfide = dps.

Polyacrylate and polystyrene-supported Schiff bases derived from substituted salicylaldehyde and optically active amino alcohols [Figure 1.17] reacted with [$VO(acac)_2$] to give polymer supported oxovanadium(IV) complexes. These reusable complexes also

catalyze the oxidation of methyl phenyl sulfide in presence of H_2O_2 and *tert*-butyl hydroperoxide [78].

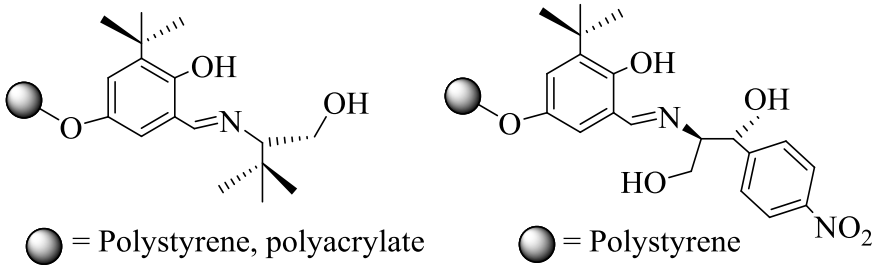

Figure 1.17. Structures of chiral Schiff base ligands supported on polymer.

Walmsley *et al.* have developed fiber-based oxidovanadium(IV) catalysts for the oxidation of thioanisole using a continuous flow set up by incorporating complexes (Figure 1.18) into polystyrene and electrospinning to produce nano-fiber mats [79]. Effect of substituent on ligands (R = NO, Br, H, MeO) was studied for the oxidation of thioanisole by hydrogen peroxide in acetonitrile at 25^{o}C and found that catalytic activity follows the order according to the derivatives: NO_2>Br>H>MeO. The electron withdrawing group nitro (NO_2) derivative gives nearly quantitative conversion of thioanisole in 10 min while methoxy (MeO) derivative produces same result in 60 min.

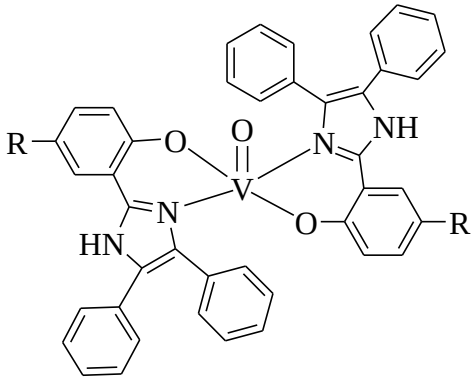

Figure 1.18. Structure of complex incorporated into polystyrene and electrospun to produce nano-fiber mats. R = NO, Br, H, MeO.

Such idea of oxidation of sulfides has been extended to model diesel fuel where catalysts PS-[$V^{IV}O$(sal-dmen)(acac)] and PS-[$V^{V}O_2$(sal-dmen)] and neat dioxidovanadium(V) complex are able to oxidize efficiently the 500 ppm concentration of model organosulfur compounds such as thiophene, benzothiophene, dibenzothiophene and 2-methylthiophene prepared in heptane (Figure 1.19, Table 1) [80].

Table 1. Desulfurization and reaction products using the anchored oxido- and dioxido-vanadium catalysts: PS-[$V^{IV}O$(fsal-dmen)(acac)] and PS-[$V^{V}O_2$(fsal-dmen)] (0.050 g), 30 % H_2O_2 (oxidant:substrate molar ratio of 3 : 1) at 60^{o}C (Taken from ref. 54).

Catalyst	Sulfur containing compound	Sulfur content (in ppm)		Sulfur removal (%)
		Initial amount	After desulfurization	
PS-[$V^{IV}O$(fsal-dmen)(acac)]	Thiophene	500	65.5	86.9
PS-[$V^{IV}O$(fsal-dmen)(acac)]	Benzothiophene	500	63	87.4
PS-[$V^{IV}O$(fsal-dmen)(acac)]	Dibenzothiophene	500	60.5	87.9
PS-[$V^{IV}O$(fsal-dmen)(acac)]	2-Methylthiophene	500	57.5	88.5
PS-[$V^{V}O_2$(fsal-dmen)]	Thiophene	500	9.5	98.1
PS-[$V^{V}O_2$(fsal-dmen)]	Benzothiophene	500	8.5	98.3
PS-[$V^{V}O_2$(fsal-dmen)]	Dibenzothiophene	500	8	98.4
PS-[$V^{V}O_2$(fsal-dmen)]	2-Methylthiophene	500	6	98.8
[$V^{IV}O$(fsal-dmen)(acac)]	Thiophene	500	148.5	70.3
[$V^{IV}O$(fsal-dmen)(acac)]	Benzothiophene	500	144.5	71.1
[$V^{IV}O$(fsal-dmen)(acac)]	Dibenzothiophene	500	141.5	71.7
[$V^{IV}O$(fsal-dmen)(acac)	2-Methylthiophene	500	140.5	71.9
[$V^{V}O_2$(fsal-dmen)]	Thiophene	500	113	77.4
[$V^{V}O_2$(fsal-dmen)]	Benzothiophene	500	109.5	78.1
[$V^{V}O_2$(fsal-dmen)]	Dibenzothiophene	500	111.5	77.7
[$V^{V}O_2$(fsal-dmen)]	2-Methylthiophene	500	108	78.4

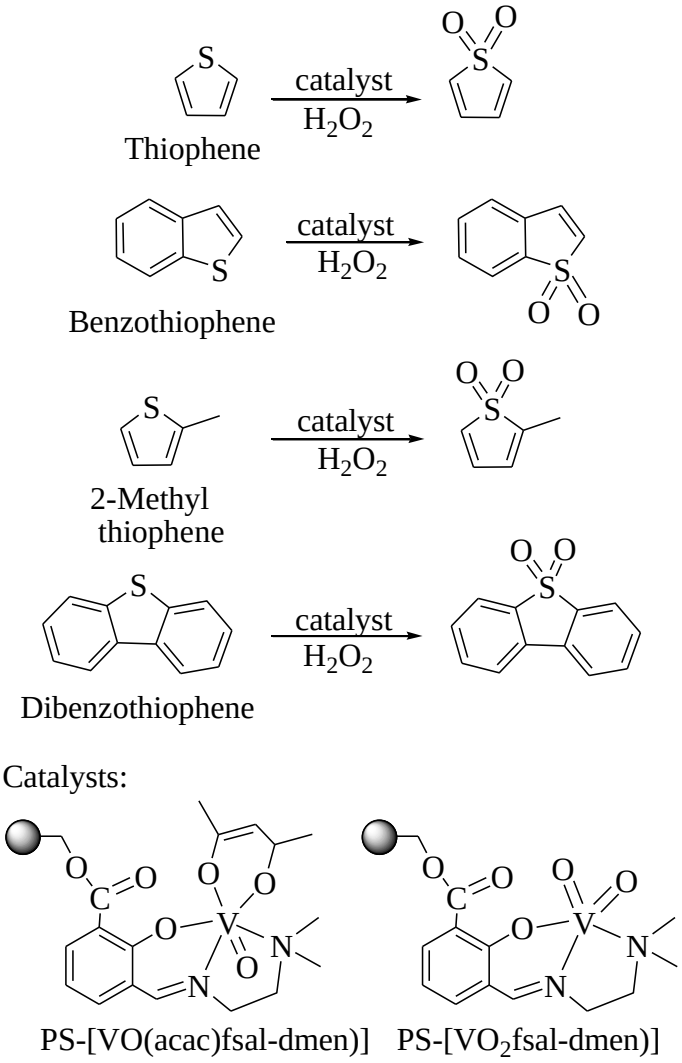

Figure 1.19. Polymer supported vanadium complexes used to catalyze oxidation of organosulfur compounds.

A suitable mechanism proposed for the catalytic formation of sulfoxide and sulfone from sulfide is presented in Figure 1.20. The sulfur atom of sulfides is electron rich and undergoes electrophilic oxidation giving sulfoxide. Generally, oxidovanadium(IV) and dioxidovanadium(V) complexes generate oxidoperoxido species [$VO(O_2)(L)$] (L = anionic unit of ligand(s)) on treatment with H_2O_2, followed by a hydroperoxidovanadium(V) complex in the presence of H^+. This species enhances the electrophilicity of the peroxido

intermediate [81,82]. The peroxide thus activated is subjected to a nucleophilic attack by the sulfide to give final product.

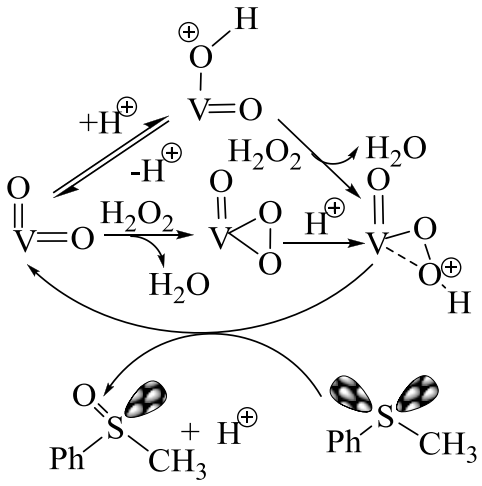

Figure 1.20. Reaction mechanism for oxidation of organic sulfides. Adopted from ref. [27].

Catalytic activity of polymer-supported complex (Figure 1.21) has been evaluated for the oxidation of various alkenes, sulfides and aromatic alcohols with 30 % H_2O_2 under mild reaction conditions. This catalyst is also selective for the oxidative bromination of salicylaldehyde with 98 % conversion to 5-bromosalicylaldehyde under optimized reaction conditions. Several other organic substrates have also been tested for this reaction and gave 80–96 % conversion with 80 – 100 % selectivity to monobrominated products [83].

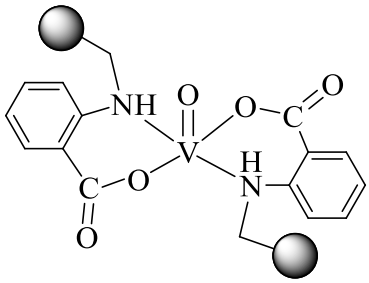

Figure 1.21. Catalyst used for oxidation/ oxidative bromination.

Polymer anchored oxidovanadium(IV) catalyst (Figure 1.22) has been used effectively for the selective oxidation of various primary and secondary alcohols to their

corresponding aldehydes in aqueous medium using molecular oxygen as an oxidant to obtain good product yield. The catalyst also shows very good activity towards oxidative bromination of various organic substrates with 90–100 % selectivity towards mono-substituted products at room temperature in aqueous medium [84].

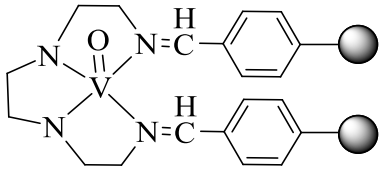

Figure 1.22. Catalyst used for oxidation/ oxidative bromination.

Oxidation of styrene catalyzed by PS–[VO(hmbmz)$_2$] in the presence of *tert*-butyl hydroperoxide gives three major products, styrene oxide, benzaldehyde and benzoic acid while ethylbenzene gave acetophenone as the major product [61]. Polymer-supported oxidoperoxidovanadium(V) complexes of 2-(2-pyridimyl)benzimidazole (2-pybmz) and 2-(3-pyridimyl)benzimidazole (3-pybmz) have also been used as catalyst for the oxidation of styrene using H_2O_2 as an oxidant. Oxidation of styrene gives five products, styrene oxide, benzaldehyde, benzoic acid, phenylacetaldehyde and 1-phenylethane-1, 2-diol; Figure 1.23. The formation of benzaldehyde is highest amongst all these products [60]. Complexes PS-[V^{IV}O(fsal-ea)(DMF)], PS-[V^{IV}O(fsal-pa)(DMF)], PS-[V^{IV}O(fsal-amp)(DMF)], PS-[V^{IV}O(fsal-β-Ala)(DMF)] also show mild to good catalytic activity towards the oxidation of styrene. Again the formation of benzaldehyde is highest for these catalyst and is justified by direct oxidative cleavage of the styrene side chain double bond via radical mechanism; Figure 1.24 [85].

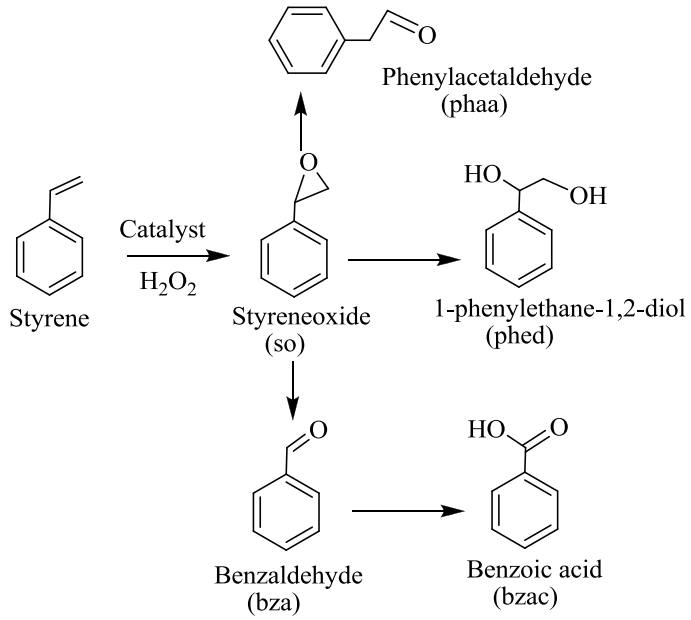

Figure 1.23. Various oxidation products of styrene.

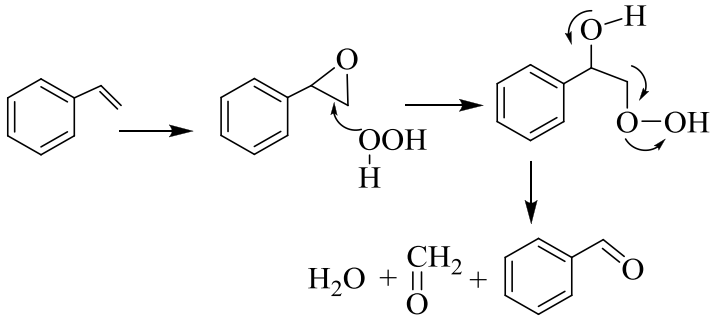

Figure 1.24. Proposed reaction mechanism.

The formation of maximum amount of benzaldehyde has also been obtained by oxidation of *trans*-stilbene catalyzed by PS-[$V^{IV}O$(fsal-β-Ala)(DMF)] in the presence of H_2O_2. Only *ca.* 16 % conversion was achieved after 6 h. Other oxidation products obtained are 1,2-diphenyl acetaldehyde (*ca.* 2 %), and benzophenone (*ca.* 1 %); Figure 1.25. Under the reaction conditions, no epoxide was detected amongst the reaction products obtained possibly due to its further oxidation to other products [62].

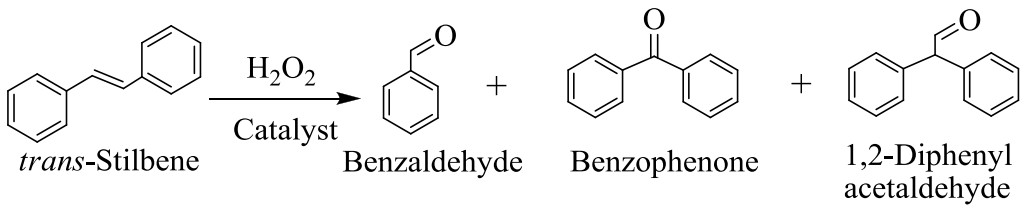

Figure 1.25. Reaction products of oxidation of *trans*-stilbene.

Complex PS–[VO(hebmz)$_2$] [Hhebmz = 2-(α-hydroxyethyl)benzimidazole] has been used as catalyst for the oxidation of benzoin using *tert*-butylhydroperoxide as an oxidant in methanol; Figure 1.26. Under the optimized reaction conditions, a maximum of 90 % conversion of the benzoin was achieved where selectivity of the obtained reaction products varies in the order: methylbenzoate (48.5 %) > benzil (19.5 %) > dimethylacetal (17.1 %) > benzoic acid (11.5 %) [86]. Complexes PS-[$V^{IV}O$(sal-hist)(acac)] and PS-[$V^{V}O_2$(sal-hist)] also catalyze the oxidation of benzoin successfully in the presence of aqueous H_2O_2 as an oxidant. A maximum of 91 % conversion of benzoin has been achieved with PS-[$V^{V}O_2$(sal-hist)] within 6 h. The selectivity of reaction products are: methylbenzoate (37.0 %) > benzil (30.5 %) > benzaldehyde-dimethylacetal (22.5 %) > benzoic acid (8.1 %). The corresponding PS–bound vanadium(IV) complex, PS–[$V^{IV}O$(sal–his)(acac)] exhibits very comparable catalytic potential [76].

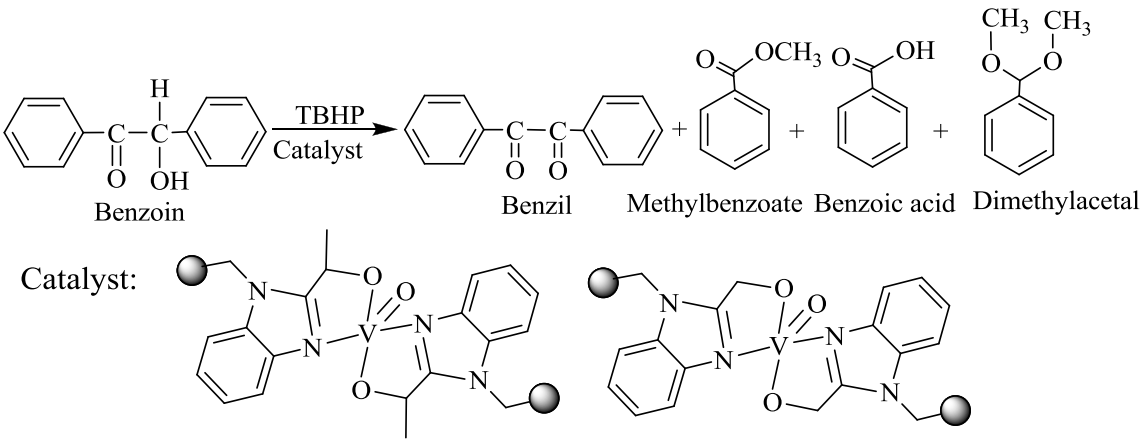

Figure 1.26. Oxidation products of benzoin and catalysts used for this reaction.

Various reaction conditions have been considered for the maximum oxidation of phenol and hydroquinone (Figure 1.27) using polymer-supported complex PS-[$V^{IV}O$(saldien)] as catalyst. It was observed that solvent plays an important role in altering the selectivity of reaction products. It gives catechol and hydroquinone upon the oxidation of phenol in acetonitrile while in water it is more selective towards catechol and *p*-benzoquinone. At lower temperature (*ca.* 70 ^{o}C) *p*-benzoquinone is stable in solution for longer period of time while at higher temperature (*ca.* 80 ^{o}C), it polymerizes slowly with the elapse of time. Oxidation of hydroquinone was also found to be pH dependent. Amongst three different buffer solutions such as acetate (pH 4.64), phosphate (pH 6.85) and carbonate (pH 10) buffer solutions used for the oxidation of hydroquinone under the optimized conditions [i.e. hydroquinone (0.55 g, 5 mmol), 30 % H_2O_2 (1.71 g, 15 mmol) and PS-[VO(saldien)] (30 mg)] carbonate buffer (10 mL) gives 16.6 % conversion of hydroquinone while others are not useful [61]. About 35 % of phenol conversion with ~60 % selectivity towards catechol and ~40 % towards p-hydroquinone has also been reported with catalysts PS-[VO(fsal-ohyba)·DMF], PS-K[VO_2(fsal-ohyba)] [87], PS-[$VO(O_2)_2$(2-pybmz)] and PS-[$VO(O_2)_2$(3-pybmz)] [60]. Vanadium complex of dithiocarbamate supported on porous methylacrylate resin catalyzes the oxidation of 2-methylphenol and 2,6-dimethylphenol to the corresponding quinones in presence of *tert*-butyl hydroperoxide [88].

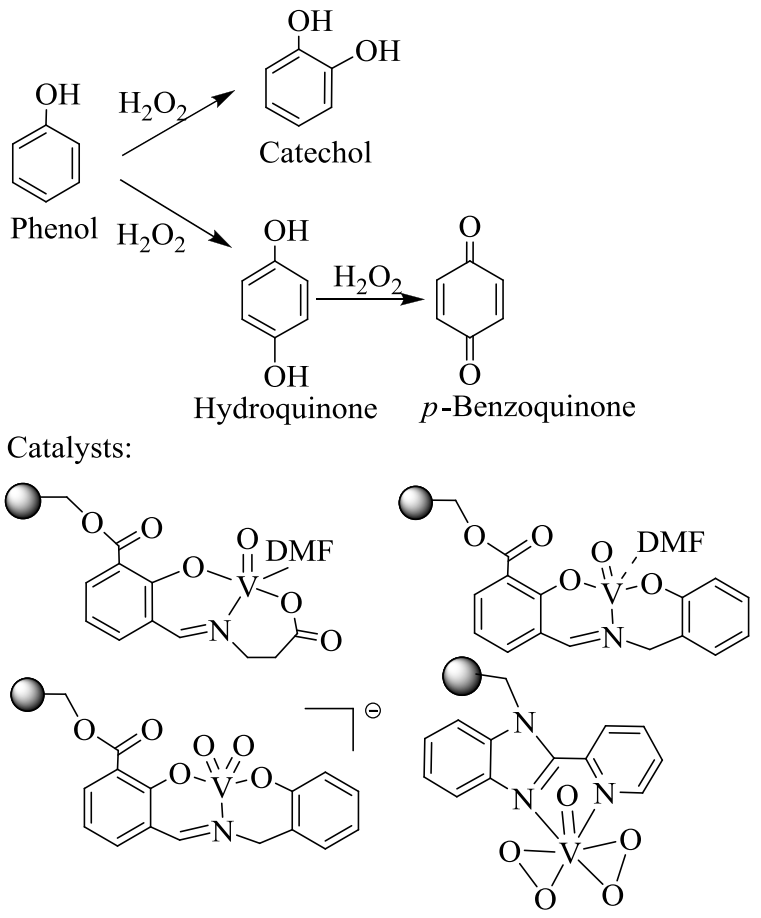

Figure 1.27. Oxidation products of phenol and further oxidation of hydroquinone to *p*-benzoquinone.

Pathak and Rao reported polymer-anchored vanadium(IV) complexes of salicylaldoxime, N,N′-bis(salicylidene)-propane-1,3-diamine and N,N′-bis(salicylidene)phenyl-1,2-diamine. These complexes catalyze the oxidation of 2,6-di-*tert*-butylphenol to give 2,6-di-*tert*-butylbenzoquinone (BQ) and 3,3’,5,5’-tetra-*tert*-butyldiphenoquinone (dPQ) in presence of *tert*-butylhydroperoxide (Figure 1.28) [89].

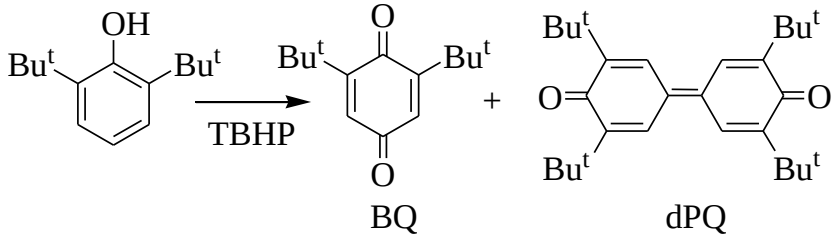

Figure 1.28. Oxidation of 2,6-di-*tert*-butylphenol.

Complexes PS-[VO(fsal-aepy)(acac)] and PS-[VO_2(fsal-aepy)] catalyse the hydroamination of styrene and vinyl pyridine with amines such as aniline and diethylamine. Amongst the mixture of two hydroaminated products formed under the optimized reaction conditions, the anti-Markownikoff product is favoured over the Markownikoff product (Figure 1.28) [90]. The fact is, regioselectivity favors anti-Markownikoff addition because this would results in least steric hindrance for the intermediate amino-styrene addition product. Intermediate amino-styrene complexes can then react in different ways, leading to hydroamination; Figure 1.29. Both the catalysts are recyclable.

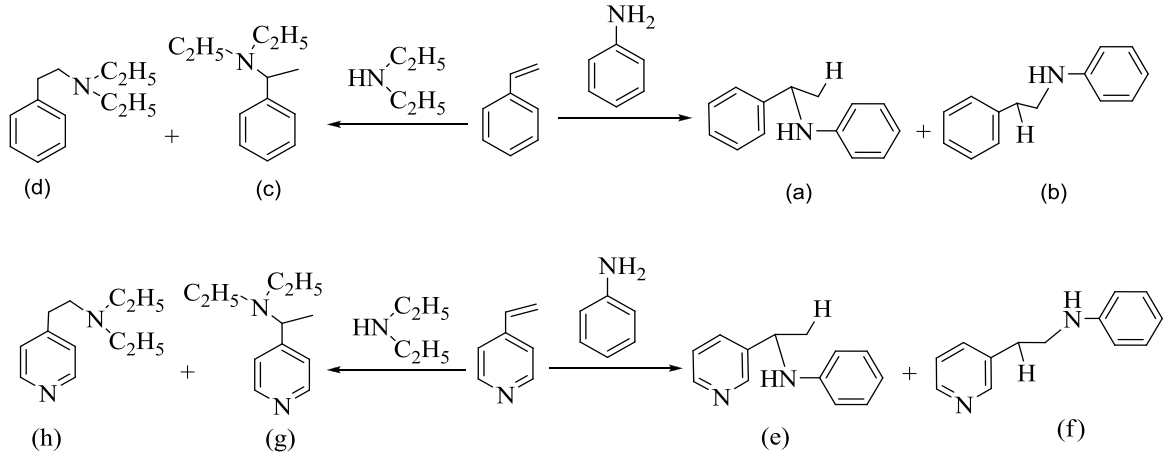

Figure 1.28 . Products of hydroamination of styrene and vinyl pyridine. Catalyst used: PS-[VO(fsal-aepy)(acac)] and PS-[VO_2(fsal-aepy)].

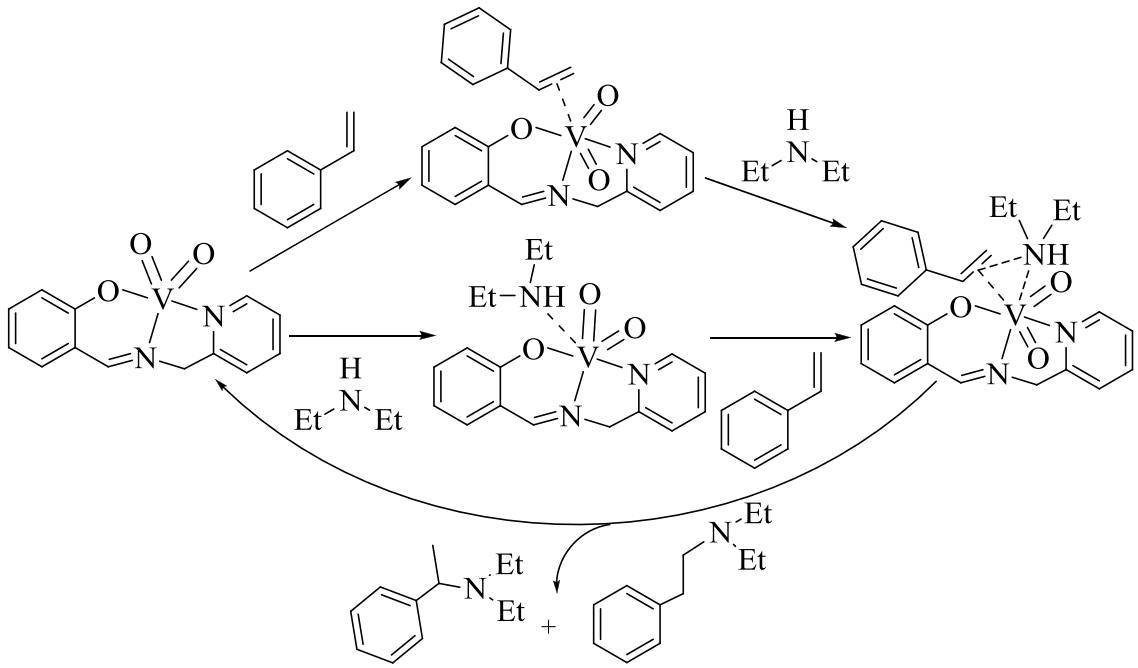

Figure 1.29. Possible reaction mechanism for the hydroamination process catalysed by [$V^{V}O_2$(sal-aepy)] (**5.4**). Mechanism considers hydroamination of styrene with diethylamine.

Oxidative amination of styrene with diethylamine, imidazole, and benzimidazole in the presence of oxygen and triethylamine has also been reported to give the corresponding enamines; Figure 1.30 presents the reaction products obtained [91]. Again, under the optimized reaction conditions, the anti-Markownikoff product was favoured over the Markownikoff one. The presence of steric hindrance due to secondary amine decreases the formation of the Markownikoff products.

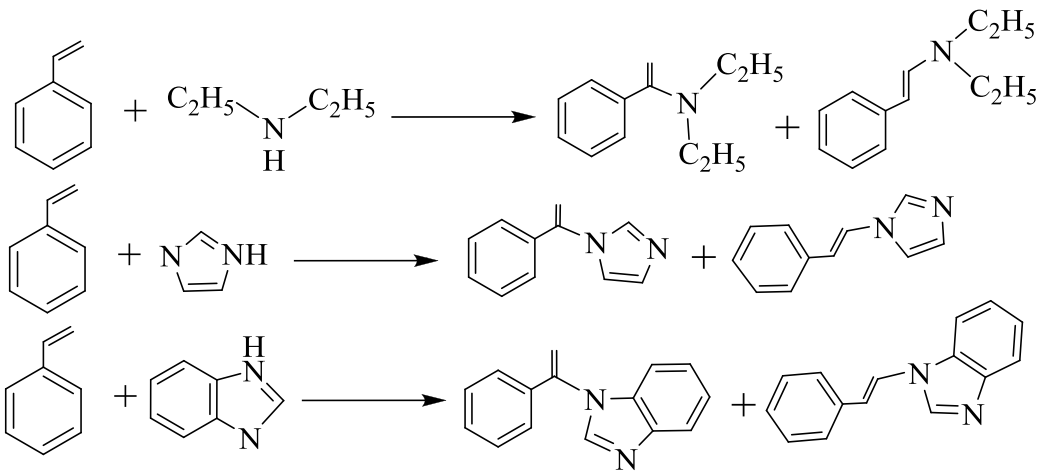

Figure 1.30. Oxidative amination of styrene with diethylamine, imidazole, and benzimidazole using catalyst precursors PS-[$V^{IV}O$(sal-cys)(DMF)].

Polymer-supported complexes PS-[$V^{IV}O$(fsal-DL-ala)(H_2O)], PS-[$V^{IV}O$(fsal-L-ile)(H_2O)] [92], PS-[$V^{IV}O$(fsal-β-ala)(DMF)] [62,92] have been used as catalysts for the oxidation of cyclohexene in presence of H_2O_2/ tert-butylhydroperoxide. The formation of at least four oxidized products, cyclohexeoxide, 2-cyclohexene-1-ol, 2-cyclohexene-1-one and cyclohexene-1,2-diol were identified by GC and characterized by GC-mass; Figure 1.31. The exact nature of the prepared catalyst PS-[$V^{IV}O(ligand)_n$] (PS-ligand is chloromethylated polystyrene covalently bonded to 2-thiomethylbenzimidazole) has not been possible but this catalyzes the oxidation of cyclohexene efficiently and gives 86% conversion with all these products mentioned above [93].

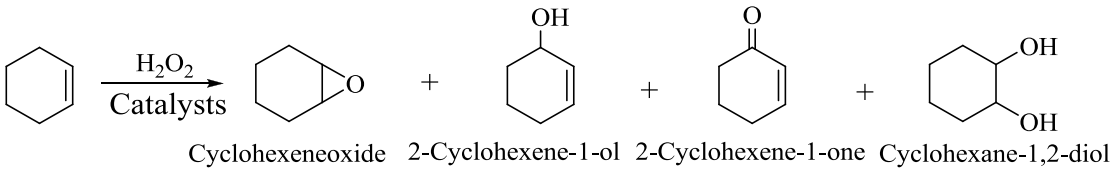

Figure 1.31. Various oxidation products of cyclohexene.

1.7. Objective of the present thesis

It is clear from the review of literature that one of the most active areas of research has been the study of catalytic potentials of vanadium complexes after screening them for the treatment of diseases [94–100] and finding insulin mimetic properties [101–104]. Polymer supported vanadium complexes have provided opportunities to explore functional mimics of vanadium based enzymes and effective catalysts for various organic transformations. Various methods have been applied to immobilize vanadium complexes on to polymer support to make them heterogeneous in nature. However, the syntheses of polymer-supported vanadium complexes via direct covalent bonding through functionalized cross-linked chloromethylpolystyrene and their catalytic applications have not been explored much. It was, therefore, reasonable to undertake systematic study on the synthesis and characterization of new polymer-supported vanadium catalysts using above methodology in addition to general method and to explore their catalytic potentials under optimized reaction conditions.

Present study is aimed to describe the synthesis of polymeric supported oxidovandium(IV)/ dioidxovanadium(V) complexes of the following ligands:

(i) Monobasic tridentate ONN donor ligands.

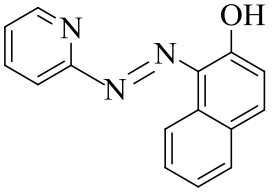

Hpan (**I**)

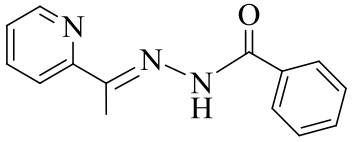

Hacpy-bhz (**II**)

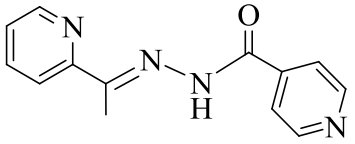

Hacpy-inh (**III**)

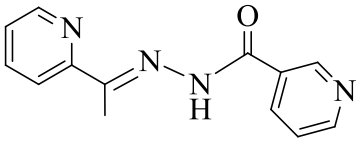

Hacpy-nah (**IV**)

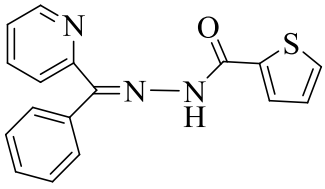

Hbzpy-tch (**V**)

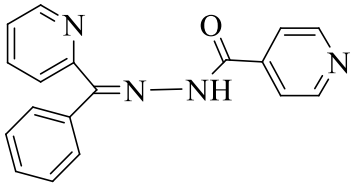

Hbzpy-inh (**VI**)

(ii) Tribasic pentadentate ligand

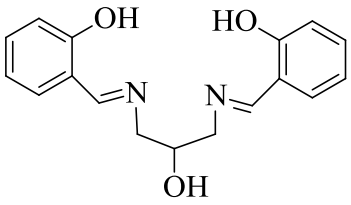

H_2sal-dahp (**VII**)

Synthesized complexes have been characterized by chemical, spectral (IR, electronic, EPR and NMR) and thermal studies, scanning electron micrographs and atomic force microscopic imaging Catalytic potential of these complexes have been explored for various organic transformations.

Chapter 2

Polymer-grafted and neat vanadium(V) complexes as functional mimics of haloperoxidases

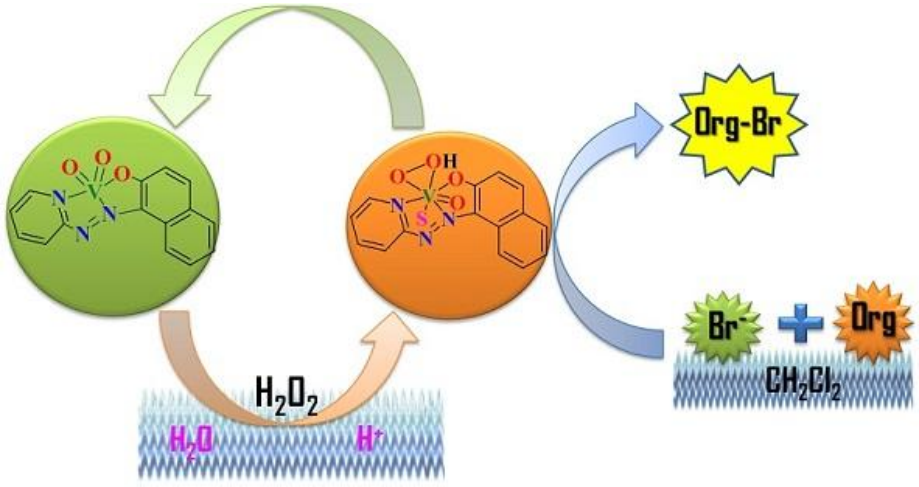

2.1. Introduction

The trigonal-bipyramidal coordination environment of vanadium center in vanadate-dependent haloperoxidases (VHPO) enzymes irrespective of their origin [19,41,105,106] has stimulated the coordination chemistry of vanadium with particular emphasis on the model character of vanadium(V) complexes having O and N functionalities. These structural models have also been extended to functional similarities including other catalytic potentials in oxygen transformations [25,29,32,33,53,54,59]. The $V^{V}O_2$ complexes with tridentate (ONO or ONN) ligand systems provide mostly a five-coordinate environment to the vanadium center similar to the enzymes. However, such complexes are coordinatively unsaturated and have a tendency to attain a six coordination environment [107]. This is mostly achieved through the coordination of a solvent molecule if suitable functional group of neighboring molecule for the formation of bridging complex is not available [108,109]. The replacement of coordinated solvent molecule in such model complexes by an imidazole moiety, one of the binding sites in VHPO, pre-grafted in the polymer produces immobilized structural models that can be modified to functional models for continuous working without losing their catalytic activities [54,69,110].

Herein, we have prepared dioxidovanadium(V) complex of a tridentate ONN donor ligand, 1-(2-pyridylazo)-2-naphthol [Hpan (**2.I**)] and grafted through coordination of imidazole functionalized chloromethylated polystyrene (cross-linked with 5 % divinylbenzene). The characterization of immobilized as well as neat complexes, their reactivity and catalytic potential as functional mimic for the oxidative bromination of organic substrates have been reported.

2.2. Experimental Section

2.2.1. Materials and methods

V_2O_5 (Loba Chemie, Mumbai, India), acetylacetone (Hacac), 1-(2-pyridylazo)-2-naphthol (Aldrich Chemicals Co., U.S.A), salicylaldehyde (Sisco research, India), styrene (Acros Organics, U.S.A.), *trans*-stilbene (Lancaster, England), and aqueous 30 % H_2O_2 (Qualigens, India) were used as obtained. Chloromethylated polystyrene [18.9% Cl (5.35 mmol Cl per gram of resin)] cross-linked with 5 % divinylbenzene was

obtained as a gift from Thermax Limited, Pune, India. [$V^{IV}O(acac)_2$] was prepared according to the method reported [111].

2.2.2. Instrumentation and characterization procedures

Elemental analyses of the ligand and complexes were obtained with an Elementar model Vario-EL-III. Vanadium content in polymer-grafted complex was checked by Inductively Coupled Plasma spectrometry (ICP; Labtam 8440 plasma lab). Thermogravimetric analyses of the complexes were carried out using Perkin-Elmer (Pyris Diamond) under oxygen atmosphere. The Energy Dispersive X-ray analyses (EDX) of the anchored ligand and the complex were recorded on a FEI Quanta 200 FEG. The samples were coated with a thin film of gold dust to protect the surface material from thermal damage by the electron beam and to make the sample conductive. IR spectra were recorded as KBr pellets on a Nicolet NEXUS Aligent 1100 FT-IR spectrometer after grinding the sample with KBr. Electronic spectrum of solid sample was recorded in Nujol using a Shimadzu 1601 UV–Vis spectrophotometer by layering the mull of the sample to the inside of one of the cuvettes while keeping the other one layered with Nujol as reference. Spectra of neat complexes were recorded in methanol or DMSO. ^{1}H NMR and ^{51}V NMR spectra were obtained on a Bruker Avance III 500 MHz and 400 MHz spectrometers, respectively, with the common parameter settings. NMR spectra were usually recorded in MeOD–d_4 or DMSO–d_6, and $\delta(^{51}V)$ values are referenced relative to neat $VOCl_3$ as external standard. EPR spectrum was recorded with a Bruker EMX EPR X-band spectrometer. The spin Hamiltonian parameters were obtained by simulation of the spectrum with the computer program of Rockenbauer and Korecz [112]. A Shimadzu 2010 plus gas-chromatograph fitted with a Rtx-1 capillary column (30 m × 0.25 mm × 0.25 μm) and a FID detector was used to analyze the reaction products. The percent conversion of substrate and selectivity of products were made on the basis of the relative peak area of the substrate/ respective product in GC using the formulae presented elsewhere [5]. The identity of the products was confirmed using a GC–MS model Perkin-Elmer, Clarus 500 by comparing the fragments of each product with the library available.

2.2.3. Preparations

2.2.3.1. Preparation of [$V^{IV}O(acac)(pan)$] (2.1)

A stirred solution of [$V^{IV}O(acac)_2$] (0.53 g, 2 mmol) dissolved in methanol (20 mL) was added to a hot solution of Hpan (0.498 g, 2 mmol) in methanol (25 mL) and the resulting reaction mixture was refluxed for *ca.* 8 h in an oil bath. The obtained dark brown precipitate was filtered off, washed with methanol and dried in vacuum. Yield 72 %. Anal. Calc. for $C_{20}H_{17}N_3O_4V$ (414.31): C, 57.98; H, 4.14; N, 10.14. Found: C, 57.5; H, 4.0; N, 10.2 %.

2.2.3.2. [{$V^{V}O(pan)$}$_2$(μ-O)$_2$] (2.2)

Complex **2.1** (0.414 g, 1 mmol) was dissolved in hot methanol (100 mL) and air passed through the solution with stirring and occasional heating. After *ca.* 3 days the solution slowly changed to wine red. After reducing the volume and keeping at room temperature complex **2.2** slowly precipitated which was filtered and dried at *ca.* 100 ^{o}C. Yield 85 %. Anal.Calc. for $C_{30}H_{20}N_6O_6V_2$ (662.41): C, 54.40; H, 3.04; N, 12.69. Found: C, 53.8; H, 2.9; N, 12.5 %. ^{1}H NMR (DMSO–d_6/ δ in ppm): 7.15–7.17 (d, 1H), 7.49–7.52 (t, 1H), 7.72–7.75 (q,br, 2H), 7.90–7.92(d, 1H), 8.12–8.14 (d, 1H), 8.26–8.28 (d, 1H), 8.38–8.41 (t, 1H), 9.33–9.34 (d, 1H), 9.36–9.37 (d, 1H). ^{51}V NMR (MeOD–d_4/ δ in ppm): −542 (major and sharp), –549 ppm (minor).

2.2.3.3. [$V^{V}O(O_2)(pan)(MeOH)$] (2.3)

An aqueous 30% H_2O_2 (*ca.* 2 mL) was added drop wise to complex **2.1** (0.414 g, 1 mmol) suspended in methanol (30 mL) with constant stirring at ambient temperature. After *ca.* 8 h, the insoluble complex slowly dissolved and gave pinkish red solution. The solution was kept for *ca.* 24 h after reducing the solution volume to *ca.* 10 mL. The precipitated solid was filtered, washed with cold methanol (2 × 4 mL) and dried in air. Yield 50 %. Anal.Calc. for $C_{16}H_{14}N_3O_5V$ (379.25): C, 50.67; H, 3.72; N, 11.07. Found: C, 51.1; H, 3.8; N, 11.2 %. IR (KBr, ν_{max}): 1359(N=N_{azo}), 935 (V=O), 848 (O–O), 771 [$V(O)_{2asym}$], 562 cm^{-1} [$V(O)_{2\ sym}$]. ^{1}H NMR (DMSO–d_6/ δ in ppm): 3.16–3.17 (d, 3H), 4.07–4.10 (q, 1H), 6.65–6.67 (d, 1H), 7.24–7.31 (t, br, 1H), 7.56–7.59 (t, 1H), 7.67–7.69

(d, 1H), 7.90–7.92 (d, 1H), 7.99 (s, 2H), 8.38–8.92 (t, 2H). ^{51}V NMR (MeOD–d_4/ δ in ppm): –597 ppm.

2.2.3.4. Preparation of PS–im[$V^{V}O_2$(pan)] (2.4)

Imidazolomethylpolystyrene (PS–im) [69] (1.00 g) was allowed to swell in DMF (20 mL) for 2 h. A solution of [{V^{V}O(pan)}$_2$(μ-O)$_2$] (**2.2**) (1.0 g, 3.02 mmol) in DMF (20 mL) was added to the above suspension and the reaction mixture was heated at 90 ^{o}C for 14 h with slow mechanical stirring. After cooling to room temperature, the dark black polymer-grafted complex **2.4** was separated by filtration, washed with hot DMF followed by hot methanol and dried at 120 ^{o}C in an air oven. Found: V, 1.12 %.

2.2.4. X-Ray crystal structure determination

Three-dimensional room temperature X–ray data for **2.3** were collected on a Bruker Kappa Apex CCD diffractometer at low temperature by the ϕ–ω scan method. Reflections were measured from a hemisphere of data collected from frames each of them covering 0.3º in ω. Of the 15840 for **2.3** reflections measured, all were corrected for Lorentz and polarization effects and for absorption by multi-scan methods based on symmetry-equivalent and repeated reflections, 1575 independent reflections exceeded the significance level ($|F|/\sigma|F|$) > 4.0. Complex scattering factors were taken from the program package SHELXTL [113]. The structure was solved by direct method and refined by full matrix least-squares on F^2. Hydrogen atoms were located in difference Fourier map and freely refined, except hydrogen atom of C(7) and O(1M), which were included in calculation positions and refined in the riding mode. Refinement was done with allowance for thermal anisotropy of all non-hydrogen atoms. Further details of the crystal structure determination are given in Table 2.1. A final difference Fourier map showed no residual density outside: 0.628 and –0.852 e.Å^{-3}. A weighting scheme, w = $1/[\sigma^2(F_o^2) + (0.057800P)^2 + 0.602000P]$, where P = $(|F_o|^2 + 2|F_c|^2)/3$, was used in the later stages of refinement.

Table 2.1. Crystal data and structure refinement for **2.3**.

Compound	$[V^{V}O(O_2)(pan)(MeOH)]$(**2.3**)
Formula	$C_{16}H_{14}N_3O_5V$
Formula weight	379.24
T, *K*	100(2)
Wavelength, Å	0.71073
Crystal system	Monoclinic
Space group	$P2_1/c$
a/Å	8.827(7)
b/Å	9.970(7)
c/Å	17.633(14)
β/º	91.39(2)
V/Å^3	1551(2)
Z	4
F_{000}	776
D_{calc}/g cm^{-3}	1.624
μ/mm^{-1}	0.674
θ/ (º)	2.31 to 27.69
R_{int}	0.2179
Crystal size/ mm^3	0.20 × 0.14 × 0.05
Goodness-of-fit on F^2	1.007
R_1 [a]	0.0819
wR_2 (all data) [b]	0.1874
Largest differences peak and hole (eÅ^{-3})	0.647 and -0.876

[a] $R_1 = \Sigma \left| \left| F_o \right| - \left| F_c \right| \right| / \Sigma \left| F_o \right|$. [b] $wR_2 = \{\Sigma[w(\left| \left| F_o \right|^2 - \left| F_c \right|^2 \right|)^2]\} / \Sigma[w(F_o^4)]\}^{1/2}$

2.2.5. Catalytic activity studies

Warning: $HClO_4$ is potential oxidant, hence must be handled carefully. The polymer-grafted complex PS–im$[V^{V}O_2(pan)]$ (**2.4**) was used for the oxidative bromination of styrene, salicylaldehyde and *trans*-stilbene. All reactions were carried

out in 50 mL round bottom flask at 40 ^{o}C. The polymer beads were allowed to swell in methanol for 2 h prior to the start of the catalytic reaction.

2.2.5.1. Oxidative bromination of styrene

Catalyst (0.010 g), styrene (1.04 g, 10 mmol), KBr (2.38 g, 20 mmol), aqueous 30 % H_2O_2 (2.27g, 20 mmol) and 70 % aqueous $HClO_4$ (5.72g, 40 mmol, added in four equal portions at t = 0, 15, 30 and 45 min) were stirred at 40 ^{o}C in a two phase CH_2Cl_2–H_2O (40 mL 50 %, v/v mixture) system for 1 h. At every 15 min small aliquot was withdrawn and after addition of 5 mL of CH_2Cl_2, it was washed with distilled water in a separatory funnel and organic layer was analyzed by gas chromatography. At the end, the organic layer after processing as above was evaporated and residue was purified by column chromatography using 1 % CH_2Cl_2 in n-hexane as an eluent. The products were identified by GC–MS and ^{1}H NMR spectroscopy.

1,2-Dibromo-1-phenylethane: ^{1}H NMR ($CDCl_3$): δ = 7.29–7.39 (m, 5H, aromatic), 5.11–5.13 (q, 1 H, CH), 3.97–4.06 (septet, 2H, CH_2) ppm.

1-Phenylethane-1,2-diol: ^{1}H NMR ($CDCl_3$): δ = 7.29–7.39 (m, 5H, aromatic), 4.9 (q, 1H, CH), 3.5 (q, 1H, CH_2), 3.6 (q, 1H, CH_2), 2.7 (br, 1H, OH) ppm.

2-Bromo-1-phenylethane-1-ol: ^{1}H NMR ($CDCl_3$): δ = 7.29–7.39 (m, 5H, aromatic), 5.1 (q, 1H, CH), 3.9 (septate, 2H, CH_2) ppm.

These data matched well with those reported earlier [95].

2.2.5.2. Oxidative bromination of salicylaldehyde

Catalyst (0.005 g), salicylaldehyde (0.61 g, 5 mmol), KBr (1.18 g, 10 mmol), 30 % H_2O_2 (1.13 g, 10 mmol) and 70 % $HClO_4$ (1.42 g, 10 mmol, added in four equal portions at t = 0, 30, 60 and 90 min) were stirred at 40 ^{o}C in distilled water (20 mL) for 2 h. After completion of the reaction, it was transferred in a separatory funnel and washed several times with water after addition of 10 mL of CH_2Cl_2. The organic layer was analyzed by gas chromatography and the reaction products were identified by GC–MS analysis.

2.2.5.3. Oxidative bromination of *trans*-stilbene

Catalyst (0.005g), *trans*-stilbene (0.90 g, 5 mmol), KBr (3.56 g, 30 mmol), 30 % H_2O_2 (3.39 g, 30 mmol), 70 % $HClO_4$ (5.72 g, 40 mmol) (added in four equal portions as mentioned before) were taken in a two phase $CHCl_3$–H_2O (40 mL, 50 %, v/v)

mixture) system and stirred at 40 ^{o}C. After 2 h the reaction mixture was washed with water and the organic layer was separated. The obtained reaction products were analyzed as mentioned above using this organic layer. For the identification of reaction products the crude mass was suspended in CH_2Cl_2; insoluble *trans*-stilbene oxide was separated by filtration, and then the solvent evaporated. Other reaction products were separated using a silica gel column. Elution of the column with 1% CH_2Cl_2 in n-hexane first separated mono bromo derivative followed by dibromo derivative. The products were identified by GC–MS and ^{1}H NMR spectroscopy.

^{1}H NMR spectral data of reaction products are as follows:

2,3-Diphenyloxirane: ^{1}H NMR ($CDCl_3$): δ = 7.35–7.55 (m, 10H, aromatic); 5.5 (d, 2H, CH).

2-Bromo-1,2-diphenylethanol: ^{1}H NMR ($CDCl_3$): δ = 8.0 (s, 1H, OH); 7.37–7.52 (m, 10H, aromatic); 5.5 (d, 2H, CH).

1,2-Dibromo-1,2-diphenylethane: ^{1}H NMR ($CDCl_3$): δ = 7.1–7.4 (m, 10H, aromatic); 6.15 (d, 2H, CH).

2.3. Results and Discussion

2.3.1. Synthesis, Characterization and solid state characteristics

Reaction between equimolar amounts of $[V^{IV}O(acac)_2]$ and Hpan (**2.I**) in dry, refluxing methanol yielded the oxidovanadium(IV) complex $[V^{IV}O(acac)(pan)]$ (**2.1**) (equation 2.1). On aerial oxidation of **2.1** in methanol, the dioxidovanadium(V) complex $[\{V^{V}O(pan)\}_2(\mu\text{-}O)_2]$ (**2.2**) was obtained (equation 2.2). The complex **2.2** can also be prepared directly by reacting $[V^{IV}O(acac)_2]$ with **2.I** followed by aerial oxidation. Addition of H_2O_2 to the methanolic solution of **2.1** yielded oxidomonoperoxidovanadium(V) complex $[V^{V}O(O_2)(pan)(MeOH)]$ (**2.3**) (equation 2.3). Same complex could also be isolated by the reaction of **2.2** with H_2O_2 in methanol (equation 2.4).

$$[V^{IV}O(acac)_2] + Hpan \rightarrow [VO^{IV}(acac)(pan)] + Hacac \quad (2.1)$$

$$2[VO^{IV}(acac)(pan)] + ½\ O_2 + H_2O \rightarrow [\{V^{V}O(pan)\}_2(\mu\text{-}O)_2] + 2Hacac \quad (2.2)$$

$$2[VO^{IV}(acac)(pan)] + 3H_2O_2 + MeOH \rightarrow [V^{V}O(O_2)(pan)(MeOH)] + 2Hacac + 2H_2O \quad (2.3)$$

$$1/2\ [\{V^{V}O(pan)\}_2(\mu\text{-}O)_2] + H_2O_2 + MeOH \rightarrow [V^{V}O(O_2)(pan)(MeOH)] + H_2O \quad (2.4)$$

All the complexes are fairly soluble in methanol, $CHCl_3$, DMF and DMSO; complex **2.1** is additionally soluble in CH_2Cl_2. Scheme 2.1 presents the structures proposed for these complexes which are based on the spectroscopic characterization (IR, electronic, EPR, ^1H and ^{51}V NMR), elemental analyses, thermogravimetric patterns and single crystal X-ray analysis of **2.3**. The ligand coordinates out through its mono anionic (ONN) functionalities.

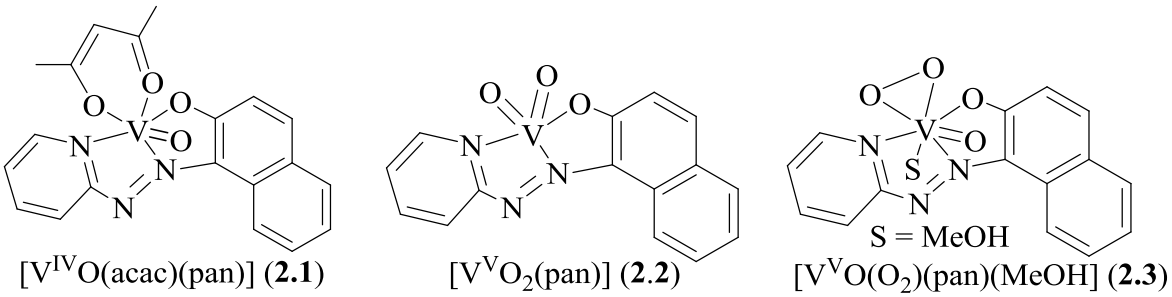

$[V^{IV}O(acac)(pan)]$ (**2.1**) $[V^{V}O_2(pan)]$ (**2.2**) $[V^{V}O(O_2)(pan)(MeOH]$ (**2.3**)

Scheme 2.1. Proposed structures of complexes prepared. Only idealized structure of **2.2** is shown.

Immobilization of imidazole through covalent attachment onto chloromethylated polystyrene, cross-linked with 5 % divinylbenzene (imidazolomethylpolystyrene, PS–im) has been achieved in acetonitrile in the presence of KI and triethylamine following the literature procedure (Scheme 2.2) [69,110]. The remaining chlorine content of 0.166 mmol/ g in imidazolomethylpolystyrene (PS–im) suggests *ca.* 97 % substitution of imidazole. Reaction of PS–im with complex **2.2** in DMF resulted in the formation of polymer-grafted dioxidovanadium(V) complex PS–im$[V^{V}O_2(pan)]$ **(2.4)**. The free chloromethyl groups of PS do not coordinate with the vanadium precursor. Scheme 2.2 presents the whole synthetic procedure. The metal ion loading calculated from the obtained vanadium content (0.21 mmol/ g of resin) for PS–im$[VO_2(pan)]$ is also close to the value determined by thermogravimetric analysis (0.18 mmol/ g of resin).

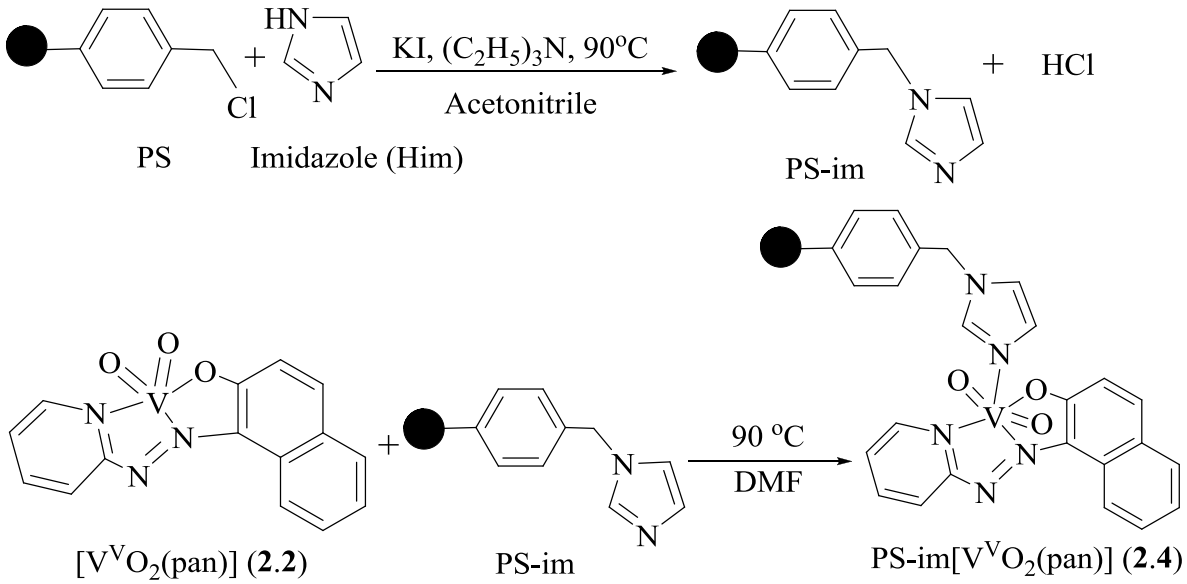

Scheme 2.2. Synthetic procedure for the isolation of polymer-grafted dioxidovanadium(V) complex, PS–im[VO_2(pan)] (**2.4**). Ball represents polystyrene back bone.

2.3.2. Structure description of $[V^VO(O_2)(pan)(MeOH)]$ (2.3)

Complex $[V^VO(O_2)(pan)(MeOH)]$ (**2.3**) crystallizes from methanol as dark red prism (crystal dimensions 0.22 × 0.21 × 0.20). Figure 2.1 shows an ORTEP representation of **2.3** and Table 2.2 contains selected bond lengths and angles. Vanadium atom is in the oxidation state V. In the molecular structure, the vanadium centre adopts a distorted seven-coordinated pentagonal bipyramidal geometry with the (pan) ligand coordinated through the one $O_{naphthol}$, one N_{azo} and one $N_{pyridine}$, and coordinated to one O_{oxide} terminal, one $O_{methanol}$ and to two $O_{peroxide}$, O(2) and O(3), atoms. The peroxide O–O distance of 1.443(5) Å lies within the range (1.38 and 1.45 Å) of the majority of peroxide compounds [114-116]; distances, V(1)-O(2) of 1.889(4) Å and V(1)-O(3) of 1.856(4) Å also indicate the presence of peroxide group.

The V=O bonds [V(1)–O(4): 1.600(4) Å] is characteristic of oxido-type O atoms with strong π bonding (see Table 2.2). The V–$O_{methanol}$ bond, which is trans to the oxo atom, is significantly longer [V(1)–O(1M): 2.241(4)Å] [29]. Intermolecular hydrogen bonds occur between the bonded methanol group and two oxygen atoms of peroxide

group of other molecule (see Figure 2.2 and Table 2.3). The pan ligand has a planar structure in the complex. The vanadium atom is displaced by about 0.2743 Å from the plane constituted for all the atoms of the ligand [C(1), C(2), C(3), C(4), C(5), C(6), C(7), C(8), C(9), C(10), C(11), C(12), C(13), C(14), C(15), N(1), N(2) and N(3)], which presents a deviation from the planarity of 0.0498(56) Å.

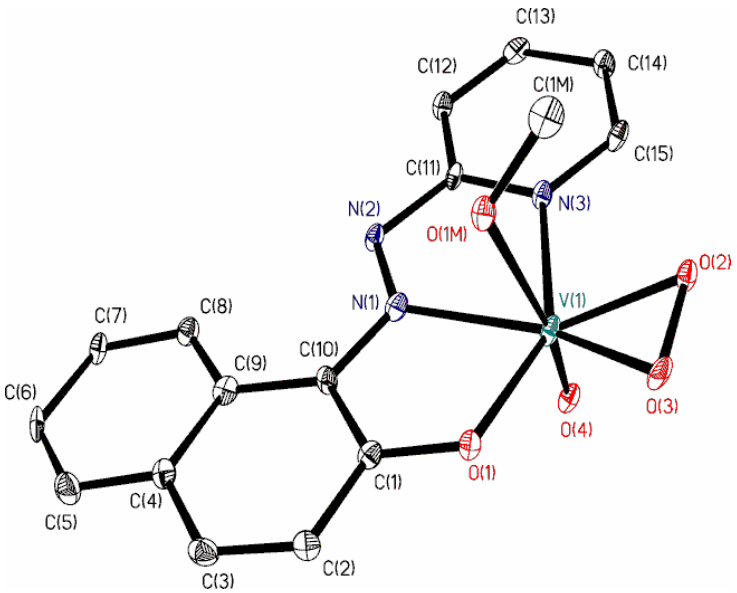

Figure 2.1. ORTEP plot of the complex [$V^{V}O(O_2)$(pan)(MeOH)] (**2.3**). All the non-hygrogen atoms are presented by their 30% probability ellipsoids. Hydrogen atoms are omitted for clarity.

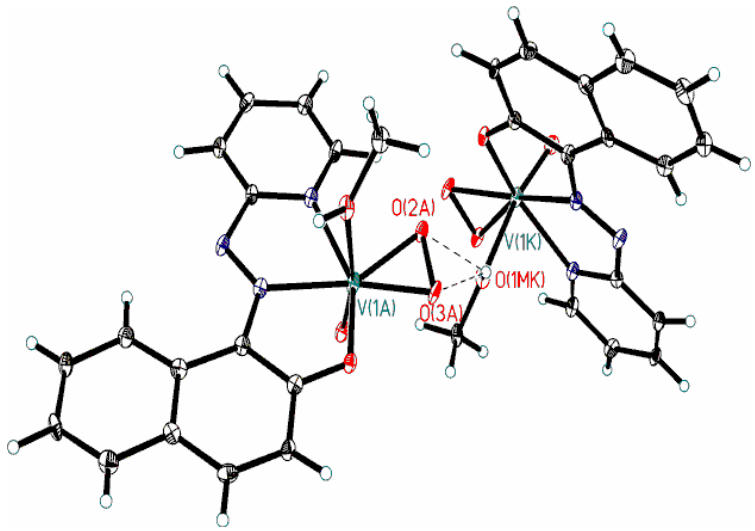

Figure 2.2. Hydrogen bonding scheme of compound [$V^{V}O(O_2)$(pan)(MeOH)] (**2.3**). All the non-hygrogen atoms are presented by their 30% probability ellipsoids.

Table 2.2. Bond lengths [Å] and angles [°] for $[V^{V}O(O_{2})(pan)(MeOH)]$ (**2.3**).

$[V^{V}O(O_{2})(pan)(MeOH)]$ (**2.3**)			
Bond lengths (Å)			
V(1)-O(1)	2.000(4)	O(2)-O(3)	1.443(5)
V(1)-O(2)	1.889(4)	V(1)-N(1)	2.135(5)
V(1)-O(3)	1.856(4)	V(1)-N(3)	2.115(5)
V(1)-O(4)	1.600(4)	N(1)-N(2)	1.275(6)
V(1)-O(1M)	2.241(4)		
Bond Angles (º)			
O(4)-V(1)-O(3)	105.5(2)	O(3)-V(1)-N(1)	152.30(19)
O(4)-V(1)-O(2)	104.1(2)	O(2)-V(1)-N(1)	151.2(2)
O(3)-V(1)-O(2)	45.30(17)	O(1)-V(1)-N(1)	75.91(19)
O(4)-V(1)-O(1)	97.7(2)	N(3)-V(1)-N(1)	72.3(2)
O(3)-V(1)-O(1)	80.05(17)	O(4)-V(1)-O(1M)	166.82(19)
O(2)-V(1)-O(1)	124.62(18)	O(3)-V(1)-O(1M)	87.52(17)
O(4)-V(1)-N(3)	91.8(2)	O(2)-V(1)-O(1M)	86.32(18)
O(3)-V(1)-N(3)	127.6(2)	O(1)-V(1)-O(1M)	82.47(17)
O(2)-V(1)-N(3)	82.79(19)	N(3)-V(1)-O(1M)	81.34(18)
O(1)-V(1)-N(3)	146.95(18)	N(1)-V(1)-O(1M)	75.95(18)
O(4)-V(1)-N(1)	91.3(2)		

Table 2.3. Hydrogen bonds for $[V^{V}O(O_{2})(pan)(MeOH)]$ (**2.3**) [Å and °].

D-H...A	d(D-H)	d(H...A)	d(D...A)	<(DHA)
O(1M)-H(1M)...O(2)#1	0.93	2.05	2.694(6)	125.1
O(1M)-H(1M)...O(3)#1	0.93	2.36	3.157(6)	143.4

Symmetry transformations used to generate equivalent atoms:
#1 -x+2,y+1/2,-z+1/2

2.3.3. Thermogravimetric Analysis (TGA) studies

The complex [VO^{IV}(acac)(pan)] (**2.1**) decomposes exothermically in two major steps. Between 200–480 ^{o}C, the weight loss corresponds to acac (Found: 23.6, Calc.: 23.9 %). On further heating the remaining residue decomposes sharply in the 480 to 550 ^{o}C to give V_2O_5 (Found: 29.0, Calc.: 30.0 %) as the end product. The polymer–grafted complex PS–im[VO_2(pan)] (**2.4**) starts losing weight at *ca.* 200 ^{o}C but major exothermic decomposition occurs in two overlapping steps in the temperature range 400–500 ^{o}C. It has been difficult to distinguish the decomposition of polymer and organic ligand fragments. However, the remaining vanadium content of 0.18 mmol/ g of resin suggest the formation of V_2O_5.

2.3.4. Field emission-scanning electron microscope (FE-SEM) and energy dispersive X-ray analysis (EDAX) studies

Field emission-scanning electron micrographs (FE–SEM) for single beads of pure chloromethylated polystyrene and polymer-grafted complex were recorded to see the morphological changes. Some of these images are reproduced in Figure 2.3 As expected, grafting of vanadium complex resulted in the roughening of the top layer of polymer-supported beads. Energy dispersive X-ray analyses (EDAX) estimate vanadium content of *ca.* 0.18 mmol/ g of resin for PS–im[$V^{V}O_2$(pan)] (**2.4**). This observation suggests the immobilization of metal complex onto polystyrene beads.

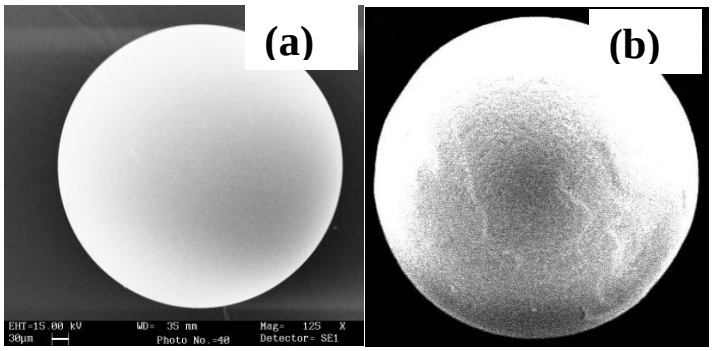

Figure 2.3. Field emission-scanning electron micrographs of (a) chloromethylated polystyrene (PS) and (b) PS–im[VO_2(pan)] (**2.4**).

2.3.5. IR spectral studies

Figure 2.4 presents IR spectra of complexes. Complex [$V^{IV}O$(acac)(pan)] (**2.1**) shows one sharp band at 955 cm^{-1} in the IR spectrum due to ν(V=O) stretch while dioxido complex [{$V^{V}O$(pan)}$_2$(μ- O)$_2$] (**2.2**) shows one sharp band at 936cm^{-1} and a broad band at 848 cm^{-1} corresponding to ν(V=O) and ν(V=O----V) modes, respectively. This observation hints towards dimerization of complex **2.2** in the solid state. This dimer breaks into monomer upon grafting into polymer and exhibits ν_{asym}(O=V=O) and ν_{sym}(O=V=O) modes at 940 and 917 cm^{-1}, respectively (Table 2.4). The peroxo complex [$V^{V}O(O_2)$(pan)(MeOH)] (**2.3**) exhibits three IR active vibrational modes associated with the peroxido moiety $[V(O_2)]^{2+}$ at 923, 721 and 565 cm^{-1} which are assigned due to the O–O intra stretching, asymmetric $V(O_2)$ stretching and symmetric $V(O_2)$ stretching, respectively. In addition, a band at 960 cm^{-1} is assigned due to ν(V=O) stretch.

The IR spectrum of Hpan (**2.I**) displays a sharp band at 1436 cm^{-1} due to ν(–N=N–) group. In complexes, this band shifts to lower wave number and appears at 1359–1364 cm^{-1}, confirming the coordination of the azo nitrogen to the metal centre [117]. Ligand also exhibits two sharp bands at 1566 and 1620 cm^{-1}due to ν(C=C/ C=N) and both of them appear at lower wave numbers (1549–1560/ 1585–1600 cm^{-1}) due to coordinated ring nitrogen to the metal. Absence of band in the 3400 cm^{-1} region (in **2.1**, **2.2** and **2.4**) indicates the coordination of phenolic oxygen after proton replacement. Thus, IR data confirm the monobasic tridentate ONN coordination behavior of ligand in these complexes.

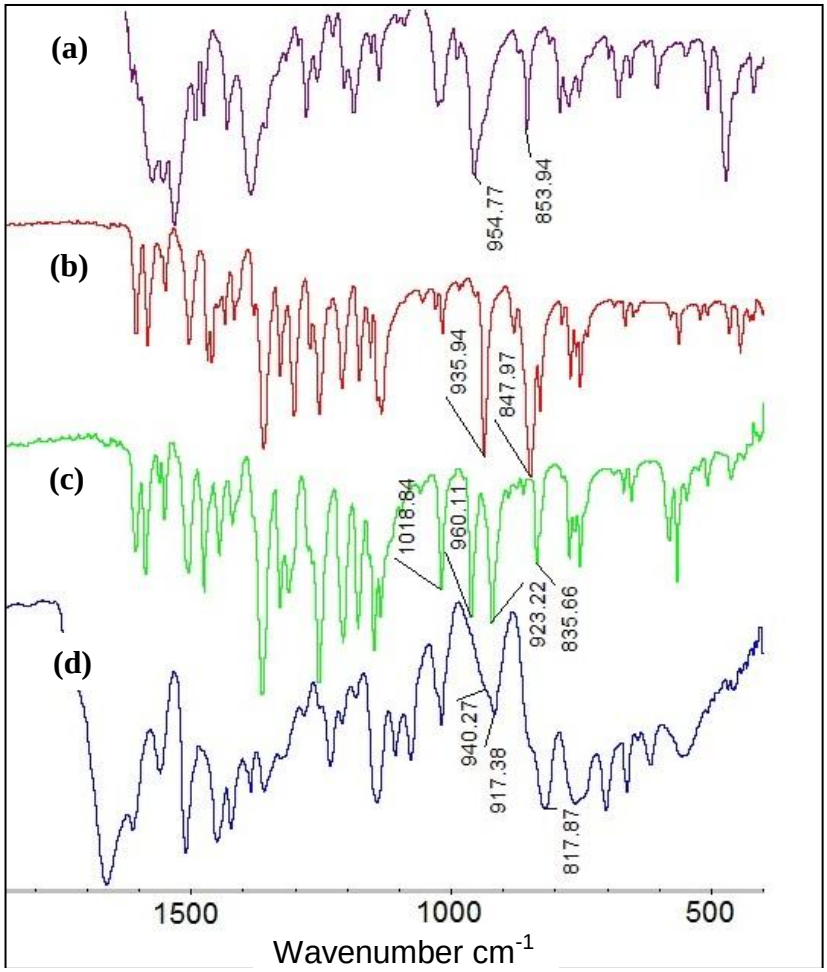

Figure 2.4. IR spectra of (a) [$V^{IV}O$(acac)(pan)] (**2.1**), (b) [{$V^{V}O$(pan)}$_2$(μ-O)$_2$] (**2.2**), (c) [$V^{V}O(O_2)$(pan)(MeOH)] (**2.3**) and (d) PS–im[$V^{V}O_2$(pan)] (**2.4**).

Table 2.4. IR spectral data of ligand and complexes.

Compounds	ν(N=N$_{azo}$)	ν(C=N$_{pyridyl}$/ C=C)	ν(V=O)
Hpan (**2.I**)	1436	1566, 1620	-
[$V^{IV}O$(acac)(pan)] (**2.1**)	1360	1549, 1586	955
[{$V^{V}O$(pan)}$_2$(μ-O)$_2$] (**2.2**)	1359	1550, 1587	936, 848
[$V^{V}O(O_2)$(pan)(MeOH)] (**2.3**) [a]	1359	1550, 1585	960
PS-im[$V^{V}O_2$(pan)] (**2.4**)	1364	1560, 1600	940, 917

[a] Bands due to peroxido group: 923, 721 and 565 cm^{-1}.

2.3.6. Electronic Spectral studies

As ligand **2.I** is an azo dye with phenolic oxygen, complexes of this ligand are highly coloured and show several bands in the visible region. We have recorded electronic spectra of complexes in MeOH and DMSO. In general, complexes $[\{V^{V}O(pan)\}_2(\mu\text{-}O)_2]$ (**2.2**) or $[V^{V}O(O_2)(pan)(MeOH)]$ (**2.3**) show good resolution of bands in MeOH while complex $[V^{IV}O(acac)(pan)]$ (**2.1**) shows better resolved bands in DMSO. Table 2.5 provides details of spectral data in both solvents but the discussion written below is based on the best spectra obtained for these complexes. The absorption bands appearing at 502, 540 and 567 nm in **2.1** and at 486, 551 and 580 nm in **2.2** are due to ligand to metal charge transfer type of transitions (LMCT). Such band in **2.3** appears at 552 and 580 nm. The band appearing at 415, 435 or 421 nm in **2.1**, **2.2** and **2.3**, respectively is due to the ligand-to-metal charge-transfer from phenolate O to d orbitals of vanadium band for monomeric dioxidovanadium(V) complexes [80,118]. Complex **2.1** also displays a weak shoulder band at 745 nm due to d–d transition. The higher energy UV region bands occurring in the range 200-330 nm are assigned to intra-ligand transitions. The electronic spectrum of polymer-grafted PS–im$[V^{V}O_2(pan)]$ (**2.4**) recorded in Nujol (Figure 2.5) exhibits spectral pattern exactly similar to that of **2.2** but with weaker intensities and thus confirm that the supported complex maintains the same coordination atmosphere as found for non–grafted one.

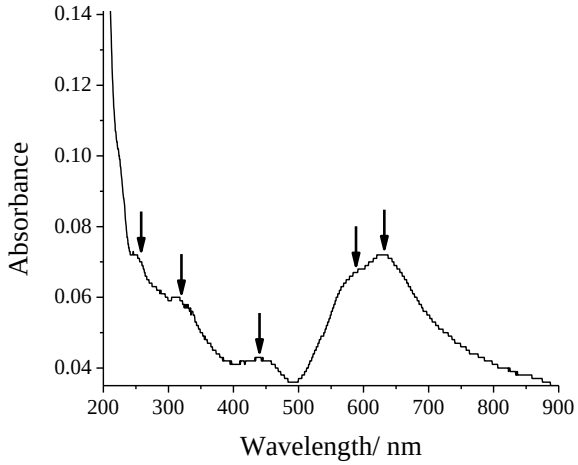

Figure 2.5. Electronic spectrum of PS–im$[V^{V}O_2(pan)]$ (**2.4**) recorded after dispersing in Nujol.

Table 2.5. Electronic spectral data of ligand and complexes

Compounds	Solvent	λ_{max}/nm (ε/M^{-1} cm^{-1})
Hpan (**2.I**)	MeOH	224, 304, 463
$[V^{IV}O(acac)(pan)]$ (**2.1**)	DMSO	257(19327), 294(10113), 340(5097), 415(6478), 502(7425)(sh), 540 (11209), 567(12414), 745(85)
	MeOH	225(20491), 292(7845), 415(7790)(sh), 462(10291), 574(604)
$[\{V^{V}O(pan)\}_2(\mu\text{-}O)_2]$ (**2.2**)	DMSO	274(13500)(sh), 309(8107)(sh), 331(6290)(sh), 410(6242), 552(13107), 573(13708)
	MeOH	228(19225), 304(4886)(sh), 435 (4842)(sh), 486(4047), 551(5970), 580(6259)
$[V^{V}O(O_2)(pan)(MeOH)]$ (**2.3**)	DMSO	271 (14491)(sh), 307(7959)(sh), 326(7167)(sh), 414(6946), 550(169450), 581(18482)
	MeOH	229 (16286), 269 (7368)(sh), 307 (3498)(sh), 326(3213)(sh), 421(3719), 552(8322), 580(8973)
PS–im$[V^{V}O_2(pan)]$ (**2.4**)	Nujol	252, 333, 435, 584, 627

2.3.7. EPR Spectral studies

Figure 2.6 presents EPR spectrum of "frozen" (77 K) solution (in MeOH) of $[V^{IV}O(acac)(pan)]$ (**2.1**). The hyperfine features and spectrum being consistent with binding modes involving $(O_{acac}, O_{phenolate}, N_{imine}, N_{py})_{equatorial}$, $(O_{acac})_{axial}$. Once a particular binding mode is assumed, the value of $A_{\parallel}$ can be estimated using the additivity relationship proposed by Wüthrich [119] and Chasteen [120], with an estimated accuracy of $\pm\ 3\times10^{-4}$ cm^{-1}. However, for the potential donor groups under consideration their predicted contributions to the parallel hyperfine coupling constant are rather similar {O_{acac}, ~41.7; $O_{phenolate}$ ~38.9; N_{imine} ~41.6; N_{py} ~40.7, O_{MeOH} ~45.5, all

$A_{\|}$ contributions in $cm^{-1} \times 10^{-4}$} [120,121], hence it is not possible to distinguish between the several plausible binding modes. The spectrum of $[V^{IV}O(acac)(pan)]$ was simulated [16] and the spin Hamiltonian parameters obtained are $g_{\|}$1.952, $A_{\|}$163.5 × 10^{-4} cm^{-1}, $A_{\perp}$63.0 × 10^{-4} cm^{-1} and $g_{\perp}$1.981. Thus, the EPR spectrum of $[V^{IV}O(acac)(pan)]$ in MeOH is in good agreement with an O_2N_2 binding mode. However, the coordination of solvent cannot be ruled out, but this implies the substitution of one of the equatorial donor atoms by an O-atom of the solvent.

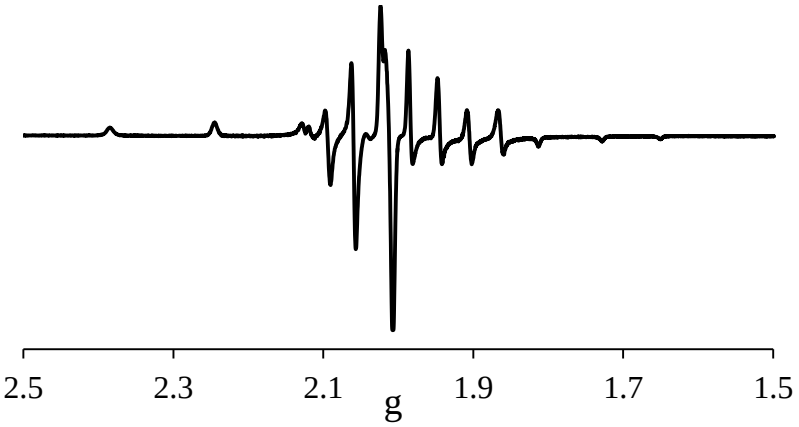

Figure 2.6. First derivative EPR spectrum of frozen solution of $[V^{IV}O(acac)(pan)]$ (**2.1**) in MeOH at 77 K.

2.3.8. ^{1}H and ^{51}V NMR studies

The ^{1}H and ^{51}V NMR chemical shift values for complexes are included in the experimental section. ^{1}H NMR spectra of complexes **2.2** and **2.3** show all expected signals. The shielded doublets at 9.33–9.34 (d, 1H), 9.36–9.37 (d, 1H) ppm in **2.2** are assignable to the protons nearest to the pyridine-nitrogen and is normally considered as characteristic of coordinated pyridinic nitrogen [117]. This signal is not very clear in complex **2.3** as signals of two protons overlap in this region. Assignments of other aromatic protons are difficult. Ligand Hpan (**2.I**) displays a signal at δ = 15.8 ppm due the naphtholic proton and the absence of this signal in complexes confirms the coordination of naphtholato-O atom.

In the ^{51}V NMR spectra, the line widths at half height are typically about 200 Hz. Complex $[\{V^{V}O(pan)\}_2(\mu\text{-}O)_2]$ (**2.2**) in MeOD–d_4 display a sharp resonance at δ = −542 and a minor one at δ = –549 ppm. These chemical shifts are within the values expected

for dioxidovanadium(V) complexes containing a O/N donor set [80,118,122]. The minor signal at δ = –549 ppm gains intensity with time in MeOD–d_4 (24 h), and therefore we assign this resonance due to [V^VO_2(pan)(MeOD)].

2.3.9. Catalytic activity studies

Vanadium haloperoxidases catalyze the oxidative bromination of organic substrates in the presence of H_2O_2 and bromide ion; vanadium(V) complexes have been reported to show functional similarities to these enzymes. During the catalytic action vanadium(V) coordinates with 1 or 2 equivalents of H_2O_2 to give oxido-monoperoxido, $[V^VO(O_2)]^+$ or oxido–diperoxido, $[VO(O_2)_2]^-$ species, that oxidize bromide ions in the presence of acid, most likely to Br_2, Br_3^- and/ or HOBr, which ultimately brominate the organic substrates [22,41].

2.3.9.1. Oxidative bromination of styrene

The dioxidovanadium(V) complexes (polymer grafted as well as non-polymer grafted) reported here satisfactorily catalyze the oxidative bromination of styrene, salicylaldehyde and *trans*–stilbene.

As observed earlier also [32,96,123], oxidative bromination of styrene in the presence of KBr, $HClO_4$ and 30 % H_2O_2 under a bi-phasic system (CH_2Cl_2–H_2O) gave mainly three major products, 1,2-dibromo-1-phenylethane, 2-bromo-1-phenylethane-1-ol and 1-phenylethane-1,2-diol; Scheme 2.3. Other minor products like benzaldehyde, styrene epoxide, benzoic acid and 4-bromostyrene have also been identified but their overall percentage is extremely low of the total of main products. All major products were separated, identified and confirmed by ^{1}H NMR spectroscopy as well as GC–MS.

Various reaction parameters *viz.* amounts of catalyst, oxidant (30 % aqueous H_2O_2), KBr and 70 % aqueous $HClO_4$ were optimized to obtain the maximum conversion of styrene. For a fixed amount of styrene (1.04 g, 0.010mol), H_2O_2 (2.27 g, 0.020 mol), KBr (2.38 g, 0.020 mol) and $HClO_4$ (2.86 g, 0.020 mol, added in four equal portions at t = 0, 15, 30 and 45 min of the reaction time) in CH_2Cl_2–H_2O (40 mL, v/v) solvent system, three different amounts of catalyst i.e. 0.010, 0.015 and 0.020 g were

taken and the reaction was carried out at 40 ^{o} C for 1 h. As shown in Figure 2.7 (a), a maximum of 65 % conversion was achieved with 0.010 g of catalyst. The conversion of styrene improved only marginally to 68 % and 70 %, on increasing catalyst amount to 0.015 and 0.020 g, respectively. Therefore, 0.010 g amount of catalyst was considered optimum for the maximum conversion of styrene.

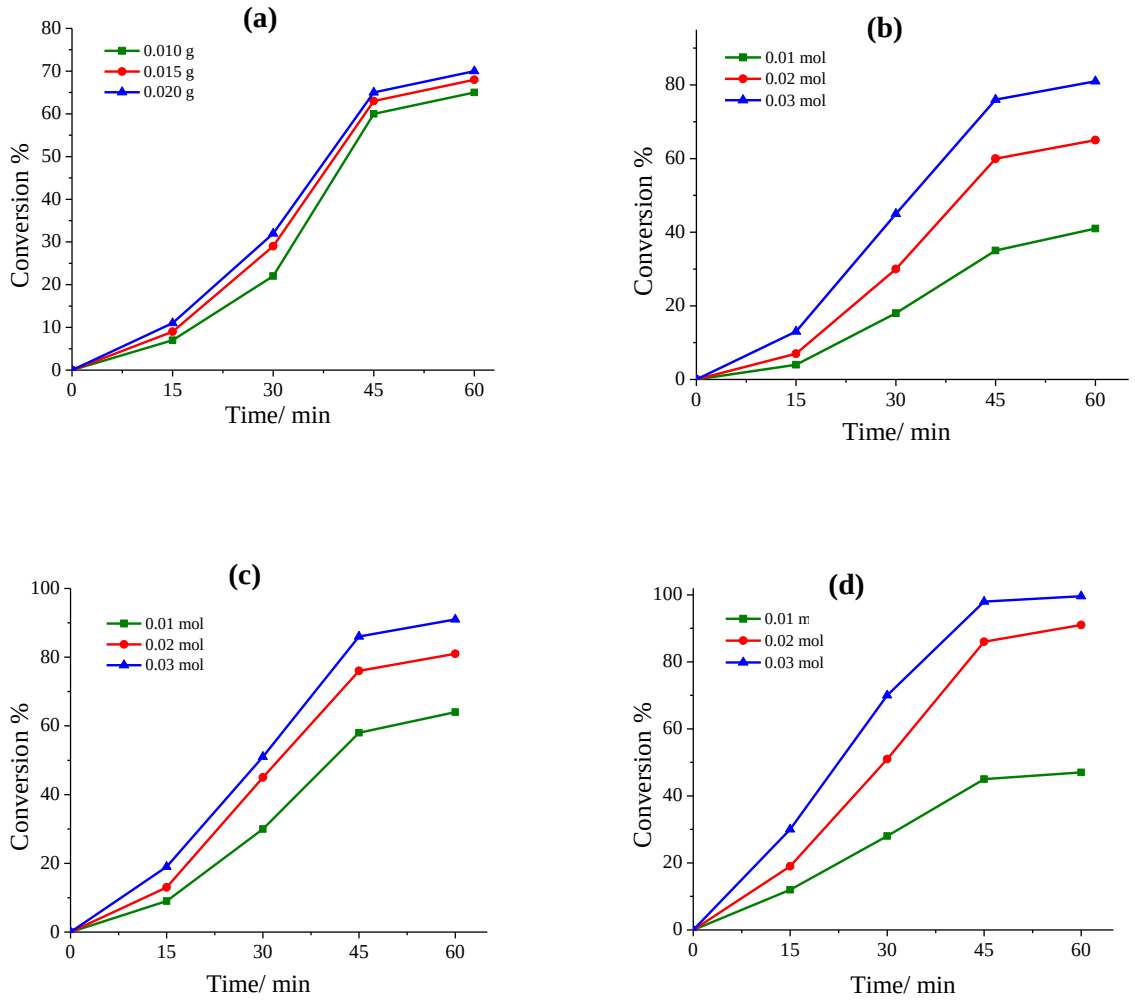

Figure 2.7. Effect of (a) amount of catalyst PS–im[VO_2(pan)] **(2.4)**, (b) amount of KBr, (c) amount of oxidant (i.e. 30 % aqueous H_2O_2) and (d) amount of 70 % $HClO_4$ on the oxidative bromination of styrene in 1 h of reaction time. For reaction conditions see text and Table 2.6.

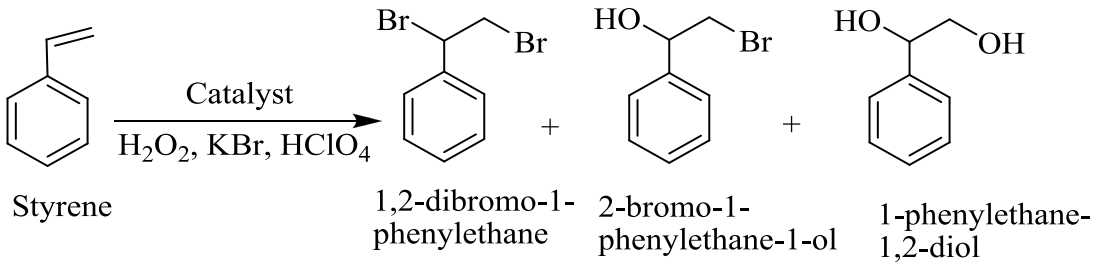

Scheme 2.3. Oxidative brominated products of styrene.

Similarly, three different amounts of KBr i.e. 10 mmol, 20 mmol and 30 mmol were taken for styrene (1.04 g, 10 mmol), catalyst (0.010 g), CH_2Cl_2–H_2O (40 mL, v/v), 30 % aqueous H_2O_2 (2.27 g, 20 mmol) and 70 % $HClO_4$ (2.86 g, 20 mmol, added as mentioned above) and the reaction was carried out at 40 ^oC. The obtained conversion was comparatively low (41 %) with 10 mmol KBr but increasing KBr amount from 10 to 20 mmol improved this conversion to 65 % which further improved to 81 % at 30 mmol KBr as shown in Figure 2.7 (b). Therefore, 30 mmol KBr was used to optimize rest of the reaction conditions.

The effect of amount of oxidant was studied considering substrate to oxidant ratios of 1:1, 1:2 and 1:3 for a fixed amount of styrene (1.04 g, 10 mmol) under above reaction conditions. A maximum of 64 % conversion was achieved with substrate to oxidant ratio of 1:1. Increasing the substrate to oxidant ratio from 1:1 to 1:2 increased the conversion from 64 to 81 %. This conversion further improved considerably (91 %) at the substrate to oxidant ratio of 1:3. Only a slight improvement in conversion was obtained upon further increasing this amount. Therefore, the oxidant amount of 30 mmol was considered to be more adequate one [Figure 2.7 (c)] for the maximum conversion of styrene in 1 h of reaction time.

Acid (here $HClO_4$) was found to be essential to carry out catalytic bromination. The amount of $HClO_4$ was optimized by taking substrate to $HClO_4$ ratios of 1:1, 1:2 and 1:3 under above reaction conditions; Figure 2.7 (d). For each condition, $HClO_4$ was added in four equal portion at t = 0, 15, 30 and 45 min reaction time. Only 47 % conversion was obtained with 10 mmol of $HClO_4$ (i.e. 1:1 substrate to $HClO_4$ ratio) but the conversion reached to 91 % with 20 mmol of $HClO_4$. Increasing this ratio to 1:3, the conversion improved to 98 % in 1 h of reaction time. At this ratio, the formation of 1-

phenylethane-1,2-diol is relatively more at the expense of 2-bromo-1-phenylethane-1-ol. However, substrate to $HClO_4$ ratio of 1:3 was considered as the best one for the maximum oxidative bromination of styrene. Similar effect along with equally good conversion of styrene has also been observed using H_2SO_4 under similar condition while use of acetic acid was not successful.

Details of all these conditions and the corresponding conversion of styrene along with the percent formation of different products are summarized in Table 2.6. Thus, the optimized reaction conditions (entry no. 9) as concluded for the oxidative bromination of 10 mmol (1.04 g) of styrene under bi-phasic system are: catalyst (0.010 g), KBr (3.57 g, 30 mmol), aqueous 30% H_2O_2 (3.39 g, 30 mmol), 70 % $HClO_4$ (4.28 g, 30 mmol) and CH_2Cl_2–H_2O (40 mL, 50 % v/v). The conversion of styrene and the formation of different reaction products under the optimized reaction conditions have been analyzed as a function of time and are presented in Figure 2.8. It is clear from the plot that the formation of all three major products starts with the consumption of styrene. The selectivity of the formation of diol improves continuously and reaches 78 % at the end of 1 h. The selectivity of mono bromo derivative improves to 20 % slowly in the first 45 min and then decreases. The formation of dibromo starts only after 30 min and ends up at 2 % in 1 h. Though no further increment was obtained after 1 h, stirring the reaction mixture further affected on the reaction products (see Figure 2.8) and at the end of 2 h, the selectivity of reaction products followed the order: 1-phenylethane-1,2-diol (85 %) > 1,2-dibromo-1-phenylethane (8.5 %) > 2-bromo-1-phenylethane-1-ol (0.5 %). It seems that monobromo derivative converts into 1-phenylethane-1,2-diol slowly.

Table 2.6. Results of oxidative bromination of styrene using catalyst PS–im[VO_2(pan)] after 1 h of reaction time.

Entry No.	KBr (g, mmol)	H_2O_2 (g, mmol)	$HClO_4$ (g, mmol)	Catalyst (g)	CH_2Cl_2/H_2O (v/v, mL)	% Conv.	% products formation			
							% mono-bromo	% di-bromo	% di-ol	% others
1	2.38, 20	2.27, 20	2.86, 20	0.010	20 /20	65	28	0	33	4
2	2.38, 20	2.27, 20	2.86, 20	0.015	20/20	68	27	0	39	2
3	2.38, 20	2.27, 20	2.86, 20	0.020	20/20	70	28	0	40	2
4	1.18, 10	2.27, 20	2.86, 20	0.010	20/20	41	22	0	17	2
5	3.56, 30	2.27, 20	2.86, 20	0.010	20/20	81	27	0	51	3
6	3.56, 30	1.13, 10	2.86, 20	0.010	20/20	64	23	0	40	1
7	3.56, 30	3.39, 30	2.86, 20	0.010	20/20	91	22	0	66	3
8	3.56, 30	3.39, 30	1.43, 10	0.010	20/20	47	16	0	29	2
9	3.56, 30	3.39, 30	2.86, 30	0.010	20/20	99	16	2	77	4

The recycle ability of **2.4** was also tested for the oxidative bromination of styrene. The reaction mixture after a contact time of 1 h was filtered and the separated catalyst was washed with acetonitrile, dried and subjected to further catalytic reactions under similar conditions. No appreciable loss in the activity (see Table 2.7) indicated that the catalyst was active even after the first cycle.

Table 2.7. Conversion of styrene and selectivity of products under optimized reaction condition after 1h of reaction time.

Sr. No.	Catalyst	% Conv.	TOF/h^{-1}	Selectivity (%)			
				mono-bromo	di-bromo	di-ol	Others
1.	PS–im[VO_2(pan)]	99	4648	16	2	78	4
2.	PS–im[VO_2(pan)][a]	95	4460	15	2	79	4
3.	[{V^VO(pan)}$_2$(μ-O)$_2$]	90	4226	24	0	73	3

[a] First cycle of used catalyst.

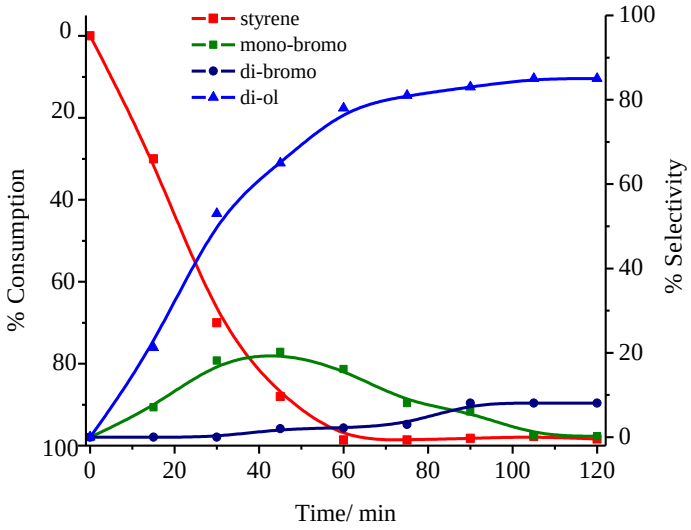

Figure 2.8. Percentage consumption of styrene and selectivity of the formation of products with time using PS–im[$V^{V}O_2$(pan)] **(2.4)** as catalyst precursor for 2 h of reaction time under the optimized conditions specified in the text.

The neat complex [{V^{V}O(pan)}$_2$(μ-O)$_2$] (**2.2**) showed 90 % conversion of styrene using 0.0007 g under the above optimized conditions. However, the turnover frequency is low compared to that of the polymer-anchored complex. The formation of only 2-bromo-1-phenylethane-1-ol and 1-phenylethane-1,2-diol was observed at the end 1 h of reaction. The 1,2-dibromo-1-phenylethane starts forming only after 1 h along with small amount of unidentified product but the overall formations of both are very low even after 2 h and the selectivity of reaction products has the following order: 1-phenylethane-1,2-diol (75 %) > 2-bromo-1-phenylethane-1-ol (20 %) > 1,2-dibromo-1-phenylethane (1.2 %). In the absence of catalyst, the reaction mixture gave about 55 % conversion in 1 h of reaction time under above optimized reaction conditions with the selectivity order of products are: 1-phenylethane-1,2-diol (58 %) > 2-bromo-1-phenylethane-1-ol (35 %) > others (7 %) > 1,2-dibromo-1-phenylethane (0 %).

Catalytic efficiency of PS–im[$V^{V}O_2$(pan)] cannot be compared with similar catalytic systems as no catalytic activity for the oxidative bromination of styrene using other polymer-grafted complexes has been reported in the literature. However, the catalytic potential of the PS–im[$V^{V}O_2$(pan)] compares well with several other mononuclear and binuclear V^{V} complexes [96] and even with manganese complex [6].

Geometry and ligand environments (e.g. ONO or ONS donor) have not much effect on the catalytic potential of complexes and exhibit almost similar conversion along with the formation of all three products. The dioxidovanadium(V) complexes with sterically hindered ONO donor ligands gave relatively more amounts of 2-bromo-1-phenylethane-1-ol (bromohydrin) [109]. However, in most cases 1-phenylethane-1,2-diol has been obtained in higher amounts.

2.3.9.2.Oxidative bromination of salicylaldehyde

Catalyst Ps–im[$V^{V}O_2$(pan)] successfully performed the oxidative bromination of salicylaldehyde using above mentioned reagents in water and gave three major products, 5-bromosalicylaldehyde, 3,5-dibromosalicylaldehyde and 2,4,6-tribromophenol (Scheme 4) at 40 ^{o}C. About 2 h was required to get maximum conversion. Oxidative bromination of salicylaldehyde has earlier been reported using vanadium complexes as catalyst [96] and these are common oxidative brominated products of salicylaldehyde. The reaction conditions were optimized for the maximum oxidative bromination considering different parameters like amounts of catalyst, aqueous 30 % H_2O_2, KBr and 70 % $HClO_4$. Thus for 5mmol (0.61 g) of salicylaldehyde, three different amounts of catalyst (0.005, 0.010 and 0.015 g), aqueous 30 % H_2O_2 (5, 10 and 15 mmol), KBr (5, 10 and 15mmol) and 70 % $HClO_4$ (5, 10 and 15mmol, added in four equal portions to the reaction mixture, first portion at t = 0 and other three portions after every 30 min intervals) were taken in water and the reaction was carried out. After several trials (see Table 2.8), the optimized reaction conditions for the maximum conversion of salicylaldehyde were obtained and these were: salicylaldehyde (0.61 g, 5mmol), KBr (1.18 g, 10 mmol), aqueous 30 % H_2O_2 (1.13 g, 10 mmol), catalyst precursor (0.005 g), aqueous 70 % $HClO_4$ (1.42 g, 10 mmol) and water (20 mL). The conversion of salicylaldehyde under various reactions conditions and the formation of different products after 2 h of reaction time are presented in Table 2.8.

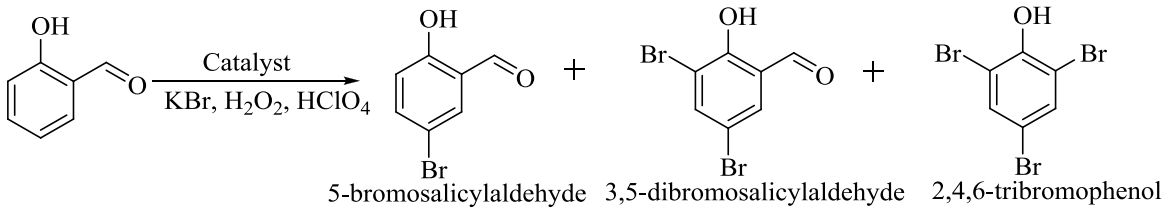

Scheme 2.4. Oxidative brominated products of salicylaldehyde.

Table 2.9 compares the selectivity of products obtained by grafted, grafted but recycled and neat catalysts. The recycled catalyst showed slightly less conversion than that obtained by fresh one but the selectivity of different products are nearly same and follows the order: 5-bromosalicylaldehyde > 2,4,6-tribromophenol > 3,5-dibromosalicylaldehyde. The non-polymer bound catalyst exhibited 80 % conversion with the formation of 5-bromosalicylaldehyde (86 %) and 3,5-dibromosalicylaldehyde (14 %), and thus also showed a good catalytic activity. In the absence of the catalyst, the reaction mixture gave about 60 % conversion of salicylaldehyde under above optimized reaction conditions with 82 % selectivity of mono-bromo and 18 % of di-bromo derivatives.

Table 2.8. Results of oxidative bromination of salicylaldehyde using catalyst PS–im[VO_2(pan)] (**2.4**) after 2 h of reaction time.

Entry No.	KBr (g, mmol)	H_2O_2 (g, mmol)	$HClO_4$ (g, mmol)	Catalyst (g)	H_2O (mL)	% Conv.	% mono-bromo	% di-bromo	% tri-bromo
1.	1.18, 10	1.13, 10	1.42, 10	0.005	20	96	80	14	0
2	1.18, 10	1.13, 10	1.42, 10	0.010	20	99	84	12	3
3	1.18, 10	1.13, 10	1.42, 10	0.015	20	99	84	10	5
4	1.18, 10	0.56, 5	1.42, 10	0.005	20	46	37	8	1
5	1.18, 10	1.69, 15	1.42, 10	0.005	20	96	78	6	12
6	0.59, 5	1.13, 10	1.42, 10	0.005	20	53	44	7	2
7	1.77, 15	1.13, 10	1.42, 10	0.005	20	98	83	12	3
8	1.18, 10	1.13, 10	0.177, 5	0.005	20	78	67	11	0
9	1.18, 10	1.13, 10	2.13, 15	0.005	20	99	85	14	0

Table 2.9. Product selectivity and % conversion under optimized reaction conditions for salicylaldehyde.

SL. No.	Catalyst (g, mmol)	% Conv.	TOF/ h^{-1}	Product selectivity (%)		
				mono-bromo	di-bromo	tri-bromo
1.	PS–im[VO_2(pan)]	96	2254	81	6	13
2.	PS–im[VO_2(pan)][a]	92	2160	80	6	14
3.	[{V^VO(pan)}$_2$(μ-O)$_2$]	80	1878	86	14	0

[a] First cycle of used catalyst.

Catalytic efficiency of the polymer-grafted complex **2.4** compares well with the non-grafted vanadium complexes reported in the literature [96] but its recyclable ability and high turnover frequency makes it better over neat ones.

2.3.9.3. Oxidative bromination of *trans*–stilbene

NH_4VO_3 catalyzed oxidative bromination of *trans*–stilbene in aqueous medium in the presence of H_2O_2, KBr and HBr has been reported by Hirao et al. [124] using dodecyltrimethylammonium bromide as a surfactant facilitated the bromination in 51 % yield with two reaction products namely 1,2-dibromo-1,2-diphenylethane and 2-bromo-1,2-diphenylethanol. We have carried out oxidative bromination of *trans*–stilbene in biphasic chloroform–water system. Chloroform was found to be better solvent in terms of solubility of *trans*–stilbene and reaction products. Oxidative bromination of *trans*–stilbene gave mainly three products: i) 2,3-diphenyloxirane (*trans*–stilbene oxide), ii) 2-bromo-1,2-diphenylethanol and iii) 1,2-dibromo-1,2-diphenylethane; Scheme 2.5. About 2 h was required to get maximum conversion. The reaction conditions for the maximum oxidative bromination of *trans*–stilbene were also optimized considering all these parameters mentioned above such as amounts of catalyst, aqueous 30 % H_2O_2, KBr and 70 % $HClO_4$. Their details, the corresponding oxidative bromination of substrate under various conditions and % selectivity of different products are summarized in Table 2.10. It is clear from the table that the optimized reaction

conditions for this reaction are different from other two reactions mentioned above and are (entry no. 7): *trans*–stilbene (0.90 g, 5 mmol)), KBr (2.36 g, 20 mmol) aqueous 30 % H_2O_2 (2.27 g, 20 mmol) catalyst precursor (0.005 g), aqueous 70 % $HClO_4$ (5.72 g, 40 mmol) and $CHCl_3$–H_2O (40 mL, 50 % v/v). Under these conditions, a maximum of 91 % conversion of *trans*–stilbene was obtained where selectivity of the reaction products follows the order: 2,3-diphenyloxirane (*trans*–stilbene oxide) (66 %) > 1,2-dibromo-1,2-diphenylethane (24 %) > 2-bromo-1,2-diphenylethanol (8 %).

Table 2.11 compares the conversion of *trans*–stilbene, obtained by fresh and recycled grafted catalysts, and non–polymer grafted catalyst along with the selectivity of products. The recycled catalyst again showed slightly less conversion (87 %) than the one obtained by fresh catalyst. The non-grafted catalyst exhibits even lower conversion (72 %). However, the selectivity of the formation of all three products is nearly same for all and follows the same order as mentioned above. In the absence of the catalyst, the reaction mixture gave about 55 % conversion under above optimized reaction conditions with 81 % selectivity of *trans*–stilbene oxide, 15 % of 1,2-dibromo-1,2-diphenylethane and 2 % of 2-bromo-1,2-diphenylethanol.

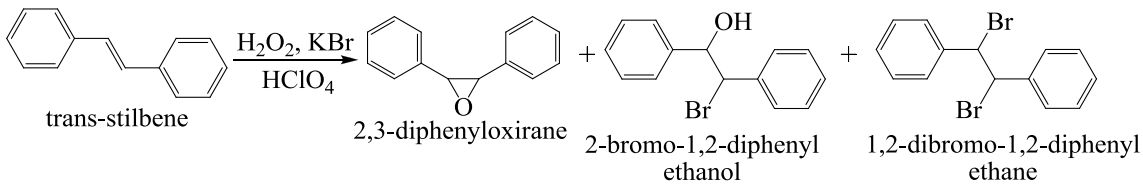

Scheme 2.5. Products obtained upon oxidative bromination of *trans*–stilbene.

Table 2.10. Results of oxidative bromination of *trans*–stilbene using catalyst PS–im[VO_2(pan)] after 2 h of reaction time.

Entry No.	KBr (g, mmol)	H_2O_2 (g, mmol)	$HClO_4$ (g, mmol)	Catalyst (g)	Solvent (mL) ($CHCl_3/H_2O$)	% Conv.	% mono-bromo	% di-bromo	% T.S.O.[a]	% others
1	3.56, 30	3.39, 30	5.72, 40	0.005	20 /20	96	4	28	62	2
2	3.56, 30	3.39, 30	5.72, 40	0.010	20 /20	98	5	28	63	2
3	3.56, 30	3.39, 30	5.72, 40	0.015	20 /20	99	5	29	63	2
4	1.18, 10	3.39, 30	5.72, 40	0.005	20 /20	79	6	22	48	3
5	2.36, 20	3.39, 30	5.72, 40	0.005	20 /20	92	3	28	58	3
6	2.36, 20	1.13, 10	5.72, 40	0.005	20 /20	85	7	21	55	2
7	2.36, 20	2.27, 20	5.72, 40	0.005 g	20 /20	91	7	22	60	2
8	2.36, 20	2.27, 20	2.86, 20	0.005	20 /20	70	5	18	45	2
9	2.36, 20	2.27, 20	4.29, 30	0.005	20 /20	86	6	22	56	2

[a] T.S.O.= *trans*–stilbene oxide

Table 2.11. Product selectivity and % conversion under optimized reaction conditions for *trans*–stilbene.

SL. No.	Catalyst	% Conv.	TOF/ h^{-1}	Selectivity (%)			
				mono-bromo	di-bromo	T.S.O	Others
1.	PS–im[VO_2(pan)]	91	2136	8	24	66	2
2.	PS–im[VO_2(pan)][a]	87	2043	11	21	65	3
3.	[{V^VO(pan)}$_2$(μ-O)$_2$]	72	1690	16	20	62	2

[a] First cycle of used catalyst

2.3.10. Reactivity of oxidovanadium(IV) and dioxidovanadium(V) complexes and possible mechanism of oxidative bromination of substrates

Generally accepted mode of action of V-BrPOs involves the presence of vanadium in their active sites, where V ion serves as a strong Lewis acid in the activation of the primary oxidant, H_2O_2 and forms a peroxido vanadium derivative. In the presence of KBr and $HClO_4$, it oxidizes a bromide ion giving bromine equivalent (most likely to HOBr) intermediate. Such an intermediate may then brominate an appropriate organic substrate. The possibility of involving the intermediate containing vanadium bound OBr^-, in the presence of H_2O_2, KBr and $HClO_4$, has recently been exploited through DFT calculations [109]. The processes occurring in the aqueous phase require acidic conditions, probably to promote the protonation of the peroxido moiety.

We have monitored the reactivity of [$V^{IV}O$(acac)(pan)] (**2.1**) with H_2O_2in DMSO by electronic absorption spectroscopy . Thus, stepwise addition of one drop portions of 30 % H_2O_2 (0.058 g, 0.513 mmol) in 10 mL of DMSO to 10 mL of *ca.* 10^{-4} M solution of **2.1** in DMSO results in the flattening of shoulder band appearing at *ca.* 745 nm (Figure 2.9 (a)). In dilute solution (*ca.* 10^{-4} M) of complex, the intensity of 540 and 567 nm bands decreases with slight red shift towards 552 and 581 nm while 502 and 411 nm bands shift to 471 and 441 nm, respectively, with slight increase in intensity; Figure 2.9 (b). In the UV region, the intensity of weak shoulder at *ca.* 298 nm decreases and a new shoulder band at 307 nm is generated (same as in peroxo complex).The intensity of the band around 257 nm slowly decreases. The shape of final spectrum is almost similar to the one obtained after treating **2.2** with H_2O_2, which, in turn, is similar to the spectrum of peroxide complex **2.3**, thus verifying the formation of similar oxidoperoxido species with both complexes.

We have also recorded spectral changes during stepwise additions of two drop portions of 30 % H_2O_2 in 5 mL of MeOH to 25 mL of 0.51×10^{-4} M solution of **2.2** in $CHCl_3$ (Figure 2.10). The spectral changes observed are very similar to the ones recorded in DMSO, showing the formation of similar type of species in both solutions.

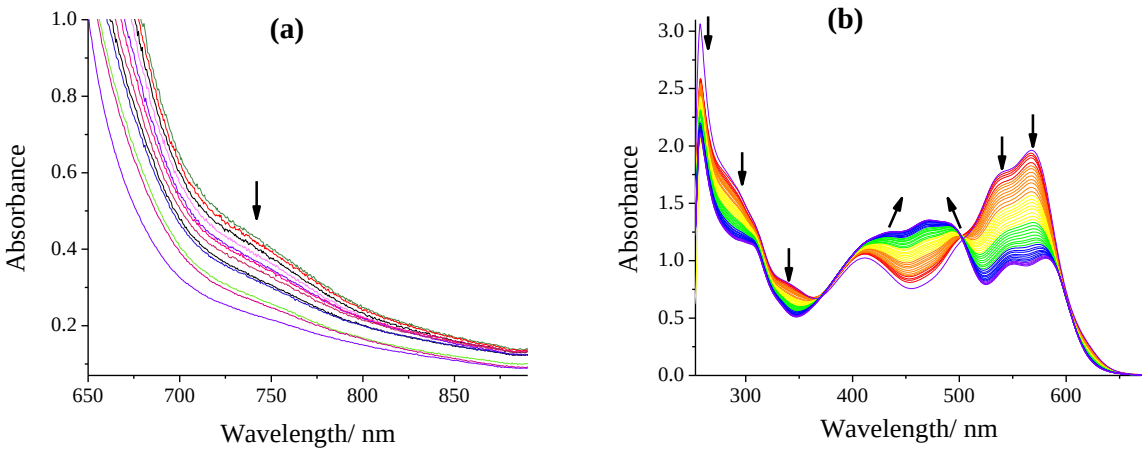

Figure 2.9. Spectral changes obtained during titration of (a) stepwise addition of one drop portions of 30 % H_2O_2 (0.058 g, 0.513 mmol) in 10 mL of DMSO to 10 mL of *ca.* 10^{-4} M solution of $[V^{IV}O(acac)(pan)]$ (**2.1**) in DMSO and (b) stepwise additions of one drop portions of aqueous 30 % (0.058 g, 0.513 mmol) in 5 mL of DMSO to 20 mL of *ca.* 1.58×10^{-4} M solution of **2.1** in DMSO.

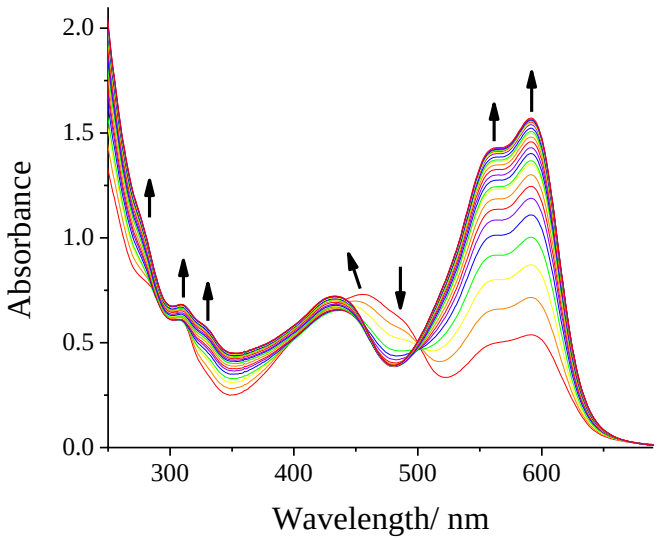

Figure 2.10. Spectral changes obtained during titration of stepwise additions of two drop portions of 30 % H_2O_2 in 5 mL of MeOH to 25 mL of *ca.* 0.51×10^{-4} M solution of $[\{V^{V}O(pan)\}_2(\mu\text{-}O)_2]$ in $CHCl_3$.

Upon addition of 1.0 equiv. of an 30 % aqueous H_2O_2 to a methanolic solution of 2.2 (*ca.* 4 mM) a peak at δ = –597 ppm emerges, which we assign due to $[V^{V}O(O_2)ONN(S)]$ (S = solvent). This signal increases intensity at the expense of the

resonances due to dioxido species (δ = –542 ppm) upon further addition of H_2O_2. The signals due to dioxido species finally disappear and another weak signal at δ = –644 ppm in addition to the signal due to peroxido complex also builds up upon addition of a total of 4 equiv. of H_2O_2, which is possibly due to $[V^VO(O_2)_2S]$ (Figure 2.11) [125]. Leaving the NMR tube open for 24 h, the only resonance at –549 ppm due to **2.2**·MeOD is recorded, indicating the reversibility of the process [126].

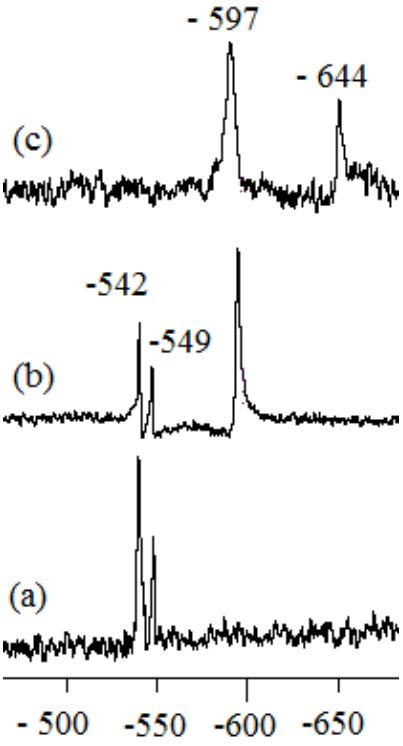

Figure 2.11. ^{51}V NMR spectra of methanolic solutions of complex **2.3** (*ca.* 4 mM): (a) after preparation of the solution, (b) solution of (a) after addition of 1 equiv. H_2O_2, (c) solution of (a) after 1 h of addition of 4 equiv. H_2O_2.

In order to identify the possible intermediate forms in the catalytic reaction, the reactivity of peroxide complex $[V^VO(O_2)(pan)(MeOH]$ (**2.3**) in methanol with one drop portions of saturated HCl solution in 5 mL of MeOH has also been studied and spectral changes are presented in Figure 2.12. The bands at 420 and 490 nm in the visible region are mainly affected in the presence of HCl. Thus, the band at 420 shifts to 410 nm with increase in intensity while 490 nm band completely disappears along with a decrease in intensity. Other bands at 550 and 590 nm gain only intensity without changing their

positions. These spectral changes have been proposed due to the formation of oxidohydroperoxido species [94,95,109,127,128].

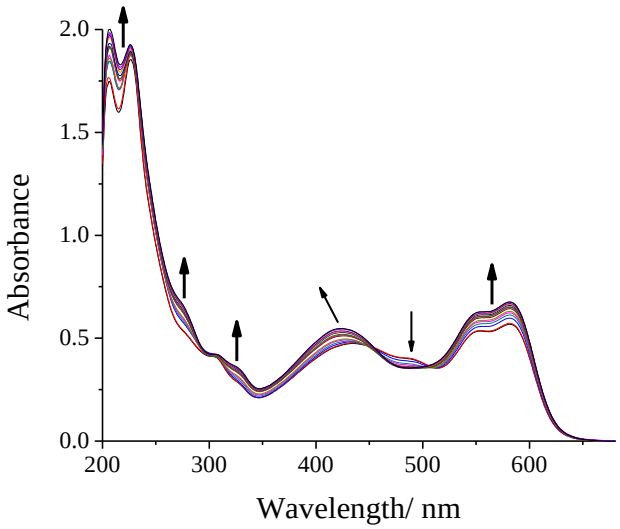

Figure 2.12. Spectral changes obtained during titration of stepwise additions of one drop portions of saturated HCl in 5 mL of MeOH to 25 mL of *ca.* 2.03×10^{-4} M solution of $[V^{V}O(O_2)(pan)(MeOH)]$ (**2.3**) in MeOH.

Thus, complexes reported here show similar behaviour as shown by other model complexes. As observed in other model vanadium complexes [29,123,129], in the presence of KBr, H_2O_2 and $HClO_4$, the generated HOBr during catalytic reaction may react with styrene to give bromonium ion as intermediate. The nucleophile Br^- as well as H_2O both may attack on the α-carbon of the intermediate to give 1,2-dibromo-1-phenylethane and 2-bromo-1-phenylethane-1-ol, respectively (Scheme 2.6). The formation of dibromo product in most cases at later stage is possibly due to (i) the presence of less amount of brominating reagent generated initially and/ or (ii) the generation of lesser amount of Br_2, another intermediate, during catalytic action. The nucleophile H_2O may further attack on the α-carbon of 2-bromo-1-phenylethane-1-ol to give 1-phenylethane-1,2-diol. All these justify the formation of 1-phenylethane-1,2-diol in higher yield.

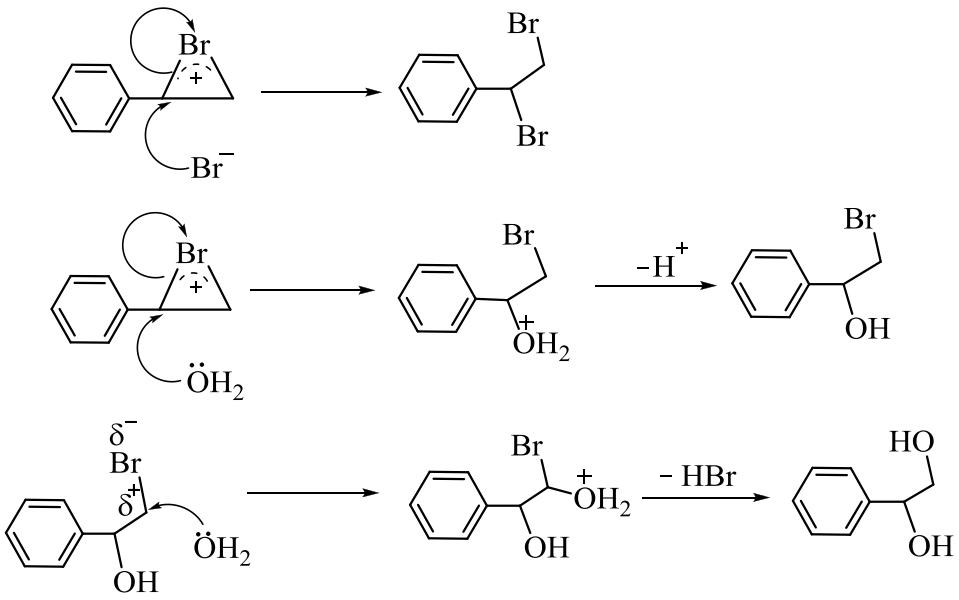

Scheme 2.6. Mechanism of action of HOBr on styrene.

The formation of 5-bromosalicylaldehyde and 3,5-dibromosalicylaldehyde upon oxidative bromination of salicylaldehyde is expected as –OH group of salicylaldehyde is *ortho*–and *para*–directing. However, the formation of 2,4,6-tribromophenol is possible only through decarbonylative bromination. Rana et al. [129] have recently shown that vanadium bound OCl^- species interacts with substrate like 2-hydroxy-1-naphthanldehyde using both functional groups which in the presence of H_2O_2 and KCl provides decarbonylated chlorinated product 1-chloronaphthalen-2-ol. Such mechanism is partly applicable here as well to give 2-bromophenol from salicylaldehyde which may undergo further bromination to give 2,4,6-tribromophenol.

The formation of 1,2-dibromo-1,2-diphenylethane and 2-bromo-1,2-diphenylethanol by oxidative bromination of *trans*–stilbene is again possible through bromonium ion intermediate as mentioned above for the oxidative bromination of styrene while that of 2,3-diphenyloxirane (*trans*–stilbene oxide) is the expected one by regular oxidation of *trans*–stilbene.

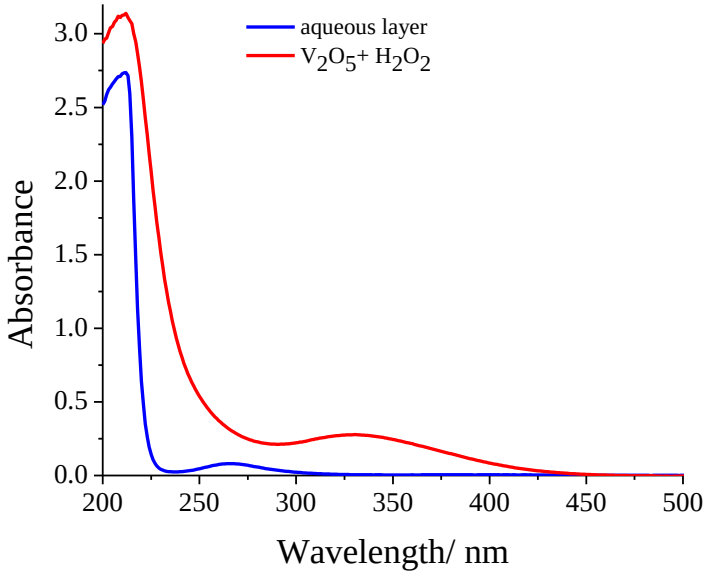

Figure 2.13. UV-visible spectra of aqueous layer from optimized reaction condition (blue line) carried out without substrate and aqueous solution of V_2O_5 treated with H_2O_2 (red line).

2.3.11. Leaching study of vanadium from polymer-anchored catalyst

To find out whether acid ($HClO_4$) added really causes leaching of vanadium ion (i.e. inorganic vanadium) we have performed blank reaction under optimized reaction conditions e.g. for oxidative bromination of *trans*–stilbene [i.e. catalyst precursor (0.005 g), KBr (2.36 g, 20 mmol), aqueous 30 % H_2O_2 (2.27 g, 20 mmol), 70 % $HClO_4$ (5.72 g, 40 mmol, added in four equal portions at 15 min intervals) and $CHCl_3$–H_2O (40 mL, 50 % v/v)] but without substrate and tested the aqueous layer after 1 h by electronic absorption spectroscopy. While aqueous layer from experiment does not show any band at *ca.* 400 nm, the standard solution made by dissolving V_2O_5 in H_2O_2 shows detectable band at *ca.* 400 nm; Figure 2.13. As H^+ ions consume continuously in the formation of possibly hydroperoxide intermediate species during catalytic reaction, the added perchloric acid consumes continuously and thus avoids the decomposition of catalysts. However, the aqueous layer from blank reaction showed vanadium content of 0.02 mmol g^{-1} of resin which indicates only partial leaching of the complex from polymer beads. Equally good catalytic activity of recycled catalyst further supports only partial decomposition of polymer-anchored complex during catalytic reactions.

2.4. Conclusions

Monobasic tridentate ONN donor ligand, 1-(2-pyridylazo)-2-naphthol [Hpan (**2.I**)] has been used to prepare oxidovanadium(IV) complex, [$V^{IV}O$(acac)(pan)] (**2.1**). Areal oxidation of **2.1** gave dioxidovanadium(V) complex, [{$V^{V}O$(pan)}$_2$(μ-O)$_2$] (**2.2**) which can be considered to be a structural model of haloperoxidase. Complex **2.2** has been grafted successfully through covalent bonding with imidazole appended methylpolystyrene cross-linked with 5% divinylbenzene {now abbreviated as PS–im[$V^{V}O_2$(pan)] (**2.4**)}. Oxidative bromination of styrene, salicylaldehyde and *trans*-stilbene has been successfully carried out using **2.4** as heterogeneous catalyst, demonstrating the functional similarity to haloperoxidases. Recyclable ability and better catalytic ability over non-grafted analog make it useful functional model of haloperoxidases. The peroxide species, similar to [$V^{V}O(O_2)$(pan)(MeOH] (**2.3**) isolated in the solid state, has also been demonstrated to form in solution which on reaction with acid possibly generates hydroperoxide intermediate during catalytic action. Possible mechanisms for the formation of different reaction products upon oxidative bromination of above substrates have been proposed.

Chapter 3

Polystyrene bound dioxidovanadium(V) complexes of 2-acetylpyridine derived ligands for catalytic oxidations

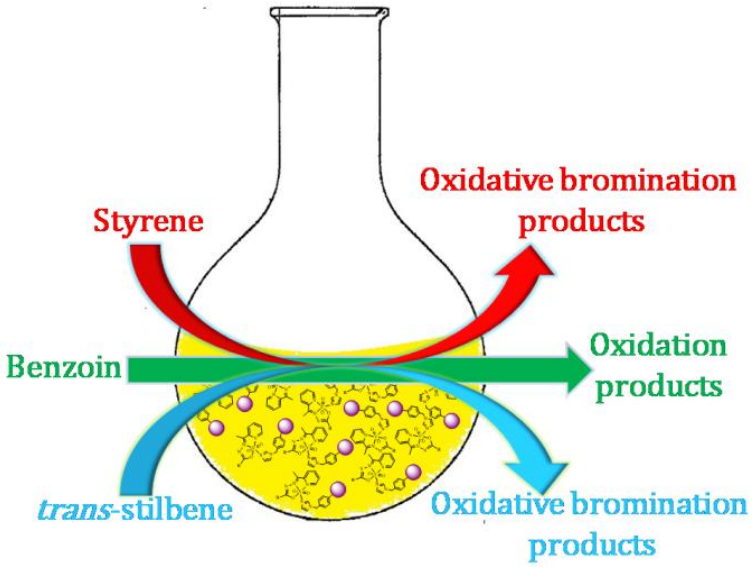

3.1. Introduction

Immobilization of homogeneous catalysts through covalent bonding with chloromethylated polystyrene cross-linked with divinylbenzene is receiving an increasing interest for developing environmental friendly greener catalytic processes which are also economically viable in industrial chemistry [54,76,80,90,91,92,130]. The development of vanadium catalytic model systems for oxidations and oxygen transfer reactions, including the oxidative halogenation of organic substrates and oxidation of organic sulfides, potentiated renewed interest in the coordination chemistry of vanadium complexes with polydentate ligands [24,25,41,81,107,131].

Dioxidovanadium(V) complexes with benzimidazole, imidazole and hydrazide derived monobasic tridentate ONN ligands have been looked at as functional models of vanadium haloperoxidases (VHPOs) [27,80,118,132]. Successful functional similarities have been demonstrated as some of these complexes mimic oxidative halogenations and sulfoxidations [27] along with the oxidation, by peroxide, of organic substrates [133].

Grafting such vanadium complexes onto polymer supports may provide extra stability to the complexes and may improve their catalytic activity and recyclable ability [53,54,91,130]. Such grafting onto polymers may also be important for the development of more environmentally benign synthetic routes to fine chemicals. For example, it has been found that polymer-supported vanadium complexes oxidize organosulfur compounds efficiently in model diesel fuels and are recyclable [80].

Two general methods have been adapted to graft vanadium complexes on polymer supports: (i) covalent bonding of a ligand to the polymer; donor atoms of this grafted ligand bind to the metal center, and (ii) the ligand bound to the metal ion possesses a functional group adequate to establish a covalent bond to the polymer. The later method has been extensively used in exploring the functional mimics and catalytic activities of polymer supported vanadium complexes [53], but only one report describes the former method for vanadium complexes [53,69]. In the present work we describe one more example of method (i); thus, in continuation of our efforts, herein we describe the synthesis of three polymer-supported dioxidovanadium(V) complexes of hydrazide derived monobasic tridentate ONN ligands via covalent bonding through imidazolomethylpolystyrene (cross-linked with 5 % divinylbenzene) (Scheme 1**)**. These complexes were applied to the oxidative bromination of styrene and *trans*-stilbene.

In addition, these catalyst precursors are shown to be active in the oxidation of benzoin, by peroxide. The oxidation of benzoin produces benzil, an alpha diketone that is an important organic intermediate; it has received an enormous attention because of its practical applications in organic and pharmaceutical industry such as for photosensitive and synthetic reagents. Benzil is extensively used as substrate in benzylic rearrangements and also acts as a starting material for the synthesis of many heterocyclic compounds [134,135] exhibiting biological activity e.g. the anticonvulsant derivative dilantin [136].

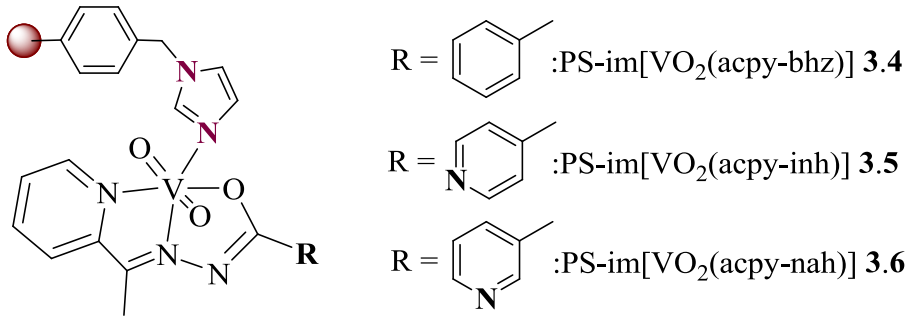

Scheme 3.1. Schematic structure of the polymer-supported complexes used in this work.

3.2. Experimental Section

3.2.1. Materials and methods

Analytical reagent grade V_2O_5, imidazole, isonicotinic acid hydrazide, hydrazine hydrate (Loba Chemie, Mumbai, India), 30 % aqueous H_2O_2, 70 % $HClO_4$ (Ranbaxy, India), KBr (Himedia, India), nicotinic acid hydrazide (Fluka Chemie, Switzerland), 2-acetylpyridine and acetylacetone (Hacac) (Aldrich, U.S.A.) were used as obtained. Benzoylhyrazide was prepared by the reaction of a twofold excess of hydrazine hydrate with ethyl benzoate. Other chemicals and solvents were of analytical reagent grades. Imidazolomethylpolystyrene (PS–im) [69,110,137], $[V^VO_2(acpy\text{-}bhz)]$ (**3.1**), $[V^VO_2(acpy\text{-}inh)]$ (**3.2**) [118] and $[\{V^VO(acpy\text{-}nah)\}_2(\mu\text{-}O)_2]$ (**3.3**) [133] were prepared according to the reported methods. Hereafter we will abbreviate dioxidovanadium(V) as (V^VO_2).

3.2.2. Instrumentation and characterization procedures

Details of instrumentation and characterization procedures are presented in Chapter 2.

3.2.3. Preparation of polymer-supported complexes

3.2.3.1. PS-im[$V^{V}O_2$(acpy-bhz)] (3.4)

The Polymer-anchored PS–im (2.0 g) was allowed to swell in DMF (20 mL) for 2 h. A solution of [$V^{V}O_2$(acpy–bhz)] (**3.1**) (2.0 g, 6.47 mmol) in 25 mL DMF was added to the above suspension and the reaction mixture was heated at *ca.* 90 ^{o}C for 20 h with very gentle mechanical stirring. After cooling to room temperature, the dark black polymer-anchored complex was separated by filtration, washed with hot DMF followed by hot methanol and dried at 120 ^{o}C in an air oven. Yield 1.70 g (85 %). Found: N, 9.26; V, 1.65 %.

3.2.3.2. PS-im[$V^{V}O_2$(acpy-inh)] (3.5) and PS-im[$V^{V}O_2$(acpy-nah)] (3.6)

Complexes **3.5** and **3.6** were prepared analogously to **3.4**, replacing **3.1** by [$V^{V}O_2$(acpy-inh)] (**3.2**) and [{V^{V}O(acpy-nah)}$_2$(μ-O)$_2$] (**3.3**), respectively.

*Data for PS-im[$V^{V}O_2$(acpy-inh)] (**3.5**):* Yield 1.66 g (83 %). Found: N, 8.13; V, 1.36 %.

*Data for PS-im[$V^{V}O_2$(acpy-nah)] (**3.6**):* Yield 1.82 g (91 %). Found: N, 10.91; V, 2.06 %.

3.2.4. X-Ray crystal structure determination

Single crystals of the monomeric form of **3.3** {now [$V^{V}O_2$(acpy-nah)]·DMSO (**3.3a**·DMSO)} were grown in DMSO by cooling the solution at *ca.* 15 ^{o}C. Three-dimensional X-ray data for **3.3a**·DMSO were collected on a Bruker SMART Apex CCD diffractometer at 100(2) K, using a graphite monochromator and Mo-K_α radiation (λ = 0.71073 Å) by the ϕ-ω scan method. Reflections were measured from a hemisphere of data collected of frames each covering 0.3 degrees in ω. Of the 18198 reflections measured, all of which were corrected for Lorentz and polarization effects, and for absorption by semi-empirical methods based on symmetry-equivalent and repeated reflections, 2245 independent reflections exceeded the significance level $|F|/\sigma(|F|) > 4.0$. Complex scattering factors were taken from the program package SHELXTL [113]. Crystal and structure refinement data are given in Table 3.1. The structures were solved

by direct methods and refined by full-matrix least-squares methods on F^2. The non-hydrogen atoms were refined with anisotropic thermal parameters in all cases. All hydrogen atoms were refined to carbon atoms, which were placed in idealized positions and refined by using a riding mode, except for C(1), C(2), C(4), C(8) and C(10) which were left to refine freely. A final difference Fourier map showed no residual density outside: 0.969 and -0.410 for **3.3a**·DMSO e.$Å^{-3}$.

Table 3.1. Crystal data and structure refinement for **3.3a**·DMSO.

Formula	$C_{15}H_{17}N_4O_4SV$
Formula weight	400.33
Temperature, K	100(2)
Wavelength, Å	0.71073
Crystal system	Monoclinic
Space group	$P2_1/n$
a/Å	9.5772(8)
b/Å	14.3085(13)
c/Å	12.2414(10)
β/º	90.607(5)
V/$Å^3$	1677.4(2)
Z	4
D_{calcd}/g cm^{-3}	1.585
Absorption coefficient/mm^{-1}	0.745
F_{000}	824
Crystal size/mm^3	0.22 x 0.20 x 0.19
θ range for data colletion ($\theta_{Min}/\theta_{Max}$)/ (º)	2.19 - 24.71
Index ranges	-11<=h<=11
	-16<=k<=15
	-14<=l<=13
Reflections collected	18198
Independent reflections	2859
R_{int}	0.0698

Completeness %/(θ)	99.8 /(24.71º)
Refinement method	Full-matrix least-squares on F^2
Restraints/parameters	2859 / 0 / 256
Goodness-of-fit on F^2	1.047
R_1 [a]	0.0407
wR_2 (all data) [b]	0.1323
Largest differences peak and hole (eÅ^{-3})	0.969 and -0.410

[a] $R_1 = \Sigma \left| \left| F_o \right| - \left| F_c \right| \right| / \Sigma \left| F_o \right|$. [b] $wR_2 = \{\Sigma[w(\left| \left| F_o \right|^2 - \left| F_c \right|^2 \right|)^2] / \Sigma[w(F_o^4)]\}^{1/2}$

3.2.5. Catalytic studies

The polymer-anchored complexes PS-im[$V^{V}O_2$(acpy-bhz)] (**3.4**), PS-im[$V^{V}O_2$(acpy-inh] (**3.5**), PS-im[$V^{V}O_2$(acpy-nah)] (**3.6**) were used as catalyst precursors to carry out the oxidative bromination of styrene and *trans*–stilbene, as well as of oxidation of benzoin. Each catalyst was allowed to swell in suitable solvent (mentioned below) prior to its use.

3.2.5.1. Oxidative bromination of styrene

Warning: $HClO_4$ is potential oxidant, hence it must be handled carefully. Complexes **3.4**, **3.5** and **3.6** were used as catalyst precursors to carry out the oxidative bromination of styrene. In a typical reaction, styrene (1.04 g, 10 mmol) was added to an aqueous solution (20 mL) of KBr (3.57 g, 30 mmol) in a 100 mL reaction flask, and then 20 mL CH_2Cl_2 and 30 % aqueous H_2O_2 (3.40 g, 30 mmol) were added. After adding 70 % $HClO_4$ (1.43 g, 10 mmol) and catalyst precursors (0.0010 g), the reaction mixture was stirred at room temperature. Three additional 10 mmol portions of 70 % $HClO_4$ were further added after every 15 minutes with continuous stirring. The experimental conditions (e.g. stirring speed, size of magnetic bar and reaction flask) in all batches were kept as similar as possible. After 1 h the orange colored organic layer was separated using a separatory funnel, washed with water and dried. The crude mass was re-dissolved in CH_2Cl_2 and insoluble material, if any, was removed by filtration. The solvent was evaporated and the reaction products were separated using a silica gel column. Elution of the column with 1 % CH_2Cl_2 in n-hexane first separated a mixture of

bromo derivatives, followed by 1-phenylethane-1,2-diol. The two bromo derivatives were finally separated from each other using another silica gel column and eluted with pure n-hexane. The products were identified by GC–MS and ^{1}H NMR spectra.

^{1}H NMR spectral data of reaction products are as follows:

1,2-Dibromo-1-phenylethane: ^{1}H NMR ($CDCl_3$): δ = 7.29–7.39 (m, 5 H, aromatic), 5.11–5.13 (q, 1 H, CH), 3.97–4.06 (septet, 2 H, CH_2) ppm.

1-Phenylethane-1,2-diol: ^{1}H NMR ($CDCl_3$): δ = 7.29–7.39 (m, 5 H, aromatic), 4.9 (q, 1 H, CH), 3.5 (q, 1 H, CH_2), 3.6 (q, 1 H, CH_2), 2.7 (br, 1 H, OH) ppm.

2-Bromo-1-phenylethane-1-ol: ^{1}H NMR ($CDCl_3$): δ = 7.29–7.39 (m, 5 H, aromatic), 5.1 (q, 1 H, CH), 3.9 (septate, 2 H, CH_2) ppm.

These data match well with those reported earlier [96,109].

3.2.5.2. Oxidative bromination of *trans*–stilbene

Similar procedures as outlined for styrene were applied for the oxidative bromination of *trans*–stilbene: *trans*–stilbene (0.90 g, 5 mmol), catalyst precursor (0.015 g), KBr (2.38 g, 20 mmol), 30 % aqueous H_2O_2 (2.27 g, 20 mmol) and 70 % $HClO_4$ (2.86 g, 20 mmol, added in four equal portions at time intervals (t = 0, 30, 60 and 90 min. of reaction time) were taken in $CHCl_3/H_2O$ (40 mL, v/v). After 2 h of stirring at room temperature the orange colored organic layer was separated using a separatory funnel, washed with water and dried. The crude mass was redissolved in CH_2Cl_2; insoluble *trans*–stilbene oxide was separated by filtration and then the solvent was evaporated. Other reaction products were separated using a silica gel column. Elution of the column with 1 % CH_2Cl_2 in n-hexane first separated a mixture of mono derivative followed by the dibromo derivative. The products were identified by GC–MS and ^{1}H NMR spectra.

^{1}H NMR spectral data of reaction products are as follows:

2,3-Diphenyloxirane: ^{1}H NMR ($CDCl_3$): δ = 7.35–7.55 (m, 10 H, aromatic); 5.5 (d, 2H, CH).

2-Bromo-1,2-diphenylethanol: ^{1}H NMR ($CDCl_3$): δ = 8.0 (s, 1 H, OH); 7.37–7.52 (m, 10 H, aromatic); 5.5 (d, 2H, CH).

1,2-Dibromo-1,2-diphenylethane: ^{1}H NMR ($CDCl_3$): δ = 7.1–7.4 (m, 10 H, aromatic); 6.15 (d, 2H, CH).

3.2.5.3. Oxidation of benzoin

Benzoin (1.06 g, 5 mmol), 30 % aqueous H_2O_2 (1.71 g, 15 mmol), and catalyst precursor (0.030 g) in 10 mL methanol were stirred at reflux temperature. The progress of the reaction was monitored by withdrawing samples at different time intervals and analyzing them quantitatively by gas chromatography. The identities of the products were confirmed by GC-MS. The effect of various parameters such as temperature, amount of oxidant and catalyst were checked to optimize the conditions for the best performance of the catalyst.

The products mainly obtained are benzil, methylbenzoate, benzoic acid and benzaldehyde-dimethylacetal.

3.3. Results and discussion

3.3.1. Synthesis, reactivity and solid state characteristics

Complexes $[VO_2(acpy\text{-}bhz)]$ (**3.1**) and $[VO_2(acpy\text{-}inh)]$ (**3.2**) were reported to be mononuclear while $[\{V^VO(acpy\text{-}nah)\}_2(\mu\text{-}O)_2]$ (**3.3**) to be dinuclear [133]. We obtained the monomeric form of **3.3** {$[VO_2(acpy\text{-}nah)]\cdot$DMSO (**3.3a**·DMSO)}, from dimethylsulfoxide, as yellow prisms suitable for single crystal x-ray diffraction analysis. Figure 3.1 shows an ORTEP representation of **3.3a**·DMSO and Table 3.2 presents selected bond lengths and angles. The complex presents an intermediate structure between the idealized square-pyramidal and trigonal-bipyramidal extremes. In fact, the geometry around the vanadium atom can be described as a distorted square-pyramidal (τ = 0.357) [138], the monobasic tridentate acpy-nah$^-$ ligand binding V^V through the pyridine-N, imine-N and the amide-O and two oxido-O ligands. The V=O distances are in the range reported for other *cis*-dioxidovanadium(V) centers (see Table 3.2). The distances of the deprotonated O-atom and the N-atom of the hydrazone group to the metal ion are consistent with the values reported for other similar complexes [80,118]. It was reported that this type of VO_2-complexes can be stabilized either in the form of monomeric or dinuclear species [139]. Monomeric species can be converted to dinuclear

ones upon heating in an appropriate solvent for a relatively long time. In this work the monomeric form of **3.3** is the relevant one.

The two external pyridine (py) rings are at an angle of 6.40(18)º with respect to each other, which is a signal of the planarity of the ligand. π-π stacking interactions are established between the external py groups [C(1), C(2), C(3), C(4), C(5) and N(1) to C(9), C(10), C(11), C(12), C(13) and N(4)] of the acpy-nah ligand of an inversion-related molecule in the crystal packing (mean separation between the py rings ca 3.617 Å). The non coordinated py groups are also involved in π-π stacking between them, with a mean separation ca 3.783 Å, see Figure 3.2.

Table 3.2. Bond lengths [Å] and angles [°] for **[**$V^{V}O_2$(acpy-nah)]·DMSO (**3.3a**·DMSO).

Bond lengths (Å)			
V(1)-O(1)	1.617(2)	V(1)-N(3)	2.099(3)
V(1)-O(2)	1.619(2)	N(2)-N(3)	1.387(4)
V(1)-O(3)	1.953(2)	N(3)-C(7)	1.293(4)
V(1)-N(4)	2.097(3)	N(2)-C(6)	1.312(4)
Bond Angles (º)			
O(1)-V(1)-O(2)	110.42(13)	O(1)-V(1)-N(4)	95.65(12)
O(1)-V(1)-O(3)	101.69(11)	O(2)-V(1)-N(4)	97.00(11)
O(2)-V(1)-O(3)	102.75(11)	O(3)-V(1)-N(4)	147.06(10)
O(1)-V(1)-N(3)	125.63(12)	O(3)-V(1)-N(3)	73.97(10)
O(2)-V(1)-N(3)	123.55(11)	N(4)-V(1)-N(3)	73.15(10)

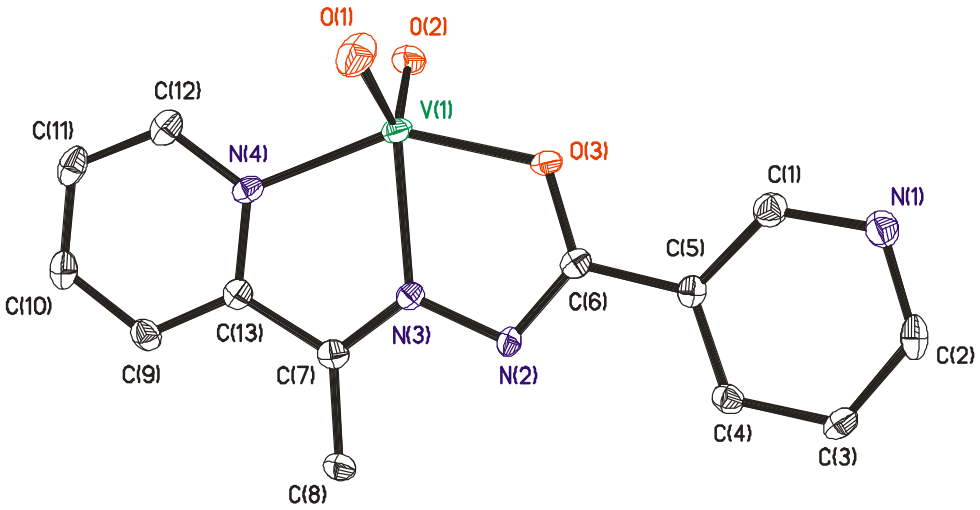

Figure 3.1. ORTEP plot of **3.3a**·DMSO. All the non-hydrogen atoms are presented by their 50% probability ellipsoids; hydrogen atoms are omitted for clarity.

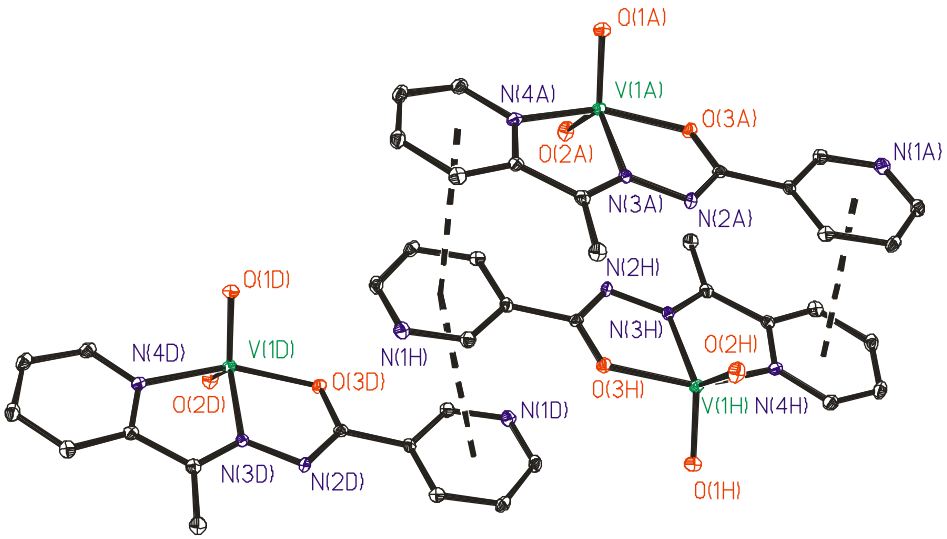

Figure 3.2. Part of the crystal packing of the **3.3a**·DMSO. π-π stacking interactions between pyridine groups are observed in the structure. Symmetry operations are: x, y, z; 1/2-x, 1/2+y, 1/2-z; -x, -y, -z; 1/2+x, 1/2-y, 1/2+z.

The reaction of imidazole with chloromethylated polystyrene, cross-linked with 5 % divinylbenzene in acetonitrole in the presence of KI and triethylamine, gave the imidazolomethylpolystyrene, PS–im [69,110,137]. The remaining chlorine content of

1.5 % (0.42 mmol Cl per gram of resin) in the PS–im suggests ~92 % loading of the imidazole. The PS-im on reaction with complexes **3.1**, **3.2** and **3.3** in DMF resulted in the formation of imidazolomethylpolystyrene-grafted $V^{V}O_2$-complexes: PS-im[$V^{V}O_2$(acpy-bhz)] (**3.4**), PS-im[$V^{V}O_2$(acpy-inh] (**3.5**) and PS-im[$V^{V}O_2$(acpy-nah)] (**3.6**). The free chloromethyl groups of PS do not coordinate with the vanadium precursor. Scheme 3.2 presents the global synthetic procedure and Table 3.3 presents the vanadium loading in supported complexes.

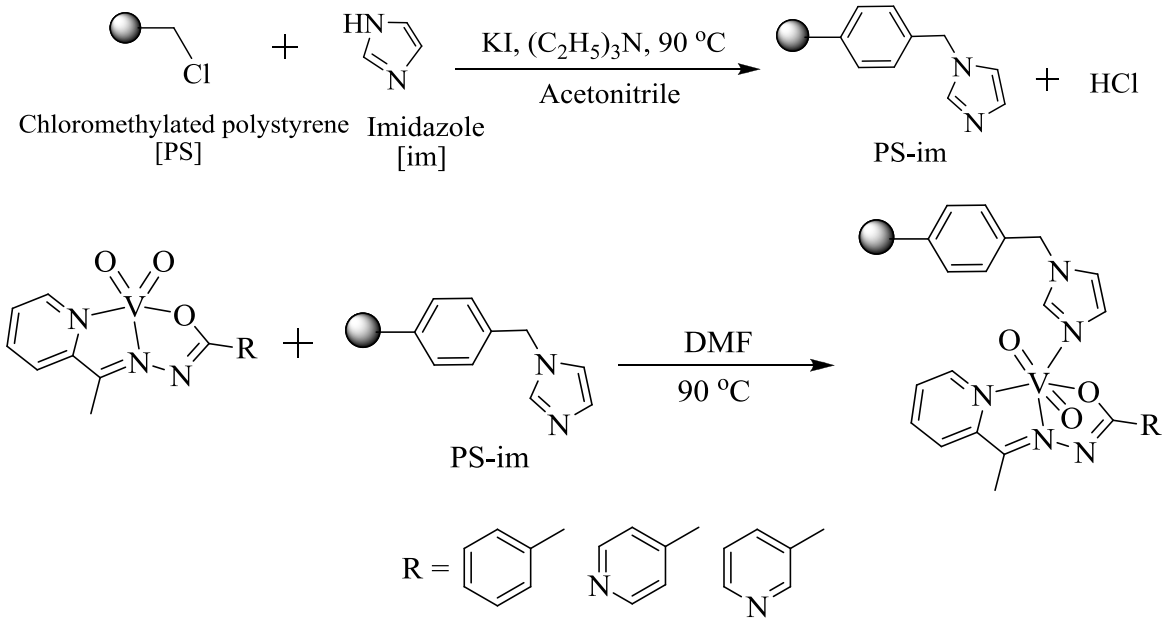

Scheme 3.2. Global synthetic procedure for the preparation of polymer bound vanadium complexes.

Table 3.3. Data of metal and loading in polymer-anchored complexes

Complexes	Metal ion loading[a] (mmol g^{-1} of resin) (obtained by ICP)	Metal ion loading[a] (mmol g^{-1} of resin) (obtained by TGA)
PS-im[VO_2(acpy-bhz)] (**3.4**)	0.324	0.30
PS-im[VO_2(acpy-inh)] (**3.5**)	0.265	0.24
PS-im[VO_2(acpy-nah)] (**3.6**)	0.403	0.38

[a]Metal ion loading = $\frac{\text{Observed metal \%} \times 10}{\text{Atomic mass of metal}}$

3.3.2. Thermogravimetric Analysis (TGA) studies

The polymer-bound complexes PS-im[$V^{V}O_2$(acpy-bhz)] (**3.4**), PS-im[$V^{V}O_2$(acpy-inh] (**3.5**) and PS-im[$V^{V}O_2$(acpy-nah)] (**3.6**) are thermally stable up to *ca.* 200 ^{o}C. Thereafter, their thermal decomposition occurs in two exothermic but overlapping steps and is completed at *ca.* 550 ^{o}C. Only very small loss in weight occurs between 550–900 ^{o}C, with the formation of V_2O_5. The vanadium content calculated from the final residues are indicated in Table 3.3, being in agreement with those obtained by ICP-MS. As reported earlier, neat complexes **3.1** and **3.2** depict continuous degradation to V_2O_5 in the 250–700 ^{o}C temperature range [118].

3.3.3. Field emission-scanning electron microscope (FE-SEM) and energy dispersive X-ray analysis (EDAX) studies

Field emission-scanning electron micrographs (FE-SEM) for single beads of pure chloromethylated polystyrene and polymer-grafted complex were recorded to observe the morphological changes, if any. Images of polymer-anchored complexes are reproduced in Figure 3.3. Though the surface of the beads is partially damaged due to interaction of beads during anchoring, the grafting of vanadium complexes only resulted in the roughening of the top layer of polymer-anchored beads. It is not possible to obtain accurate information on the morphological changes in terms of the exact orientation of the covalently bonded metal complexes due to their poor loading. However, the estimated vanadium content of *ca.* 0.38 mmol g^{-1} of resin in PS-im[$V^{V}O_2$(acpy-bhz)], 0.25 mmol g^{-1} in PS-im[$V^{V}O_2$(acpy-inh)] and 0.39 mmol g^{-1} of PS-im[$V^{V}O_2$(acpy-nah)] obtained by EDAX (see Figure 3.4), which are close to the contents obtained through ICP-MS and TGA, suggest that the catalyst sites are uniformly distributed over the polymer upon immobilization.

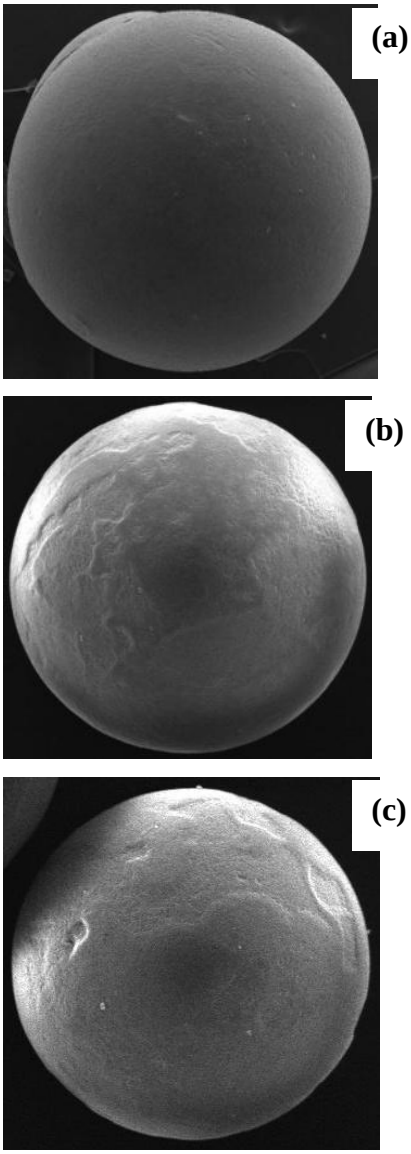

Figure 3.3. FE-SEM profiles of (a) PS-im[$V^{V}O_2$(acpy-bhz)] (**3.4**), (b) PS-im[$V^{V}O_2$(acpy-inh)] (**3.5**) and (c) PS-im[$V^{V}O_2$(acpy-nah)] (**3.6**).

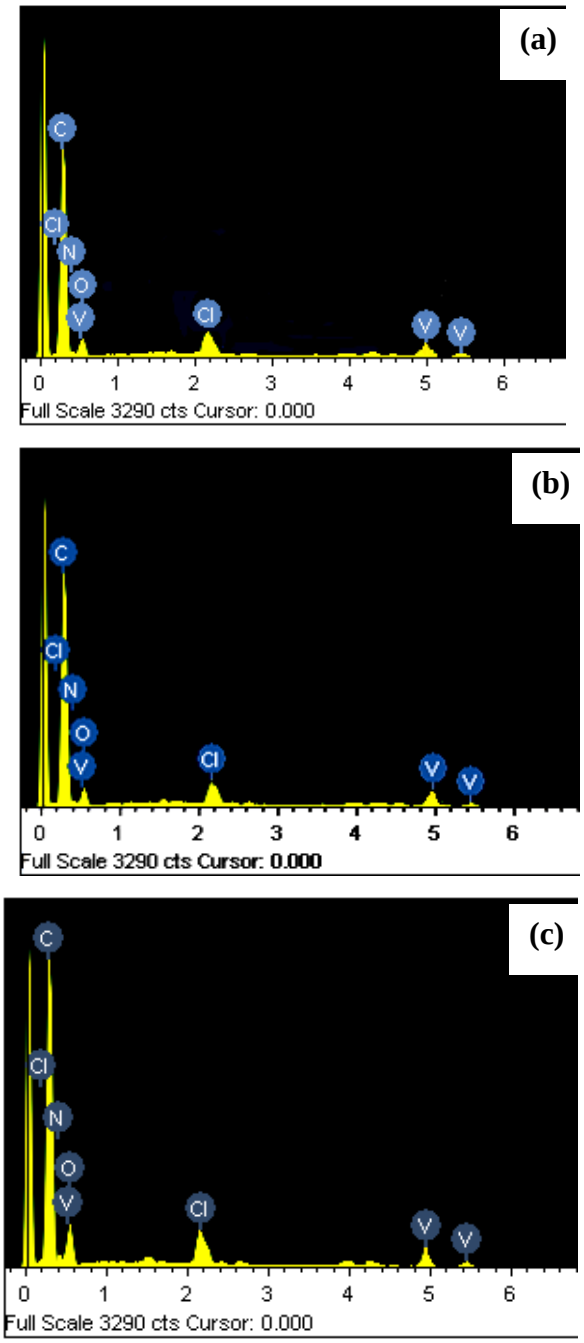

Figure 3.4. Energy-dispersive X-ray analysis (EDAX) profiles of (a) PS-im[$V^{V}O_2$(acpy-bhz)] (**3.4**), (b) PS-im[$V^{V}O_2$(acpy-inh)] (**3.5**) and (c) PS-im[$V^{V}O_2$(acpy-nah)] (**3.6**).

3.3.4. IR spectral studies

The important IR bands for the neat and polymer-bound ligands and their vanadium complexes are given in Table 3.4. The 1500-1650 cm^{-1} range appears quite complex in the IR of all compounds and assignments were made by comparison with previously reported results obtained from the DFT calculations recently carried out with similar types of ligands and binding sets around the vanadium center [109] (see Table

3.4). The ν(C=N) (azomethine) for the complexes are indicated in Table 3.4, the vibrations being also coupled to the aromatic ring, as was the case of [$V^{IV}O$(sal-ama)] complexes (sal-ama = N-salicylideneamino acidato) [140].

The $V^{V}O_2$-complexes exhibit bands due to ν_{sym}(O=V=O) and ν_{asym}(O=V=O) as assigned in Table 3.4; however, we note that recent DFT calculations for complex K[$V^{V}O_2${Hdfmp(nah)$_2$}] {Hdfmp(nah)$_2$ = Schiff base obtained by the condensation of 2,6-diformyl-4-methylphenol and nicotinoylhydrazide} showed that these two vibrations are isolated (each band corresponds to stretching of one V=O bond) [109].

Polymer supported complexes exhibit two well separated bands in the 915 – 940 cm^{-1} region characteristic of *cis*-[$V^{V}O_2$] species. These bands are similar to those reported for the mononuclear neat complexes **3.1** and **3.2**. The dinuclear form of **3.3** displays only one band at 958 cm^{-1} while its mononuclear analogue **3.3a** exhibits two sharp bands, as observed for other neat $V^{V}O_2$-complexes [53]. In polymer-supported complexes, other characteristic bands due to coordination of ligands are similar to those reported for the corresponding non-polymer-supported complexes.

Table 3.4. IR spectra of compounds (ν in cm^{-1}). The DFT calculated vibrational frequencies for K[$V^{V}O_2${Hdfmp(nah)$_2$}], scaled by a factor of 0.9, are given in parentheses [109].

Complexes	ν(C=C_{ring})	ν(C=$N_{azomethine}$)	ν(V=O) / [V-(μ-O)-V]
[$V^{V}O_2$(acpy-bhz)] (**3.1**)	1598	1565	946, 909
[$V^{V}O_2$(acpy-inh)] (**3.2**)	1598,	1565	946, 899
[{$V^{V}O$(acpy-nah)}$_2$(μ-O)$_2$] (**3.3**)	1600	1582	958, 778
[VO_2(acpy-nah)]·DMSO (**3.3a**)	1595,	1572	945, 898
PS-im[$V^{V}O_2$(acpy-bhz)] (**3.4**)	1600	1559	915, 926
PS-im[$V^{V}O_2$(acpy-inh)] (**3.5**)	1597	1570	920, 939
PS-im[$V^{V}O_2$(acpy-nah)] (**3.6**)	1605	1572	919, 926
K[$V^{V}O_2${Hdfmp(nah)$_2$}]		1556 (1529, 1523) [109]	934, 900 (954, 944) [109]

3.3.5. Electronic spectral studies

Electronic spectral data of neat complexes have been discussed in the literature [141,142]. The polymer anchored complexes show similar spectral patters, Figure 3.5 and Table 3.5. The electronic spectral studies of polymer anchored complexes have been described earlier [54,76,80,90,91,92,130]. A band appearing at 394 nm in PS-im[$V^{V}O_2$(acpy-bhz)] is assigned to a ligand-to-metal charge transfer (lmct) transition, but may also contain bands localized in the C═N group. Thus, a medium intensity band at *ca.* 400 nm is assigned to n-π (imine) and to LMCT bands. Other bands appearing in the UV region correspond to intra-ligand bands.

Table 3.5. Electronic spectral data of polymer-anchored complexes.

Complexes	Solvent	λ_{max} / nm
PS-im[$V^{V}O_2$(acpy-bhz)] (**3.4**)	Nujol	394, 277, 240
PS-im[$V^{V}O_2$(acpy-inh)] (**3.5**)	Nujol	404, 295, 253
PS-im[$V^{V}O_2$(acpy-nah)] (**3.6**)	Nujol	415, 318, 260

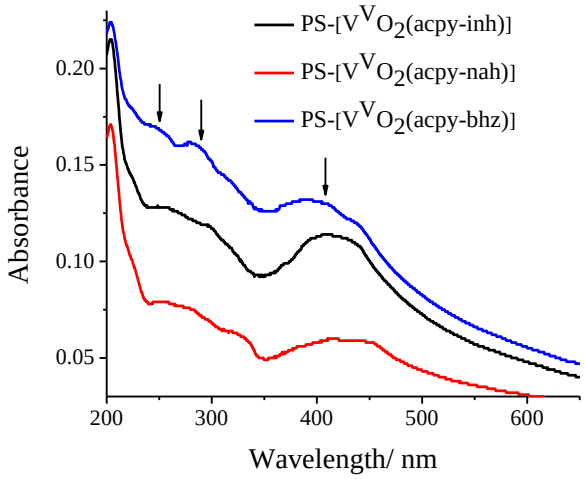

Figure 3.5. Electronic spectra recorded for the polymer-anchored complexes dispersed in Nujol.

3.3.6. ^{51}V NMR studies

Further characterization of the V^V-complexes was obtained from ^{51}V NMR spectra recorded in DMSO-d_6. The δ_V (^{51}V) values measured may be used to establish their behavior upon modifications of the composition of the solutions. In the present study we reinvestigated complexes **3.1**, **3.2** and **3.3** in solution, trying to establish speciation in conditions simulating those existing during the catalytic experiments (see Scheme 3.3 and Table 3.6). All three complexes show strong resonances at *ca.* δ_V = −500 to −505 ppm. Compound, [V^VO_2(acpy-nah)] (**3.3a)** was chosen as representative for the studies. The ^{51}V NMR spectrum of **3.3a** (*ca.* 4 mM) dissolved in DMSO-d_6 shows a strong resonance δ_V = −505 ppm [Figure 3.6 (a)]. The assignment of this and other resonances was done by considering both the experiments and comparison with DFT calculations described in previously reported studies [25,90,96,109]. Thus, the resonances at δ_V = –505 ppm may be tentatively assigned to species such as **CI** in Scheme 3.3; in fact, the observed chemical shifts are within the values expected for V^VO_2-complexes containing O/N donor sets [122,143,144]. Upon addition of methanol (50% v/v) to a 4 mM solution of **3.3a** in DMSO-d_6 a new resonance at δ_V = –538 ppm shows up; we tentatively assign this resonance to species **CII**: [V^VO_2(acpy-nah)(S)], (S = solvent) [Figure 3.6, (b)]. Similar species were also reported, e.g. [V^VO_2(sal-dmenH^+)(MeOH)] at δ_V = –543 ppm [80].

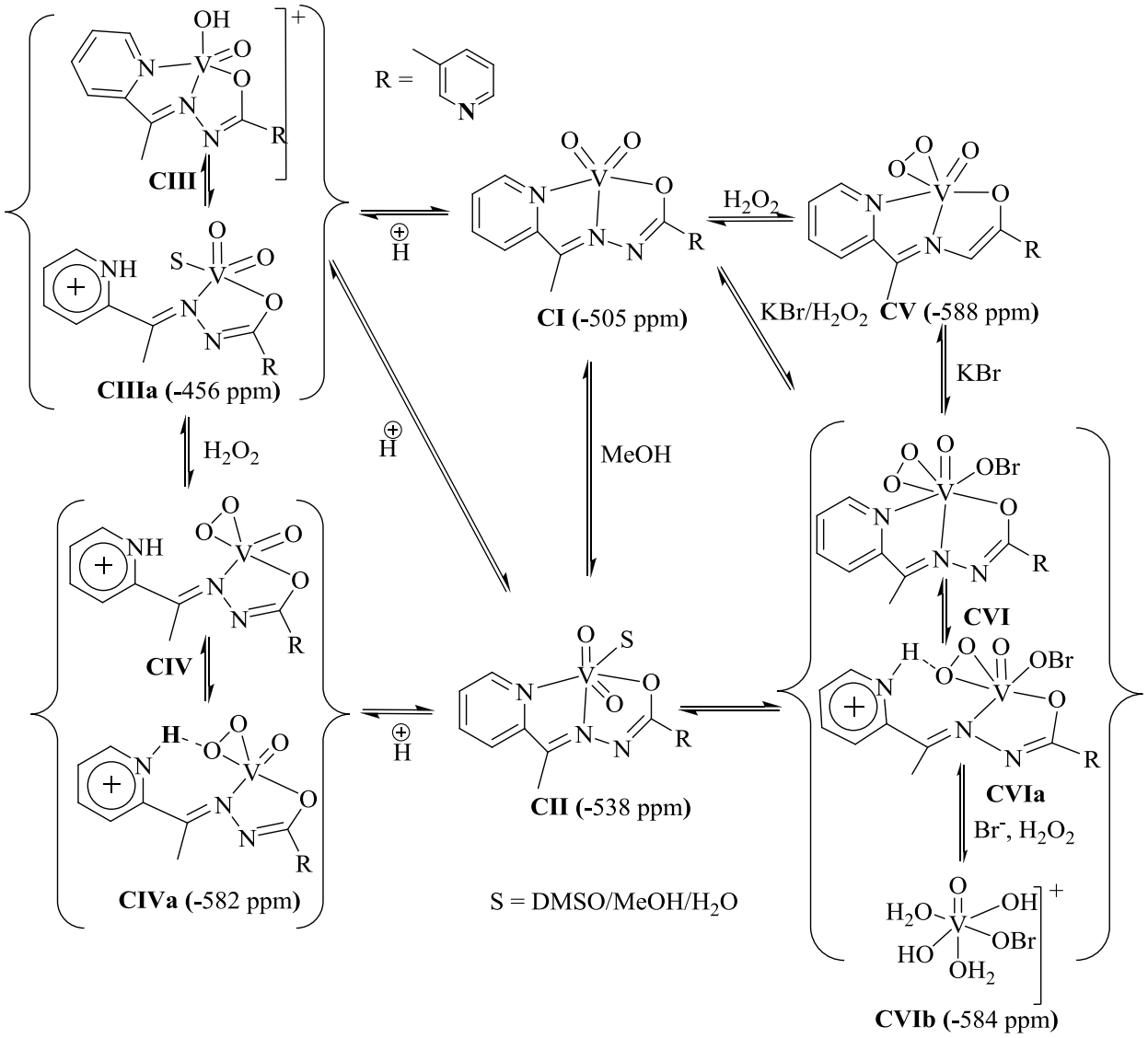

Scheme 3.3. Summary of speciation of V^V-containing species in solutions of complex **3.3a**. The δ values of $[V^VO_2(acpy\text{-}nah)]$ in DMSO-d_6 were (tentatively) established through the present ^{51}V NMR experiments and by comparison with previous experimental and theoretical studies [76,80,96,109].

Upon additions of 0.5 and 1.0 (total) equivalents of a HCl solution a new peak at δ_V = –456 ppm is detected [Figure 3.6, (c)]. We tentatively assign this resonance to species **CIII**, an oxidohydroxido-V^V complex. Another possible assignment is **CIIIa**, as both species correspond to the same degree of protonation, and both types of complexes have been previously considered plausible [76,80,109,142] in the case of rather similar complexes. Upon further addition of 2 equiv. of 30 % H_2O_2 to this solution a resonance

at δ_V = –582 ppm is detected and could correspond to the oxido–peroxido [$V^VO(O_2)$(acpy-nahH^+)] species **CIV** or **CIVa,** Scheme 3.3) [Figure 3.6, (d)]. Similar types of $V^VO(O_2)$-complexes were also considered plausible in previous studies [76,80,109,142]. However, the δ_V = –582 ppm resonance may also correspond to the tetravanadate (V4) [145].

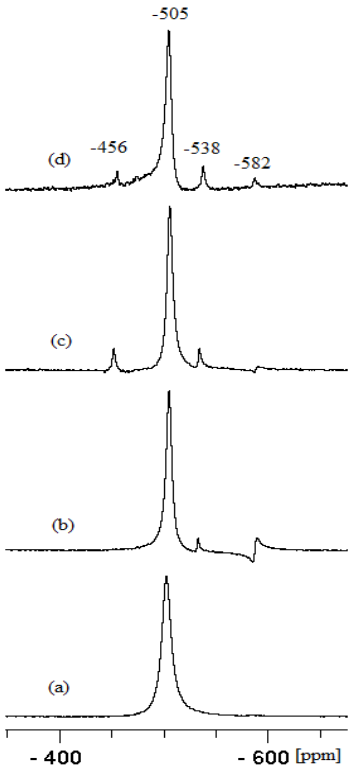

Figure 3.6. ^{51}V NMR spectra of solutions of compound **3.3a** (*ca.* 4 mM) in DMSO-d_6. (a) solution of **3.3a** (b) solution of (a) after addition of methanol (50 % v/v); (c) solution of (b) after addition of 1.0 equiv. of HCl solution; (d) solution of (c) upon adding 2.0 equiv. of H_2O_2 (solution of 30 % H_2O_2)

Upon addition of 30 % H_2O_2 (3 equiv.) to a 4 mM solution of **3.3a** in DMSO-d_6 a resonance at δ_V = –588 ppm shows up [Figure 3.7, (d)] which we tentatively assign as [$V^VO(O_2)$(acpy-nah)] (**CV,** Scheme 3.3); in fact this matches with the chemical shift of the authentic oxido–peroxido complexes of **3.3** previously reported [133]. Further additions of 3.0 equiv. KBr and 2.0 equiv. 30% H_2O_2 generates resonances at δ_V = –584 ppm and δ_V = –601 ppm [Figure 3.7, (c)]. The resonance at δ_V = –584 ppm is tentatively assigned to a species containing coordinated OBr^- (vanadium bound hypobromite ion) reported as probably responsible for the formation of bromohydrin (see structures **CVI**, **CVIa** or **CVIb** Scheme 3.3) [32,96,123].

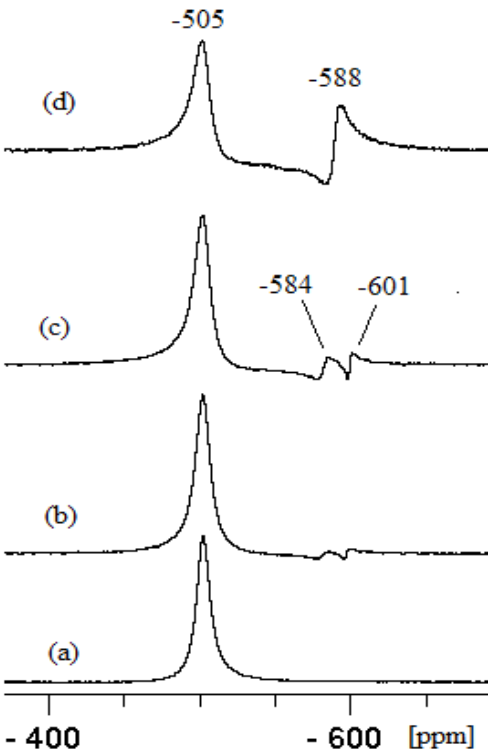

Figure 3.7. ^{51}V NMR spectra of solutions of compound **3.3a** (*ca.* 4 mM) in DMSO-d_6 (a) solution of **3.3a**; (b) solution of (a) after addition of 3.0 equiv. KBr and 2.0 equiv. H_2O_2 (solution of 30 % H_2O_2); (c) solution of (b) after *ca.* 15 min. (d) solution of (a) after addition of 3.0 equiv. of H_2O_2 (solution of 30 % H_2O_2).

The other two complexes, [V^VO_2(acpy-bhz)] (**3.1**) and [V^VO_2(acpy-inh)] (**3.2**) were also studied under similar conditions and these experiments confirmed that V^V species are quite stable to moderate additions of acid and/or H_2O_2 solutions, and also show similar patterns for intermediate species formation as complex **3.3a**. The experimental ^{51}V chemical shifts and assignments are summarized in Table 3.6.

Suspensions of PS-[V^VO_2(acpy-bhz)] (**3.4**), PS-[V^VO_2(acpy-inh)] (**3.5**) and PS-[V^VO_2(acpy-nah)] (**3.6**) were kept under the conditions used for the brominations of styrene and *trans*–stilbene, and then the polymer-anchored complexes were separated by filtration. ^{51}V NMR spectra were recorded for the solutions left after removing the catalyst. These solutions do not show any ^{51}V NMR resonances, suggesting that there is no leaching. We repeated this experiment up to 3 times at room temperature detecting no leaching by this procedure. However, under refluxing conditions these catalytic precursors partially leached into solvent and the solution show ^{51}V NMR resonances corresponding to neat complexes.

Table 3.6. Summary of the experimental ^{51}V NMR data (ppm) and tentative assignments of the vanadium complexes studied in this work (see Scheme 3.3)

Complexes	**CI**	**CII**	**CIII**	**CIV**	**CV**	**CVI**
3.1	–504	–532	–451	–583	–591	–584
3.2	–500	–538	–456	–578	–591	–586
3.3a	–505	–538	–456	–582	–588	–584

3.3.7. Catalytic activity studies

3.3.7.1. Oxidative bromination of styrene

Before use in catalytic reactions the polymer beads were swelled in CH_2Cl_2 for 4 h. For the oxidative bromination of styrene a two phase solvent system H_2O-CH_2Cl_2 was used, taking the polymer supported complexes as catalyst precursors in the presence of KBr, aqueous H_2O_2 and $HClO_4$. Three main products were obtained: 1,2-dibromo-1-phenylethane, 2-bromo-1-phenylethane-1-ol and 1-phenylethane-1,2-diol; Scheme 3.4.

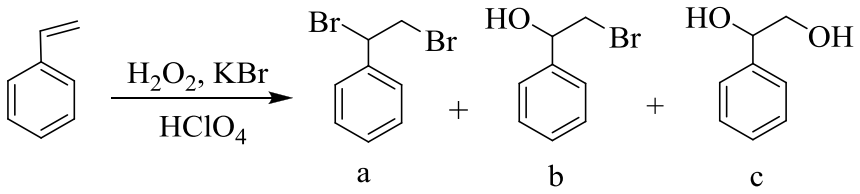

Scheme 3.4. Main products of catalytic oxidative bromination of styrene: (a) 1,2-dibromo-1-phenylethane, (b) 2-bromo-1-phenylethane-1-ol and (c) 1-phenylethane-1,2-diol

The obtained major products are the same as those reported by Conte *et al.* [32,123] and others [76,92,96]. Formation of some minor products such as benzaldehyde, styrene epoxide, benzoic acid and 4-bromostyrene was also observed; these are among the usual oxidation products of styrene, but their overall formation corresponds to ~5 % of the total conversion of styrene. Addition of $HClO_4$ in four equal portions was required to obtain better yields in the oxidative bromination.

Amongst these catalyst precursors preliminary experiments showed the good catalytic activity of PS-im[V^VO_2(acpy-bhz)] (**3.4**). Therefore it was taken as a representative catalyst precursor and parameters such as the amounts of catalyst,

oxidant, KBr and $HClO_4$ were studied to optimize the reaction conditions for: i) the maximum conversion of styrene irrespective of the selectivity of products and ii) the maximum oxidative bromination of styrene. Taking the mixture of styrene (1.04 g, 10 mmol), KBr (3.57 g, 30 mmol) and 70 % $HClO_4$ (5.72 g, 40 mmol) in 40 mL dichloromethane-water (1:1 v/v), five different amounts of catalyst viz. 0.010, 0.015, 0.020, 0.025 and 0.030 g were taken and the reaction was carried out at room temperature. Three additional 10 mmol portions of 70 % $HClO_4$ were further added to the reaction mixture after every 15 min. intervals. This was necessary to avoid leaching of complex from the polymer support. As shown in Figure 3.8, 0.010 g of catalyst gave 84 % conversion with 6 % of monobromo, 2 % dibromo and 82 % diol derivatives. Increasing the amount to 0.015 improved this conversion to 99 % with 2 % of monobromo, 6 % dibromo and 84 % diol derivatives. Further increasing of the catalyst did not improve the final overall conversion of the substrate; however, some impact on the selectivity of the different products was observed (entries no. 1 to 5 of Table 3.7). Therefore, an amount of 0.015 g of catalyst was selected to optimize other conditions.

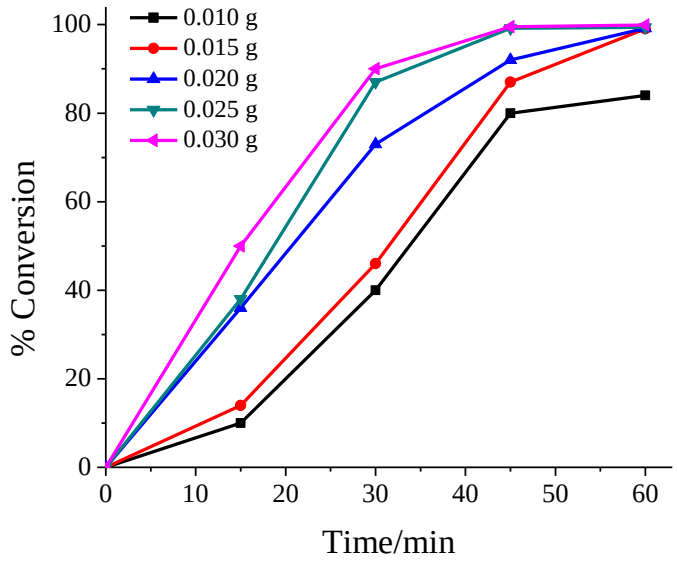

Figure 3.8. Effect of the amount of catalyst PS-im[VO_2(acpy-bhz)] on oxidative bromination of styrene. Reaction conditions: Styrene (1.04 g, 10 mmol), CH_2Cl_2/H_2O (40 mL, 50 % v/v), 30 % aqueous H_2O_2 (3.39 g, 30 mmol), KBr (3.57 g, 30 mmol), $HClO_4$ (5.72 g, 40 mmol, added in four equal portions at t = 0, 15, 30 and 45 min. of reaction time) at room temperature for 1 h.

The effect of amount of oxidant (30 % aqueous H_2O_2) on the oxidative bromination of styrene is illustrated in Figure 3.9. Under the reaction conditions of styrene (1.04 g, 10 mmol), CH_2Cl_2-H_2O (40 mL, 50 % v/v), KBr (3.57 g, 30 mmol) and $HClO_4$ (5.72 g, 40 mmol, added as mentioned above), a substrate to oxidant ratio of 1:1 gave 79 % conversion with 48 % selectivity of mono-bromo, 0 % of dibromo and 51 % of diol derivatives. Increasing this ratio to 1:2 improved the conversion to 99 % but no improvement in the conversion was noted on further increasing this ratio (entries no. 1, 6 to 9 of Table 3.7). Therefore, a substrate to H_2O_2 ratio of 1:2 was considered suitable to optimize other conditions.

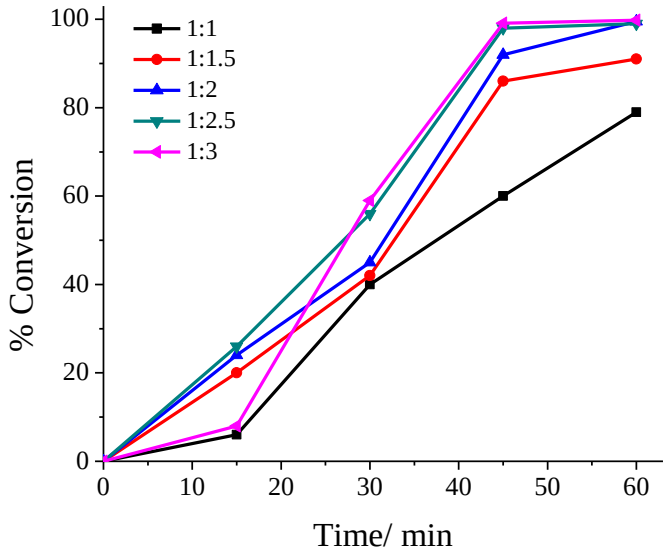

Figure 3.9. Effect of the amount of oxidant (i.e. 30 % H_2O_2) on oxidative bromination of styrene. Reaction conditions: Catalyst (0.015 g), styrene (1.04 g, 10 mmol), CH_2Cl_2/H_2O 40 mL, 50 % v/v), KBr (3.57 g, 30 mmol), $HClO_4$ (5.72 g, 40 mmol).

Similarly, five different amounts (viz. 20 mmol, 25 mmol, 30 mmol, 35 mmol and 40 mmol) of KBr were used while other reaction parameters such as catalyst (0.015 g), styrene (1.04 g, 10 mmol), 30 % H_2O_2 (2.27 g, 20 mmol) and $HClO_4$ (5.72g, 40 mmol, added in four equal portions at t = 0, 15, 30 and 45 min. of reaction time) in 40 mL dichloromethane-water (1:1 v/v) mixture and the reaction was monitored at room temperature for 1 h. As shown in Figure 3.10, increasing the KBr amount from 20 mmol to 25 mmol increased the conversion from 74 % to 89 % while 30 mmol KBr gave 99 % conversion. But further increment of KBr does not make much difference in the

conversion or the selectivity of the products (Entries no. 8 and 10 to 13 of Table 3.7). A 35 % selectivity of mono-bromo derivative and 63 % selectivity of diol derivative was obtained with 20 mmol of KBr, while 30 mmol KBr gave three main products with the following order of selectivity: diol 79 % > monobromo (11 %) > dibromo (5 %).

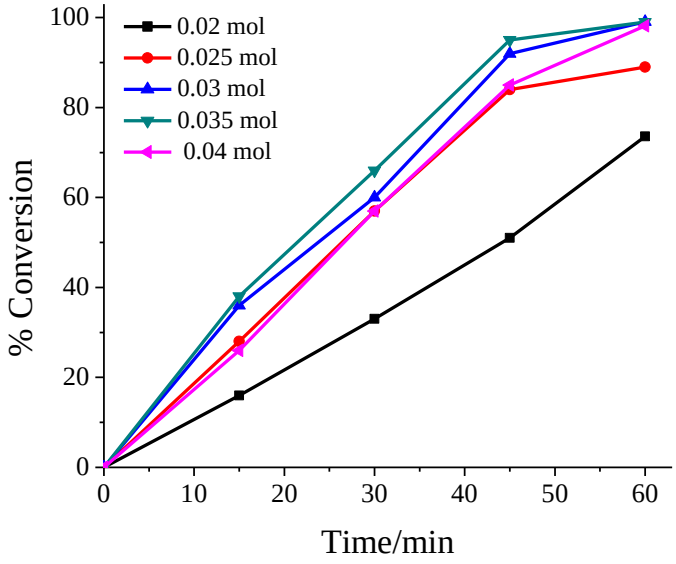

Figure 3.10. Effect of the amount of KBr on the oxidative bromination of styrene. Reaction conditions: Catalyst (0.015 g), styrene (1.04 g, 10 mmol), CH_2Cl_2/H_2O 40 mL, 50 % v/v), H_2O_2 (2.27 g, 20 mmol), $HClO_4$ (5.72 g, 40 mmol).

The effect of various amounts of $HClO_4$ added in the reaction mixture as a function of the conversion of substrate is shown in Figure 3.11. The way of addition of acid (here $HClO_4$) to the reaction mixture may affect the stability of the catalyst, while its amount has great influence on the conversion and selectivity of products. It was found that addition of $HClO_4$ successively in four equal portions at t = 0, 15, 30 and 45 min. of reaction time decreased the decomposition of catalyst. From the plot it is clear that 40 mmol of $HClO_4$ are needed to achieve 99 % conversion in a period of 1 h and from the analysis of the selectivity of products we conclude that upon increasing the amount of $HClO_4$ it is the formation of the diol derivative that mainly increases. Equally good conversion of styrene has also been observed using H_2SO_4 under similar conditions, while the use of acetic acid was not successful.

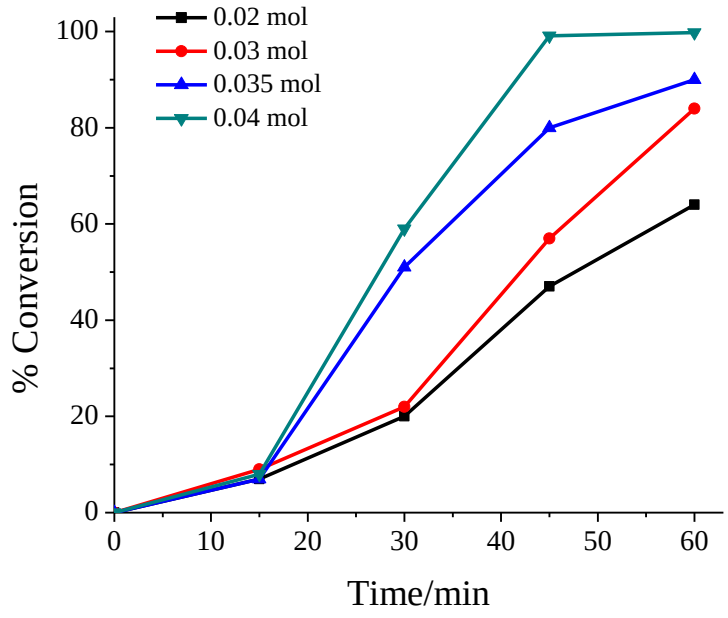

Figure 3.11. Effect of the amount of $HClO_4$ on the oxidative bromination of styrene. Reaction conditions: Catalyst (0.015 g), styrene (1.04 g, 10 mmol), CH_2Cl_2/ H_2O (40 mL, 50 % v/v), H_2O_2 (2.27 g, 20 mmol), KBr (3.57 g, 30 mmol).

Table 3.7 summarizes the various reaction conditions applied to optimize the reaction conditions for the maximum oxidative bromination as well as maximum conversion of styrene considering PS-im[V^VO_2(acpy-bhz)] (**3.4**). Thus, the optimized reaction conditions for the maximum conversion of 10 mmol (1.04 g) of styrene are: catalyst precursor (0.015 g), 30 % aqueous H_2O_2 (2.27 g, 20 mmol), KBr (3.57 g, 30 mmol), $HClO_4$ (5.72 g, 40 mmol, added in four equal portions at t = 0, 15, 30 and 45 min. of reaction time) and CH_2Cl_2-H_2O (40 mL, 50 % v/v) at room temperature for 1 h (entry no. 8, Table 3.7). Entry no. 6 presents reaction conditions {i.e. styrene (1.04 g, 10 mmol) catalyst precursor (0.015 g), 30 % aqueous H_2O_2 (1.135, 10 mmol), KBr (3.57 g, 30 mmol), $HClO_4$ (5.72 g, 40 mmol} for the maximum formation of 2-bromo-1-phenylethane-1-ol (48 % selectivity) along with 51 % selectivity of diol and no formation of the dibromo derivative; however, under these conditions the maximum conversion obtained was only 79 %. Reducing the amount of $HClO_4$ from 40 mmol to 30 mmol (entry no. 17) improved the conversion to 96 % with the formation reasonably good amount of both bromo derivatives (8 % selectivity of mono bromo and 27 % of

dibromo) and less amount of diol (64 % selectivity). Thus, lower amounts of H_2O_2 and $HClO_4$ both direct the reaction to the formation of bromo derivatives in satisfactory amounts.

Table 3.7. Results of oxidative bromination of 1.04 g (10 mmol) of styrene after 1 h of reaction time using PS-im[V^VO_2(acpy-bhz)] (**3.4**) as catalyst precursor.

Entry No.	Catalyst (g)	KBr (g, mmol)	H_2O_2 (g, mmol)	$HClO_4$ (g, mmol)	Solvent (CH_2Cl_2/H_2O)	% Conv.	% selectivity			
							Mono-bromo	dibromo	diol	others
1	0.010	3.57, 30	3.405, 30	5.72, 40	20/20	84	6	2	82	10
2	0.015	3.57, 30	3.405, 30	5.72, 40	20/20	99	2	6	84	8
3	0.020	3.57, 30	3.405, 30	5.72, 40	20/20	99	5	4	86	5
4	0.025	3.57, 30	3.405, 30	5.72, 40	20/20	99	3	6	81	10
5	0.030	3.57, 30	3.405, 30	5.72, 40	20/20	99	3	8	80	9
6	0.015	3.57, 30	1.135, 10	5.72, 40	20/20	79	48	0	51	1
7	0.015	3.57, 30	1.69, 15	5.72, 40	20/20	91	35	2	57	6
8	0.015	3.57, 30	2.27, 20	5.72, 40	20/20	99	11	5	79	5
9	0.015	3.57, 30	2.83, 25	5.72, 40	20/20	99	12	3	80	5
10	0.015	2.38, 20	2.27, 20	5.72, 40	20/20	74	35	0	63	2
11	0.015	2.97, 25	2.27, 20	5.72, 40	20/20	89	29	2	64	5
12	0.015	4.165, 35	2.27, 20	5.72, 40	20/20	99	16	2	78	4
13	0.015	4.76, 40	2.27, 20	5.72, 40	20/20	98	12	5	79	4
14	0.015	3.57, 30	2.27, 20	2.86, 20	20/20	64	11	31	57	1
15	0.015	3.57, 30	2.27, 20	4.29, 30	20/20	84	13	22	62	3
16	0.015	3.57, 30	2.27, 20	5.00, 35	20/20	90	14	5	76	5
17	0.015	3.57, 30	1.135, 10	4.29, 30	20/20	96	8	27	64	1
18	0.015	3.57, 30	2.27, 20	2.86, 20	20/20	99	11	21	67	1

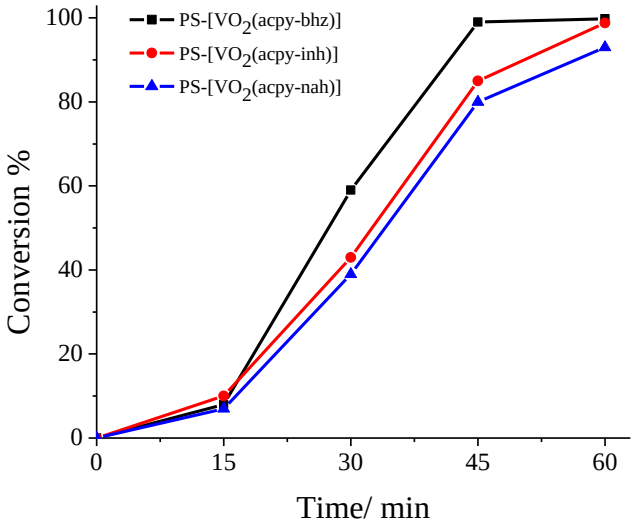

Figure 3.12. Effect of different catalyst on the oxidative bromination of styrene under optimized reaction conditions for the maximum conversion of styrene i.e. styrene ((1.04 g, 10 mmol), catalyst precursor (0.015 g), 30 % aqueous H_2O_2 (2.27 g, 20 mmol), KBr (3.57 g, 30 mmol), $HClO_4$ (5.72 g, 40 mmol, added in four equal portions at t = 0, 15, 30 and 45 min. of reaction time) and CH_2Cl_2/H_2O (40 mL, 50 % v/v) at room temperature for 1 h.

The other two catalyst precursors, PS-im[VO_2(acpy-inh)] (**3.5**) and PS-im[VO_2(acpy-nah)] (**6**), along with neat complexes were also tested under the above optimized reaction conditions for the maximum conversion of styrene. The results are presented in Table 3.8 (and Figure 3.12). It is clear from the data that all three supported complexes show comparable catalytic activity (94 to 99 %); PS-im[VO_2(acpy-nah)] being less active. Amongst the products formed after 1 h of reaction time the selectivity of 1-phenylethane-1,2-diol is higher (76–80 %) while that of 2-bromo-1-phenylethane-1-ol (bromohydrin) is 11–13 %. It was observed that, extending the reaction time for another 1 h resulted in the formation of more dibromo product. These catalyst precursors were also tested for their recyclability and the results (Table 3.8) show that upon use they are still active and have slightly lower but equally good catalytic potential.

Details of time-on analysis i.e. the consumption of styrene and the selectivity of the formation of major products for all three catalysts are presented in Figures 3.13, 3.14 and 3.15. Under the experimental conditions presented in entry no. 8 of Table 3.7, the formation of 1-phenylethane-1,2-diol and 2-bromo-1-phenylethane-1-ol (bromohydrin)

starts with the consumption of styrene. However, the selectivity of 1-phenylethane-1,2-diol reaches 79 % after 1 h, while that of 2-bromo-1-phenylethane-1-ol (bromohydrin) is only 12 %. The formation of diol was always found to be high [96]. Either no formation of dibromo derivative or its formation in very low yield has been noted with these catalysts precursors under the above conditions. After 2 h of the reaction the selectivity of mono bromo product rolls back to nearly zero in all cases. It seems that formation of 1-phenylethane-1,2-diol occurs at the expense of the mono bromo derivative. The selectivity profiles were very similar for catalyst precursors **3.5** and **3.6** (Figures 3.14 and 3.15). The neat complexes are equally active and exhibit similar selectivity behavior (Table 3.8). However, the recycle ability of the polymer-supported complexes makes them better catalysts over non polymer-supported ones. Blank reaction gave *ca.* 60 % oxidative bromination of styrene under above optimized reaction conditions.

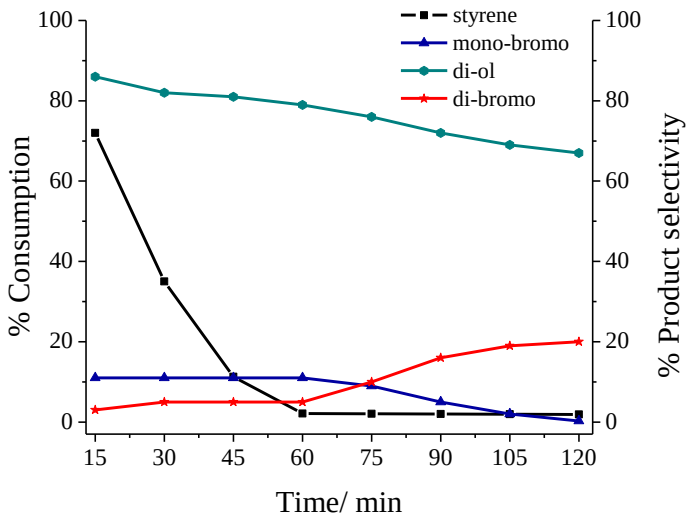

Figure 3.13. Percentage consumption of styrene and selectivity of the formation of products with time using PS-im[$V^{V}O_2$(acpy-bhz)] (**3.4**) as catalyst precursor under the optimized conditions specified in the text.

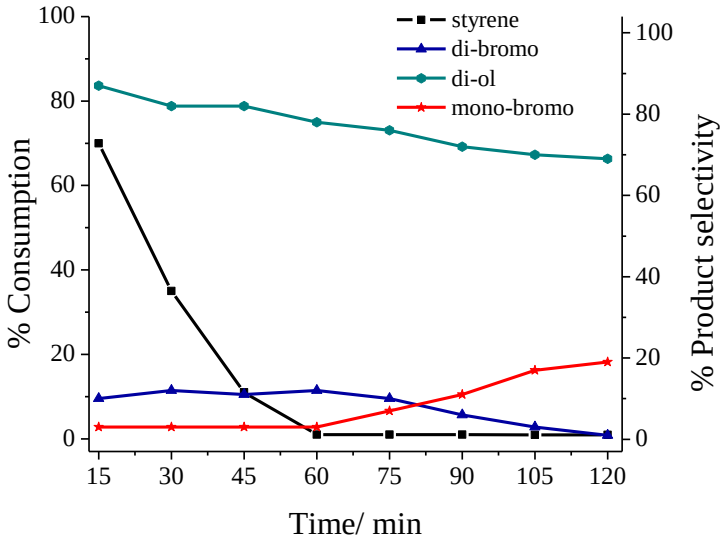

Figure 3.14. Percentage consumption of styrene and selectivity of the formation of products with time using PS-im[$V^{V}O_2$(acpy-inh)] (**3.5**) as catalyst precursor under the optimized conditions specified in the text.

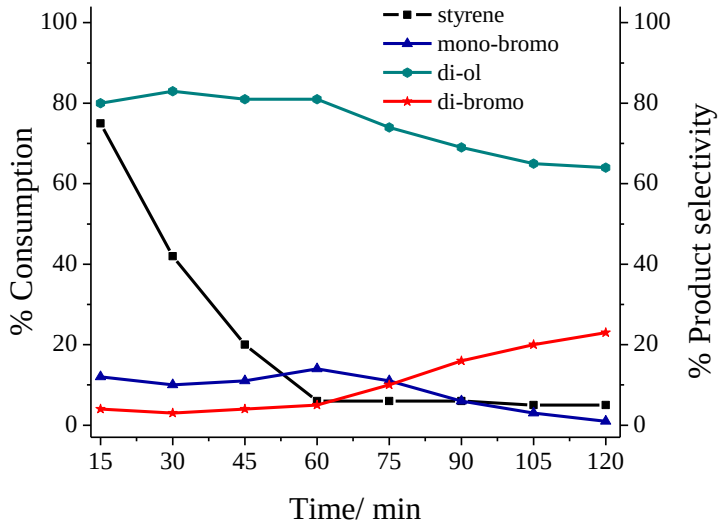

Figure 3.15. Percentage consumption of styrene and selectivity of the formation of products with time using PS-im[$V^{V}O_2$(acpy-nah)] (**3.6**) as catalyst precursor under the optimized conditions specified in the text.

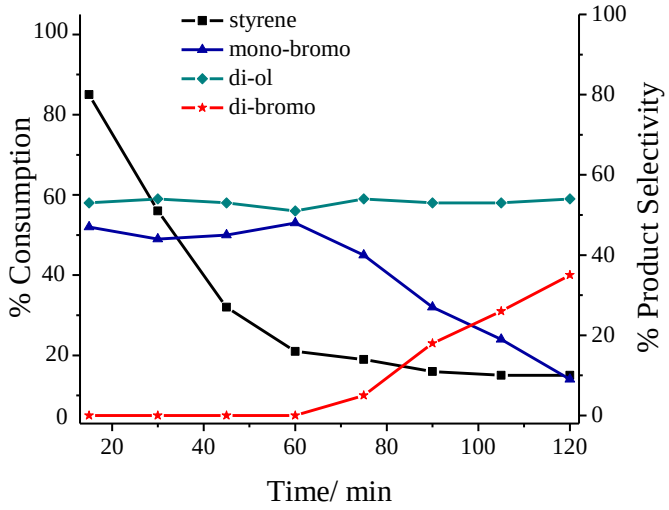

Figure 3.16. Percentage consumption of styrene and selectivity of the formation of products with time using PS-im[$V^{V}O_2$(acpy-bhz)] (**3.4**) as catalyst precursor for the conditions of entry no. 6 in Table 3.7 (maximum brominated products).

Time on analysis of the results for the experimental conditions i.e. for the maximum oxidative bromination of styrene presented in entry no. 6 of Table 3.7 shows that the selectivity of 2-bromo-1-phenylethane-1-ol and 1-phenylethane-1,2-diol both increases with the consumption of styrene and reaches 48 and 51 %, respectively, after 1 h. During the next 1 h the formation of 1,2-dibromo-1-phenylethane starts and its selectivity reaches 35 %, while those of 2-bromo-1-phenylethane-1-ol and 1-phenylethane-1,2-diol reach 8 and 55 %, respectively (Figure 3.16).

Table 3.8. Product selectivity and % conversion at optimum reaction conditions, chosen for maximum conversion of styrene.

Sr. No	Catalyst	% Conv.	Selectivity (%)				
			Mono-bromo	dibromo	diol	Others	TOF/h^{-1}
1	PS-im[$V^{V}O_2$(acpy-bhz)] (**3.4**)	98	11	5	79	5	2016
2	PS-im[$V^{V}O_2$(acpy-inh)] (**3.5**)	99	12	3	78	7	2037
3	PS-im[$V^{V}O_2$(acpy-nah)] (**3.6**)	94	13	5	76	6	1934
4	PS-im[$V^{V}O_2$(acpy-bhz)] (**3.4**)[a]	96	12	3	78	7	1954
5	PS-im[$V^{V}O_2$(acpy-inh)] (**3.5**)[a]	97	13	4	78	5	1996
6	PS-im[$V^{V}O_2$(acpy-nah)] (**3.6**)[a]	94	14	5	75	6	1934
7	[$V^{V}O_2$(acpy-bhz)] (**3.1**)	97	26		73	1	1996
8	[$V^{V}O_2$(acpy-inh)] (**3.2**)	98	30		68	2	2016
9	[$V^{V}O_2$(acpy-nah)]·DMSO (**3.3a**)	85	36		63	1	1749
10	Blank reaction	60	15	1	80	4	-

[a] Data for used catalyst (first cycle).

The reaction mechanisms presented in Scheme 3.5 throw some light on the sequential conversion of initially formed dibromo derivative into the mono-bromo one, which in turn converts into diol. Thus catalytically in situ generated HOBr, by the reaction of vanadium complex with KBr in the presence of H_2O_2 and $HClO_4$, reacts with styrene to give the bromonium ion as intermediate. The nucleophile Br^- as well as H_2O may both attack the α-carbon of the intermediate to give 1,2-dibromo-1-phenylethane and 2-bromo-1-phenylethane-1-ol, respectively. The nucleophile H_2O may further attack the α-carbon of 2-bromo-1-phenylethane-1-ol to give 1-phenylethane-1,2-diol. These steps justify the formation of 1-phenylethane-1,2-diol in highest yield under any experimental conditions mentioned in Table 3.7.

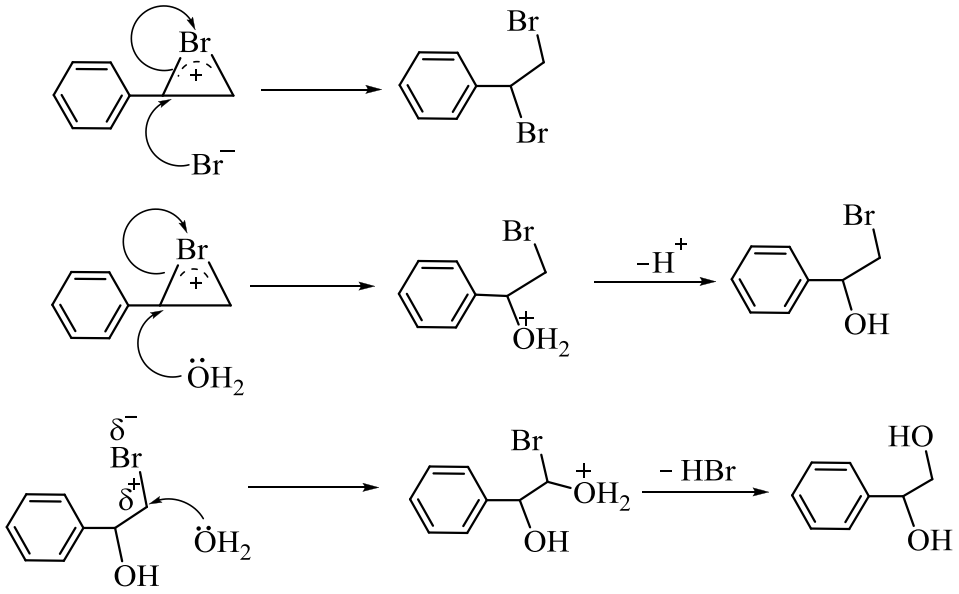

Scheme 3.5. Possible mechanisms operating to yield the three main products detected, after the bromonium ion is formed by action of catalytically generated HOBr on styrene.

3.3.7.2. Oxidative bromination of *trans*–stilbene

Oxidative bromination of *trans*–stilbene was carried out with the biphasic chloroform-water solvent system. Chloroform was found to be better solvent in terms of solubility of *trans*–stilbene. Polymer beads were allowed to swell in chloroform for 4 h prior to the reaction. Oxidative bromination of *trans*–stilbene gave mainly three products: i) 2,3-diphenyloxirane (TSO = *trans*–stilbene oxide), ii) 2-bromo-1,2-diphenylethanol and iii) 1,2-dibromo-1,2-diphenylethane; Scheme 3.6.

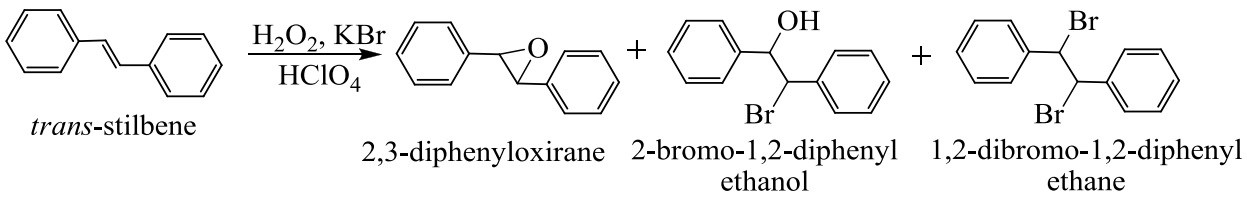

Scheme 3.6. Products of the oxidative bromination of *trans*–stilbene.

Again PS-im[$V^{V}O_2$(acpy-bhz)] (**3.4**) was taken as catalyst precursor and all parameters as stated above were studied in order to maximize the oxidative bromination of *trans*–stilbene. Reaction requires *ca.* 2 h to achieve the equilibrium. Table 3.9

summarizes various trials with experimental details for the oxidative bromination of *trans*–stilbene and the obtained conversions under several different reaction conditions applied.

Thus, the optimized reaction conditions settled for the maximum conversion of 0.90 g (5 mmol) of *trans*–stilbene (entry No. 8; Table 3.9) are: catalyst precursor (0.015 g), KBr (2.38 g, 20 mmol), H_2O_2 (2.27 g, 20 mmol), $HClO_4$ (2.86 g, 20 mmol, added in four equal portions at t = 0, 30, 60 and 90 min. of reaction time) in $CHCl_3$–H_2O (40 mL, 1 : 1, v/v). Again addition of $HClO_4$ in four equal portions, instead of only one portion, was necessary to avoid leaching of complex from the polymer support. Under these conditions, a reasonably good amount of 2-bromo-1,2-diphenylethanol (8 % selectivity) and 1,2-dibromo-1,2-diphenylethane (26 % selectivity) with a maximum of 93 % conversion of *trans*–stilbene was achieved. Higher amounts of oxidant does not improve the conversion of *trans*–stilbene, while higher amounts of $HClO_4$ causes the partial leaching of complex from the polymer support resulting in lower conversion.

Table 3.9

Results of oxidative bromination of 0.90 g (5 mmol) of *trans*–stilbene after 2 h of reaction time using PS-im[V^VO_2(acpy-bhz)] (**3.4**) as catalyst precursor.

Entry No.	KBr (g, mmol)	H_2O_2 (g, mmol)	$HClO_4$ (g, mmol)	Catalyst (g)	$CHCl_3/H_2O_2$ (1:1) (mL)	% Conv.	% Selectivity			
							Mono-bromo	dibromo	TSO	Others
1.	3.57, 30	3.405, 30	5.72, 40	0.015	40	91	7	15	75	3
2	3.57, 30	3.405, 30	5.72, 40	0.020	40	93	5	13	80	2
3	3.57, 30	3.405, 30	5.72, 40	0.025	40	92	6	13	79	2
4	1.18, 10	3.405, 30	5.72, 40	0.015	40	80	9	32	58	1
5	2.38, 20	3.405, 30	5.72, 40	0.015	40	95	4	22	73	1
6	2.38, 20	1.13, 10	5.72, 40	0.015	40	83	5	25	67	3
7	2.38, 20	2.27, 20	5.72, 40	0.015	40	93	4	29	65	2
8	2.38, 20	2.27, 20	2.86, 20	0.015	40	93	8	26	74	2
9	2.38, 20	2.27, 20	4.29, 30	0.015	40	95	4	26	77	3
10	0.00, 0	2.27, 20	2.86, 20	0.015	40	2	0	0	0	2
11	2.38, 20	2.27, 20	2.86, 20	-	40	55	8	15	72	5

The high amount of *trans*–stilbene oxide formed under all experimental conditions presented in Table 3.9 led us to extend experimental trials without KBr (entry no. 10) or without catalyst (entry no. 11) under the above optimized conditions. Only 2 % conversion of *trans*–stilbene was obtained in the experiments in the absence of KBr,

while 55 % conversion was achieved in the absence of catalyst. This suggests the importance of KBr in this reaction. Further, the formation of highest amount of *trans*–stilbene oxide (72 % selectivity) in the later case led us to propose the following mechanisms (Scheme 3.7) for the formation of different products.

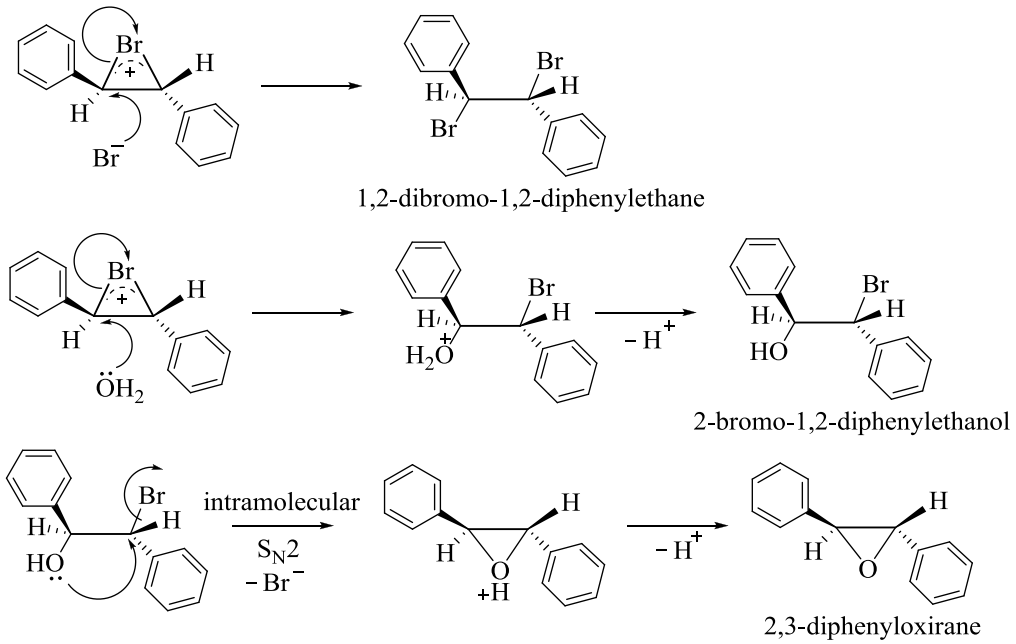

Scheme 3.7. Proposed mechanisms operating to yield products, after the bromonium ion is formed by action of catalytically generated HOBr on *trans*–stilbene.

Other two polymer anchored complexes PS-im[V^VO_2(acpy-inh)] and PS-im[V^VO_2(acpy-nah)] along with non polymer-anchored complexes were also used to carry out the transformation and the results are summarized in Table 3.10. Under these conditions the catalytic activity of the different polymer-supported catalysts follows the order: PS-im[V^VO_2(acpy-inh)] (95 %) > PS-im[V^VO_2(acpy-bhz)] (93 %) > PS-im[V^VO_2(acpy-nah)] (88 %). In the case of the neat complexes the conversion is slightly lower [V^VO_2(acpy-inh)] (94 %) > [V^VO_2(acpy-bhz)] (90 %) > [V^VO_2(acpy-nah)] (82 %) but follow the same trend and selectivity profiles. Amongst the three products formed, the selectivity of the formation of *trans*-stilbene oxide is highest (71–76 %), which is followed by 1,2-dibromo-1,2-diphenylethane (22–25 %) and the formation of 2-bromo-1,2-diphenylethanol is minimum.

Table 3.10. Results of oxidative bromination of *trans*–stilbene catalysed by different catalyst precursors. Conversion and relative amounts of products obtained after 2 h of reaction.

Catalyst	% Conv.	Selectivity (%)				
		Mono-bromo	Di-bromo	*T.S.O.	Others	TOF /h^{-1}
PS-im[$V^{V}O_2$(acpy-bhz)] (**3.4**)	93	1	23	74	2	359
PS-im[$V^{V}O_2$(acpy-inh)] (**3.5**)	95	1	22	74	3	366
PS-im[$V^{V}O_2$(acpy-nah)] (**3.6**)	88	1	24	72	3	339
PS-im[$V^{V}O_2$(acpy-bhz)] (**3.4**) [a]	91	1	20	74	5	347
PS-im[$V^{V}O_2$(acpy-inh)] (**3.5**) [a]	94	1	23	73	3	355
PS-im[$V^{V}O_2$(acpy-nah)] (**3.6**) [a]	86	1	25	72	2	328
[$V^{V}O_2$(acpy-bhz)] (**3.1**)	90	1	25	71	3	347
[$V^{V}O_2$(acpy-inh)] (**3.2**)	94	1	22	76	1	363
[$V^{V}O_2$(acpy-nah)]·DMSO (**3.3a**)	82	1	25	71	3	316

[a] Data for used catalyst (first cycle).

*T.S.O. = *trans*–stilbene oxide

3.3.7.2.1. Mechanism of oxidative bromination

From the mechanistic point of view involving the oxybromination reactions, one of the efforts was the elucidation of the main reaction pathway and identification of intermediates using spectroscopic techniques, namely ^{51}V NMR.

The catalytic reactions of styrene described in this study follows the approach of using a two phase system. The mode of action of V-dependent bromoperoxidase enzymes (V-BrPOs) has received much attention [23,32,123,142,146,147] and it is normally accepted that vanadium, in the presence of hydrogen peroxide [148–151], forms a peroxido vanadium derivative. Oxidation of the bromide ion is followed by the formation of a bromine equivalent intermediate, which may then either brominate an organic substrate or react with another molecule of Br^- to form bromine. The primary oxidant is H_2O_2 and the role of the V^V ion is to serve as a strong Lewis acid in the activation process. The high efficacy of the bromination process is associated to the formation of the intermediate, and the reaction has been considered to take place in two different 'compartments' of the enzymes: one first step in a hydrophilic region of the protein, and the second in a hydrophobic region. This has led to model the reaction by the development of two-phase systems [141]: (1) the vanadium

precursor, H_2O_2 and KBr are dissolved in water, where the formation of a V^V-peroxido derivative, and the oxidation of Br^- occurs with the formation of an intermediate; (2) this intermediate is transferred to the organic phase, often a chlorinated solvent (e.g. $CHCl_3$ or CH_2Cl_2), where the bromination of substrate takes place. The process in the aqueous phase requires acidic conditions, probably to promote the protonation of the peroxido moiety.

V^VO_2-complexes catalyze the oxidative bromination of styrene in the presence of H_2O_2. In this reaction vanadium complexes react with 1 or 2 equiv. of H_2O_2, forming oxidomonoperoxido complexes which ultimately oxidize the bromide species (to Br_2, Br_3^- and/or HOBr), the bromination of the substrate then proceeding with the liberation of a proton [146], which may act as a reservoir of the active oxidant. We clearly identified monoperoxido V^V-complexes, *e.g.* **CV** δ_V = –588 ppm Figure 3.17; more details of the suggested speciation of the system are shown in Scheme 3.3. Upon addition of Br^- brominated species may form (see **CVI or CVIa** or **CVIb**, Scheme 3) which may be responsible for the formation of bromohydrin. Accordingly, the hypobromite-like species should be directly involved in the ‘‘Br^+” transfer process or, at least, it is one of the active species in the bromination process [23]. The occurrence, during the catalytic cycle, of a similar species, where the equatorial peroxido oxygen is protonated and the Br^- is prone to coordinate the other peroxidic oxygen, has been proposed [147], which ultimately oxidize the bromide species (most likely to HOBr) and brominates the substrate. Therefore the halogenations may proceed involving the intermediates containing bound OBr^-, namely the intermediates included in Scheme 3.3, where we tentatively suggest assignments for the resonances observed in the ^{51}V NMR experiments to V^V-complexes containing OBr^- as also suggested in previous studies [109]. Hypobromite intermediates have been detected by ESI-MS on model systems [152].

It is plausible that in the present systems the V^V-catalysts act mainly to produce the bromide-containing species, e.g. a bromonium ion intermediate; the reactions then proceed to form other species, some not containing the Br atom. In the absence of a V^V-complex the reaction also proceeds with reasonable conversion, but with distinct selectivity profiles. The presence of KBr is essential to get reasonable conversion, although in many cases the brominated compounds are not the main products obtained.

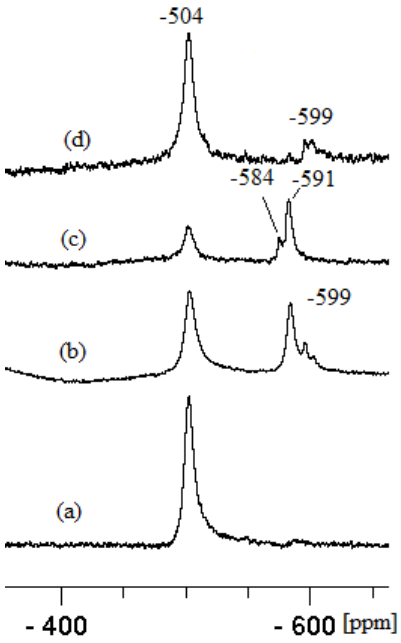

Figure 3.17. ^{51}V NMR spectra of solutions (*ca.* 4 mM) in DMSO-d_6 (a) of compound **3.1**; (b) solution of (a) after addition of 3.0 equiv. KBr and 2.0 equiv. H_2O_2 (solution of 30 % H_2O_2); (c) solution of (b) after *ca.* 15 min. (d) solution of (a) after addition of 3.0 equiv. of H_2O_2 (solution of 30 % H_2O_2).

Figure 3.17 depicts ^{51}V NMR experiments with catalytic precursor (**3.1**) upon additions of H_2O_2 and KBr. New resonances appear at –584 ppm (and at –599 to –601 ppm). The resonance observed here at δ_V = –584 ppm is tentatively assigned to a species containing coordinated OBr^- which, as mentioned, could be responsible for the formation of the bromohydrin (see structures **CVI**, **CVIa** or **CVIb** Scheme 3.3). Therefore the halogenations may indeed proceed involving the intermediates outlined in Scheme 3.3. However, the resonance at $\delta_V \approx$ –584 ppm may also be ascribed to other formulations not containing bound hypobromite ion, thus definite assignments for these resonances cannot be made in the present systems.

3.3.7.3. Oxidation of benzoin

The production of benzil from benzoin has attracted much attention, as benzil is a particularly useful intermediate for the synthesis of heterocyclic compounds and benzylic acid rearrangements [76,153–155]. The catalytic oxidation of benzoin was achieved successfully with these polymer-supported complexes using 30 % aqueous H_2O_2 as oxidant. The polymer beads were allowed to swell in methanol for 2 h prior to

the reaction. The main products obtained were: benzil, methylbenzoate, benzoic acid and benzaldehyde-dimethylacetal; Scheme 3.8.

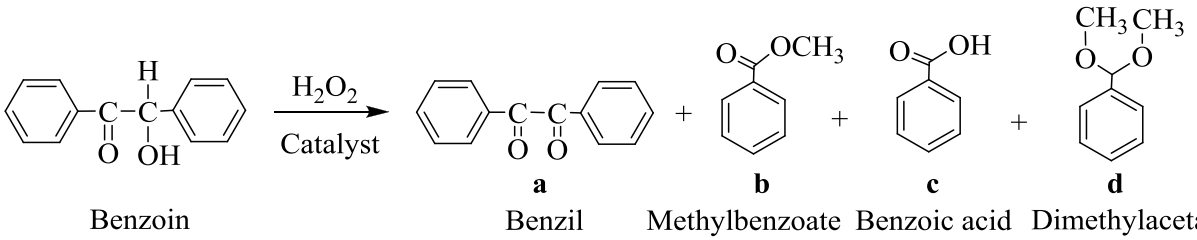

Scheme 3.8. Oxidation products of benzoin: (a) benzil, (b) methyl benzoate, (c) benzoic acid and (d) benzaldehyde-dimethylacetal.

To optimize the reaction conditions for the maximum oxidation of benzoin, the effect of various amounts of catalyst on the oxidation of benzoin for the fixed conditions of: benzoin (1.06 g, 5 mmol) and 30 % H_2O_2 (1.13 g, 10 mmol) in 15 mL of methanol at reflux temperature was studied as a function of time for 6 h and the results are illustrated in Figure 3.18. Increasing the catalyst precursor amount from 0.010 g to 0.015 g increases the conversion from 56 % to 69 %. This conversion further improved to 74 % on increasing the catalyst amount to 0.020 g, but no significant improvement in the conversion was noted on further increasing its amount. Therefore an amount of 0.020 g was considered the best for optimum conversion of benzoin in 6 h of reaction time, and the experiments described below were carried out using this amount of catalyst precursor.

Variation in the volume of the solvent was also studied by taking 10, 15 and 20 mL of methanol; Figure 3.19. It was observed that 15 mL of methanol for 1.06 g (5 mmol) of benzoin, 0.020 g of catalyst and 1.13 g 30 % H_2O_2 was sufficient enough to carry out the reaction at reflux temperature for satisfactory transformation (73 %) of benzoin.

The effect of amount of oxidant was studied considering three different benzoin to H_2O_2 molar ratios of 1 : 1, 1 : 2 and 1 : 3 under the above optimized conditions i.e. amount of benzoin (1.06 g, 5 mmol) and PS-im[V^VO_2(acpy-bhz)] (0.020 g) in refluxing methanol (15 mL). A maximum of 87.0 % conversion was achieved at a benzoin to H_2O_2 molar ratio of 1 : 3 in 6 h of reaction time while 1 : 1 and 1 : 2 ratios resulted in 60.0 and 75.0 % conversion, respectively; Figure 3.20. Thus, the substrate to oxidant

ratio of 1:3 was considered the best ratio to obtain maximum oxidation of benzoin (87 %) in 6 h of reaction time.

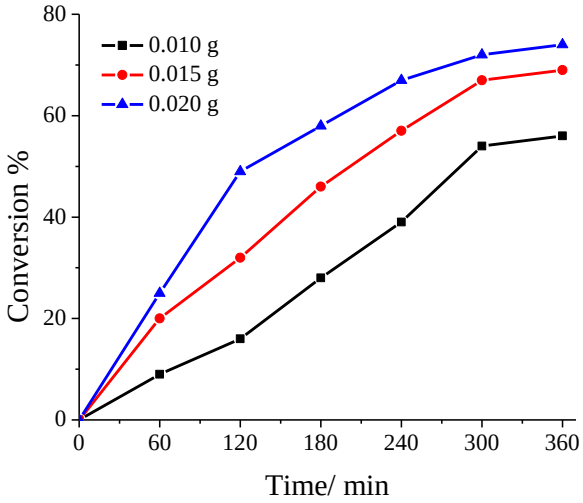

Figure 3.18. Effect of the amount of catalyst PS-im[$V^{V}O_2$(acpy-bhz)] (**3.4**) on oxidation of benzoin. Reaction conditions: benzoin (1.06 g, 5 mmol) and 30 % H_2O_2 (1.13 g, 10 mmol) in methanol (15 mL) at reflux temperature.

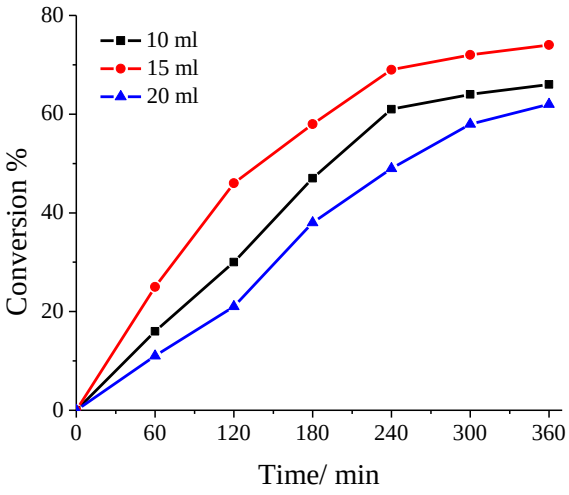

Figure 3.19. Effect of the amount of solvent methanol on oxidation of benzoin. Reaction conditions: PS-im[$V^{V}O_2$(acpy-bhz)] (**3.4**) (0.020 g), benzoin (1.06 g, 5 mmol) and 30 % H_2O_2 (1.13 g, 10 mmol) at reflux temperature of methanol.

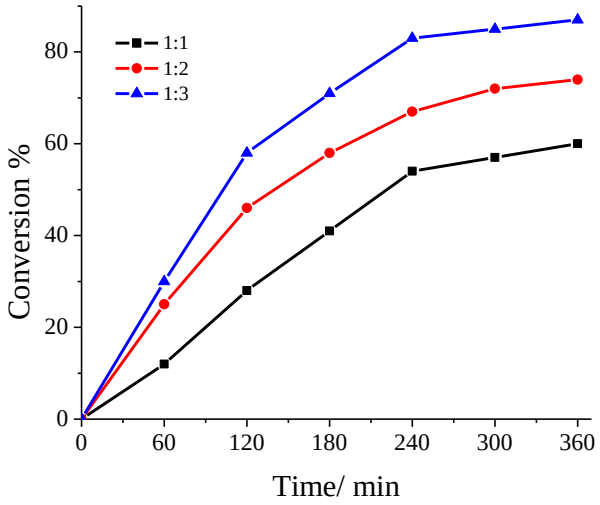

Figure 3.20. Effect of the amount of oxidant (i.e. 30 % H_2O_2) on the oxidation of benzoin. Reaction conditions: PS-im[VO_2(acpy-bhz)] (0.020 g) and benzoin (1.06 g, 5 mmol) in refluxing methanol (15 mL).

Thus, optimized operating reaction conditions for the maximum oxidation of benzoin were fixed as follows: benzoin (1.06 g, 5 mmol), PS-im[VO_2(acpy-bhz)] (0.020 g), 30 % H_2O_2 (1.7 g, 15 mmol) and methanol (15 ml) at reflux temperature. Under these conditions other catalysts were also tested and the results are summarized in Table 3.11. It is clear from the table that the catalytic activity of polymer-supported catalysts PS-im[VO_2(acpy-bhz)] (**3.4**) and PS-im[VO_2(acpy-inh)] (**3.5**) is comparable, but in similar conditions PS-im[VO_2(acpy-nah)] (**3.6**) shows lower catalytic activity. The corresponding neat complexes showed lower conversions and distinct selectivity: the formation of different products for polymer-anchored catalysts follows the order: benzil (a) > benzaldehyde-dimethylacetal (d) > benzoic acid (c) > methylbenzoate (b) . With the corresponding neat complexes this order is benzil (a) > methylbenzoate (b) > benzoic acid (c) > benzaldehyde-dimethylacetal (d). The relative amount of benzil is higher, and that of benzoic acid is lower when using the systems in homogeneous conditions. The distinct changes in the conversion and selectivity of products for catalyst (**3.3**) from other two may be due to its partial existence as a dinuclear species in methanol under the catalytic conditions. The global conversion of benzoin is comparable with that previously reported for the catalytic activity of PS–[V^VO_2(sal–his)] (Hsal-his = Schiff

base derived from the reaction of salicylaldehyde and histamine) [76], but the selectivity toward benzil is significantly improved in present study, as well as the TOF values.

Table 3.11. Conversion of benzoin and selectivity of the formation of various products after 6 h of reaction.

Catalyst	Conv. %	Product selectivity (%)[a]					
		a	b	c	d	Others	TOF/h^{-1}
Ps-[$V^{V}O_2$(acpy-bhz)] (**3.4**)	87	46	5	35	13	1	111
Ps-[$V^{V}O_2$(acpy-inh)] (**3.5**)	90	47	8	33	12	1	116
Ps-[$V^{V}O_2$(acpy-nah)] (**3.6**)	81	49	6	30	14	1	104
Ps-[$V^{V}O_2$(acpy-bhz)] (**3.4**)[b]	84	44	5	36	14	1	108
Ps-[$V^{V}O_2$(acpy-inh)] (**3.5**)[b]	86	46	8	34	10	2	111
Ps-[$V^{V}O_2$(acpy-nah)] (**3.6**)[b]	78	50	6	29	13	2	100
[$V^{V}O_2$(acpy-bhz)] (**3.1**)	67	54	5	10	31	-	86
[$V^{V}O_2$(acpy-inh) (**3.2**)	70	56	2	12	30	-	90
[$V^{V}O_2$(acpy-nah)]·DMSO (**3.3a**)	60	54	3	20	23	-	77
Blank reaction	48	41	8	34	15	2	-

[a] a: benzil, b: methylbenzoate, c: benzoic acid and d: benzaldehyde-dimethylacetal.

[b] Data for used catalyst (first cycle).

Figure 3.21 shows percentage consumption of benzoin for PS-im[$V^{V}O_2$(acpy-bhz)] (**3.4**) along with the percentage product formation with the course of time (6 h), under the optimized reaction conditions as described above. It is clear from the plot that formation of all four products start from the beginning of the consumption of the benzoin. The consumption of benzoin is relatively fast for the first 4 h (83 %) and within the next 2 h reaches 87 % (at the end of 6 h). Similarly, the rate of formation of benzil is highest among all the products up to 4 h (35 %) and then improves slowly for the remaining 2 h (up to 40 %). Methyl benzoate, benzoic acid and benzaldehyde-dimethylacetal form slowly for initial 1 h (3 %, 2 % and 1 % respectively); after that the amount of methyl benzoate increases more rapidly, with 30 % formation at the end of 5 h. The amounts of benzoic acid and benzaldehyde-dimethylacetal increase very slowly throughout the 6 h of reaction, with an overall 11 % and 5 % formation, respectively, till the end of the process.

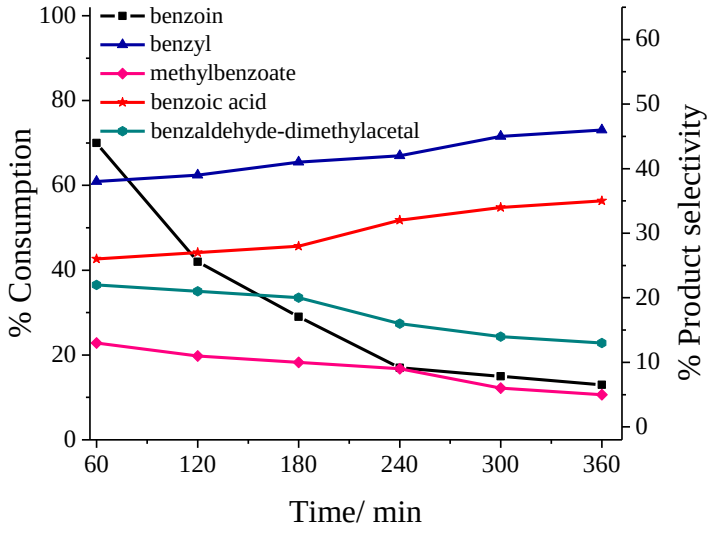

Figure 3.21. Percentage conversion of benzoin and selectivity of the formation of products with time using PS-im[$V^{V}O_2$(acpy-bhz)] (**3.4**) as catalyst precursor under the optimized conditions specified in the text.

Similar trends were observed for PS-im[$V^{V}O_2$(acpy-inh)] (**3.5**) and PS-im[$V^{V}O_2$(acpy-nah)] (**3.6**) (Figs. 3.22 and 3.23). For PS-im[$V^{V}O_2$(acpy-inh)], the percentage product formation of benzil, methylbenzoate, benzoic acid and benzaldehyde-dimethylacetal is 42 %, 30 %, 10 %, 7 % respectively with 90 % consumption of benzoin. For PS-im[$V^{V}O_2$(acpy-nah)] (**3.6**) the percentage product formation of benzil, methylbenzoate, benzoic acid and benzaldehyde-dimethylacetal is 40 %, 24 %, 11 %, 5 %, respectively, with 81 % consumption of benzoin at the end of 6 h.

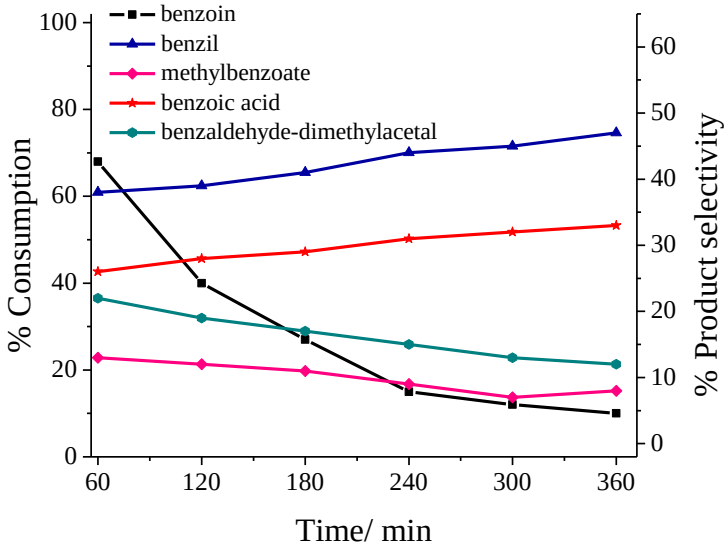

Figure 3.22. Percentage consumption of benzoin and selectivity of the formation of products with time using PS-im[$V^{V}O_2$(acpy-inh)] (**3.5**) as catalyst precursor

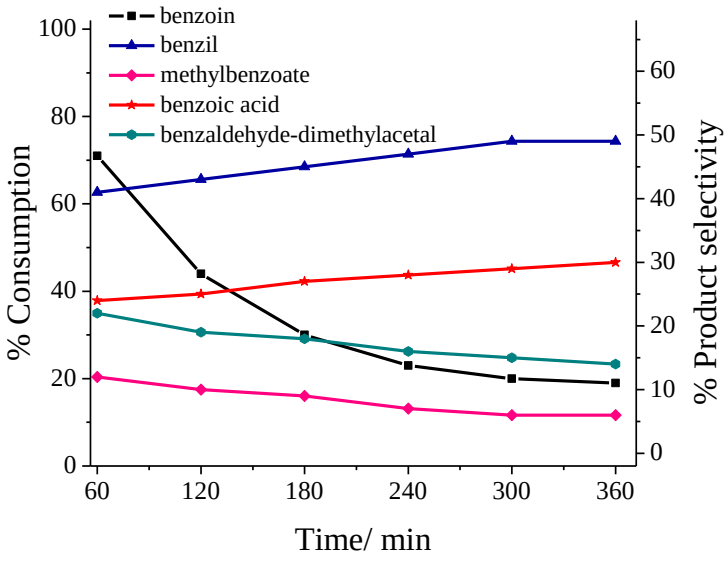

Figure 3.23. Percentage consumption of benzoin and selectivity of the formation of products with time using PS-im[$V^{V}O_2$(acpy-nah)] (**3.6**) as catalyst precursor.

3.4. Conclusions

Three potentially polymer-supported (PS) $V^{V}O_2$-complexes with ONN donor ligands, abbreviated herein as PS-im[$V^{V}O_2$(acpy-bhz] (**3.4**) PS-im[$V^{V}O_2$(acpy-inh)] (**3.5**) and PS-im[$V^{V}O_2$(acpy-nah] (**3.6**), were designed, synthesized and characterized. The corresponding neat complexes were also characterized by analytical and spectroscopic techniques. A monomeric version of complex **3.3** was also characterized by single crystal X-ray diffraction analysis.

The prepared $V^{V}O_2$-complexes, polymer-supported as well as neat complexes, were successively used as catalyst precursors for the oxidative bromination of styrene and *trans*-stilbene using 30 % aqueous H_2O_2 as an oxidant. Thus these V^{V}-complexes may be considered as functional models of VHPOs. Their catalytic potential for benzoin oxidation was also demostrated. The polymer-supported catalysts are thermally more stable, selective, easy recoverable from the reaction mixture and recyclable without much decrease of activity. Interestingly, reactions take place in the absence of the vanadium complexes, with moderate conversions of the substrates, but the selectivity profiles of the reaction products differ; namely much lower amounts of brominated products are obtained. In the absence of KBr almost no conversion of e.g. *trans*-stilbene was achieved under the experimental conditions used.

The complexes can also be converted, by treatment with H_2O_2, to the corresponding peroxido-complexes, similar to what is expected to be one of the intermediates in the catalytic cycle of the activity of VHPO. ^{51}V NMR experiments with DMSO solutions of the neat complexes, by adding methanol, acid, KBr and/or H_2O_2 allowed to detect several distinct $V^{V}O_2$-, $V^{V}O$-, $V^{V}O(OH)$- and $V^{V}O(O_2)$-species in solution. Some of these, namely the $V^{V}O(O_2)$-L and species probably containing coordinated OBr^{-}, are plausible intermediates in the catalytic reactions to produce the bromine-containing intermediates.

Chapter 4

Oxidovanadium(IV) and dioxidovanadium(V) complexes of hydrazones of 2-benzoylpyridine and their catalytic applications

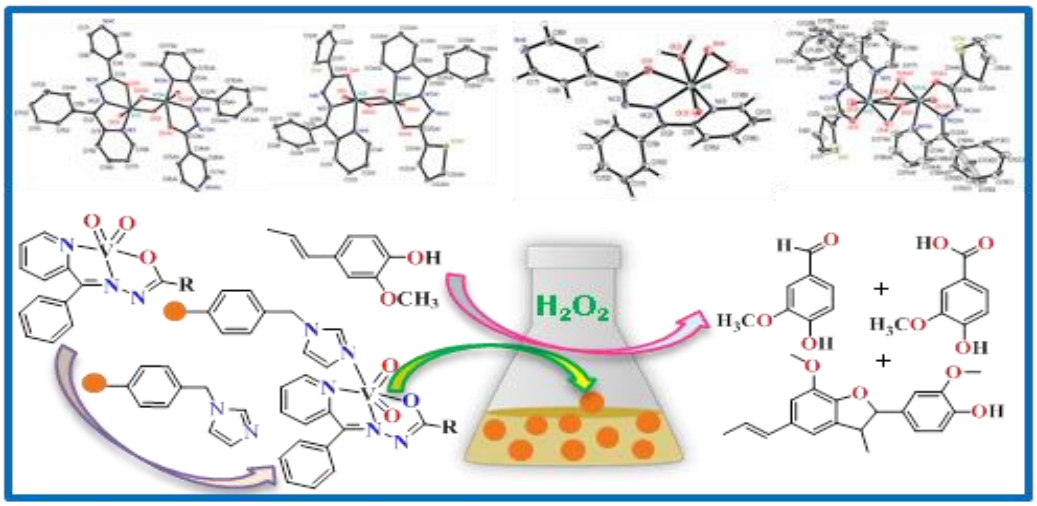

4.1. Introduction

Trigonal bipyramidal dioxidovanadium(V) complexes particularly with benzimidazole, imidazole, pyridyl and hydrazide derived monobasic tridentate ONN ligands have been considered not only as good structural models of vanadium haloperoxidades (VHPOs) [118,132] but functional models as well because some of these complexes mimic oxidative halogenations and sulfoxidations [27,80,133] along with the oxidation, by peroxide, of organic substrates [76,89,156,157]. It has been generally observed that interaction between monobasic tridentate ligands and $[VO(acac)_2]$ under aerobic conditions produces dinuclear, pseudo-octahedral complexes with the $[(VO)_2(\mu\text{-}O)_2]$ core unless bulky groups are attached to the ligand to provide sufficient steric hindrance [141,158,159,160,161]. We observed that such condition is not necessary and even dioxidovanadium(V) complex of ligand having less steric hindrance can be crystallized in mono- as well as dinuclear both forms in different solvent systems [133]. However, they exist in the mononuclear form in solvent. Our effort in this direction led us to design monobasic tridentate ONN donor ligands having bulky group (Scheme 4.1) and isolate dioxidovanadium(V) complexes in order to see if both types of complexes can be isolated from similar ligand systems.

Recently we observed that model trigonal bipyrimidal dioxidovanadium(V) complexes can expand their coordination sphere and coordinate covalently with the nitrogen of the imidazole functionalized chloromethylated polystyrene, cross-linked with 5 % divinylbenzene [69,133]. Such method of immobilizing molybdenum complexes has also been reported by others [137]. This method is quite simple over the other methods where free linkage like carboxylate, hydroxyl, sulphonate, imine etc. must be present in the ligand sphere of the metal complexes to immobilize e.g. on chloromethylated polystyrene [53,54].

The development of immobilized polymer vanadium complexes based catalytic systems have shown considerable interest in recent years for oxidations and oxygen transfer reactions, including the oxidative halogenation of organic substrates [53,54]. Such environmentally benign systems provide extra stability to the metal complexes and have recyclability along with high turnover numbers [53,54].

Continuing our efforts on the above method, we describe herein the synthesis of two polymer-supported dioxidovanadium(V) complexes of ONN donor hydrazones of 2-benzoylpyridine via covalent bonding through imidazolomethylpolystyrene (cross-linked with 5 % divinylbenzene**)** (Scheme 4.1). Model polymer-supported dioxidovanadium(V) complexes as well as the corresponding neat analogues have been used for the oxidation of isoeugenol. Intermediate peroxide species involved during catalytic action have also been isolated as solid as well as generated in solution and studied. It has also been observed that bulky group present on the ligands has no impact on the crystallization of dioxidovanadium(V) complexes in the mononuclear or dinuclear forms. Similar neat dioxidovanadium(V) complexes derived from 2-benzoylpyridine have been reported by Kurup et al. but no catalytic activities of those are reported [162].

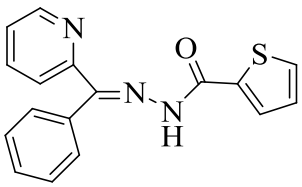

Hbzpy-tch (**4.I**)

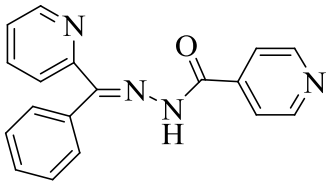

Hbzpy-inh (**4.II**)

Scheme 4.1. Structure of ligands used in this study.

4.2. Experimental Section

4.2.1. Materials and methods

Analytical reagent grade V_2O_5, thiophene-2-carboxylic acid hydrazide (Fluka Chemie, Switzerland), isonicotinic acid hydrazide, imidazole, (Loba Chemie, Mumbai, India), 2-benzoylpyridine, acetylacetone (Hacac) (Aldrich, U.S.A.), isoeugenol (S.D. Fine, India) and 30 % aqueous H_2O_2 were used as obtained. A gift sample of chloromethylated polystyrene [18.9 % Cl (5.35 mmol Cl per gram of resin)] cross-linked with 5 % divinylbenzene was provided by Thermax Limited, Pune, India. Other chemicals and solvents were of analytical reagent grades. Imidazolomethylpolystyrene (PS–im) [69,137], $[V^{IV}O(acac)_2]$ [111] were prepared according to the reported methods.

4.2.2. Instrumentation and characterization procedures

The atomic force microscopic imaging was performed on a scanning probe microscope from NTEGRA (NT-MDT) in a semi-contact mode. Other instrumentation details are presented in Chapter 2.

4.2.3. Preparation of ligands and complexes

4.2.3.1. Hbzpy-tch (4.I)

This was prepared using procedure reported in the literature with certain modifications [163,164]. A solution of 2-benzoylpyridine (0.915 g, 5 mmol) in methanol (15 mL) was added to a solution of thiophene-2-carboxylic acid hydrazide (0.710 g, 5 mmol) in methanol (10 mL) and the resulting reaction mixture was refluxed for 5 h on a water bath. After reducing the volume of the solution to *ca.* 5 mL, it was kept at room temperature where pale yellow solid separated out which was filtered off, washed with small amount of methanol and dried in air. Yield: 85 %. Anal. calcd. for $C_{17}H_{13}N_3OS$ (307.37): C, 66.42; H, 4.26; N, 13.67; S, 10.43 %. Found: C, 66.2; H, 4.0; N, 13.5; S, 10.1 %.

4.2.3.2. Hbzpy-inh (4.II)

This ligand was prepared analogously to **4.I** considering 2-benzoylpyridine (0.915 g, 5 mmol) and isonicotinic acid hydrazide (0.685 g, 5 mmol) in methanol. Yield: 92 %. Anal. calcd. for $C_{18}H_{14}N_4O$ (302.32): C, 71.50; H, 4.66; N, 14.0 %. Found: C, 72.1; H, 4.4; N, 14.2 %.

4.2.3.3. $[V^{IV}O(acac)(bzpy\text{-}tch)]$ (4.1)

A solution of Hbzpy-tch (0.307 g, 1 mmol) in methanol (10 mL) was treated with $[V^{IV}O(acac)_2]$ (0.265 g, 1 mmol) dissolved in methanol (10 mL) in one portion and the resulting reaction mixture was refluxed under stirring in an oil bath for 2 h. Upon reducing the solvent volume to *ca.* 10 mL and cooling to room temperature resulted in the precipitation of green solid which was filtered off, washed with methanol and dried under *vacuum.* Yield: 87%. EPR (X-Band, DMF, 77 K): $g_z = 1.946$, $A_z = 167.3 \times 10^{-4}$

cm^{-1}. Anal. calcd. for $C_{22}H_{19}N_3O_4SV$ (472.41): C, 55.93; H, 4.05; N, 8.89; S, 6.78 %. Found: C, 55.4; H, 4.1; N, 9.1; S, 6.5 %.

4.2.3.4. $[V^{IV}O(OMe)(bzpy\text{-}inh)]$ (4.2)

Complex **4.2** was prepared analogously to **4.1**, replacing **4.I** by (bzpy-inh) (**4.II**). Yield: 85 %. EPR (X-Band, DMF, 77 K): $g_z^1 = 1.951$, $A_z^1 = 167 \times 10^{-4}$ cm^{-1}, $A_z^2 = 159.4 \times 10^{-4}$ cm^{-1}. Anal. calcd. for $C_{19}H_{16}N_4O_3V$ (399.29): C, 57.15; H, 4.03; N, 14.03 %. Found: C, 57.4; H, 4.2; N, 14.2 %.

4.2.3.5 $[\{V^{V}O(bzpy\text{-}tch)\}_2(\mu\text{-}O)_2]$ (4.3)

Method A. Complex **4.1** (0.472 g, 1 mmol) was dissolved in hot methanol (100 mL) and air was passed through the solution with occasional shaking for 12 h. The color of the solution changed gradually from green to yellow. After reducing the volume to *ca.* 20 mL the solution was kept open for slow evaporation where yellow solid of **4.3** obtained within overnight. This was filtered and dried in air. Yield: 84 %. ^{51}V NMR (400 MHz, DMF/acetone–d_6 4:1, ppm): δ –501. Anal. calcd. for $C_{34}H_{24}N_6O_6S_2V_2$ (778.60): C, 52.44; H, 3.10; N, 10.79; S, 8.23 %. Found: C, 52.5; H, 3.0; N, 10.7; S, 8.1 %. Yellow crystals of **4.3** were grown by slow evaporation of its DMF solution in a week period time.

Method B. Complex **4.3** can be prepared in nearly same yield by direct oxidation of solution obtained for **4.1** without isolating it.

4.2.3.6 $[\{V^{V}O(bzpy\text{-}inh)\}_2(\mu\text{-}O)_2]$ (4.4)

Complex **4.4** was prepared adopting the procedure described for **4.3** and replacing **4.1** by $[VO^{IV}(OMe)(bzpy\text{-}inh)]$ (**4.2**). X-ray diffraction quality crystals for **4.4** were obtained by slow evaporation of its methanolic solution in air. Yield: 86 %. ^{51}V NMR (400 MHz, DMF/acetone–d_6 4:1, ppm): δ –502. Anal. calcd. for $C_{36}H_{26}N_8O_6V_2$ (768.52): C, 56.26; H, 3.41; N, 14.58 %. Found: C, 56.0; H, 3.5; N, 14.4 %.

4.2.3.7 [$V^{V}O(O_2)$(bzpy-tch)] (4.5)

An aqueous 30 % H_2O_2 (*ca.* 2 mL) was added drop wise to complex **4.3** (0.389 g, 0.5 mmol) dissolved in methanol (20 mL) with constant stirring at ambient temperature for 8 h. After reducing the solvent volume to *ca.* 10 mL it was kept for *ca.* 24 h where orange solid precipitated which was filtered off, washed with cold methanol (2 × 2 mL) and dried in air. Yield 70 %. ^{51}V NMR (400 MHz, DMF/acetone–d_6 4:1, ppm): δ –571. *Anal.* calcd. for $C_{17}H_{12}N_3O_4SV$ (405.30): C, 50.37; H, 2.98; N, 10.36; S, 7.91 %. Found: C, 50.7; H, 2.9; N, 10.2; S, 8.2 %.

4.2.3.8 [$V^{V}O(O_2)$(bzpy-inh)] (4.6)

Complex **4.6** was prepared analogously to **4.5**, taking 0.5 mmol of **4.4**. X-ray diffraction quality crystals for [$V^{V}O(O_2)$(bzpy-inh)]·0.5MeOH (**4.6**) were obtained by slow evaporation of its methanolic solution in air. Yield: 62 %. ^{51}V NMR (400 MHz, DMF/acetone–d_6 4:1, ppm): δ –570. Anal. calcd. for $C_{18}H_{13}N_4O_4V$ (400.26): C, 54.01; H, 3.27; N, 13.99 %. Found: C, 54.2; H, 3.2; N, 13.7 %.

4.2.3.9. PS–im[$V^{V}O_2$(bzpy-tch)] (4.7)

The polystyrene bound imidazole (Ps–im, 1.0 g) was suspended in DMF (10 mL) for 2 h prior to the reaction. A solution of [{$V^{V}O$(bzpy-tch)}$_2$(μ-O)$_2$] (**4.3**) (1.56 g, 2 mmol) in DMF (20 mL) was then added to the above suspension of PS–im and the mixture was heated in an oil bath for 24 h at *ca.* 90 ^{o}C with slow mechanical stirring. Then polystyrene bound PS–im[$V^{V}O_2$(bzpy-tch)] (**4.4**) was filtered and washed with DMF followed by hot methanol. It was dried at 120 ^{o}C in an air oven. Recovery yield: 95 %.

4.2.3.10. PS–im[$V^{V}O_2$(bzpy-inh)] (4.8)

Complex **4.8** was prepared analogously to **4.7**, replacing **4.3** by **4.4** (1.54 g, 2 mmol). Recovery yield: 90 %.

4.2.4. X-Ray crystal structure determination

Three-dimensional X-ray data were collected on a Bruker Kappa Apex CCD diffractometer at low temperature for **4.3**, **4.4**, and **4.6** by the ϕ-ω scan method. Reflections were measured from a hemisphere of data collected from frames each of them covering 0.3º in ω. Of the 55659 for **4.3**, 60921 for **4.4** and 34088 for **4.6** reflections measured, all were corrected for Lorentz and polarization effects and for absorption by multi-scan methods based on symmetry-equivalent and repeated reflections, 5018, 2965 and 2188 respectively, independent reflections exceeded the significance level ($|F|/\sigma|F|$) > 4.0. Complex scattering factors were taken from the program package SHELXTL [113]. The structures were solved by direct methods and refined by full matrix least-squares on F^2. In **4.3**, hydrogen atoms were located in difference Fourier map and left to refine freely. In **4.4**, hydrogen atoms were included in calculation positions and refined in the riding mode. In **4.6**, hydrogen atoms were located in difference Fourier map and left to refine freely, except for C(5), C(6), C(14) and C(16), which were included in calculation positions and refined in the riding mode. In **4.6**, hydrogen atoms of water molecule were located in difference Fourier map and fixed to oxygen atom. Refinements were done with allowance for thermal anisotropy of all non-hydrogen atoms. Further details of the crystal structure determination are given in Table 4.1. A final difference Fourier map showed no residual density outside: 0.565 and -0.836 e.Å^{-3} for **4.3** and 2.055, -0.709 e.Å^{-3} for **4.4** and 0.987 and -0.599 e.Å^{-3} for **4.6**. A weighting scheme w = $1/[\sigma^2(F_o^2) + (0.081100\ \ P)^2 + 0.219200\ P]$ for **4.3**, w = $1/[\sigma^2(F_o^2) + (0.129400\ P)^2 + 0.908600\ P]$ for **4.4** and w = $1/[\sigma^2(F_o^2) + (0.115100\ P)^2 + 0.000000\ P]$ for **4.6**, where P = $(|F_o|^2 + 2|F_c|^2)/3$, were used in the latter stages of refinement.

4.2.5. Catalytic oxidation of isoeugenol

The polymer anchored catalysts were dipped in acetonitrile for 2 h prior to the reaction. In a double neck round bottom flask, isoeugenol (0.82 g, 5 mmol) and 30 % H_2O_2 (1.13 g, 10 mmol) were mixed in 7 mL of acetonitrile and after addition of appropriate catalyst (20 mg) the reaction mixture was heated in an oil bath at 80 ^oC with

very slow mechanical stirring (to avoid crushing of polymer beads) for 4 h. To monitor the progress of the reaction, samples were taken out at every 30 min interval using a syringe and analyzed by a gas chromatograph equipped with a FID detector.

Table 4.1. Crystal data and structure refinement for $[\{V^{V}O(bzpy\text{-}tch)\}_2(\mu\text{-}O)_2]$ (**4.3**), for $[\{V^{V}O(bzpy\text{-}inh)\}_2(\mu\text{-}O)_2]$ (**4.4**) and for $[V^{V}O(O_2)(bzpy\text{-}inh)]\cdot 0.5MeOH$ (**4.6**).

	4.3	**4.4**	**4.6**
Formula	$C_{34}H_{24}N_6O_6S_2V_2$	$C_{36}H_{26}N_8O_6V_2$	$C_{18.5}H_{17}N_4O_{5.5}V$
Formula weight	778.59	768.53	434.3
T, *K*	100(2)	100(2)	100(2)
Wavelength, Å	0.71073	0.71073	0.71073
Crystal system	Triclinic	Monoclinic	Monoclinic
Space group	$P\bar{1}$	$P2_1/c$	$P2_1/c$
a/Å	8.3281(6)	14.6312(5)	10.2637(12)
b/Å	9.6580(8)	8.2122(3)	22.806(3)
c/Å	22.010(2)	14.4503(5)	8.1173(9)
α/°	81.235(6)	90	90
β/°	87.348(6)	110.765(2)	105.364(7)
γ/°	68.383(5)	90	90
V/Å^3	1626.5(2)	1623.48(10)	1832.2(4)
Z	2	2	2
F_{000}	792	784	892
D_{calc}/g cm^{-3}	1.590	1.572	1.574
μ/mm^{-1}	0.760	0.638	0.585
θ/ (°)	0.94 to 27.57	1.49 to 27.58	1.79 to 26.52
R_{int}	0.1076	0.0951	0.1672
Crystal size/ mm^3	0.22 × 0.09 × 0.06	0.25 × 0.18 × 0.08	0.14 × 0.09 × 0.07
Goodness-of-fit on F^2	1.028	1.088	1.030
$R_1[I>2\sigma(I)]$ [a]	0.0502	0.0698	0.0673
wR_2 (all data) [b]	0.1530	0.2035	0.2124
Largest differences peak and hole (eÅ^{-3})	0.565 and -0.836	2.055 and -0.709	0.987 and -0.599

[a] $R_1 = \Sigma ||F_o| - |F_c|| / \Sigma |F_o|$. [b] $wR_2 = \{\Sigma[w(|F_o|^2 - |F_c|^2)^2] / \Sigma[w(F_o^4)]\}^{1/2}$

4.3. Results and discussion

Scheme 4.2 provides an overview of the complexes described in this contribution and structural formulae of the complexes are based on their characterization by elemental analysis, spectroscopy (IR, UV/Vis, EPR, ^{1}H, ^{13}C and ^{51}V NMR) and for **4.3**, **4.4** and **4.6** by single crystal X–ray diffraction analysis.

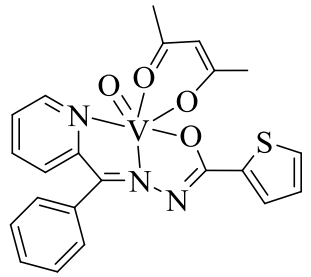

$[V^{IV}O(acac)(bzpy\text{-}tch)]$ (**4.1**)

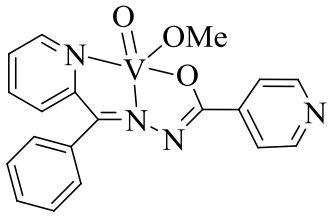

$[V^{IV}O(OMe)(bzpy\text{-}inh)]$ (**4.2**)

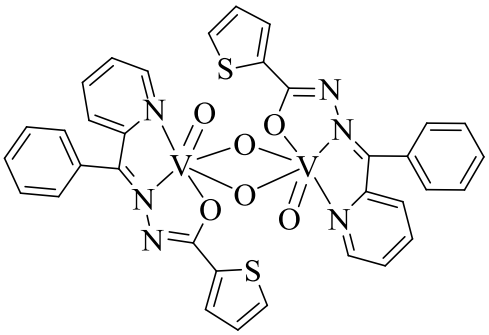

$[\{V^{V}O(bzpy\text{-}tch)\}(\mu\text{-}O_2)]$ (**4.3**)

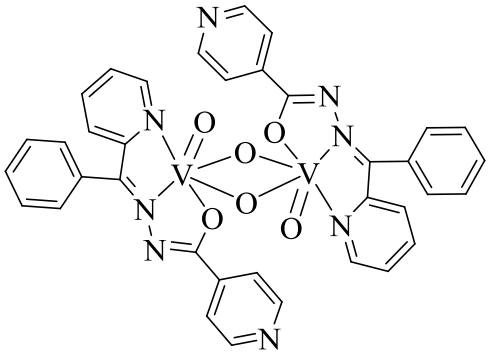

$[\{V^{V}O(bzpy\text{-}inh)\}(\mu\text{-}O_2)]$ (**4.4**)

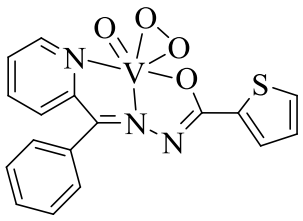

$[V^{V}O(O_2)(bzpy\text{-}tch)]$ (**4.5**)

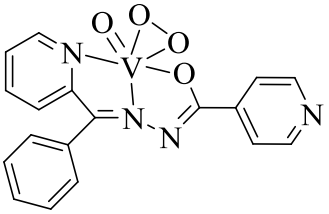

$[V^{V}O(O_2)(bzpy\text{-}inh)]$ (**4.6**)

Scheme 4.2. Proposed structure of complexes reported in this contribution.

4.3.1. Synthesis, Characterization and solid state characteristics

Precursor $[V^{IV}O(acac)_2]$ reacts with an equimolar amount of very similar ligands, Hbzpy-tch (**4.I**), and Hbzpy-inh (**4.II**) and gives two different types of complexes, $[VO^{IV}(acac)(bzpy\text{-}tch)]$ (**4.1**) (equation 4.1) and $[VO^{IV}(OMe)(bzpy\text{-}inh)]$ (**4.2**) (equation 4.2), respectively. However, their aerial oxidation in methanol gave

dioxidovanadium(V) complexes which on crystallization from methanol have formulae, $[\{V^{V}O(bzpy\text{-}tch)\}_2(\mu\text{-}O_2)]$ (**4.3**) (equation 4.3) and $[\{V^{V}O(bzpy\text{-}inh)\}_2(\mu\text{-}O_2)]$ (**4.4**) (equation 4.4). Here, either solvent or steric hindrance has no definite trend on the formulation of the complexes. However, all these dioxido complexes behave as monomer in solution. These complexes can also be prepared directly by reacting ligands with $[V^{IV}O(acac)_2]$ in methanol followed by aerial oxidation.

$$[V^{IV}O(acac)_2] + Hbzpy\text{-}tch \rightarrow [VO^{IV}(acac)(bzpy\text{-}tch)] + Hacac \quad (4.1)$$

$$[V^{IV}O(acac)_2] + Hbzpy\text{-}inh + MeOH \rightarrow [VO^{IV}(OMe)(bzpy\text{-}inh)] + 2Hacac \quad (4.2)$$

$$2[VO^{IV}(acac)(bzpy\text{-}tch)] + \tfrac{1}{2}\, O_2 + H_2O \rightarrow [\{V^{V}O(bzpy\text{-}tch)\}_2(\mu\text{-}O)_2] + 2Hacac \quad (4.3)$$

$$2[VO^{IV}(OMe)(bzpy\text{-}inh)] + \tfrac{1}{2}\, O_2 + H_2O \rightarrow [\{V^{V}O(bzpy\text{-}inh)\}_2(\mu\text{-}O)_2] + 2MeOH \quad (4.4)$$

Addition of H_2O_2 to the methanolic solutions of **4.3** and **4.4** yielded corresponding oxidomonoperoxidovanadium(V) complexes $[V^{V}O(O_2)(bzpy\text{-}tch)]$ (**4.5**) and $[V^{V}O(O_2)(bzpy\text{-}inh)]$ (**4.6**) (equation 5 considering **4.3** as a representative), respectively.

$$[\{V^{V}O(bzpy\text{-}tch)\}_2(\mu\text{-}O)_2] + 2H_2O_2 \rightarrow 2[V^{V}O(O_2)(bzpy\text{-}tch)] + 2H_2O \quad (4.5)$$

All the complexes are fairly soluble in methanol, DMF and DMSO. Reaction of $[\{V^{V}O(bzpy\text{-}tch)\}_2(\mu\text{-}O_2)]$ (**4.3**) and $[\{V^{V}O(bzpy\text{-}inh)\}_2(\mu\text{-}O_2)]$ (**4.4**) with PS-im in DMF and ethyl acetate in the presence of triethylamine resulted in the formation of polymer-suported dioxidovanadium(V) complexes PS–im$[V^{V}O_2(bzpy\text{-}tch)]$ (**4.7**) and PS–im$[V^{V}O_2(bzpy\text{-}inh)]$ (**4.8**), respectively. Here nitrogen of the imidazolomethylpolystyrene covalently binds with vanadium of complex; Scheme 4.3. The free chloromethyl groups, present if any, of PS do not coordinate to the vanadium precursor. The metal ion loadings calculated from the obtained vanadium content (Table

4.2) for the polymer-supported complexes are also close to the value determined by thermogravimetric analyses (vide infra).

Table 4.2. Data of metal ion loading in polymer-anchored complexes

Complexes	Metal ion loading[a] (mmol g^{-1} of resin) (obtained by ICP)	Metal ion loading[a] (mmol g^{-1} of resin) (obtained by TGA)
PS–im[$V^{V}O_2$(bzpy-tch)] (**4.7**)	0.224	0.24
PS–im[$V^{V}O_2$(bzpy-inh)] (**4.8**)	0.248	0.27

[a]Metal ion loading = $\frac{\text{Observed metal \%} \times 10}{\text{Atomic mass of metal}}$

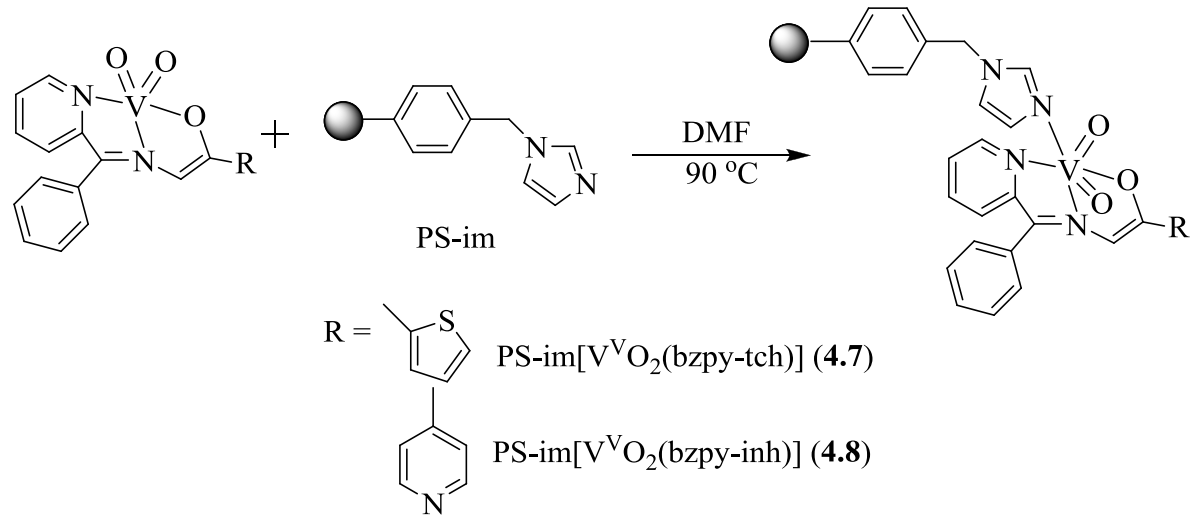

Scheme 4.3. Synthetic scheme for the isolation of polymer-supported complexes. Only monomeric form of VO_2-complexes are shown.

4.3.2. TGA studies

Thermal studies of $V^{V}O_2$-complexes and their polymer-supported analogues, all dried at *ca.* 100 °C, were carried out to see their thermal stability. Both types of complexes are stable up to *ca.* 160 °C. The $V^{V}O_2$-complexes complexes start decomposing thereafter in multiple exothermic but overlapping steps and complete above *ca.* 520 °C to give V_2O_5 as the final product. The observed V_2O_5 contents of 23.8 % (for [{V^{V}O(bzpy-tch)}$_2$(μ-O_2)] (**4.3**) and 23.3 % (for [{V^{V}O(bzpy-inh)}$_2$(μ-O_2)] (**4.4**) match closely with the calculated values of 23.4 and 23.7 %, respectively. Further,

small weight loss of 0.2–0.4 % occurs between 520–900 ^{o}C which was ignored. The polymer-supported complexes PS–im[{$V^{V}O_2$(bzpy-tch)] (**4.7**) and PS–im[$V^{V}O_2$(bzpy-inh)] (**4.8**) are relatively better thermally stable but show weight loss of 1–2 % above *ca.* 120 ^{o}C possibly due to residual moisture absorbed. The complete decomposition of complexes along with polymer occurs exothermically in two overlapping steps between *ca.* 200–500 ^{o}C. Again only very small loss (0.2–0.4 %) in weight occurs between 500–900 ^{o}C. As polymer-support in only organic based in these complexes, the stable content indicates the formation of V_2O_5. The vanadium content from their V_2O_5 contents calculated for these complexes are also reported in Table 4.3, being in agreement with the values obtained by ICP-MS.

4.3.3. FE–SEM and EDAX analysis

FE–SEM images of PS–im and polymer anchored complexes **4.7** and **4.8** show major morphological changes after anchoring; Figure 4.1. Darkening of beads, significant increase in bead size and change in surface morphology of **4.7** and **4.8** as compared to PS–im were observed by FE–SEM studies. The presence of peak for nitrogen in EDAX of PS–im confirms binding of imidazole to chloromethylated polystyrene. The peaks due to O and V other than N also confirm the presence of part of the vanadium complex on the surface of PS-im beads; Figure 4.2. The average vanadium content obtained by EDAX by spotting two particular places was 0.20$\pm$0.02 mmol g^{-1} of resin for **4.7** and 0.21$\pm$0.03 mmol g^{-1} of resin for **4.8** which is almost similar to the data of ICP-MS and TGA.

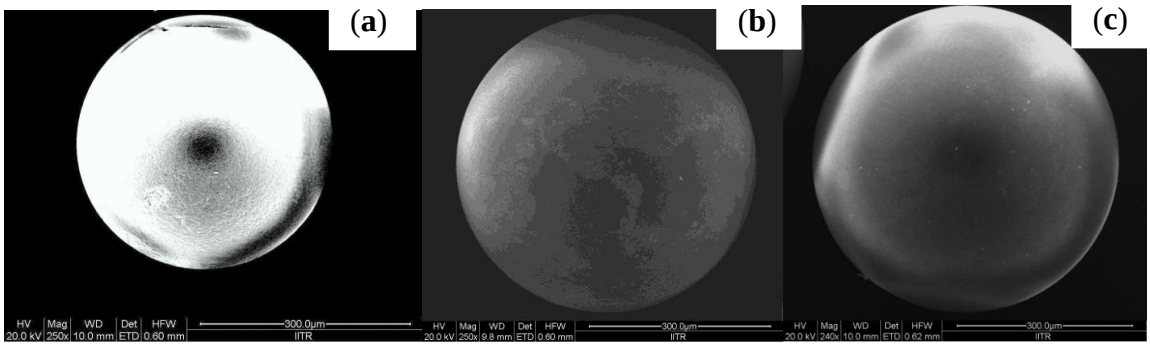

Figure 4.1. Field emission scanning electron micrographs of PS–im (**a**), PS–[$V^{V}O_2$(bzpy-tch)] (**b**) and PS–[$V^{V}O_2$(bzpy-inh)] (**c**).

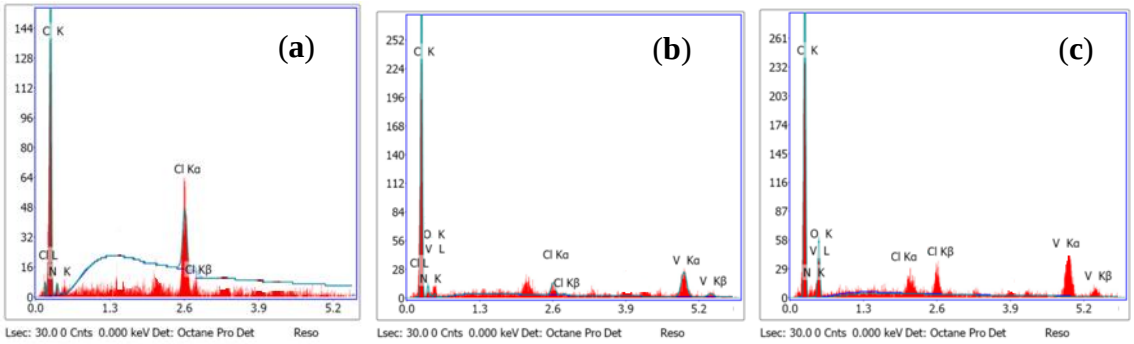

Figure 4.2. Energy dispersive x-ray analysis graphs of PS–im (**a**), PS–[$V^{V}O_2$(bzpy-tch)] (**b**) and PS–[$V^{V}O_2$(bzpy-inh)] (**c**).

4.3.4. AFM study

AFM images (Figure 4.3, left) of imidazolomethylpolystyrene beads show morphological changes before and after complex anchoring. The surface roughness and mean height as measured by AFM are 83.1102 nm and 362.523 nm, respectively for PS–im whereas these values were decreased after reaction of PS–im with dioxidovanadium(V) complexes **4.3** and **4.4** which confirm that the complexes are immobilized in the pores of PS–im beads thereby reducing the surface roughness (surface roughness and mean height for PS–im[$V^{V}O_2$(bzpy-tch)] (**4.7**) are 25.6553 nm, 149.738 nm, respectively, and for PS–im[$V^{V}O_2$(bzpy-inh)] (**4.8**) are 19.7321 nm, 100.3285 nm, respectively) (Figure 4.3, right). Comparatively lower surface roughness and mean height of **4.8** than **4.7** indicates more complex anchoring in the pores of **4.8**,

this observation is also in agreement with the vanadium content obtained from ICP-MS, TGA and EDAX.

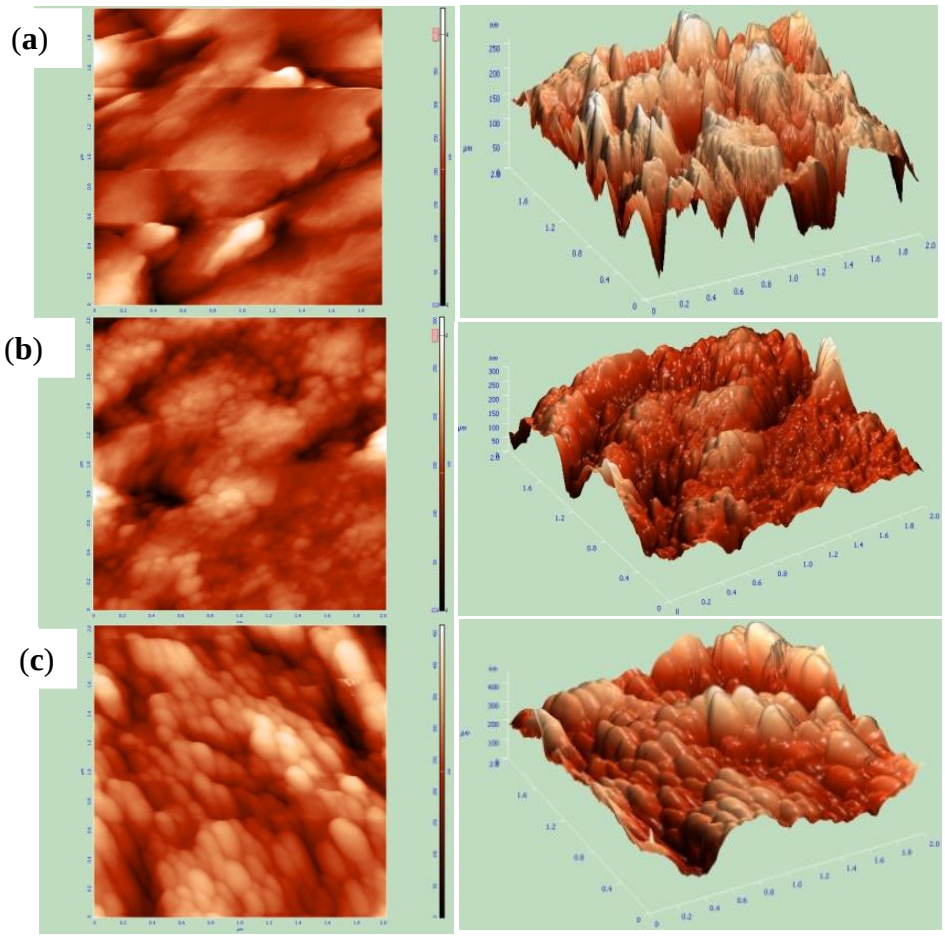

Figure 4.3. AFM images (left) and respective 3d-views (right) of PS–im (**a**), PS–im[$V^{V}O_2$(bzpy-tch)] (**b**) and PS–im[$V^{V}O_2$(bzpy-inh)] (**c**).

4.3.5. Molecular structure of [{$V^{V}O$(bzpy-tch)}$_2$(μ-O)$_2$] (4.3), [{$V^{V}O$(bzpy-inh)}$_2$(μ-O)$_2$] (4.4) and [$V^{V}O(O_2)$(bzpy-inh)]·0.5MeOH (4.6)

The asymmetric unit of **4.3** contains two half of two dinuclear complexes and only one half of one dinuclear complex in the structure of **4.4**. The asymmetric unit of **4.6** contains one peroxido complex and half methanol molecule. In all three complexes, ligands bzpy-tch and bzpy-inh act as ONN donors. Table 4.2 includes selected bond lengths and angles.

The complex **4.3** crystallized from DMF and **4.4** from methanol as yellow prisms. Figures 4.4 and 4.5 show their ORTEP representation. X-ray structure analysis

of **4.4** shows two complexes with difference twist of the phenyl group bound to pyridine group (see Figure 4.5). The structures of **4.3** and **4.4** show that each V^V centre is six-coordinated in a distorted octahedral geometry, with terminal oxygen atoms, O3 (O3A by symmetry transformation) and O5, only in compound **4.3,** (O5A by symmetry transformation), and two bridging oxygen atoms, O2 (by symmetry transformation O2A) and O6, only in compound **3.3,** (O6A by symmetry transformation). The V1–O3 and V2–O5 bonds have typical V=O bonds, with strong π-bonding, and the distances are 1.613(2) and 1.615(2) Å, respectively. O2 is strongly coordinated to V1 [V1–O2, 1.655(2) Å in **4.3** and 1.662(2) Å in **4.4**] and O6 to V2 [V2–O6, 1.662(2) Å in **4.3**]. O2A is weakly associated with V1 [V1–O2A, 2.358(2) Å in **4.3** and 2.340(2) Å in **4.4**] and O6A with V2 [V2–O6A, 2.327(2) Å in **4.3**] (see Figure 4.4. and Figure 4.5.), which reinforces that the V-μ-oxido bonds trans to the azomethine groups show the π-bonding character. The remaining three coordination sites are occupied by the pyridine N atoms [V1–N1, 2.104(3) Å in **4.3** and 2.113(3) Å in **4.4** and V2–N4, 2.110(3) Å in **4.3**], azomethine N atoms [V1–N2, 2.119(3) Å in **4.3** and 2.128(3) in **4.4**, and V2–N5, 2.122(3) Å in **4.3**] and ketonic O atoms [V1–O1, 1.956(2) Å in **4.3** and 1.972(2) Å in **4.4**, and V2–O4, 1.963(2) Å in **4.3**]. The V–V distances are V1-V1A, 3.158 Å and V2-V2A, 3.143 Å in **4.3**, and V1-V1A, 3.132 Å in **4.4**, and the O3–V1–O2 angles are, 107.21(12)º in **4.3** and 107.01(11)º in **4.4**, and O(5)-V(2)-O(6) is 106.55(12)º in **4.3**, also similar to those observed in other compounds [28,165]. Within the possible configurations for the $[VO(\mu\text{-}O)_2VO]^+$ core in complexes consisting of two edge-sharing octahedrally coordinated oxidovanadium centers, we can classify these cores as *anti*-coplanar [166,167]. The vanadium atoms are displaced by about 0.0923 Å in **4.3** and about 0.2007 in **4.4** from the planes constituted for the atoms (C1, C2, C3, N1, N2, N3, C14, C15, C16, C17 in **4.3** and C1, C2, C3, N1, N2, N3, C15, C16, C17, C18 in **4.4**), which present a deviation from planarity of 0.0575(26) Å in **4.3** and 0.0518(24) in **4.4**.

The complex of **4.6** crystallizes from methanol as orange prisms and Figure 4.6 shows an ORTEP representation. The vanadium atom is in the oxidation state V. In the molecular structure, the vanadium center adopts a distorted seven-coordinated

pentagonal bypyramidal geometry with the bzpy-inh ligand coordinated through the pyridine N atom [V1–N1, 2.146(4) Å], azomethine N atom [V1–N2, 2.106(4) Å] and ketonic O atom [V1–O1, 2.019(3) Å]. Terminal oxygen atom, O3 with V(1)-O(3) of 1.593(3) Å has strong π-bonding. One water molecule and two peroxide oxygen atoms, O4 and O5, are also coordinated to the vanadium center. The peroxide O-O distance of 1.443(4) Å lies within the range (1.38-1.45 Å) of the majority of peroxide compounds [116]. The V-O_{water} bond, which is trans to the oxido atom, is significantly longer [V1-O2, 2.255(3) Å]. The vanadium atom is displaced by about 0.1288 Å from the plane constituted for the atoms (C1, C2, C3, N1, N2, N3, C15, C16, C17, C18), which presents a deviation from planarity of 0.0680(40) Å. Intermolecular hydrogen bonds occur between coordinated water molecule and other complexes in the crystal packing (see Table 4.3).

Table 4.3. Bond lengths [Å] and angles [°] for [{$V^{V}O$(bzpy-tch)}$_2$(μ-O)$_2$] (**4.3**), for [{$V^{V}O$(bzpy-inh)}$_2$(μ-O)$_2$] (**4.4**) and for [$V^{V}O(O_2)$(bzpy-inh)(H_2O)]·0.5MeOH (**4.6**).

Bond lengths	**4.3**	**4.4**	**4.6**
V(1)-O(1)	1.956(2)	1.972(2)	2.019(3)
V(1)-O(2)	1.655(2)	1.662(2)	2.255(3)
V(1)-O(3)	1.613(2)	1.615(2)	1.593(3)
V(1)-O(4)			1.876(3)
V(1)-O(5)			1.855(3)
V(1)-N(1)	2.104(3)	2.113(3)	2.146(4)
V(1)-N(2)	2.119(3)	2.128(3)	2.106(4)
V(1)-O(2A)#1	2.358(2)	2.340(2)	
V(2)-O(5)	1.615(2)		
V(2)-O(6)	1.662(2)		
V(2)-O(4)	1.963(2)		
V(2)-N(4)	2.110(3)		
V(2)-N(5)	2.122(3)		
V(2)-O(6A)#2	2.327(2)		
O(4)-O(5)			1.443(4)
Bond angles	**4.3**	**4.4**	**4.6**

O(3)-V(1)-O(2)	107.21(12)		107.01(11)	169.46(15)
O(3)-V(1)-O(1)	98.48(11)		98.89(10)	97.42(16)
O(2)-V(1)-O(1)	105.34(11)		105.19(10)	85.42(13)
O(3)-V(1)-N(1)	95.78(11)		93.48(10)	91.54(16)
O(2)-V(1)-N(1)	98.47(11)		100.21(10)	80.68(14)
O(1)-V(1)-N(1)	147.06(10)		146.93(9)	146.05(14)
O(3)-V(1)-N(2)	101.60(11)		98.89(11)	92.85(16)
O(2)-V(1)-N(2)	150.73(11)		153.68(11)	78.14(14)
O(1)-V(1)-N(2)	74.86(10)		74.70(9)	73.95(14)
N(1)-V(1)-N(2)	73.26(10)		73.14(9)	72.94(15)
O(3)-V(1)-O(5)				103.52(17)
O(3)-V(1)-O(4)				104.02(17)
O(5)-V(1)-O(4)				45.49(14)
O(5)-V(1)-O(1)				126.60(15)
O(4)-V(1)-O(1)				82.04(13)
O(5)-V(1)-N(2)				150.53(16)
O(4)-V(1)-N(2)				152.26(16)
O(5)-V(1)-N(1)				82.16(15)
O(4)-V(1)-N(1)				127.35(14)
O(5)-V(1)-O(2)				82.56(14)
O(4)-V(1)-O(2)				86.39(14)
O(3)-V(1)-O(2A)#1	174.81(10)	#3	174.22(10)	
O(2)-V(1)-O(2A)#1	77.63(11)	#3	78.32(10)	
O(1)-V(1)-O(2A)#1	81.79(9)	#3	81.57(8)	
N(1)-V(1)-O(2A)#1	81.46(9)	#3	83.23(9)	
N(2)-V(1)-O(2A)#1	73.42(9)	#3	75.63(8)	
O(5)-V(2)-O(6)	106.55(12)			
O(5)-V(2)-O(4)	98.91(11)			
O(6)-V(2)-O(4)	105.87(10)			
O(5)-V(2)-N(4)	95.11(11)			
O(6)-V(2)-N(4)	99.38(11)			
O(4)-V(2)-N(4)	146.09(10)			
O(5)-V(2)-N(5)	100.73(12)			
O(6)-V(2)-N(5)	152.29(11)			
O(4)-V(2)-N(5)	74.06(10)			

N(4)-V(2)-N(5)	73.07(10)		
O(5)-V(2)-O(6A)#2	175.32(10)		
O(6)-V(2)-O(6A)#2	77.28(10)		
O(4)-V(2)-O(6A)#2	82.39(9)		
N(4)-V(2)-O(6A)#2	81.49(9)		
N(5)-V(2)-O(6A)#2	75.25(9)		
V(1)-O(2)-V(1A)#1	102.37(11)	#3	101.68(10)
V(2)-O(6)-V(2A)#2	102.72(10)		

Symmetry transformations used to generate equivalent atoms:

#1 -x+1,-y+1,-z+2 #2 -x+1,-y+2,-z+1 #3 -x+1,-y,-z+1

Table 4.4. Hydrogen bonds for $[V^{V}O(O_2)(bzpy\text{-}inh)]\cdot 0.5MeOH$ (**4.6**).

D-H...A	d(D-H)	d(H...A)	d(D...A)	<(DHA)
O(2)-H(2OA)...N(4)#4	1.03	1.77	2.781(5)	167.3
O(2)-H(2OB)...O(4)#5	1.01	1.87	2.863(5)	170.1
O(2)-H(2OB)...O(5)#5	1.01	2.44	3.345(5)	149.3

Symmetry transformations used to generate equivalent atoms:

#4 -x,-y+1,-z #5 -x+1,-y+1,-z+1

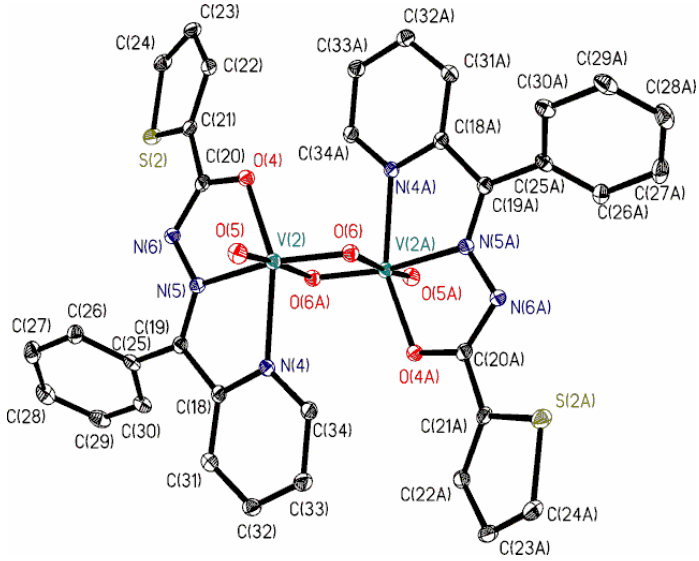

Figure 4.4. ORTEP plot of complex $[\{V^{V}O(bzpy\text{-}tch)\}_2(\mu\text{-}O)_2]$ (**4.3**) All the non-hydrogen atoms are presented by their 30 % probability ellipsoids. Hydrogen atoms are omitted for clarity.

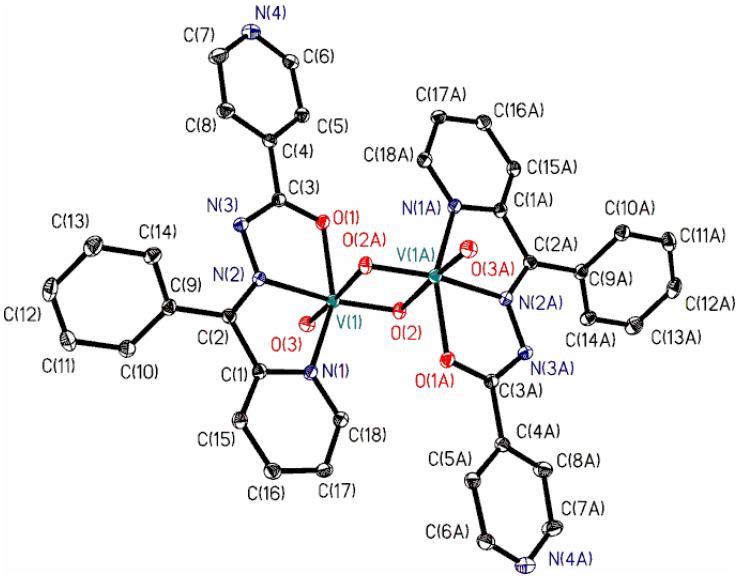

Figure 4.5. ORTEP plot of complex $[\{V^{V}O(bzpy\text{-}inh)\}_2(\mu\text{-}O)_2]$ (**4.4**). All the non-hydrogen atoms are presented by their 30 % probability ellipsoids. Hydrogen atoms are omitted for clarity.

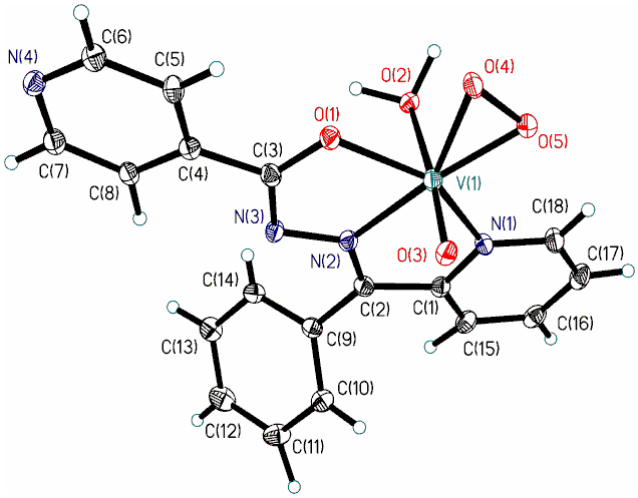

Figure 4.6. ORTEP plot of complex $[V^{V}O(O_2)(bzpy\text{-}inh)]$ (**4.6**). All the non-hydrogen atoms are presented by their 30 % probability ellipsoids. Hydrogen atoms are omitted for clarity.

4.3.6. IR spectral studies

A partial list of IR spectral data of ligands and complexes is presented in the experimental section. All the oxidovanadium(IV) complexes exhibit one sharp band at 948–989 cm^{-1} due to ν(V=O) mode. The dinuclear $[(V^{V}O)_2(\mu\text{-}O)_2]^{2+}$ complexes **4.3** and **4.4** exhibit one sharp band at 936 cm^{-1} due to ν(V=O) and a broad band at 856–870 cm^{-1} due to ν[V–(μ-O)–V]. The mononuclear $[V^{V}O(O_2)]^{+}$ complexes **4.5** and **4.6** exhibit a sharp band at 958–967 cm^{-1} due to ν(V=O) mode. In addition they exhibit three active vibrational bands at 920–923, 661–662 and 571–575 cm^{-1} due to peroxide moiety which can be assigned due to the O–O intra stretching, asymmetric $V(O_2)$ stretching and symmetric $V(O_2)$ stretching, respectively. All these signatures indicate the η^2–coordination of the peroxido group.

The IR spectra of the ligands exhibit three sharp bands at 3053–3062, 1667–1690 and 1635–1637 cm^{-1} due to ν(NH), ν(C=O) (of the hydrazide moiety) and ν(C=N) (azomethine), respectively. The first two bands are indicative of their ketonic nature in the solid state. Absence of these bands in the IR spectra of all complexes indicates their enolisation and replacement of H by the metal ion. The ν(C=N) undergoes to lower wave number in complexes, indicating the coordination of the azomethine nitrogen to

the vanadium ion. All polymer anchored complexes exhibit spectral patterns very similar to mononuclear $[V^{V}O_2]^{+}$ complexes but with relatively weak intensity. The coordination of pyridinic nitrogen of benzoylpyridine residue to vanadium could not be assigned unequivocally due to the complexity of the spectra in the relevant region. However, in the light of X-ray single crystal study (vide supra) it is clear that ring nitrogen take part in coordination.

Table 4.5. IR spectral data (cm^{-1}) of ligands and complexes.

S. No.	Compounds	ν (NH)	ν (C=O)	ν (C=N)	ν (V=O)/ [V-(μ-O)-V]
1	Hbzpy-tch (**4.I**)	3053	1667	1637	-
2	Hbzpy-inh (**4.II**)	3062	1690	1635	-
3	$[VO^{IV}(acac)(bzpy\text{-}tch)]$ (**4.1**)	-	-	1593	948
4	$[VO^{IV}(OMe)(bzpy\text{-}inh)]$ (**4.2**)	-	-	1589	989
5	$[\{V^{V}O(bzpy\text{-}tch)\}_2(\mu\text{-}O_2)]$ (**4.3**)	-	-	1591	936, 856
6	$[\{V^{V}O(bzpy\text{-}inh)\}_2(\mu\text{-}O_2)]$ (**4.4**)	-	-	1590	936, 870
7	$[V^{V}O(O_2)(bzpy\text{-}tch)]$ (**4.5**)	-	-	1586	967
8	$[V^{V}O(O_2)(bzpy\text{-}inh)]$ (**4.6**)	-	-	1585	958
9	PS–im$[V^{V}O_2(bzpy\text{-}tch)]$ (**4.7**)	-	-	1609	917
10	PS–im$[V^{V}O_2(bzpy\text{-}inh)]$ (**4.8**)	-	-	1609	940

***** Bands due to peroxide moiety: Complex **4.5**: 923, 662, 571 cm^{-1}. Complex **4.6**: 920, 661, 575 cm^{-1}.

4.3.7. Electronic spectral studies

Electronic absorption spectra for all the ligands and neat complexes were recorded in methanol; spectra of visible region for oxidovanadium(IV) complexes were recorded in DMF. Figure 4.7 and 4.8 provide spectra of oxidoperoxido and polymer-supported complexes. The absorption maxima with their extinction coefficients (wherever possible) are given in Table 4.6. The ligand Hbzpy-inh (**4.II**) displays three bands at 203, 265 and 317 nm while Hbzpy-tch (**4.I**) exhibits one additional band at 247

nm along with the above bands at nearly same positions. These bands are assignable to φ → φ*, π→ π* and n → π*, transitions; an additional band at 247 nm is probably a split band of π→ π* transition. These ligand bands are also observable in complexes with some variations in their positions. All the complexes display a medium intensity band in the visible region at *ca.* 400 nm which is assigned to a ligand-to-metal charge-transfer (LMCT) transition. In addition, $V^{IV}O$-complexes display two medium intensity bands at 525 and 760 nm in **4.1** while at 645 and 805 nm in **4.2** which are assigned to d–d transition. Oxidoperoxidovanadium(V) complexes exhibit LMCT bands at same position as observed in the corresponding $V^{V}O_2$-complexes. The intensity of the bands of the polymer-supported complexes is, in general, poor but they exhibit all bands at nearly same position as observed for the corresponding $V^{V}O_2$-complexes. All these suggest the immobilization of these $V^{V}O_2$-complexes onto polymer support.

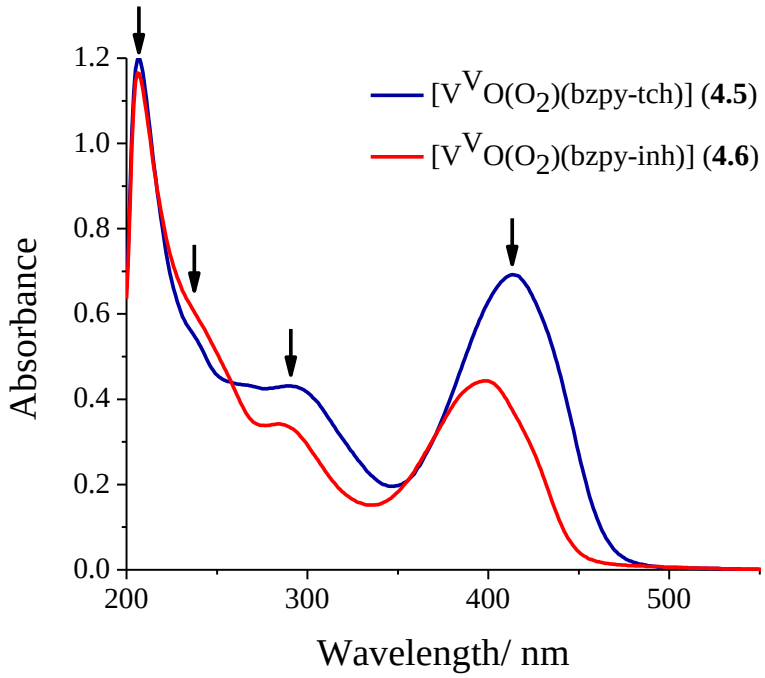

Figure 4.7. Electronic spectra of oxidoperoxidovanadium(V) complexes recorded in methanol.

Table 4.6. Electronic spectral data of ligands and complexes

Compounds	Solvent	λ_{max}/nm (ε/M^{-1} cm^{-1})
Hbzpy-tch (**4.I**)	MeOH	203 (2.73×10^4), 247 (1.83×10^4), 271 (1.85×10^4), 320 (2.15×10^4)
Hbzpy-inh (**4.II**)	MeOH	203 (2.57×10^4), 265 (1.45×10^4), 317 (0.59×10^4)
$[VO^{IV}(acac)(bzpy\text{-}tch)]$ (**4.1**)	MeOH DMF	206 (1.40×10^4), 271(1.44×10^4), 306 (1.37×10^4), 402 (0.16×10^4) 525 (0.74×10^2), 766 (0.16×10^2)
$[VO^{IV}(OMe)(bzpy\text{-}inh)]$ (**4.2**)	MeOH DMF	208 (2.93×10^4), 222 (3.06×10^4), 272 (1.79×10^4), 340 (1.52×10^4), 420 (0.50×10^4), 645 (0.91×10^2), 805 (0.15×10^2)
$[\{V^{V}O(bzpy\text{-}tch)\}_2(\mu\text{-}O_2)]$ (**4.3**)	MeOH	205 (2.50×10^4), 240 (1.60×10^4), 279 (1.34×10^4), 306 (1.50×10^4), 418 (1.05×10^4)
$[\{V^{V}O(bzpy\text{-}inh)\}_2(\mu\text{-}O_2)]$ (**4.4**)	MeOH	206 (1.22×10^4), 238 (sh) (0.75×10^4), 256 (w) (0.67×10^4), 306 (1.15×10^4), 405 (0.61×10^4),
$[V^{V}O(O_2)(bzpy\text{-}tch)]$ (**4.5**)	MeOH	206 (3.45×10^4), 240 (1.41×10^4), 290 (1.15×10^4), 415 (1.70×10^4)
$[V^{V}O(O_2)(bzpy\text{-}inh)]$ (**4.6**)	MeOH	206 (3.83×10^4), 249 (1.55×10^4), 283 (1.04×10^4), 400 (1.24×10^4)
PS–im$[V^{V}O_2(bzpy\text{-}tch)]$ (**4.7**)	Nujol	235, 270, 308, 395
PS–im$[V^{V}O_2(bzpy\text{-}inh)]$ (**4.8**)	Nujol	231, 265, 309, 380

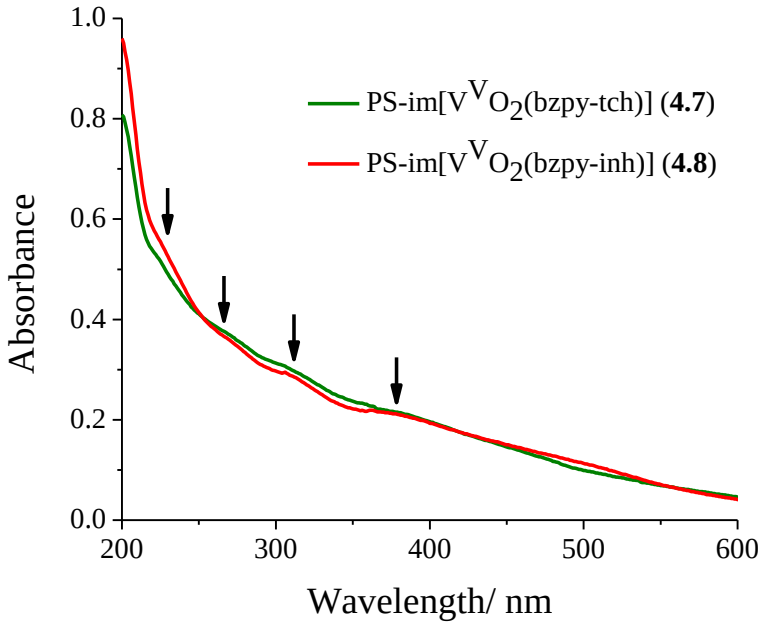

Figure 4.8. Electronic spectra of polymer-supported dioxidovanadium(V) complexes after dispersing in Nujol.

4.3.8. NMR spectral studies

4.3.8.1. ^{1}H NMR spectral studies

The mode of the coordination of the ligands was also confirmed by studying ^{1}H NMR chemical shifts of the ligands and complexes. ^{1}H NMR spectra (Figures 4.9 – 4.12) were recorded in DMSO–d_6 and the data pertaining to ligands as well as complexes are presented in Table 4.7. A broad signal appearing at δ value 8.94 and 10.16 ppm in Hbzpy-tch (**4.I**) and Hbzpy-inh (**4.II**), respectively due to –NH– proton disappears in the spectra of the complexes which demonstrate the enolization of the NH group and consequent replacement of H and coordination of the enolate oxygen. Signals for aromatic protons of the ligands and complexes appear within the expected region but substantial downfield shift was observed for some signals in the complexes. In dioxidovanadium(V) a downfield shift of $\Delta\delta$ = 0.83 ppm (in **4.3**) and 0.24 ppm (in **4.4**) in the signal of the protons adjacent to pyridyl nitrogen (of bzpy) in comparison to the free ligand confirms its coordination. In oxidoperoxiovanadium(V) complexes signal for

the same proton appears at more downfield shift ($\Delta\delta$ = 0.86 ppm in **4.5** and 1.03 ppm in **4.6**) which can be attributed to the presence of peroxide moiety.

Table 4.7. ^{1}H NMR spectral data of ligand and complexes

Compounds	–NH	Aromatic H		
		(pyridyl ring)$_{bzpy}$	(phenyl ring)$_{bzpy}$	(pyridyl ring)$_{inh}$/ (thiophene ring)$_{tch}$
Hbzpy-tch (**4.I**)	8.94	8.06-8.02(m, 1H), 7.58-7.56(m, 2H), 7.40-7.36(m, 1H)	7.65-7.62(m, 2H), 7.52-7.51(m, 3H)	7.99-7.95(m, 2H), 7.26-7.25(m, 1H)
Hbzpy-inh (**4.II**)	10.16	8.68-8.67(m, 1H), 8.056-8.024(m, 1H), 7.98-7.97(d, 1H), 7.96-7.94(m, 1H)	7.65-7.63(m, 2H), 7.53-7.50 (m, 3H)	8.71-8.69(d, 2H), 7.74-7.73(d, 2H)
[{$V^{V}O$(bzpy-tch)}$_2$(μ-O)$_2$] (**4.3**)	–	8.89-8.88(d, 1H), 8.28-8.24(m, 1H), 7.82-7.80(m, 2H)	7.78-7.76(m, 1H), 7.68-7.65(m, 4H)	7.87-7.86(d, 1H), 7.71-7.70(d, 1H), 7.20-7.18(m,1H)
[{$V^{V}O$(bzpy-inh)}$_2$(μ-O)$_2$] (**4.4**)	–	8.92-8.91(d, 1H), 8.31-8.28(m, 1H), 7.87-7.86(d, 1H), 7.86-7.85(m, 1H)	7.83-7.80(m, 1H), 7.73-7.70(m, 4H)	8.72-8.71(d, 2H), 7.78-7.76(d, 2H)
[$V^{V}O(O_2)$(bzpy- tch)] (**4.5**)	–	9.69-9.68(d,1H), 8.30-8.27(m, 1H), 7.81-7.77(m, 2H)	7.66-7.62(m, 5H)	7.96-7.93(m, 1H), 7.61-7.59(d, 1H), 7.21-7.19(m, 1H)
[$V^{V}O(O_2)$(bzpy- inh)] (**4.6**)	–	9.71-9.72(d, 1H), 8.33-8.28(m, 1H), 8.01-7.99(m, 1H), 7.70-7.68(m, 1H)	7.67- 7.65(m, 5H)	8.74-8.73(d, 2H), 7.90-7.89(d, 2H)

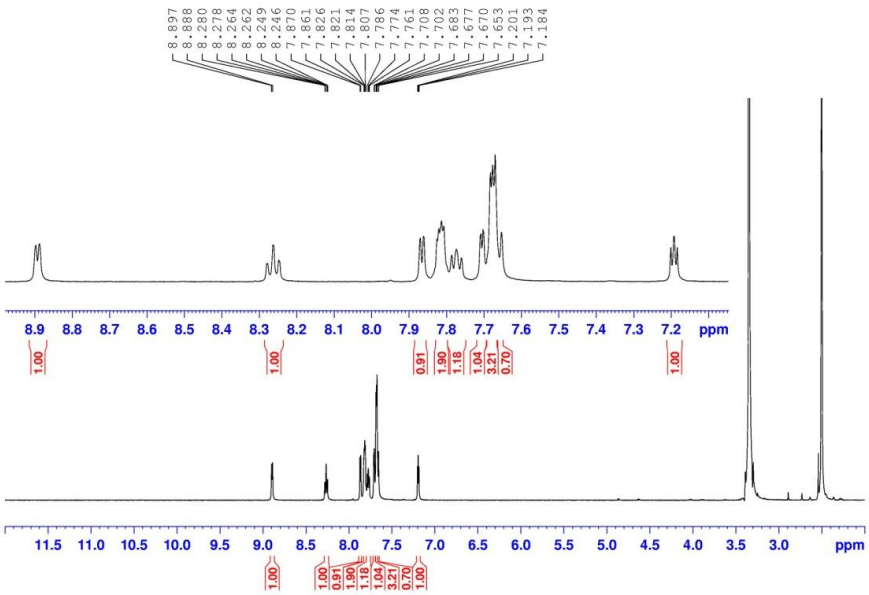

Figure 4.9. ^{1}H NMR spectrum of [{$V^{V}O$(bzpy-tch)}$_2$(μ-O)$_2$] (**4.3**).

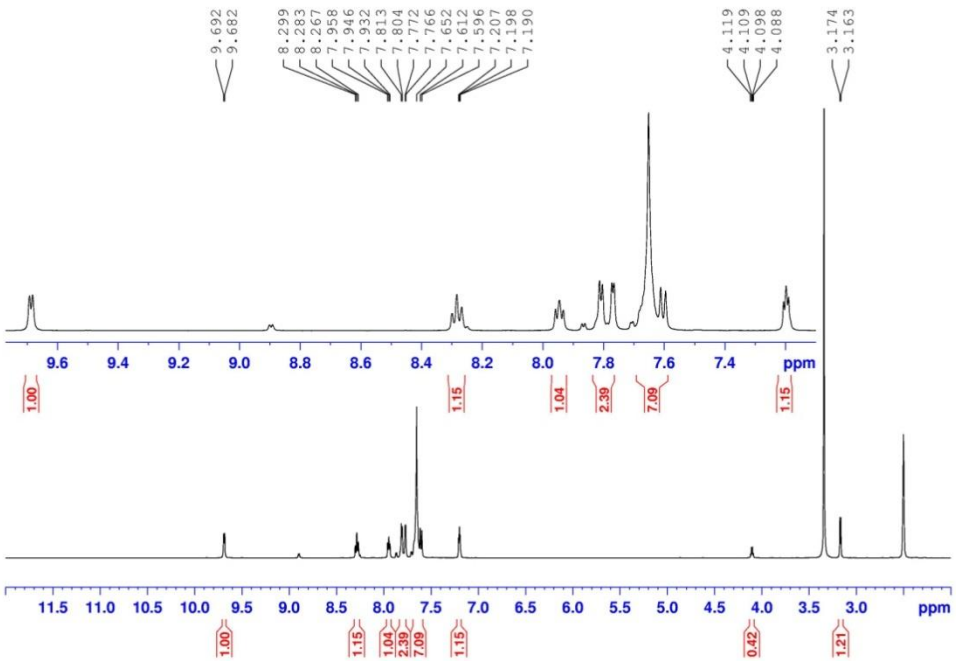

Figure 4.10. ^{1}H NMR spectrum of [$V^{V}O(O_2)$(bzpy-tch)] (**4.5**).

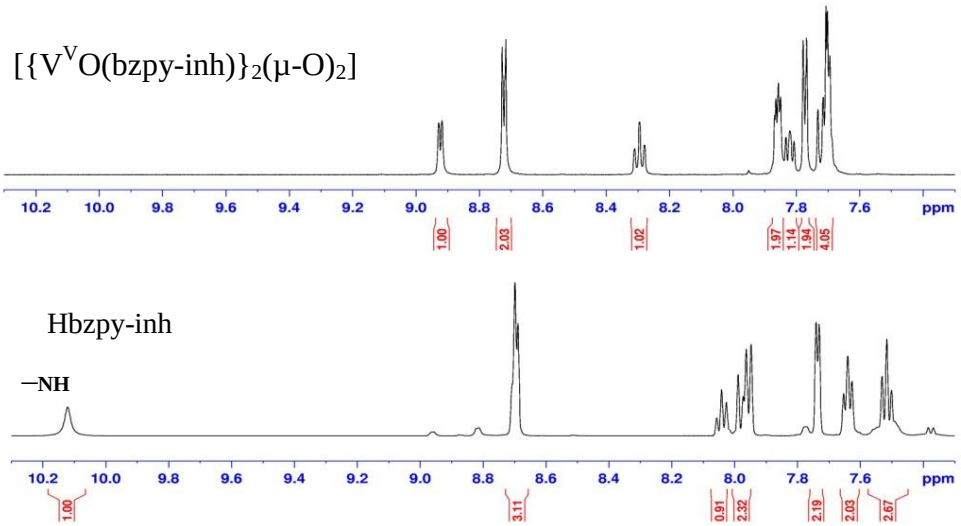

Figure 4.11. ^{1}H NMR spectra of (Hbzpy-inh) (**4.II**) and [{$V^{V}O$(bzpy-inh)}$_2$(μ-O)$_2$] (**4.4**).

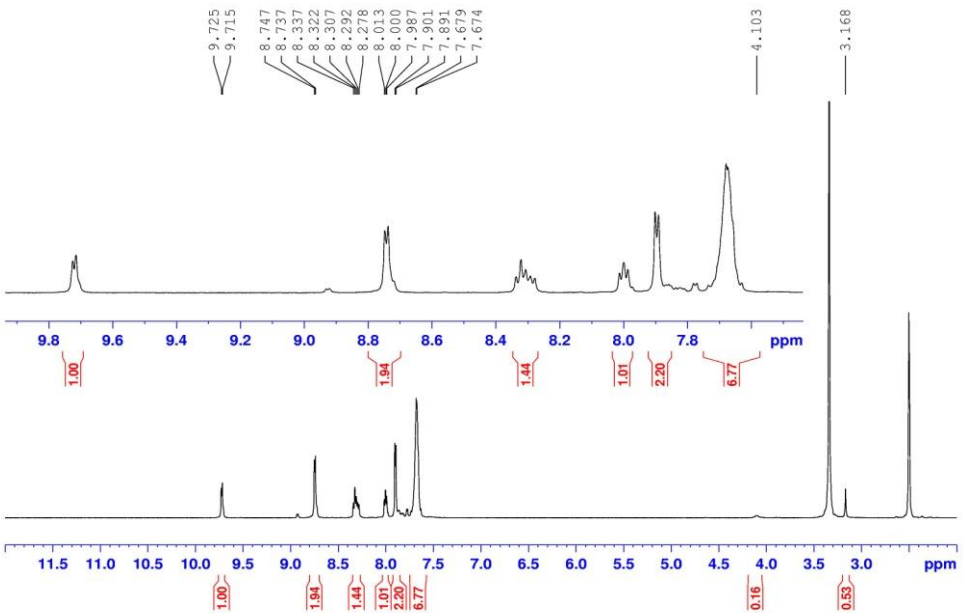

Figure 4.12. ^{1}H NMR spectrum of [$V^{V}O(O_2)$(bzpy-inh)] (**4.6**).

4.3.8.2. ^{13}C NMR spectral studies

The coordinating modes of ligands were further supported by the study of coordination-induced ^{13}C NMR chemical shifts (Figures 4.13 – 4.16). ^{13}C NMR signals were recorded in DMSO–d_6 for ligands and complexes and are assigned in Table 4.8 and 4.9 A significant downfield shift, $\Delta\delta$ = [δ(complex) – δ(ligand)] was observed in the signals of the carbon atoms in the vicinity of the coordinating atoms. Coordination of the enolate oxygen was indicated by a large downfield shift, $\Delta\delta$ = 20.44 ppm in the signal of enolate carbon i.e. C3 in case of **4.3** and $\Delta\delta$ = 23.62 ppm in case of **4.4** [118]. Similarly, the peak due to azomethine carbon i.e. C2 also appeared at lower field in the spectrum of **4.3** and **4.4** as compared to the ligands **4.I** and **4.II**. Even the signals due to carbon atoms C17 (in case of **4.I**) and C18 (in case of **4.II**) also showed noticeable downfield shift in complexes **4.3** and **4.4,** repectively confirming the coordination of pyridyl nitrogen of bzpy. Similar trend for carbon atoms C3, C2 and C17 or C18 was observed in the spectrum of oxidoperoxidovanadium(V) complexes **4.5** and **4.6.** In ligands the peaks due to the carbon atoms of phenyl ring and thiophene or pyridyl ring appeared at expected δ values which also appeared in the ^{13}C NMR spectra of complexes **4.3, 4.4, 4.5** and **4.6** with slight shifting.

Table 4.8. ^{13}C NMR spectral data of ligand and complexes

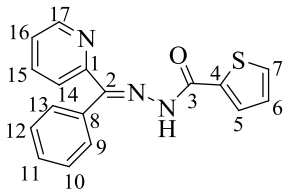

Compounds	C3	C2	C1	C17	C10/C12	C9/C13	C4, C5, C6, C7, C8, C11, C14, C15, C16
Hbzpy-tch (**4.I**)	154.92	151.60	148.93	138.27	128.84	128.46	136.81,129.42,128.88,126.16, 129.38,124.96,121.89,131.45, 124.07
[{$V^{V}O$(bzpy-tch)}$_2$(μ-$O)_2$] (**4.3**)	175.36	158.16	154.73	153.67	130.19	128.46	143.10,132.49,131.11,128.50, 133.41,128.43,126.72,134.00, 126.92
[$V^{V}O(O_2)$(bzpy- tch)] (**4.5**)	173.91	155.75	151.79	149.93	129.81	128.51	141.97,131.62,130.30,129.69, 132.21,128.21,125.77,135.76, 126.32

Table 4.9. ^{13}C NMR spectral data of ligand and complexes

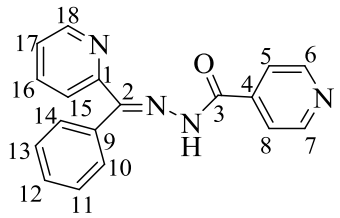

Compounds	C3	C2	C1	C18	C6/C7	C11/C13	C10/C14	C5/C8	C4, C9, C12, C16, C17, C15
Hbzpy-inh (**4.II**)	151.78	149.99	148.94	140.39	150.83	129.52	128.31	121.18	138.51,136.88, 128.31,137.26, 126.53,125.22
[{$V^{V}O$(bzpy-inh)}$_2$(μ-$O)_2$] (**4.4**)	175.40	154.41	153.79	143.16	150.41	130.25	128.53	122.04	138.26,131.29, 128.25,131.97, 127.56,127.28
[$V^{V}O(O_2)$(bzpy-inh)] (**4.6**)	175.87	155.43	154.78	150.14	150.41	129.82	128.60	122.36	142.16,130.61, 128.29,139.72, 127.02,126.52

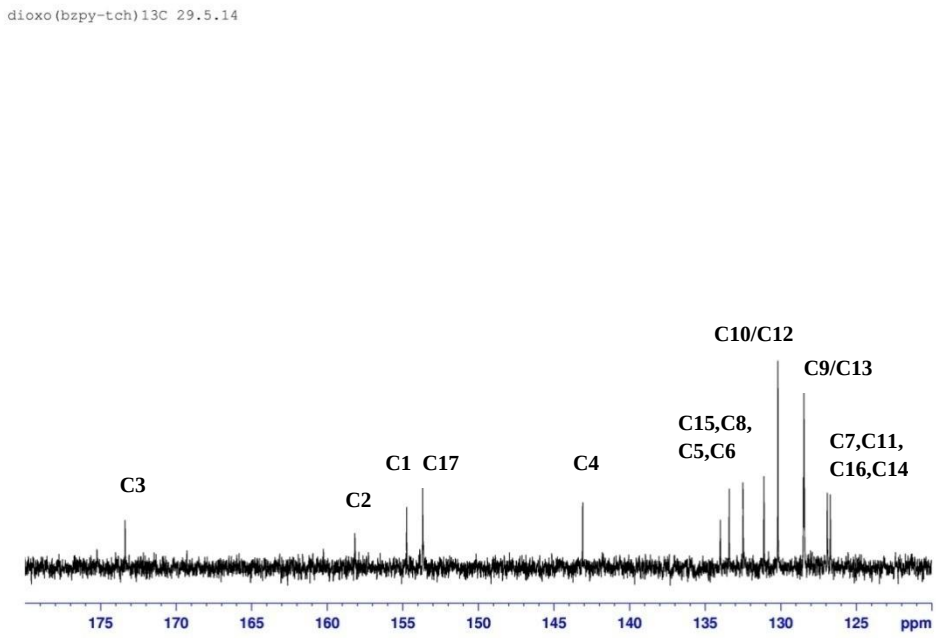

Figure 4.13. ^{13}C NMR spectrum of $[\{V^{V}O(bzpy\text{-}tch)\}_2(\mu\text{-}O)_2]$ (**4.3**).

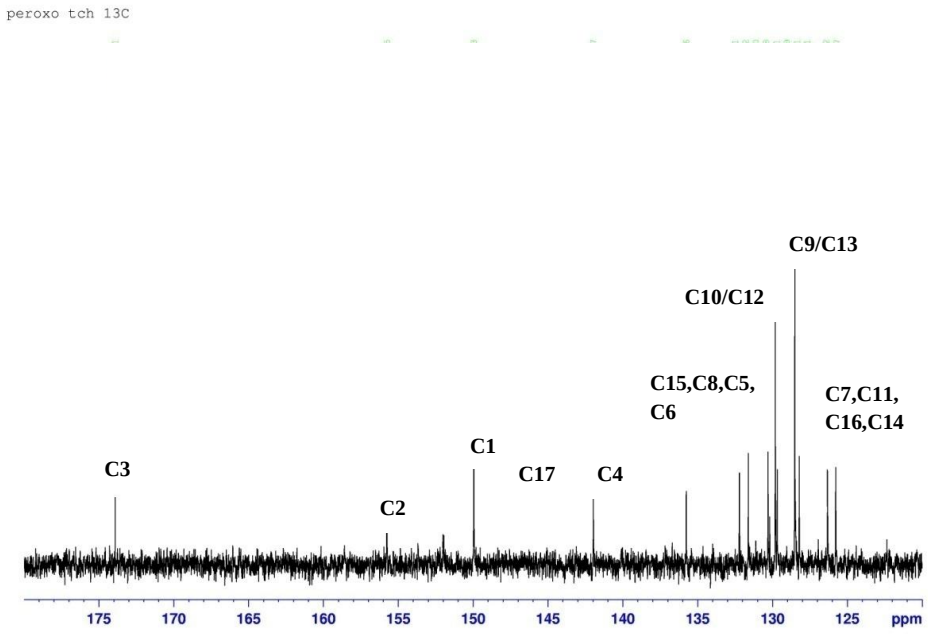

Figure 4.14. ^{13}C NMR spectrum of $[V^{V}O(O_2)(bzpy\text{-}tch)]$ (**4.5**)

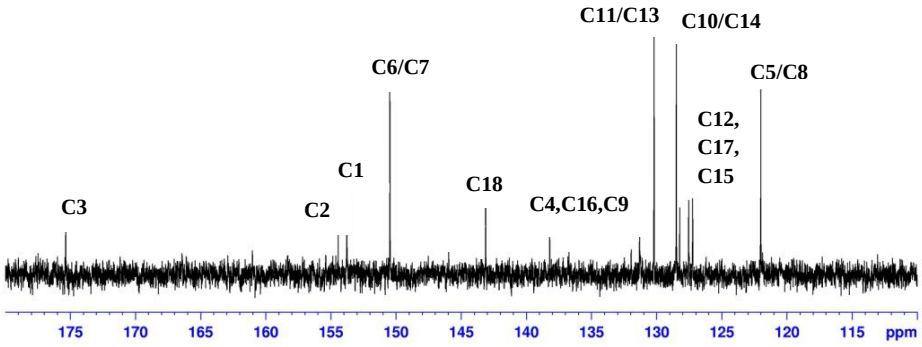

Figure 4.15. ^{13}C NMR spectrum of [{$V^{V}O$(bzpy-inh)}$_2$(μ-O)$_2$] (**4.4**)

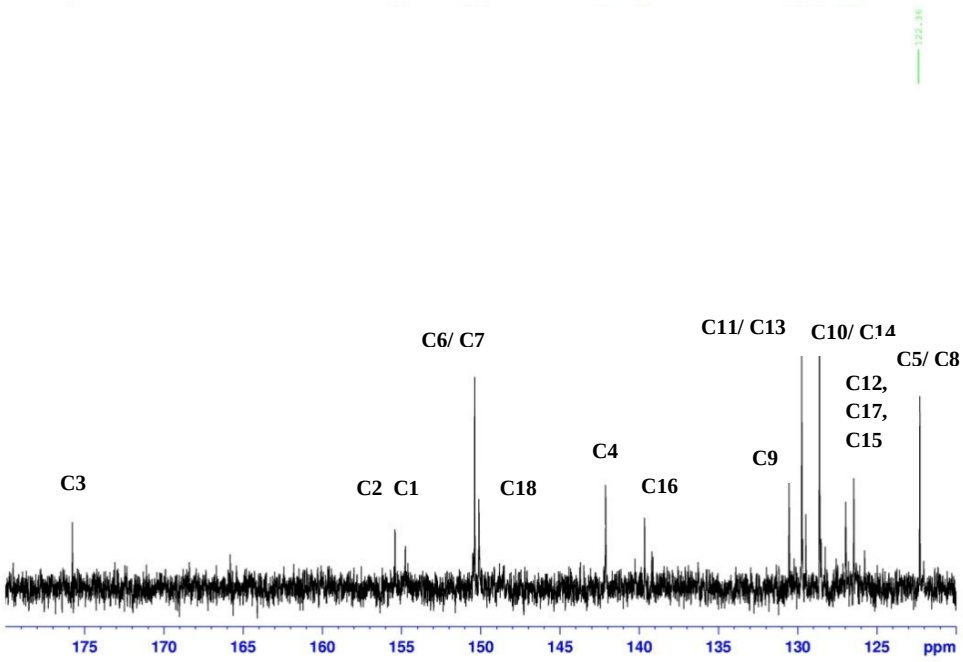

Figure 4.16. ^{13}C NMR spectrum of [$V^{V}O(O_2)$(bzpy- inh)] (**4.6**)

4.3.9. Electrospray Ionization Mass Spectrometry studies

The compounds **4.1** to **4.4** were studied by ESI-MS as a means to observe what species are formed in acetonitrile solution. The respective spectra are included in Figure 4.17 to Figure 4.20. For compound **4.1**, one of the major species detected is assigned to the sodium adduct of HBzpy-tch ($[Na(HBzpy\text{-}tch)]^+$, m/z = 330). The species at m/z = 767 may be assigned to either the dimeric molecular ion $[\{V^{IV}O(bzpy\text{-}tch)\}_2O]^+$ or the mixed valence dimer $[\{V^{V}O(bzpy\text{-}tch)\}O\{V^{IV}O(bzpy\text{-}tch)\}]^+$. The species at m/z = 844 may be due to adduct of two acetonitrile molecules with either one of the species assigned to m/z = 762. For compound **4.2**, two of the major species detected correspond to the protonated ligand $H_2Bzpy\text{-}inh^+$ (m/z = 303) and the respective sodium adduct ($[Na(HBzpy\text{-}inh)]^+$, m/z = 325). Minor species are assigned to the following: $[Na(Bzpy\text{-}inh)]^+$ at m/z = 365; $[H\{V^{V}O_2(bzpy\text{-}inh)(inh)(MeOH)_2\}]^+$ at m/z = 585 and the respective acetonitrile adducts at m/z = 627 and 667; the species at m/z = 752 may be assigned to either the dimeric molecular ion $[V^{IV}O(bzpy\text{-}inh)_2O]^+$ or the mixed valence dimer $[\{V^{V}O(bzpy\text{-}inh)\}O\{V^{IV}O(bzpy\text{-}inh)\}]^+$. For compound **4.3** the major species detected was assigned to $[\{V^{V}O(bzpy\text{-}tch)\}O\{V^{IV}O(bzpy\text{-}tch)\}]^+$ at m/z = 762. For compound **4.4**, the following species were assigned; the species at m/z = 309 is assigned to the double charged $[H\{V^{V}O(bzpy\text{-}inh)(bzpy)(H_2O)(MeOH)\}]^{2+}$; the sodium adduct ($[Na(HBzpy\text{-}inh)]^+$ is detected at m/z = 325; the species at m/z = 385 is assigned to $[H\{V^{V}O_2(bzpy\text{-}tch)\}]^+$; the species at m/z = 611 is assigned to $[V^{V}O_2(bzpy\text{-}tch)(inh)(CH_3CN)(MeOH)(H_2O)]^+$, the species at m/z = 752 is assigned to the mixed valence dimer $[\{V^{V}O(bzpy\text{-}inh)\}O\{V^{IV}O(bzpy\text{-}inh)\}]^+$; the species at m/z = 775 is assigned to the mixed valence dimer $[Na\{V^{IV}O(bzpy\text{-}inh)\}O\{V^{IV}O(bzpy\text{-}inh)\}]^+$. Overall, all compounds exhibit a tendency to aggregate into μ-oxido-bridged species even under the ESI-MS conditions. Noteworthy are the V^{V} compounds that exhibit peaks that are in agreement with mixed valence species, thus possibly indicating that the synthetic preparation of these compounds did not allow for the complete oxidation of V^{IV} to V^{V}. With the exception of compound **4.3**, free ligand was detected in all cases. Ligand fragmentation was also observed with the isonicotinoylhydrazide compounds

4.2 and **4.4**, also indicating their relatively lower stability compared to compounds **4.1** and **4.3**.

4.3.10. EPR Spectral studies

Compounds $[V^{IV}O(acac)(bzpy\text{-}tch)]$ (**4.1**), $[V^{IV}O(MeO)(bzpy\text{-}inh)]$ (**4.2**) were characterized by low temperature EPR. The V^{V} compounds $[\{V^{V}O(bzpy\text{-}tch)\}_2(\mu\text{-}O)_2]$ (**4.3**), $[\{V^{V}O(bzpy\text{-}inh)\}_2(\mu\text{-}O)_2]$ (**4.4**), PS– $[V^{V}O_2(bzpy\text{-}tch)]$ (**4.7**) and PS– $[V^{V}O_2(bzpy\text{-}inh)]$ (**4.8**) were also analyzed by EPR in order to ascertain if the respective synthetic procedures afforded the complete oxidation of the precursor V^{IV} species. The respective EPR spectra are presented in Figure 4.21 and the obtained spin Hamiltonian parameter are listed in Table 4.10.

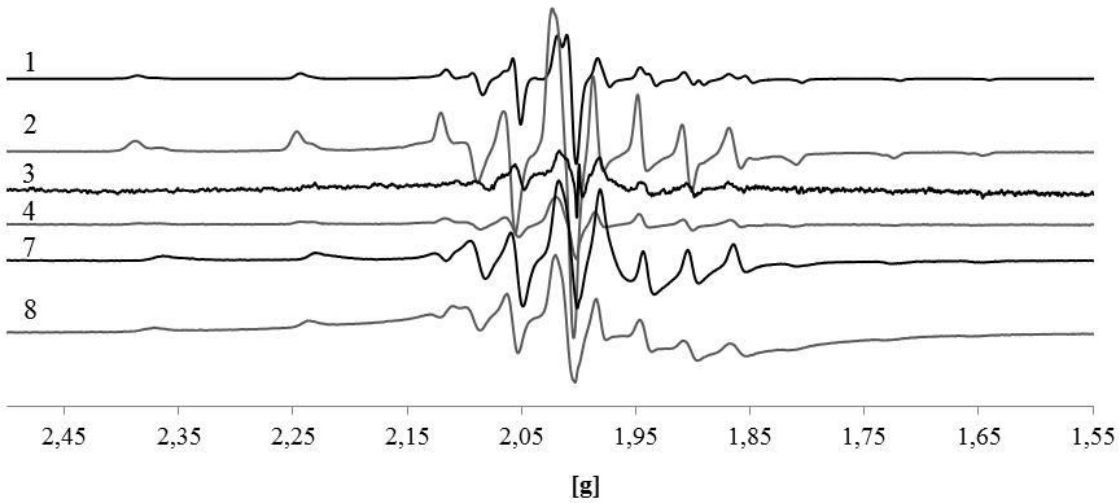

Figure 4.21. First derivative of the EPR spectra measured from compounds **4.1, 4.2, 4.3, 4.4, 4.7**, and **4.8**. The spectra for compounds **4.1** to **4.4** were recorded from DMF solutions at 77 K, while for **4.7** and **4.8** the spectra were obtained from the neat solids at room temperature.

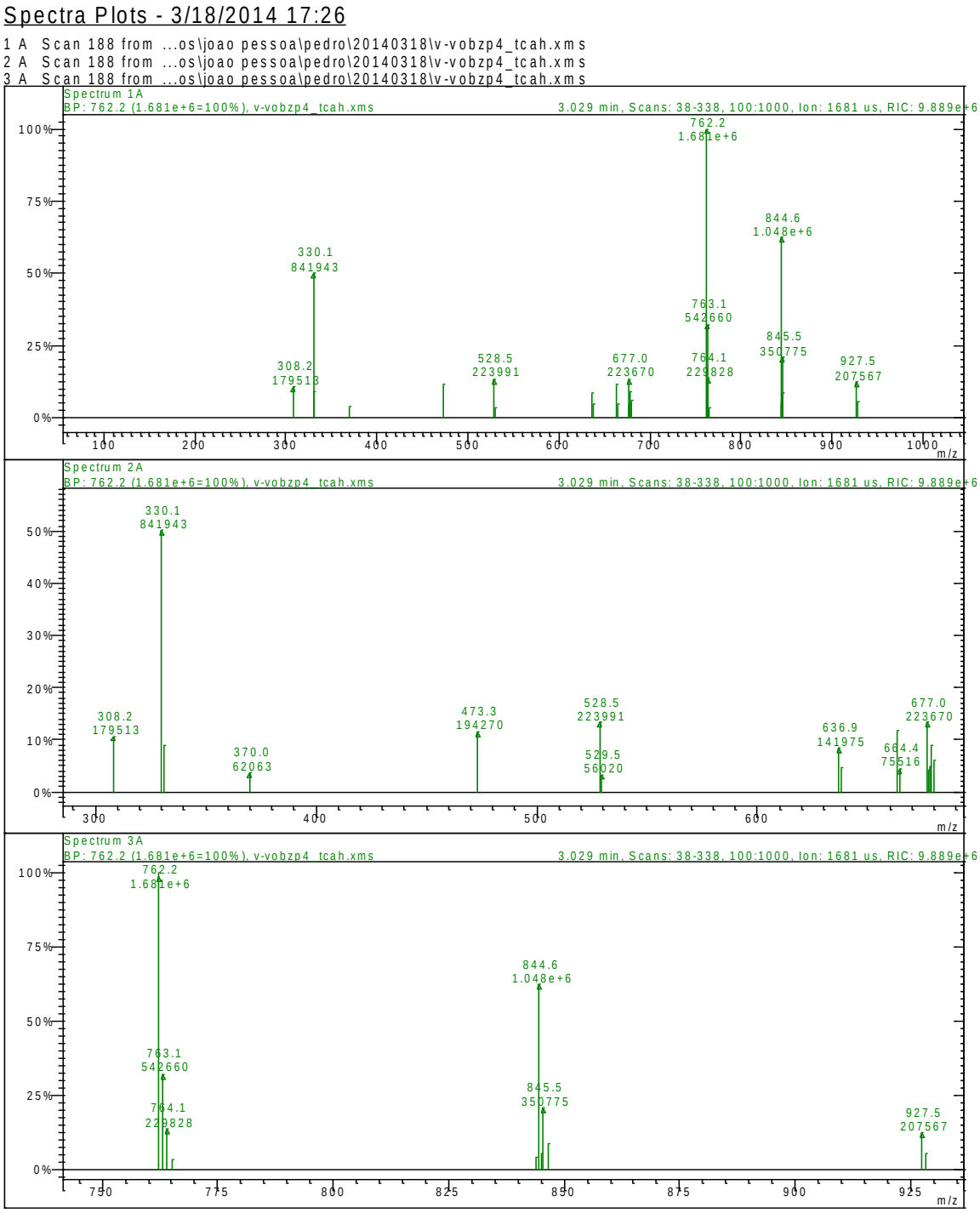

Figure 4.17. (a) ESI-MS spectrum of [VO^{IV}(acac)(bzpy-tch)] (**4.1**) in acetonitrile.

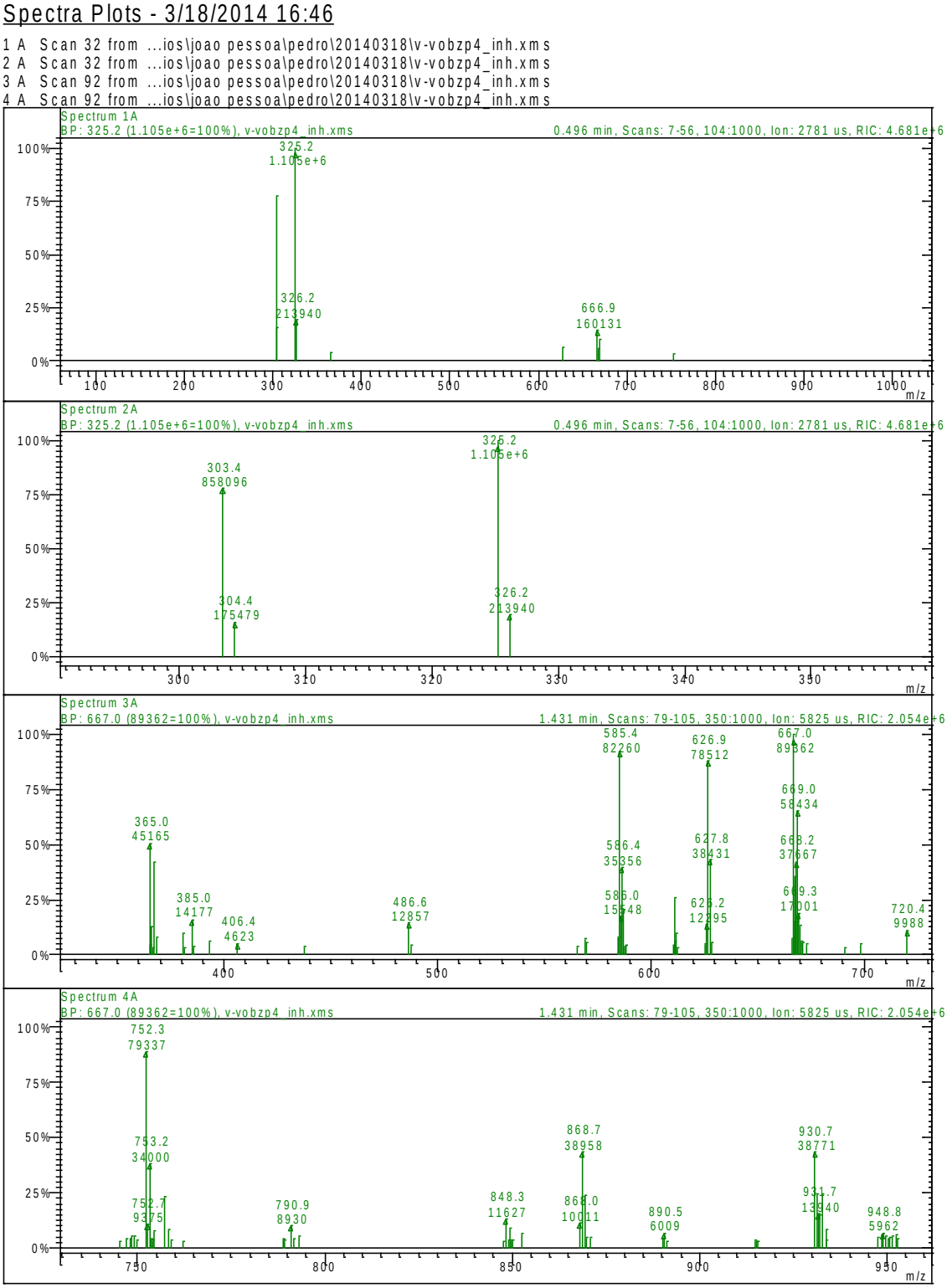

Figure 4.18. (b) ESI-MS spectrum of [VO^{IV}(OMe)(bzpy-inh)] (**4.2**) in acetonitrile.

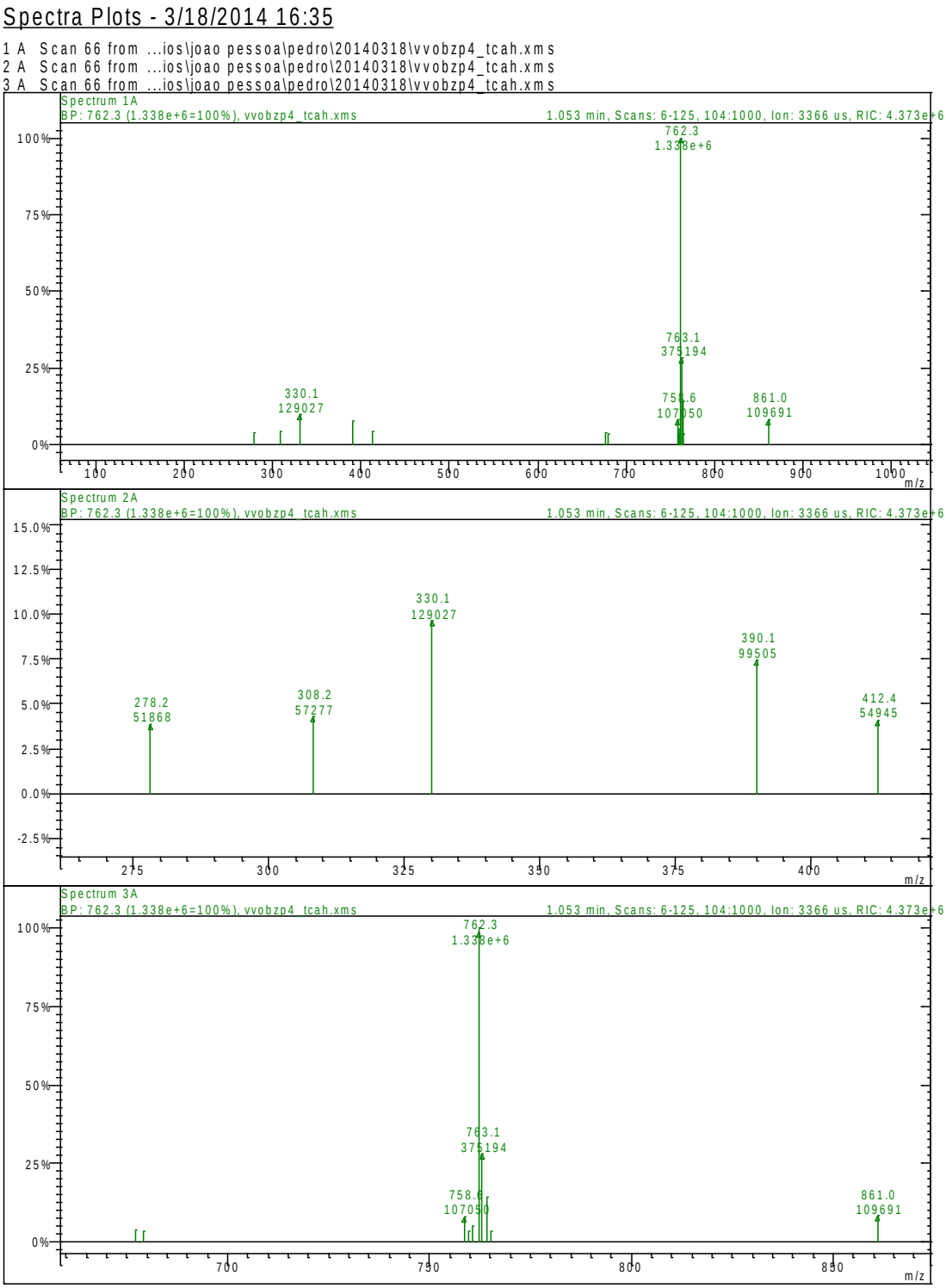

Figure 4.19. (a) ESI-MS spectrum of $[\{V^{V}O(bzpy\text{-}tch)\}_2(\mu\text{-}O)_2]$ (**4.3**) in acetonitrile.

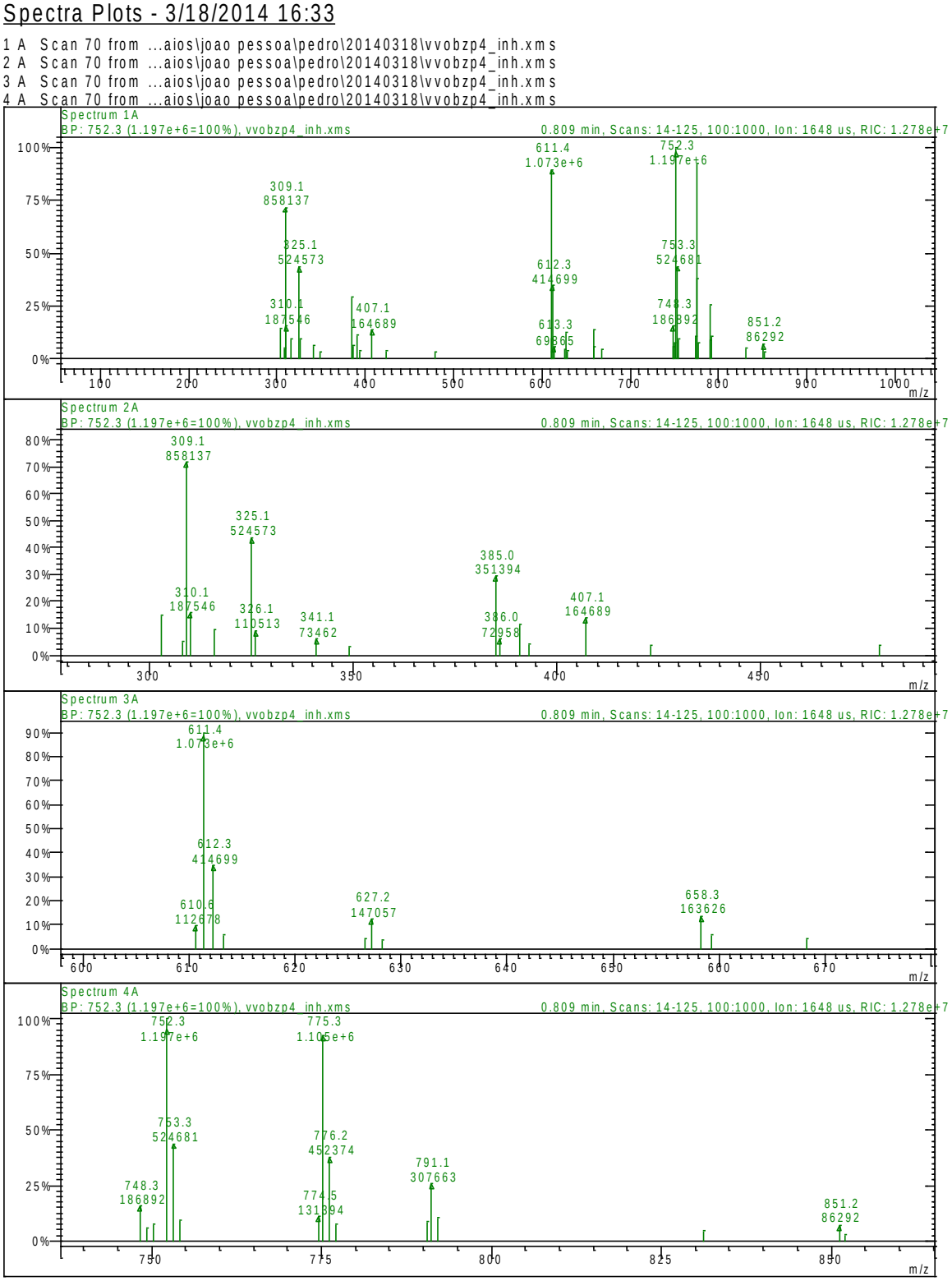

Figure 4.20. (b) ESI-MS spectrum of $[\{V^{V}O(bzpy\text{-}inh)\}_2(\mu\text{-}O)_2]$ (**4.4**) in acetonitrile.

Table 4.10. Spin Hamiltonian parameters obtained for compounds **4.1, 4.2, 4.3, 4.4, 4.7**, and **4.8**.

Compound	g_x, g_y (or $g_\perp$)	A_x, A_y (or $A_\perp$) $\times 10^4$ cm^{-1}	g_z (or $g_{//}$)	A_z (or $A_{//}$) $\times 10^4$ cm^{-1}	Donor atom set
4.1[a]	1.974, 1.979	61.7, 54.9	1.946	167.3	N_{imine}, N_{pyr}, O_{DMF}, O_{ArO}
4.2[a]	1.982	57.6	1.951	167	N_{imine}, N_{pyr}, O_{DMF}, O_{ArO}
			1.951	159.4	N_{imine}, N_{pyr}, O_{RO}, O_{ArO}
4.4[a]	1.977, 1.983	55.6, 54.2	1.95	163	N_{imine}, N_{pyr}, O_{acac}, O_{ArO}
4.7[b]	1.979	63	1.946	162.6	N_{imine}, N_{pyr}, O_{acac}, O_{ArO}
4.8[b]	1.981	58.5	1.95	161.2	N_{imine}, N_{pyr}, O_{acac}, O_{ArO}

[a] Spectrum measured from a DMF solution at 77 K. [b] Spectrum measured from the neat solid at room temperature.

The probable equatorial donor atom coordinated to the $V^{IV}O$ center were assigned using the additivity rule developed by Wüthrich and Chasteen [119,120]. For compounds **4.1** and **4.2**, the obtained spin Hamiltonian parameters are in agreement with the expected tridentate donor atom set [N_{imine}, N_{pyr}, O_{DMF}, O_{ArO}] which includes also a coordinated solvent molecule. The spectrum of **4.2** shows also a minor species that exhibits *z*-component parameters consistent with a coordinated methoxido ligand. Thus the assigned donor atom set [N_{imine}, N_{pyr}, O_{RO}, O_{ArO}] is in agreement with the expected formula of [$V^{IV}O$(MeO)(bzpy-inh)]. All of the V^V compounds exhibit strong V^{IV} signals, confirming the incomplete oxidation of the respective $V^{IV}O$ precursor compounds. In the case of compounds **4.4, 4.7** and **4.8,** the $V^{IV}O$ signal was strong enough to allow the estimation of the respective spin Hamiltonian parameters. The *z*-component parameters for these cases are in agreement with a [N_{imine}, N_{pyr}, O_{acac}, O_{ArO}] donor atom set, which is consistent with the presence of [$V^{IV}O$(acac)(bzpy-tch)] in **4.7** and [$V^{IV}O$(acac)(bzpy-inh)] in both **4.4** and **4.8.**

4.3.11. Reactivity of oxidovanadium(IV) and oxidovanadium(V) complexes

4.3.11.1. Reactivity of $[V^{IV}O(acac)(bzpy\text{-}tch)]$ (4.1) and $[\{V^{V}O(bzpy\text{-}tch)\}\mu\text{-}O_2]$ (4.3) towards H_2O_2

Oxidoperoxidovanadium(V) complexes of all ligands have been isolated and characterized. The in-situ generation of the peroxido species in solution from the corresponding oxidovanadium(IV) complexes by their treatment with H_2O_2 have also been followed by electronic absorption spectroscopy and show very interesting spectral changes. Thus, at least two different sets of electronic spectral patterns were observed during stepwise addition of 0.051 g (0.45 mmol) of 30 % H_2O_2 taken in 15 mL of MeOH to 25 mL of *ca.* 0.23×10^{-4} M solution of $[VO^{IV}(acac)(bzpy\text{-}tch)]$ (**4.3**) in MeOH. As presented in Figure 4.22 for first set, the band at 307 nm shifts to 321 nm with rapid decrease in intensity while band at 271 nm increases its intensity without changing its position. A weak shoulder appearing at *ca.* 418 nm maintains its position with slight decrease in intensity while band at 204 nm maintains its position with slight increase in intensity. Further addition of H_2O_2 causes no change in the positions of all bands but sharp increase in the intensity of 204 band, and only marginal increase in the intensities of 271, 321 and 418 nm bands. We interpret these spectral changes as corresponding to: (a) oxidation of the $V^{IV}O$-complex, yielding a V^{V}-species (**3** or most probably its mononuclear $V^{V}O_2$-counterpart), followed by the generation of oxidoperoxidovanadium(V) species in solution.

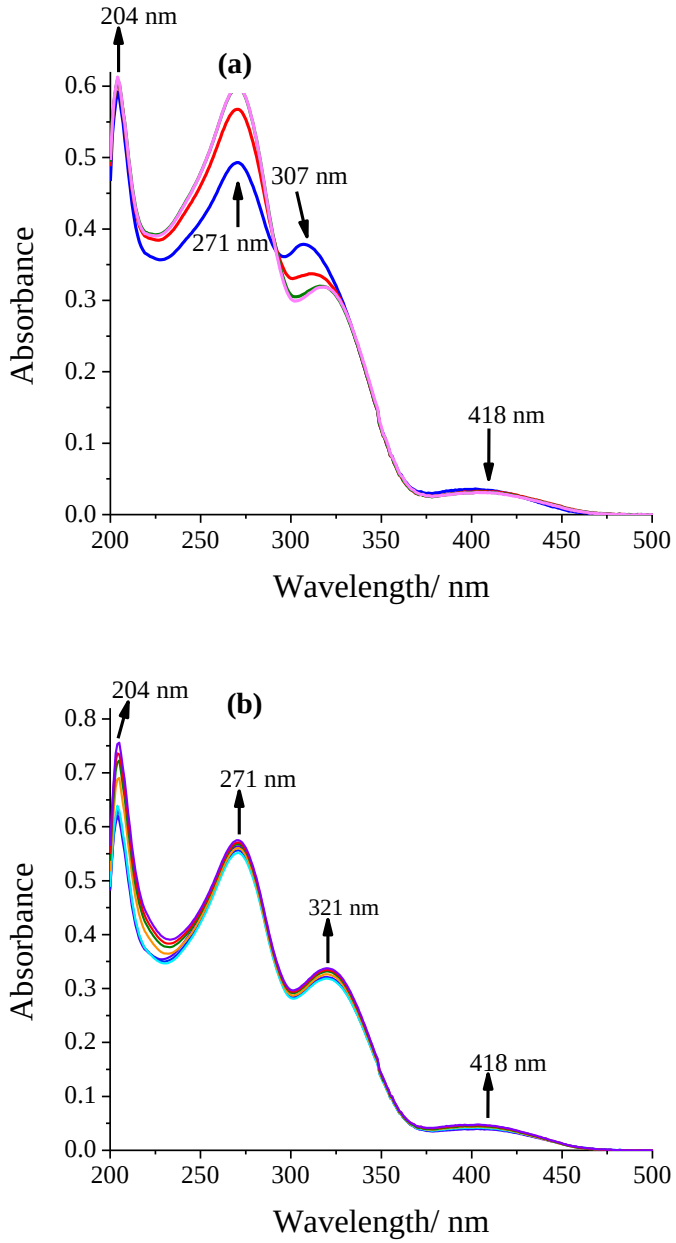

Figure 4.22. Two sets (a) and (b) of spectral changes obtained during the titration of stepwise additions of a solution prepared from 0.051 g (0.45 mmol) of 30 % H_2O_2 dissolved in 15 mL of MeOH to 25 mL of *ca.* 0.23 × 10^{-4} M solution of [$V^{IV}O$ (acac)(bzpy-tch)] in MeOH.

The two d-d bands present at 570 and 766 nm are also sensitive towards H_2O_2 as observed with its concentrated solution in DMF. Stepwise addition of a solution prepared from 0.051 g (0.45 mmol) of 30 % H_2O_2 dissolved in 15 mL of DMF to 4 mL of

ca. 0.38 × 10^{-2} M solution of [$V^{IV}O$ (acac)(bzpy-tch)] in DMF causes a considerable reduction in intensity of the 766 nm band followed by its flattening, while the 570 nm band slowly moves to *ca.* 540 nm, along with a slight broadening and considerable increase in intensity (Figure 4.23 (a)). Further addition of H_2O_2 causes considerable reduction in the intensity along with disappearance of both bands (Figure 4.23 (b)).

Solution of [{$V^{V}O$(bzpy-tch)}μ-O_2] in MeOH is also sensitive towards H_2O_2, as monitored by electronic absorption spectroscopy. Again two different sets of electronic spectral patterns were observed upon stepwise additions of a solution prepared from 0.051 g (0.45 mmol) of 30 % H_2O_2 dissolved in 10 mL of MeOH to 25 mL of *ca.* 0.6 × 10^{-4} M solution of [{$V^{V}O$(bzpy-tch)}μ-O_2] in MeOH. Here, the band at 418 nm continuously increases its intensity while the band at 306 nm decreases its intensity but positions of both remain nearly same and form isosbestic point at 332 nm. A weak shoulder at 238 nm shifts to 234 nm with slight decrease in intensity while 207 nm band gains only intensity (Figure 4.24 (a)). Further addition of H_2O_2 (second set) two bands at 418 and 306 nm gains intensity while maintaining their positions. A weak shoulder appearing at 234 nm weakens with increase in intensity and finally disappears (Figure 4.24 (b)) while the band at 207 nm only gains intensity and finally disappears. The initial spectrum of second set is similar to that recorded for the corresponding oxidoperoxidovanadium(V) complex [$V^{V}O(O_2)$(bzpy-tch)]. This observation suggests that dioxido complex initially changes to the corresponding peroxide complex and then possibly converts into ligand free peroxide $[V^{V}O(O_2)]^{2+}$ species.

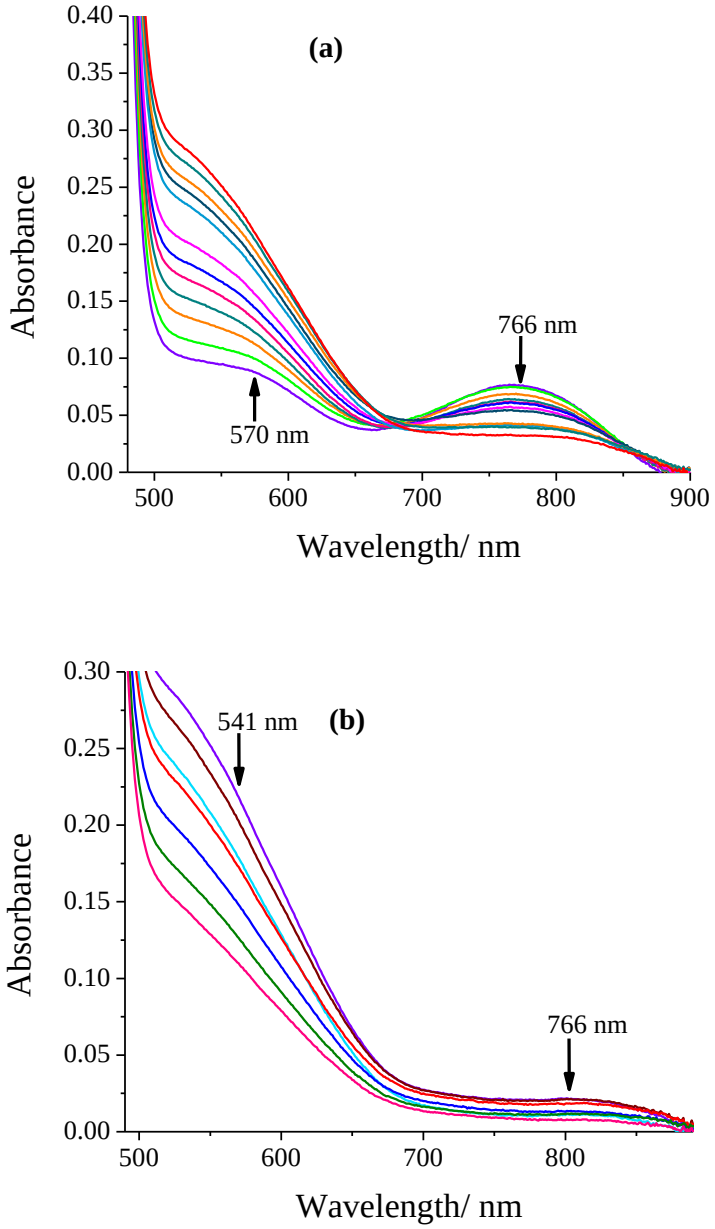

Figure 4.23. Two sets of spectral changes obtained during titration of stepwise additions of a solution prepared from 0.051 g (0.45 mmol) of 30 % H_2O_2 in 15 mL of DMF to 4 mL of *ca.* 0.38 × 10^{-2} M solution of [$V^{IV}O$ (acac)(bzpy-tch)] in DMF. (a) showing flattening of 766 nm band and movement of 570 nm band slowly to *ca.* 540 nm and (b) showing flattening of both bands with decrease in intensity.

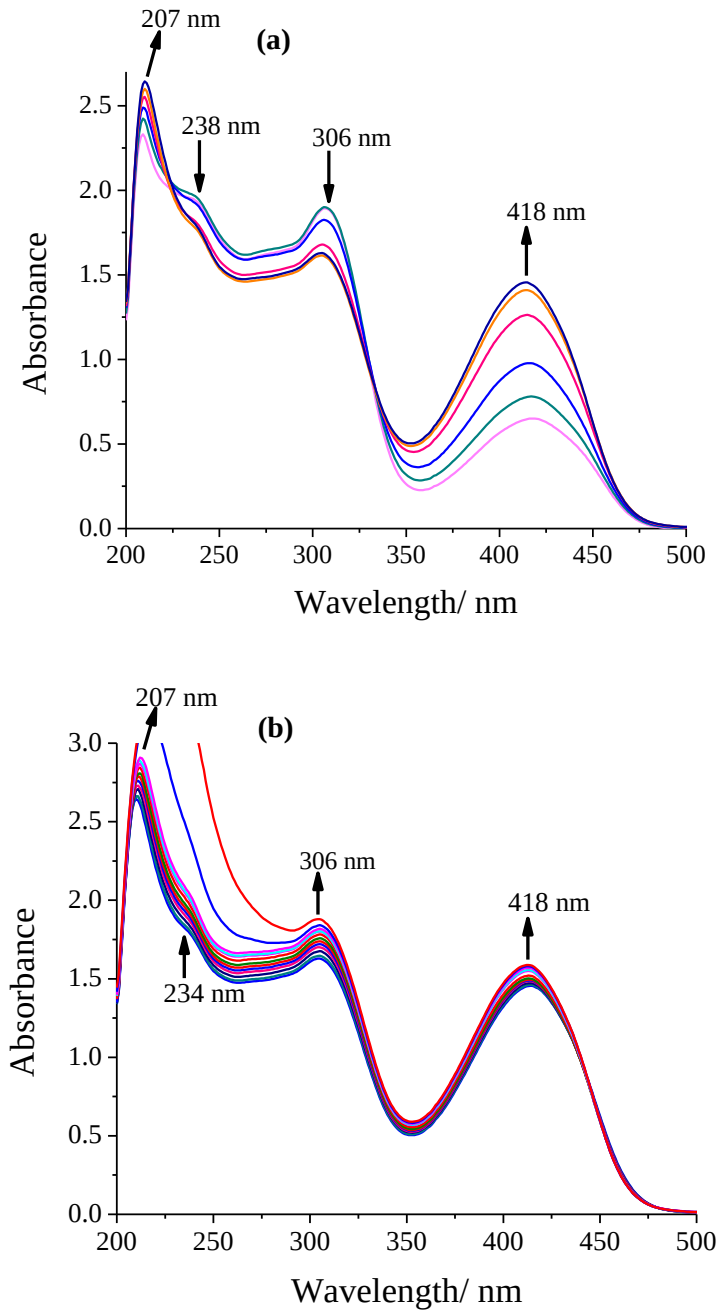

Figure 4.24. Two sets (a) and (b) of spectral changes obtained during titration of stepwise additions of a solution prepared from 0.051 g (0.45 mmol) of 30 % H_2O_2 in 10 mL of MeOH to 25 mL of *ca.* 0.6 × 10^{-4} M solution of [{$V^{V}O$(bzpy-tch)}μ-O_2] in MeOH.

The interaction of [$V^{IV}O$(acac)(bzpy-tch)] with H_2O_2 was also monitored by ^{51}V NMR. Figure 4.25 shows the change in chemical shifts of the V^{V} species in solution in the presence of oxidant and substrate. Additional ^{51}V NMR spectra of [{$V^{V}O$(bzpy-

tch)}μ-O_2] and [{$V^{V}O(O_2)$(bzpy-tch)}] were also measured, each showing a single resonance at –501 and –571 ppm, respectively (Figure 4.26 and Figure 4.27).

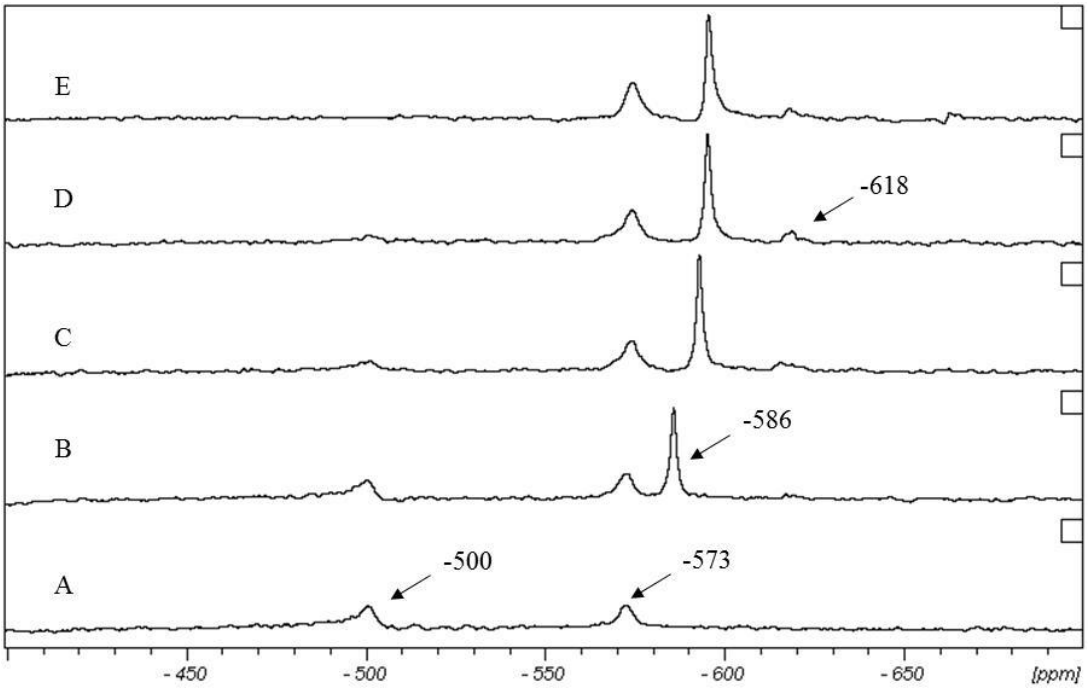

Figure 4.25. ^{51}V NMR spectra of [VO^{IV}(acac)(bzpy-tch)] (2 mM, DMF/acetone–d_6 4:1) in the presence of: A) 1 molar equivalents of H_2O_2 (0.1 M, acetone), 5 h after addition; B) 4 equivalents of H_2O_2; C) 100 equivalents of H_2O_2; D) 100 equivalents of H_2O_2 and isoeugenol; E) 24 h after the addition of 100 equivalents of isoeugenol.

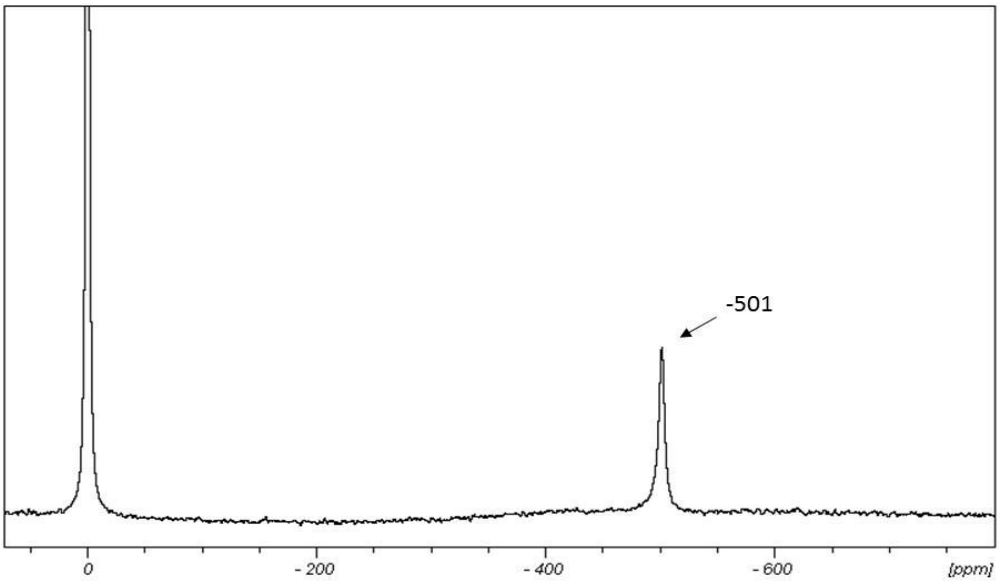

Figure 4.26. ^{51}V NMR spectrum of **4.1** in DMF/acetone–d_6 4:1 solution.

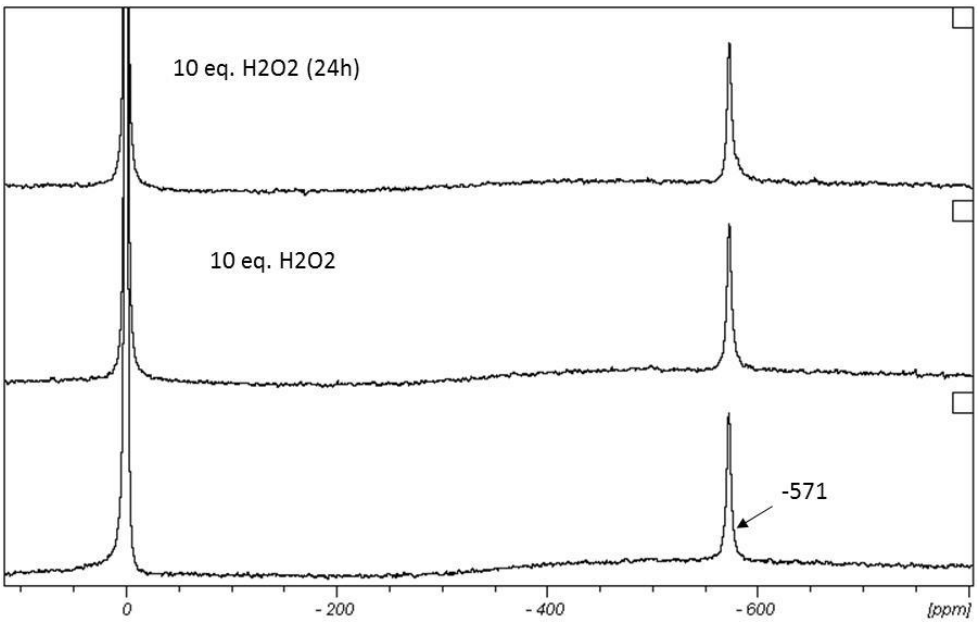

Figure 4.27. ^{51}V NMR spectrum of **4.5** in DMF/acetone–d_6 4:1 solution before and after the addition of 10 equivalents of H_2O_2.

The first observation is that in the presence of equimolar amounts of H_2O_2, [$V^{IV}O$(acac)(bzpy-tch)] is converted into [$V^{V}O_2$(bzpy-tch)], at –500 ppm, and the corresponding peroxide species [{$V^{V}O(O_2)$(bzpy-tch)}], at –571. Further addition of

H_2O_2 induces the appearance of another species at –586 ppm and the disappearance of $[V^VO_2(bzpy\text{-}tch)]$. The species at –586 ppm may be due to a oxidoperoxidovanadium(V) species such as $[\{V^VO(O_2)(HOO)(Hbzpy\text{-}tch)\}]$ bearing an end-on bound hydroperoxido ligand, with a protonated pyridine N donor atom. Replacement of this donor atom by a more electronegative O donor atom, the respective ^{51}V resonance is shifted upfield [122]. After the addition of 100 equivalents of oxidant, a new species appears at – 618 ppm. This could be indicative of hydrolysis of the ligand, forming either as $[\{V^VO(O_2)(HOO)(Hbzpy)\}]$ or as $[\{V^VO(O_2)(HOO)(tch)\}]$ as a result of ligand hydrolysis. The resonances at –586 and –618 ppm did not change after the addition of isoeugenol. Moreover, there was no observable alteration to the spectrum even after an additional 48 h period at room temperature and another 24 h at 40º C. This is in agreement with observed stability of $[\{V^VO(O_2)(bzpy\text{-}tch)\}]$, which could be easily isolated as a solid.

4.3.11.2. Reactivity of $[V^{IV}O(OMe)(bzpy\text{-}inh)]$ (4.2) and $[\{V^VO(bzpy\text{-}inh)\}\mu\text{-}O_2]$ (4.4) towards H_2O_2

Behaviour of $[V^{IV}O(OMe)(bzpy\text{-}inh)]$ (**4.2**) towards H_2O_2 is entirely different than observed for $[V^{IV}O(acac)(bzpy\text{-}tch)]$ (**4.1**). At least four different sets of spectral changes could be identified from this experiment. Initial addition of H_2O_2 to a methanolic solution of $[VO^{IV}(OMe)(bzpy\text{-}inh)]$ (**4.2**) results in the increment in the intensity of 215, 272 and 333 nm bands of the UV region without changing their positions. A new shoulder band at *ca.* 420 nm also generates with the formation of two isosbestic points at 370 nm and 430 nm (Figure 4.28 (a)). In the next set, the 272 and 333 nm bands remain at the same position with only slight loss in intensity, 215 nm band gains intensity slightly and shoulder band at *ca.* 420 moves to *ca.* 380 with slight increment of intensity causing shift of isosbestic point at 365 nm (Figure 4.28 (b)). Further addition of H_2O_2 causes again the formation of a band at *ca.* 438 nm along with

shift of 380 nm band to 390 nm. A small shift of 333 nm band to 320 nm along with decreased intensity, shift of 265 nm band to 260 along with increased intensity and shift of 215 nm band to 220 nm with sharp increased intensity have also been observed (Figure 4.28 (c)). In the fourth and last set (Figure 4.28 (d)), the two bands at 438 and 390 nm gradually merge with loss in intensity and appear as a broad band at *ca.* 400 nm The 333 nm band continuously decreases while the 260 nm band slowly broadens and disappears with increase in intensity. Simultaneously, the band at 220 nm moves to higher wave length along with sharp increase in intensity.

Spectral changes in the d–d bands could be observed only in higher concentration of $[V^{IV}O(OMe)(bzpy\text{-}inh)]$ (**4.2**). Both shoulder bands i.e. 645 and 805 nm slowly disappear upon addition of H_2O_2 (0.051 g (0.45 mmol) of 30 % H_2O_2 dissolved in 15 mL of DMF) to **4.2** taken in DMF (5 mL of *ca.* 0.7×10^{-2} M solution in DMF) (Figure 4.29). This in line of the oxidation of oxidovanadium(IV) species to dioxido which in turn to oxidoperoxido species.

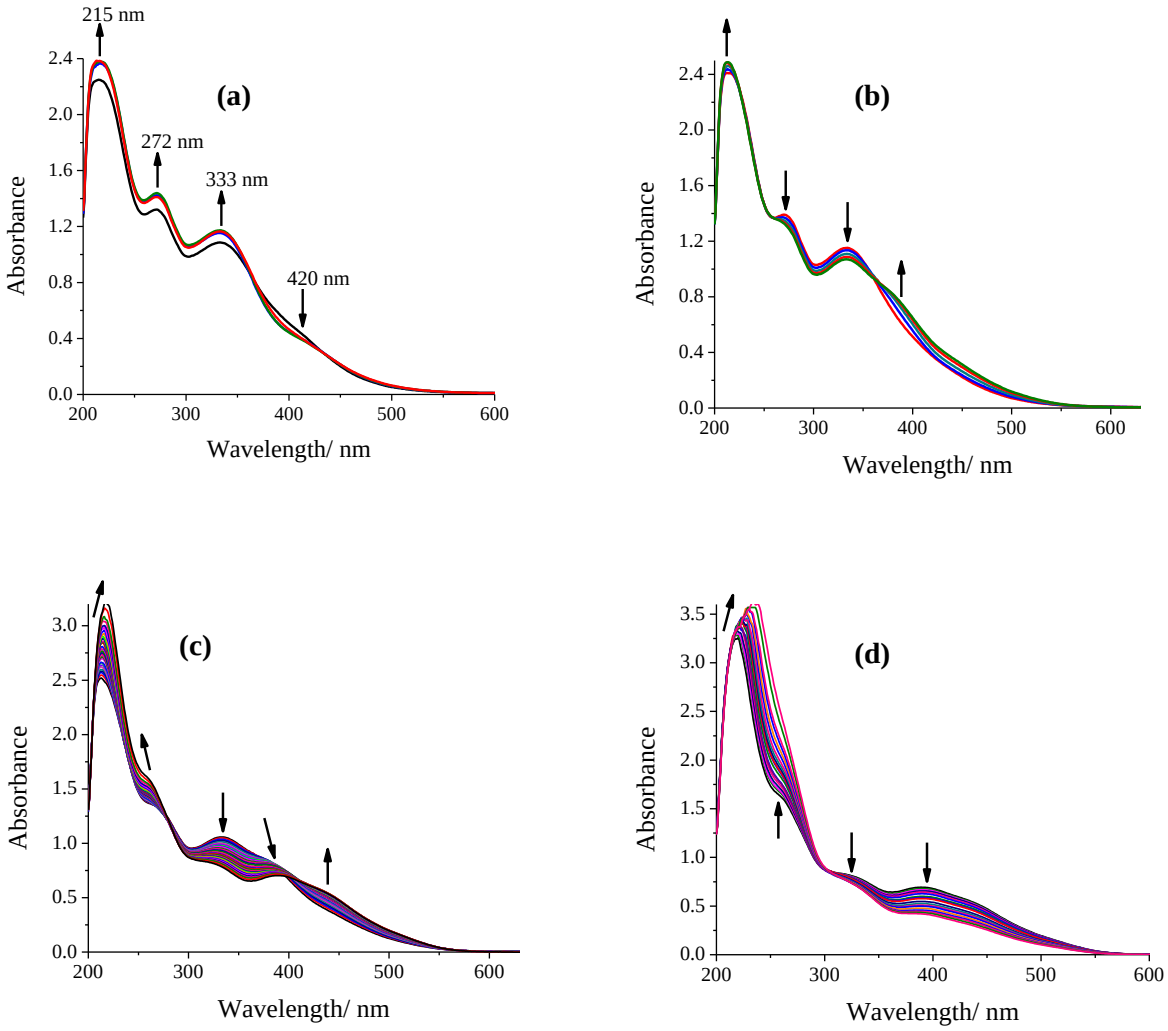

Figure 4.28. Four sets (a), (b), (c) and (d) of spectral changes obtained during the titration of stepwise additions of a methanolic solution of H_2O_2 prepared from 0.051 g (0.45 mmol) of 30 % H_2O_2 dissolved in 5 mL of MeOH to 25 mL of *ca.* 0.90×10^{-4} M solution of [$V^{IV}O$ (OMe)(bzpy-inh)] in MeOH.

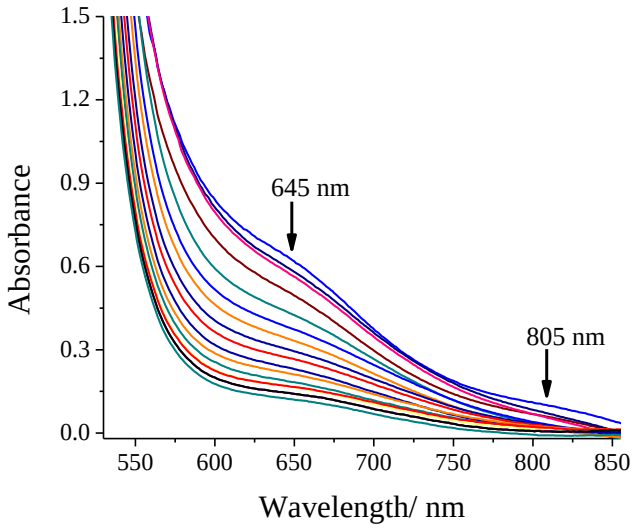

Figure 4.29. Spectral changes obtained during the titration of stepwise additions of a solution prepared from 0.051 g (0.45 mmol) of 30 % H_2O_2 dissolved in 15 mL of DMF to 5 mL of *ca.* 0.7×10^{-2} M solution of $[V^{IV}O(OMe)(bzpy\text{-}inh)]$ in DMF.

During drop wise addition of a methanolic solution of H_2O_2 to $[\{V^{V}O(bzpy\text{-}inh)\}\mu\text{-}O_2]$, 396 nm band slightly increases its intensity with a shift to 391 nm while 280 nm band moves to 284 nm with slightly decrease in intensity. The band at 209 nm shifts only slightly towards higher wave number with slight increase in intensity. The whole process generates two isosbestic points at 232 nm and 330 nm. Further addition of H_2O_2 causes increase in intensity of two bands with no change of 391 nm band and change of 284 nm band to a shoulder. The band at 284 nm shifts to higher wave length with sharp increase in intensity.

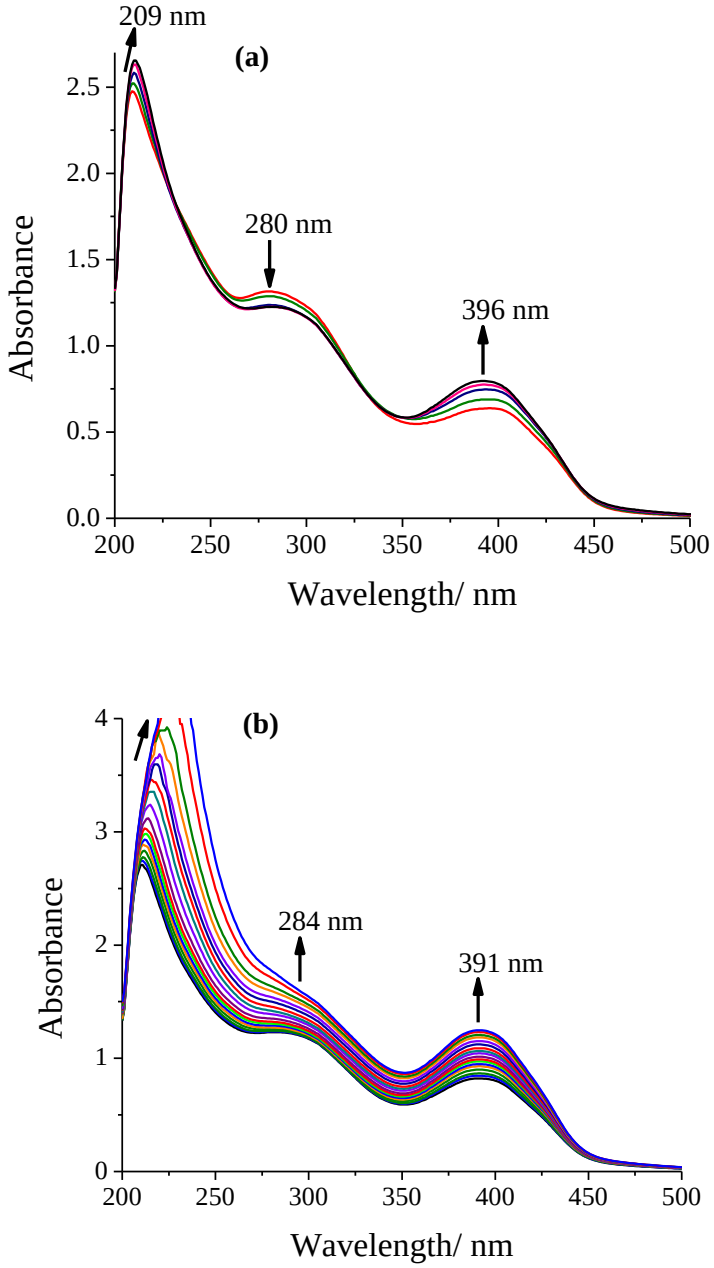

Figure 4.30. Two sets of spectral changes (a) and (b) obtained during the titration of stepwise additions of a solution prepared from 0.051 g (0.45 mmol) of 30 % H_2O_2 dissolved in 5 mL of MeOH to 30 mL of *ca.* 0.48 × 10^{-4} M solution of [{$V^{V}O$(bzpy-inh)}μ-O_2] in MeOH.

The interaction of [$V^{IV}O$(OMe)(bzpy-inh)] with H_2O_2 was also monitored by ^{51}V NMR (Figure 4.31). ^{51}V NMR spectra of [{$V^{V}O$(bzpy-inh)}μ-O_2] and [{$V^{V}O(O_2)$(bzpy-

inh)}] were measured, each showing a single resonance at –502 and –570 ppm, respectively (See Figures 4.32 and 4.33).

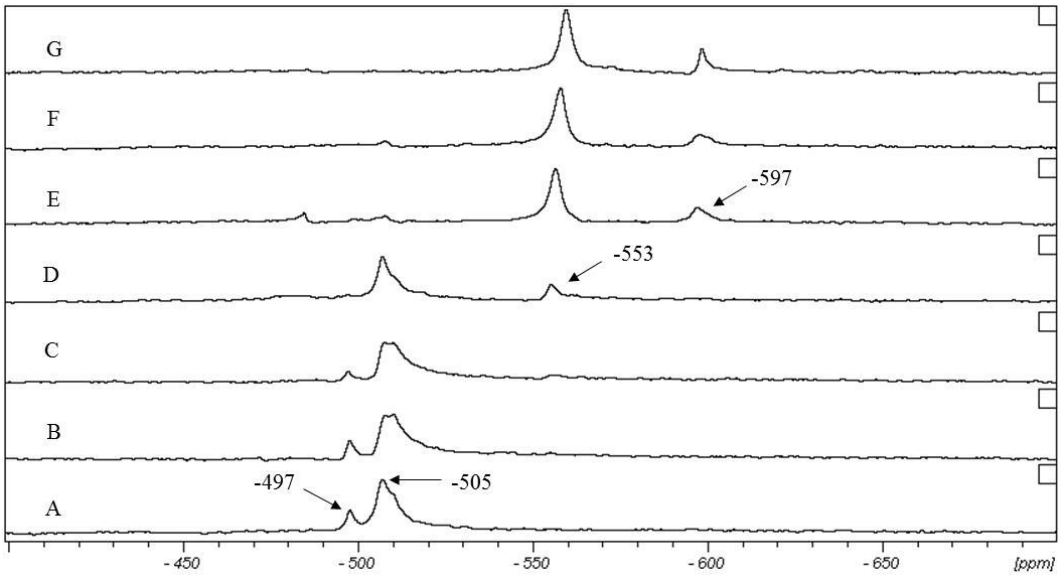

Figure 4.31. ^{51}V NMR spectra of [$V^{IV}O$(OMe)(bzpy-inh)] (2 mM, DMF/acetone–d_6 4:1) in the presence of: (A) 1 molar equivalent of H_2O_2 (0.1 M, acetone), 5 h after addition. (B) 2 equivalents of H_2O_2. (C) 5 equivalents of H_2O_2. (D) 10 equivalents of H_2O_2. (E) 100 equivalents of H_2O_2. (F) 100 equivalents of H_2O_2 and isoeugenol. (G) 24 h after the addition of 100 equivalents of isoeugenol.

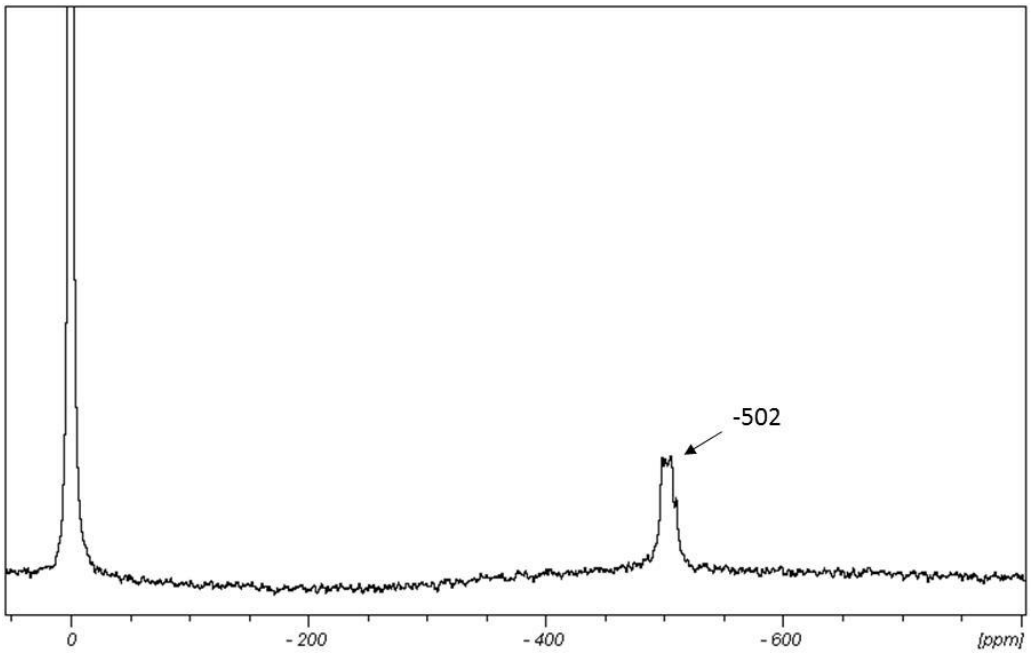

Figure 4.32. ^{51}V NMR spectrum of **4.2** in DMF/acetone–d_6 4:1 solution.

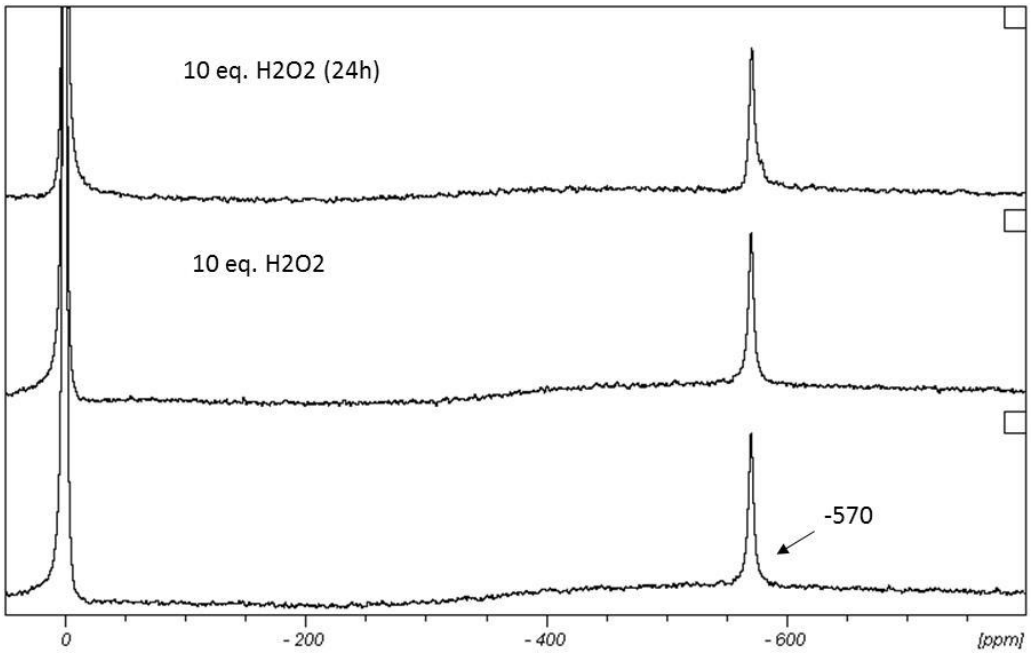

Figure 4.33. ^{51}V NMR spectrum of **4.6** in DMF/acetone–d_6 4:1 solution before and after the addition of 10 equivalents of H_2O_2.

In the presence of one equivalent of H_2O_2, [$V^{IV}O(OMe)$(bzpy-inh)] is converted into [$V^{V}O_2$(bzpy-inh)] with a major signal at –505 ppm, alongwith a minor species at –

497 ppm which is assigned to a conformer of $[V^{V}O_2(bzpy\text{-}inh)]$. A new resonance appears at –553 ppm only after the addition of 10 equivalents of H_2O_2. This resonance is assigned to a V^{V} species such as $[V^{V}O(HOO)(OMe)(bzpy\text{-}inh)]$ bearing a side-on bound hydroperoxo ligand. The corresponding peroxido species $[\{V^{V}O(O_2)(bzpy\text{-}inh)\}]$ was observed to appear further upfield at –570 ppm. Another species appears at –597 ppm upon the addition of oxidant and as in the case of $[V^{IV}O(acac)(bzpy\text{-}tch)]$, this resonance is tentatively assigned to $[\{V^{V}O(O_2)(HOO)(Hbzpy\text{-}inh)\}]$. The addition of isoeugenol did not cause any observable changes in the spectrum even after an additional 48 h period at room temperature and another 24 h period at 40º C. As in the case of $[\{V^{V}O(O_2)(bzpy\text{-}tch)\}]$, this is in agreement with the observed stability of $[\{V^{V}O(O_2)(bzpy\text{-}inh)\}]$.

4.3.12. Catalytic oxidation of 2-methoxy-4-(prop-1-en-1-yl)phenol (isoeugenol)

With an output of about 15,000 tons/year [168], vanillin is possibly the second largest produced aroma chemical in the world because this is the key compound in food industry to provide characteristic aroma and flavour of vanilla bean. It is mainly produced by the oxidation of isoeugenol. Microbial biotransformations of isoeugenol have been the key method to produce vanillin and vanillic acid and reported extensively in the literature [169,170]. Vanillic acid can be reduced to vanillin. Photocatalytic oxidation of isoeugenol over TiO_2 also produces vanillin [171]. Catalytic transformation of isoeugenol to vanillin using Bu_4NVO_3/pyrazine-2-carboxylic acid in the presence of H_2O_2 as oxidant has been reported by Gusevskaya et al. [172]

We have carried out the catalytic oxidation of isoeugenol using polymer supported as well as non-polymer supported $V^{V}O_2$-complexes as catalysts. At least formation of three different products namely vanillin, vanillic acid and dehydroisoeugenol were observed; Scheme 4.4. The supported complex PS–im$[V^{V}O_2(bzpy\text{-}inh)]$ was used as a representative catalyst for the optimization of different reaction parameters *viz.* amounts of catalyst, oxidant (30 % aqueous H_2O_2) and solvent, and temperature at which reaction was carried out while maintaining other condition e.g. stirring speed around 100 rpm in all reactions.

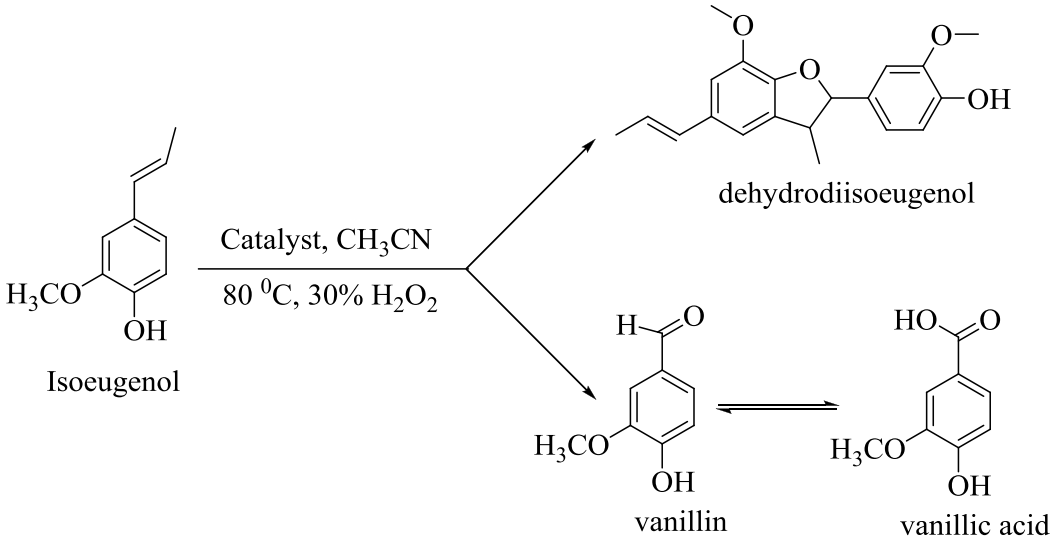

Scheme 4.4: The proposed scheme for the oxidation reaction of isoeugenol

To optimize the catalyst amount, four different amounts of catalyst (0.01, 0.02, 0.03 and 0.04 g) were taken while considering isoeugenol (0.82 g, 5 mmol) and other reaction parameters consistent such as aqueous 30 % H_2O_2 (1.13 g, 10 mmol), acetonitrile (5 mL) and reaction temperature (80 ^oC). Details of the reaction products analyzed for 2 h are presented in Figure 4.34. Increasing catalyst amount from 0.01 g to 0.02 g, conversion enhanced from 61% to 89 %; but there was no considerable improvement in conversion further on increasing catalyst amount up to 0.04 g. Only the amount of vanillic acid slightly increased and of vanillin slightly decreased. Therefore, 0.02 g of catalyst was chosen as most appropriate amount for optimizing remaining conditions.

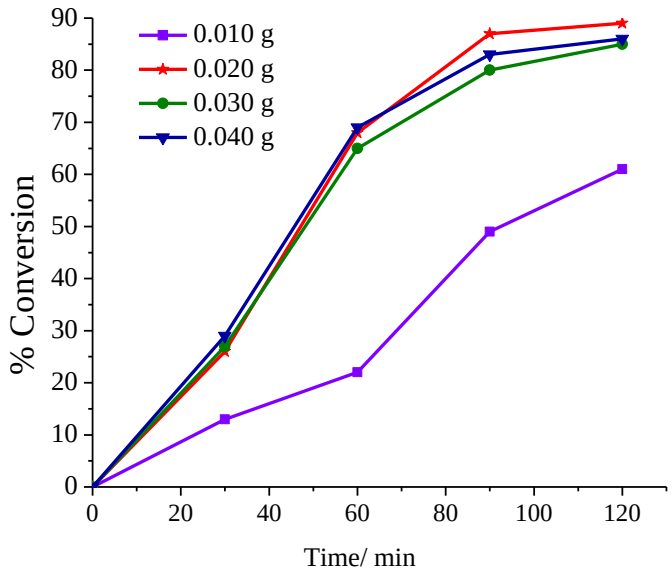

Figiure 4.34. Effect of the amount of catalyst PS–im[VO_2(bzpy-inh)] on the oxidation of isoeugenol. Reaction conditions: isoeugenol (0.82 g, 5 mmol), acetonitrile (7 mL), 30 % aqueous H_2O_2 (1.13 g, 10 mmol), reaction temperature (80 ^oC) and reaction time 2 h.

Considering 0.02 g of optimized catalyst for 5 mmol of isoeugenol in 7 mL of acetonitrile and 80 ^oC reaction temperature, three different amounts of oxidant (30% H_2O_2) *viz.* 5, 10 and 15 mmol were tested. The lowest i.e. 76 % conversion of isoeugenol was obtained with 5 mmol oxidant under above reaction conditions whereas a maximum of 89 % conversion was obtained using 10 mmol oxidant (product distribution: vanillic acid = 20 %, vanillin = 17 % and dehydroisoeugenol = 52 %) (Figure 4.35). Further increasing the amount of oxidant to 15 mmol did not improve any conversion; in fact, this condition decreases the formation of vanilin (product distribution: vanillic acid = 18 %, vanillin = 14 %, dehydroisoeugenol = 53 %). Considering all these facts 10 mmol of oxidant was found suitable for the maximum conversion of isoeugenol.

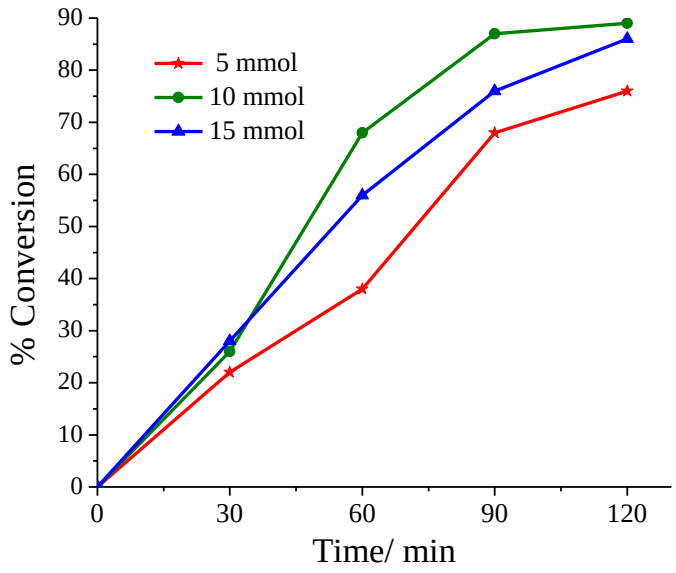

Figiure 4.35. Effect of the amount of oxidant i.e. 30 % aqueous H_2O_2 on the oxidation of isoeugenol. Reaction conditions: isoeugenol (0.82 g, 5 mmol), acetonitrile (7 mL), catalyst PS–im[VO_2(bzpy-inh)] (0.020 g), reaction temperature (80 ^oC) and reaction time 2 h.

The solvent (acetonitrile) also affects on the oxidation of substrate (Figure 4.36). Under above optimized reaction conditions i.e. PS–im[V^VO_2(bzpy-inh)] (0.020 g) and 30 % aqueous H_2O_2 (1.13 g, 10 mmol), three different solvent volumes i.e. 4, 7 and 10 mL for isoeugenol (0.82 g, 5 mmol) were taken and reaction was carried out at 80 ^oC for 2 h. It was found that 4 mL solvent gave highest conversion (91 %) with product distribution: vanilic acid = 31 %, vanillin = 10 % and dehydroisoeugenol = 50 %. Increasing the solvent volume decreases the conversion as well as percentage of vanillin. Thus, 4 mL solvent amount was considered to be the best one for maximum conversion of isoeugenol.

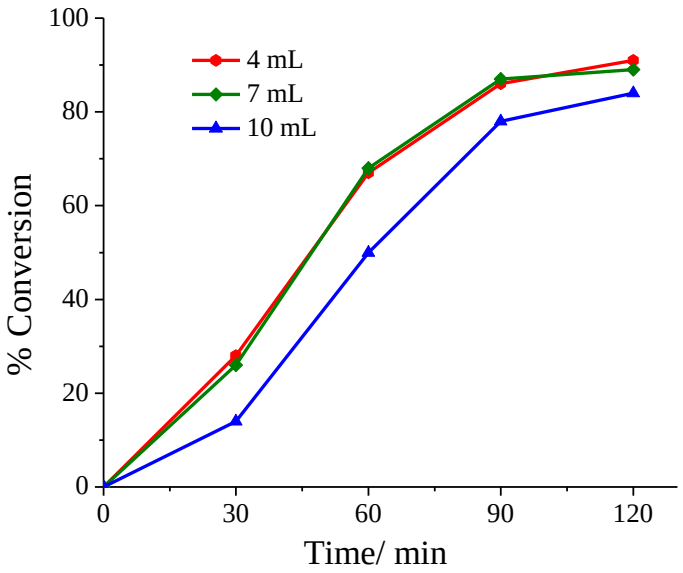

Figure 4.36. Effect of the amount of solvent (acetonitrile) on the oxidation of isoeugenol. Reaction conditions: isoeugenol (0.82 g, 5 mmol), PS–im[$V^{V}O_2$(bzpy-inh)] (0.020 g), 30 % aqueous H_2O_2 (1.13 g, 10 mmol), reaction temperature (80 ^{o}C) and reaction time 2 h.

The effect of temperature on oxidation of isoeugenol is presented in Figure 4.37. To a 5 mmol (0.82 g) isoeugenol in 4 mL of acetonitrile, PS–im[$V^{V}O_2$(bzpy-inh)] (0.020 g) and 30 % aqueous H_2O_2 (1.13 g, 10 mmol) were added and the reaction was monitored at three different temperatures viz. 60, 70 and 80 ^{o}C for 2 h. The conversion was lowest (42 %) at 60 ^{o}C but improved to 84 % at 70 ^{o}C. However, running the reaction at 80 ^{o}C improved this conversion to 91 % with a product distribution of 31 % vanillic acid, 10 % vanillin and 50 % dehydroisoeugenol.

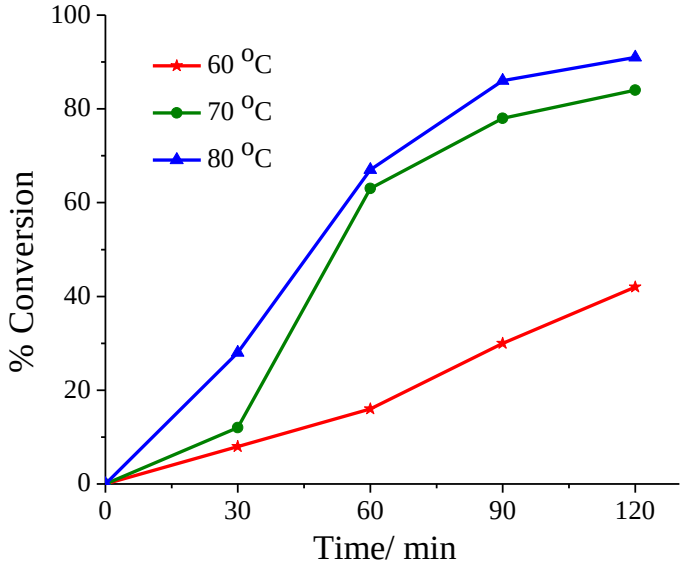

Figure 4.37. Effect of the temperature on oxidation of isoeugenol. Reaction conditions: isoeugenol (0.82 g, 5 mmol), acetonitrile (4 mL), PS–im[$V^{V}O_2$(bzpy-inh)] (0.020 g), 30 % aqueous H_2O_2 (1.13 g, 10 mmol) for 2 h.

Details of all experimental conditions are presented in Table 4.11. Thus, the optimized reaction conditions (entry no. 7) for the oxidation of 5 mmol of isoeugenol are: catalyst PS–im[$V^{V}O_2$(bzpy-inh)] (0.02 g), 30 % aqueous H_2O_2 (1.13 g, 10 mmol), acetonitrile (4 mL) and temperature 80 ^{o}C. A maximum of 18 % conversion was achieved after 2 h using 70 % aqueous TBHP as oxidant under above optimized reaction conditions with a product distribution: vanillic acid = 1 %, vanillin = 9 % and dehydroisoeugenol = 8 %. Blank reaction gave only 12 % conversion.

Details of the consumption of isoeugenol and formation of products for the catalyst PS–im[$V^{V}O_2$(bzpy-inh)] are presented in Figure 4.38. Under the experimental conditions presented in entry no. 7 of Table 4.11, the formation of all three products starts with the consumption of isoeugenol and increase with time. The formation of vanillic acid is better compared to vanillin in the beginning but improves and reaches 30 % while that of vanillin could reach only 10 %. The formation of dehydroisoeugenol reaches 50 % after 2 h of reaction time. Literature also reports similar trend of the formation of these products and in all cases the overall percent formation of vanillin is

low. Non polymer-anchored complexes are equally active and exhibit similar trend of formation of different products (Table 4.12). However, the recycle ability of the polymer-supported complexes makes them better catalysts over non polymer-supported ones.

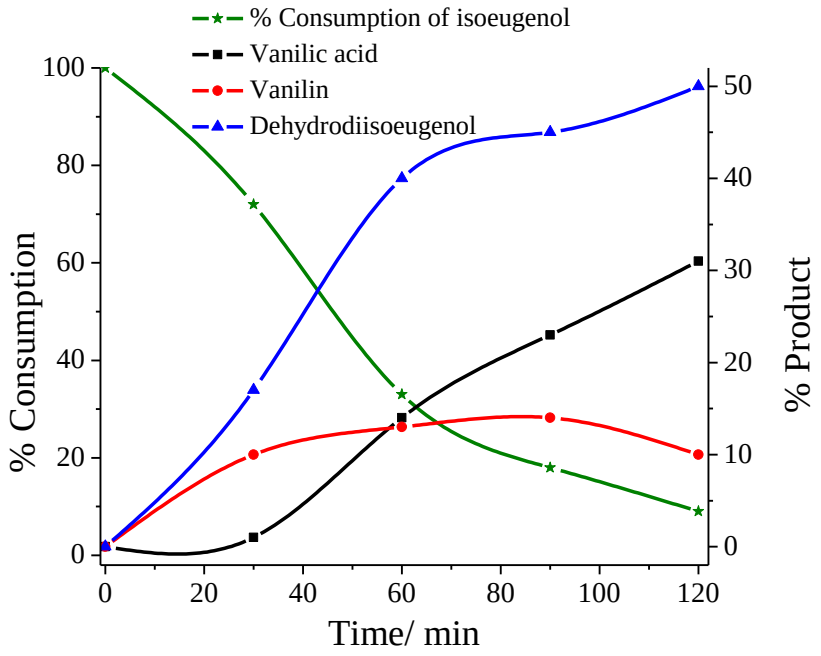

Figure 4.38. Percentage consumption of isoeugenol and formation of products with time using PS–im[$V^{V}O_2$(bzpy-inh)] as catalyst precursor under the optimized conditions specified in the text.

Table 4.11.

Results of the oxidation of 0.82 g (5 mmol) of isoeugenol after 2 h of reaction time using PS–im[$V^{V}O_2$(bzpy-inh)] (**4.7**) as catalyst precursor.

Entry No.	Catalyst (g)	H_2O_2 (g, mmol)	CH_3CN (mL)	Temp. (^oC)	% Conv.	% products formation*			TOF
						VA	Vanillin	DDI	
1	0.010	1.13, 10	7	80	61	13	6	42	307
2	0.020	1.13, 10	7	80	89	20	17	52	449
3	0.030	1.13, 10	7	80	85	21	15	49	428
4	0.040	1.13, 10	7	80	86	22	14	50	433
5	0.020	0.565, 5	7	80	76	15	7	54	383
6	0.020	1.69, 15	7	80	86	18	14	53	433
7	0.020	1.13, 10	4	80	91	31	10	50	459
8	0.020	1.13, 10	10	80	84	20	9	55	423
9	0.020	1.13, 10	4	60	42	10	5	27	212
10	0.020	1.13, 10	4	70	84	26	8	50	423
11.	-	1.13, 10	4	80	10	1	8	1	-

*VA = Vanilic acid, DDI = Dehydrodiisoeugenol

Table 4.12.

Product selectivity and % conversion at optimum reaction conditions, chosen for maximum conversion of isoeugenol.

S. No.	Catalyst	Catalyst (g)	% Conv.	TOF (h^{-1})	% products formation*		
					VA	Vanillin	DDI
1	PS–im[$V^{V}O_2$(bzpy-tch)] (**4.7**)	0.022	85	428	25	9	51
2.	PS–im[$V^{V}O_2$(bzpy-inh)] (**4.8**)	0.020	91	459	31	10	50
3.	[{$V^{V}O$(bzpy-tch)}$_2$μ-O_2] (**4.3**)	1.93×10^{-3}	70	353	19	5	46
4.	[{$V^{V}O$(bzpy-inh)}$_2$μ-O_2] (**4.4**)	1.96×10^{-3}	74	373	20	7	47

*VA = Vanilic acid, DDI = Dehydrodiisoeugenol

4.4. Conclusions

Two hydrazones of 2-benzoylpyridine has been used as monobasic tridentate ONN donor ligands to prepare oxidovanadium(IV) complexes $[VO^{IV}(acac)(bzpy\text{-}tch)]$ (**4.1**)and $[VO^{IV}(OMe)(bzpy\text{-}inh)]$ (**4.2**). The dioxidovanadium(V) complexes $[\{V^{V}O(bzpy\text{-}tch)\}_2(\mu\text{-}O)_2]$ (**4.3**) and $[\{V^{V}O(bzpy\text{-}inh)\}_2(\mu\text{-}O)_2]$ (**4.4**) have been synthesized by the aerial oxidation of oxidovanadium(IV) complexes. Reaction of dioxidovanadium(V) complexes with H_2O_2 yielded oxidiperoxidovanadium(V) complexes $[V^{V}O(O_2)(bzpy\text{-}tch)(MeOH)]$ (**4.5**) and $[V^{V}O(O_2)(bzpy\text{-}inh)(MeOH)]$ (**4.6**).The structure of the complexes **4.3, 4.4, 4.6** has been established by single crystal X-ray analysis. All the complexes have been characterized well by various spectroscopic techniques. EPR, ^{51}V NMR and ESI-MS studies shows the dual nature of the dioxidovanadium(V) complexes as in solution they exists in both V(IV) and V(V) species. The dioxidovanadium(V) complexes have been supported on imidazolomethylpolytyrene (PS-im) to prepare polymer-anchored complexes PS–im$[V^{V}O_2(bzpy\text{-}tch)]$ (**4.7**) and PS–im$[V^{V}O_2(bzpy\text{-}inh)]$ (**4.8**). EPR studies shows that after anchoring dioxidovanadium(V) species has been converted into oxidovanadium(IV) species. Acting as model polymer supported complexes of VHPO's, they have been used as for the oxidation of isoeugenol effectively.

Chapter 5

Polymer supported oxidovanadium (IV) complexes of Schiff base derived from salicylaldehyde and 1,3-diamino-2-hydroxypropane as peroxidase mimetic catalyst towards oxidation of pyrogallol

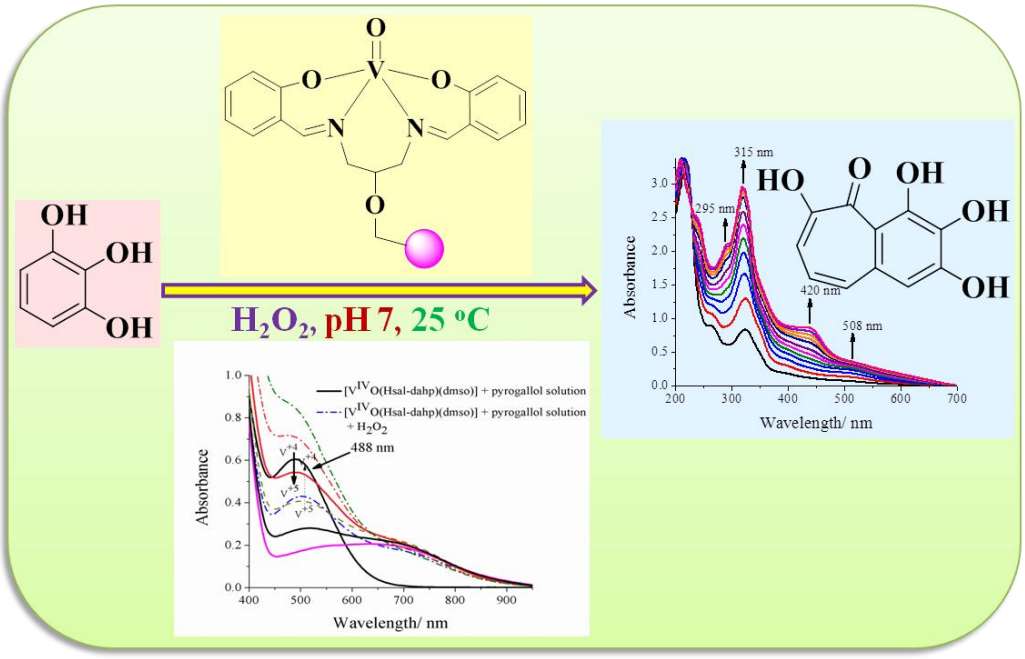

5.1. Introduction

Peroxidase enzymes have significant applications in many physiological reactions. Peoxidase-like activity of haloperoxidases has also been reported towards classical peroxidase substrates using recombinant VHPO [173]. However, the use of natural or recombinant enzyme is not economically viable in terms of their industrial application due to difficulty in bulk production, higher production cost, poor stability and very specific reaction conditions (such as pH and reaction medium). Application of heterogeneous vanadium containing catalysts can overcome these problems. V_2O_5 nanowire [174] has been used as heterogeneous catalyst mimicking peroxidase activity. However, no example of peroxidase like activity of polymer supported vanadium complexes has been reported to the best of our knowledge.

Dinuclearorganophosphorus-bridged vanadium complex of formula {(LVO(μ-O_2PRR')}$_2$[L = η^5-cyclopentadienyltris(diethylphosphito-κ^1P) cobaltate(III)] has been used as effective catalyst in the oxidation of 3,5-di-tertbutylcatechol to the corresponding quinone [175]. This complex could also be explored for the oxidation of pyrogallol. Similar other complexes reported by Mc Lauchlan et al. are expected to be potential catalysts for mimicking peroxidase activity [176,177].

Applications of polymer supported vanadium complexes as catalysts have grown tremendously over the past few years [53,54]. Vanadium complexes, in the presence of oxidants like H_2O_2 and *tert*-butylhydroperoxide (TBHP) act as good oxidation catalysts as they easily form intermediate complex with electron rich peroxido group, which in turn transfer oxygen to the organic substrates [25,32,33]. The polymer support acts as protein mantle and prevents the decomposition of the complexes which in turn enhances their turn over numbers.These observations inspired us to design the vanadium complex which can easily be linked covalently to the Merrifield resin (chloromethylated polystyrene) to obtain the supported vanadium complex as heterogeneous biological catalyst. Several strategies have been adopted to modify chloromethylated polystyrene depending upon the structure of ligands and metal complexes in order to prepare chloromethylated polystyrene-supported metal complexes [53,54,55].

Smith et al. [178] have prepared oxidovanadium(IV) complex [V^{IV}O(Hsal-dahp)]$_n$ of tribasic pentadentate ligand derived from salicylaldehyde and 1,3-diaminohydroxypropane [Scheme 5.1, H_3sal-dahp (**5.I**)] which is similar to salen type

ligands but has additional free hydroxyl group which could be used for immobilization e.g. on to chloromethylated polystyrene. Complex $[V^{IV}O(Hsal\text{-}dahp)]_n$, though, shows good catalytic properties, it could not be immobilized on to chloromethylated polystyrene to make it recyclable during catalytic reaction due to its existence in polymeric form with ---(L)V=O---(L)V=O--- structure. We observed that this complex could easily be converted into monomeric species using polar solvents like DMSO/ DMF and can be made suitable for immobilization on to chloromethylated polystyrene. In this contribution, we therefore report the isolation of monomeric $[V^{IV}O(Hsal\text{-}dahp)(dmso)]$, its immobilization on to chloromethylated polystyrene and characterization. This polymer supported complex (abbreviated now as PS-$[V^{IV}O(sal\text{-}dahp)]$) shows good peroxidase like activity in aqueous medium. Very similar complex $[V^{V}O(hap\text{-}dahp)]$ (derived from *o*-hydroxyacetophenone and 1,3-diaminohydroxypropane) has been encapsulated in the nano-pores of zeolite-Y and used as catalyst for oxidation reactions [179].

5.2. Experimental Section

5.2.1. Materials and methods

$[V^{IV}O(acac)_2]$ [111] and H_3sal-dahp (**5.I**) [178] were prepared according to methods reported in the literature. Vanadium content in PS-$[V^{IV}O(sal\text{-}dahp)]$ (**5.2**) was determined by ICP-MS. Sample for ICP-MS was prepared by taking 0.02 g of **5.2** in a beaker and treating with 6 mL of nitric acid-hydrochloric acid (1 : 1) mixture on a hot plate. After complete leaching the residue was dissolved in deionized-distilled water, filtered and diluted up to 50 mL. Other details are presented in Chapters 2 and 4.

5.2.2. Synthesis

5.2.2.1. $[V^{IV}O(Hsal\text{-}dahp)(dmso)]$ (5.1)

Polymeric complex $[V^{IV}O(Hsal\text{-}dahp)]_n$ was prepared by the reaction of $VOSO_4{\cdot}5H_2O$ (0.506 g, 2 mmol) and H_3sal-dahp (0.596 g, 2 mmol) in methanol as reported in the literature [178]. It was also prepared by another method given here. To a stirred solution of H_3sal-dahp (0.596 g, 2 mmol) in methanol (10 mL) was added a solution of $[V^{IV}O(acac)_2]$ (0.530 g, 2 mmol) in methanol (10 mL) and the reaction mixture was refluxed on a water bath for 1 h where light orange solid separated. This

was filtered off, washed with methanol and dried in vacuo over silica gel. Yield: 0.580 g **(**80 %). $[V^{IV}O(sal\text{-}dahp)]_n$ was dissolved in minimum hot dimethyl sulfoxide (dmso), filtered and left for slow evaporation at room temperature. Light orange crystals of $[V^{IV}O(Hsal\text{-}dahp)(dmso)]$ (**5.1**) suitable for X-ray diffraction study slowly formed which were filtered, washed with methanol and dried at room temperature. Anal. Calc. for $C_{19}H_{22}N_2O_5SV$ (441.39): C, 51.70; H, 5.02; N, 6.34; S, 7.26%. Found: C, 52.14; H, 4.9; N, 6.5; S, 6.9%.

5.2.2.2. PS-$[V^{IV}O(sal\text{-}dahp)]$ (5.2)

Cholоromethylated polystyrene beads (1.00 g) were suspended in DMF (20 mL) and left for 2 h. A solution of $[V^{IV}O(Hsal\text{-}dahp)]_n$ (1.0 g, 2.75 mmol) in 30 mL DMF was added to the above suspension of beads. After adding triethylamine (3 mL) and K_2CO_3 (0.069 g, 0.5 mmol) the resulting mixture was heated at 90 ^oC for 2 days with slow mechanical stirring. Finally, the beads were filtered off, washed with DMF followed by hot methanol and dried in oven at 80 ^oC. Recovery yield: 94%. Found vanadium content by ICP-MS: 0.145 mmol g^{-1} of resin.

5.2.2.3. Catalytic oxidation of pyrogallol: a peroxidase mimetic activity

Catalyst PS-$[V^{IV}O(sal\text{-}dahp)]$ was suspended in acetonitrile for 2 h before starting the reaction. The reaction was carried out in a 50 mL round bottom flask. In a typical reaction 1 mL of 0.25×10^{-1} M (0.025 mmol) pyrogallol solution was mixed in a phosphate buffer of pH 7 and the reaction was started with the addition of 0.25×10^{-1} M (0.025 mmol) solution of 30% H_2O_2 and catalyst (0.64 mg, 0.00145 mmol). The progress of the reaction was monitored by measuring the successive increase the in the intensity of a new band at 420 nm up to 2 h using UV-Vis spectrophotometer.

5.2.4. X-Ray crystal structure determination

Three-dimensional X-ray data were collected on a Bruker Kappa Apex CCD diffractometer at low temperature for **5.1** by the ϕ-ω scan method. Reflections were measured from a hemisphere of data collected from frames each of them covering 0.3º in ω. Of the 18878 reflections measured, all were corrected for Lorentz and polarization

effects and for absorption by multi-scan methods based on symmetry-equivalent and repeated reflections, 2200 independent reflections exceeded the significance level ($|F|/\sigma|F|$) > 4.0. Complex scattering factors were taken from the program package SHELXTL [113]. The structures were solved by direct methods and refined by full matrix least-squares on F^2. Hydrogen atoms were left to refine freely. Refinements were done with allowance for thermal anisotropy of all non-hydrogen atoms. Further details of the crystal structure determination are given in Table 5.1. A final difference Fourier map showed no residual density outside: 0.412 and –0.368 e.Å^{-3}. A weighting scheme $w = 1/[\sigma^2(F_o^2) + (0.038600\ P)^2 + 1.162400\ P$, where $P = (|F_o|^2 + 2|F_c|^2)/3$, was used in the latter stages of refinement.

Table 5.1. Crystal data and structure refinement for [$V^{IV}O$(Hsal-dahp)(dmso)] (**5.1**).

	5.1
Formula	$C_{19}H_{24}N_2O_6SV$
Formula weight	459.40
T, *K*	100(2)
Wavelength, Å	0.71073
Crystal system	Orthorhombic
Space group	Pnma
a/Å	16.9139(5)
b/Å	15.8319(4)
c/Å	7.3289(2)
V/Å^3	1962.53(9)
Z	4
F_{000}	956
D_{calc}/g cm^{-3}	1.555
μ/mm^{-1}	0.652
θ/ (º)	2.73 to 28.32
R_{int}	0.0376
Crystal size/ mm^3	0.22 x 0.19 x 0.15

Goodness-of-fit on F^2	1.063
$R_1[I>2\sigma(I)]$ [a]	0.0284
wR_2 (all data) [b]	0.0780
Largest differences peak and hole ($eÅ^{-3}$)	0.412 and -0.368

[a] $R_1 = \Sigma \left| \left| F_o \right| - \left| F_c \right| \right| / \Sigma \left| F_o \right|$. [b] $wR_2 = \{\Sigma[w(\left| \left| F_o \right|^2 - \left| F_c \right|^2 \right|)^2] / \Sigma[w(F_o^4)]\}^{1/2}$

5.3. Results and discussion

Reaction between $[V^{IV}O(acac)_2]$ (Hacac = acetylacetone) and tribasic pentadentate Schiff base H_3sal-dahp (**5.I**, Scheme 5.1) in methanol leads to the formation of oxidovanadium(IV) complex where ligand behaves as dibasic tetradentate coordinating through both of the phenolic oxygens and azomethine nitrogens. Alcoholic oxygen of the ligand does not take part in coordination. However, complex is polymeric in nature having formula $[V^{IV}O(Hsal\text{-}dahp)]_n$ in the solid state with polymeric chain of V=O----V=O [178]. Dissolving $[V^{IV}O(Hsal\text{-}dahp)]_n$ in hot (80 ^oC) dimethyl sulfoxide and leaving for crystallization at room temperature results in the breaking of V=O----V=O chain and formation of a monomeric species of formula $[V^{IV}O(Hsal\text{-}dahp)(dmso)]$ (**5.1**). Structures of the ligand and complex are presented in Scheme 5.1.

Interaction of chloromethylpolystyrene cross-linked with 5% divinylbenzene (PS–Cl) with **5.1** in DMF in presence of triethylamine resulted in the formation of the corresponding polymer-grafted oxidovanadium(IV) complex, PS–$[V^{IV}O(sal\text{-}hdap)]$ (**5.2**) (Scheme 5.2). Both complexes were characterized by various spectroscopic techniques (IR, electronic and EPR), thermal, atomic force microscopy (AFM) and field-emission scanning electron micrographs (FE–SEM) as well as energy dispersive X-ray (EDAX) studies.

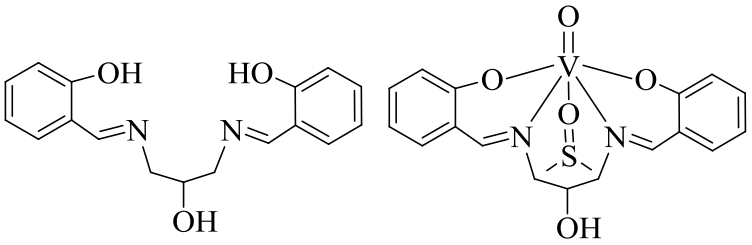

(H_3sal-dahp) (**5.I**) [V^{IV}O(Hsal-dahp)(dmso)] (**5.1**)

Scheme 5.1. Structures of H_3sal-dahp (**5.I**) and its monomeric vanadium complex [V^{IV}O(Hsal-dahp)(dmso)] (**5.1**).

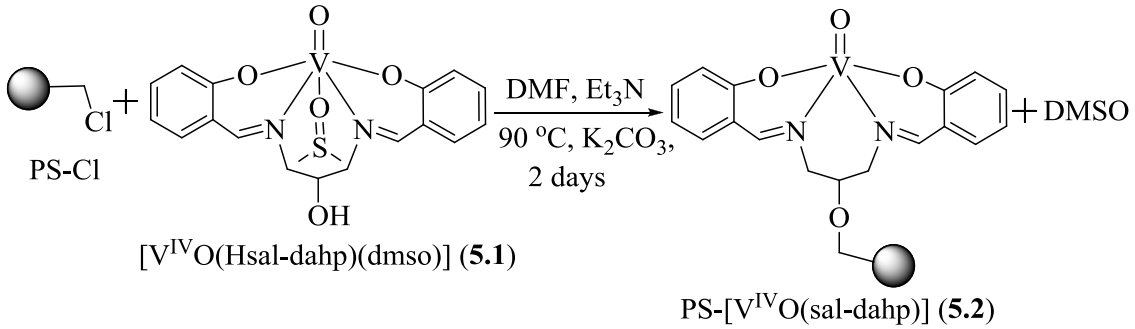

Scheme 5.2. Synthetic route to prepare polymer-supported complex PS–[V^{IV}O(sal-dahp)] (**5.2**).

5.3.1. TGA studies

Thermal stability of neat as well as polymer supported complexes was studied by thermo gravimetric analysis. Neat complex [V^{IV}O(Hsal-dahp)(dmso)] (**5.1**) is stable up to *ca.*160 ^{o}C. Thereafter organic part starts decomposing in three consecutive exothermic steps and the final residue of 21.0% at *ca.* 500 ^{o}C corresponds to V_2O_5; the theoretical value of 20.5% being close to the obtained one. The thermal decomposition of PS-[V^{IV}O(sal-dahp)] (**5.2**) occurs in three steps. A total weight loss of 4.8% observed in the temperature range of 100-200 ^{o}C may be due to loss of trapped solvent and water molecules. The weight loss in the temperature range 200-400 ^{o}C is possibly due to collapse of part of the complex moiety. The major decomposition occurs between 400-500 ^{o}C which may be attributed to the decomposition of major part of polymer residue along with the decomposition of remaining part of organic ligand. Further weight loss of 1.8% was observed between 500-900 ^{o}C. The final obtained residue of 0.9% is due to

V_2O_5 and the vanadium content calculated from this value is 0.17 mmol g^{-1} of resin which is almost similar to the vanadium content obtained from ICP-MS (0.145 mmol g^{-1}) and EDAX (0.127 mmol g^{-1} of resin).

5.3.2. Single Crystal Structure of [V^{IV}O(Hsal-dahp)(dmso)] (5.1)

Complex [V^{IV}O(Hsal-dahp)(dmso)] (**5.1**) crystallizes in a centrosymmetric orthorhombic space group, Pnma. Half water molecule and half [V^{IV}O(Hsal-dahp)(dmso)] complex are present in the asymmetric unit and grow through x, -y+1/2, z (#1) symmetry transformation for generating the equivalent atoms. This complex adopts a six-coordinated structure in a distorted octahedral geometry. The phenolic oxygen and the imine nitrogen atoms of the ligands coordinate to the vanadium centre while hydroxyl group of the ligand does not participate in coordination. One dmso molecule and oxo group completes the coordination sphere. The equatorial plane therefore comprises a [N(1), O(1), N(1A), O(1A)] donor atom set (mean deviation from the plane = 0.0000 Å), and the V^{V}O center is projected from this plane by 0.3455 Å.

Figure 5.1 shows an ORTEP representation of [V^{IV}O(Hsal-dahp)(dmso)] (**5.1**) and Figure 5.2 shows an ORTEP representation of the crystal packing in which the complexes form an antiparallel dimer through π-π interactions between phenol rings and C=N bonds of two complexes. Table 5.2 presents selected bond lengths and bond angles. The distance between centroids are: $d_{c1–c2}$ = 3.457 Å [c1 (C7AB-N1AB), c2 (C1AF-C2AF-C3AF-C4AF-C5AF-C6AF)], $d_{c3–c4}$ = 3.457 Å [c3 (C7AF-N1AF), c4 (C1AB-C2AB-C3AB-C4AB-C5AB-C6AB)]. Intermolecular hydrogen bonds between water molecules and complexes are present in the crystal packing (see Table 5.3). An intramolecular hydrogen bond is present between hydroxyl group and DMSO coordinated molecule, too.

5.3.3. IR spectral studies

IR spectra of [V^{IV}O(Hsal-dahp)(dmso)], PS-Cl and PS-[V^{IV}O(sal-dahp)] are reproduced in Figure 5.3 and a partial list of spectral data are presented in Table 5.4. The ligand displays a broad band at 3390 cm^{-1} due to free –OH groups. The bonding of hydroxyl oxygen to PS-Cl could not be ascertained by IR spectra as PS-[V^{IV}O(sal-

dahp)] (**5.2**) also exhibits weak band at 3400 cm^{-1} due to the trapped residual water in the polymer matrices. The band appearing at 1607 cm^{-1} due to azomethine group shifts to lower wave number in complexes suggesting the coordination of nitrogen to the vanadium. Neat complex **5.1** exhibits a sharp band at *ca.* 950 cm^{-1} due to ν(V = O) mode while supported complex exhibits such band at 992 cm^{-1}. Other characteristic bands of polystyrene as well as of neat complex are also present in supported complex.

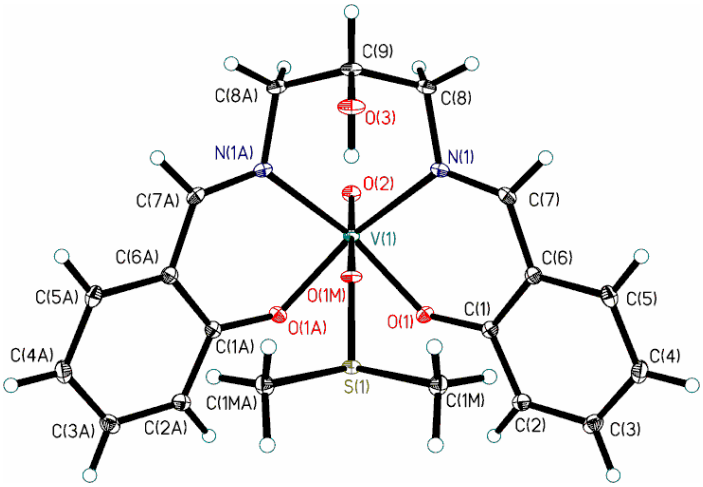

Figure 5.1. ORTEP representation of [V^{IV}O(Hsal-dahp)(dmso)] (**5.1**).

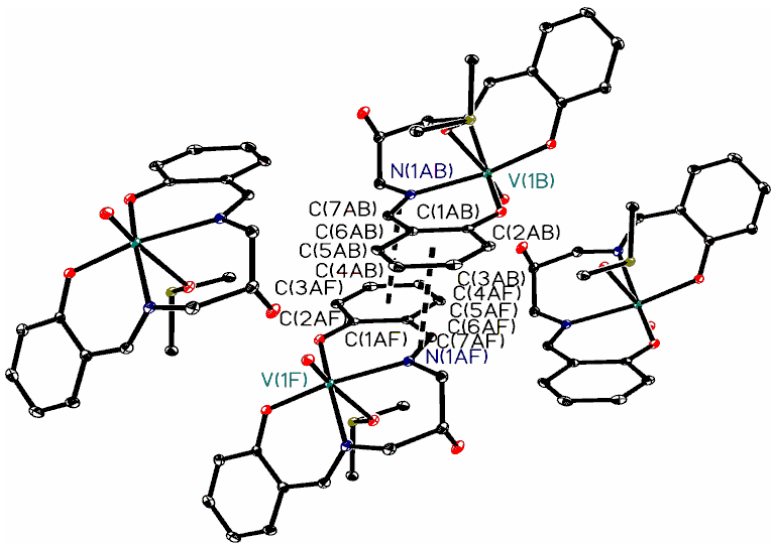

Figure 5.2. ORTEP representation of the crystal packing in [V^{IV}O(Hsal-dahp)(dmso)] (**5.1**).

Table 5.2. Bond lengths [Å] and angles [°] for [V^{IV}O(Hsal-dahp)(dmso)] (**5.1**).

Bond lengths	**5.1**
V(1)-O(1)	1.9571(10)
V(1)-O(2)	1.6025(15)
V(1)-N(1)	2.1064(12)
V(1)-O(1M)	2.3177(14)
N(1)-C(7)	1.280(2)
N(1)-C(8)	1.4647(18)
Bond angles	**5.1**
O(2)-V(1)-O(1)	104.55(5)
O(2)-V(1)-N(1)	95.31(5)
O(1)-V(1)-N(1)	87.89(4)
O(2)-V(1)-O(1M)	167.21(6)
O(1)-V(1)-O(1M)	84.78(4)
N(1)-V(1)-O(1M)	76.03(4)

Table 5.3. Hydrogen bonds for [V^{IV}O(Hsal-dahp)(dmso)] (**5.1**).

D-H...A	d(D-H)	d(H...A)	d(D...A)	<(DHA)
O(1W)-H(2WA)...O(3)#2	0.88(4)	1.91(4)	2.793(2)	175(3)
O(1W)-H(1WA)...O(1)#3	0.81(5)	2.51(4)	3.195(2)	143(2)
O(1W)-H(1WA)...O(1)#4	0.81(5)	2.51(4)	3.195(2)	143(2)
O(3)-H(3O)...O(1M)	0.80(3)	2.11(3)	2.902(2)	172(3)

Symmetry transformations used to generate equivalent atoms:

#1 x,-y+1/2,z #2 x+1/2,y,-z+5/2 #3 x,-y+1/2,z+1 #4 x,y,z+1

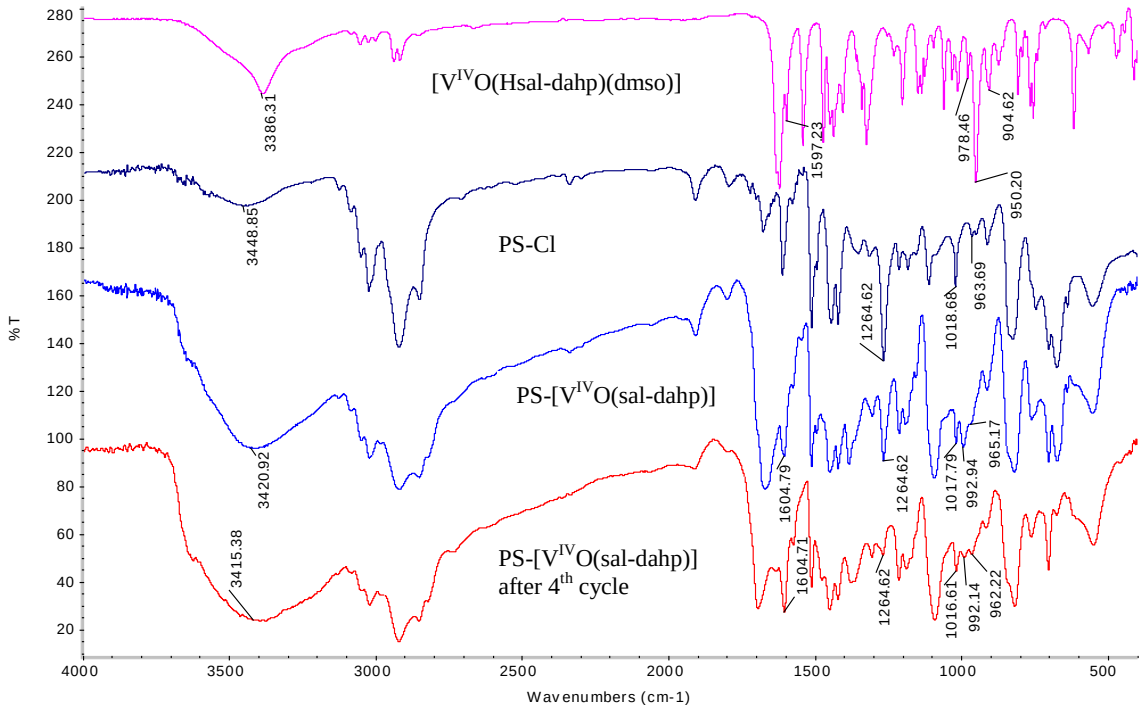

Figure 5.3. IR spectra of [$V^{IV}O$(Hsal-dahp)(dmso)], PS-Cl , PS-[$V^{IV}O$(sal-dahp)] and PS-[$V^{IV}O$(sal-dahp)] after 4th cycle.

Table 4. IR spectral data (cm^{-1}) of ligand and complexes.

S. No.	Compounds	ν(OH)	ν(C=N)	ν(V=O)
1	H_3sal-dahp (**5.I**)	3390 (broad)	1607	-
2	[$V^{IV}O$(Hsal-dahp)(dmso)] (**5.1**)	3386	1597	950
3	PS-[$V^{IV}O$(sal-dahp)] (**5.2**)	3400 (broad)	1604	992

5.3.4. Electronic spectral studies

Electronic spectra of similar ligand, its vanadium complex and zeolite-Y encapsulated complexes have been described in the literature [179]. Data of the ligand H_3sal-dahp (**5.I**) and complex recorded in methanol are very similar to [$V^{V}O$(hap-dahp)] [179]; Table 5.5. All ligand bands also appear in complexes with slight variations in their positions; Figure 5.4. Bands due to ligand to metal charge transfer and d – d transition for [$V^{IV}O$(Hsal-dahp)(dmso)] (**5.1**) become more clear in DMF and appear at 488 (ε/M^{-1} cm^{-1} = 0.98×10^2) and 748 nm (ε/M^{-1} cm^{-1} = 0.07×10^2), respectively.

Polymer supported complex PS-[$V^{IV}O$(sal-dahp)] (**5.2**) exhibits LMCT band at 386 nm (Figure 5.5). In addition, one d – d band (515 nm) could only be located due to poor loading of the complex on to polymer.

Table 5.5. Electronic spectral data of ligand and complexes

Compounds	Solvent	λ_{max}/nm (ε/M^{-1} cm^{-1})
H_3sal-dahp (**5.I**)	MeOH	215 (4.42×10^4), 256 (2.30×10^4), 282 (0.6×10^4), 316 (0.75×10^4), 402 (0.22×10^4)
[$V^{IV}O$(Hsal-dahp)(dmso)] (**5.1**)	MeOH	232 (4.37×10^4), 270 (2.21×10^4), 361 (0.82×10^4)
	DMF	488 (0.98×10^2), 748 (0.07×10^2)
PS-[$V^{IV}O$(sal-dahp)] (**5.2**)	Nujol	280, 386, 515

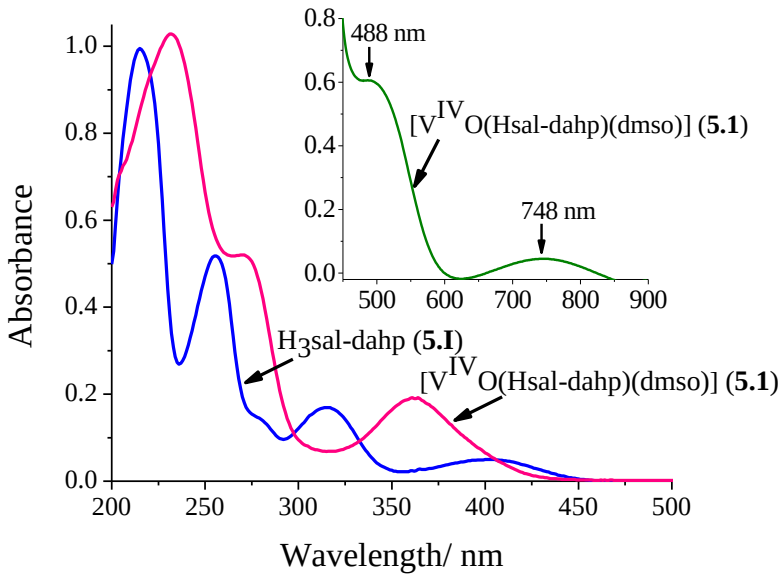

Figure 5.4. Electronic spectra of H_3sal-dahp (**5.I**) and [$V^{IV}O$(Hsal-dahp)(dmso)] (**5.1**) recorded in methanol. Inset shows d-bands in **5.1** in the visible region.

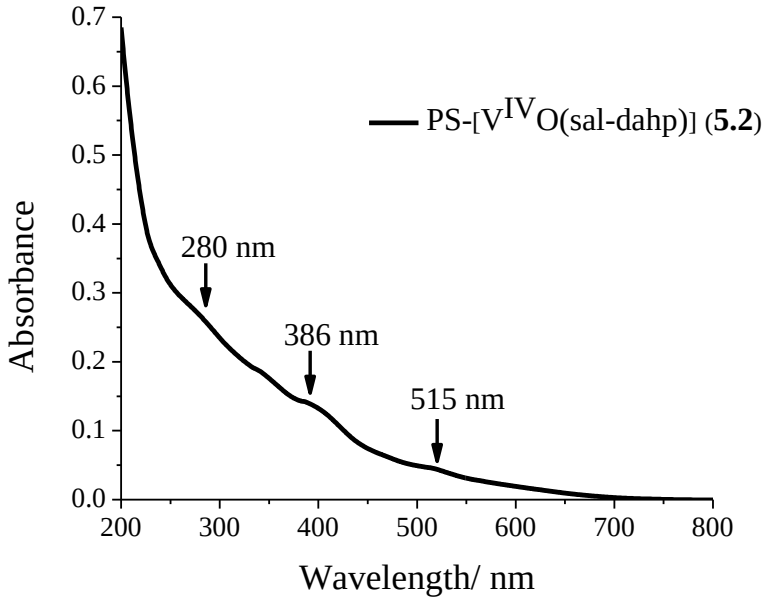

Figure 5.5. Electronic spectrum of PS-[$V^{IV}O$(sal-dahp)] (**5.2**) recorded in nujol.

5.3.5. EPR spectral study

The 1st derivative EPR spectra of "frozen" (77 K) solution of [$V^{IV}O$(Hsal-dahp)(dmso)] (**5.1**) in DMF and that of solid PS-[$V^{IV}O$(sal-dahp)] (**5.2**) at room temperature are presented in Figure 5.6. The spectra of both complexes are well resolved. The spectrum of **5.2** is characteristic of magnetically diluted $V^{IV}O$-complex and the well-resolved EPR hyperfine features indicate that the vanadium(IV) centers are well dispersed in the polymer matrix. Both the spectra were simulated and the obtained spin Hamiltonian parameters g_z and A_z agree well with the values estimated using the additivity relationship proposed by Wüthrich [119] and Chasteen [120] with estimated accuracy of $\pm 3\times10^{-4}$ cm^{-1}. The spin Hamiltonian parameters obtained by simulation of the experimental EPR spectra are given in Table 5.6. The predicted contributions to the parallel hyperfine coupling constant for the donor groups under consideration are same {2 × N_{imine}, 2 × $O_{phenolate}$ (161×10^{-4} cm^{-1})} [29,119,120]. In general, the hyperfine features of the spectra are consistent with a binding set involving ($O_{phenolate}$, N_{imine}, N_{imine}, $O_{phenolate}$)$_{equatorial}$. However, the possibility of the interaction of solvent with vanadium center could not be ascertained [29].

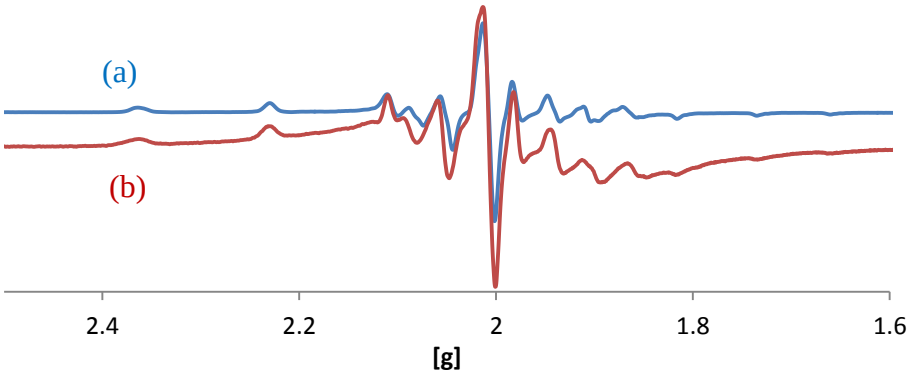

Figure 5.6. 1st derivative EPR spectra of [$V^{IV}O$(Hsal-dahp)(dmso)] (**5.1**) (a) recorded from DMF solution at 77 K, and of PS-[$V^{IV}O$(sal-dahp)] (**5.2**) (b) recorded from neat solid at room temperature.

Table 5.6. EPR spectral parameters of complexes

Compound	g_x, g_y (or $g_\perp$)	A_x, A_y (or $A_\perp$) $\times 10^4$ cm^{-1}	g_z (or $g_{//}$)	A_z (or $A_{//}$) $\times 10^4$ cm^{-1}
[$V^{IV}O$(Hsal-dahp)(dmso)] (**5.1**)	1.983	53.9	1.956	158.9
PS-[$V^{IV}O$(sal-dahp)] (**5.2**)	1.981	57.3	1.951	160.9

5.3.6. Field emission-scanning electron microscope (FE-SEM) and energy dispersive X-ray analysis (EDX) studies

Field emission scanning electron micrographs (FE-SEM) of chloromethylated polystyrene (PS-Cl) beads and PS-[$V^{IV}O$(sal-dahp)] (**5.2**) were recorded and their images are shown in Figure 5.7 (a and b). Only small morphological changes could be observed between plain polymer bead (PS-Cl) and polymer-anchored complex. However, a considerable increase in the diameter of beads could be noted. After complex anchoring EDX (Figure 5.7 (a' and b')) analysis shows 0.127 mmol g^{-1} of resin of vanadium content on the surface which is in agreement with the data obtained from ICP-MS (0.145 mmol g^{-1}).

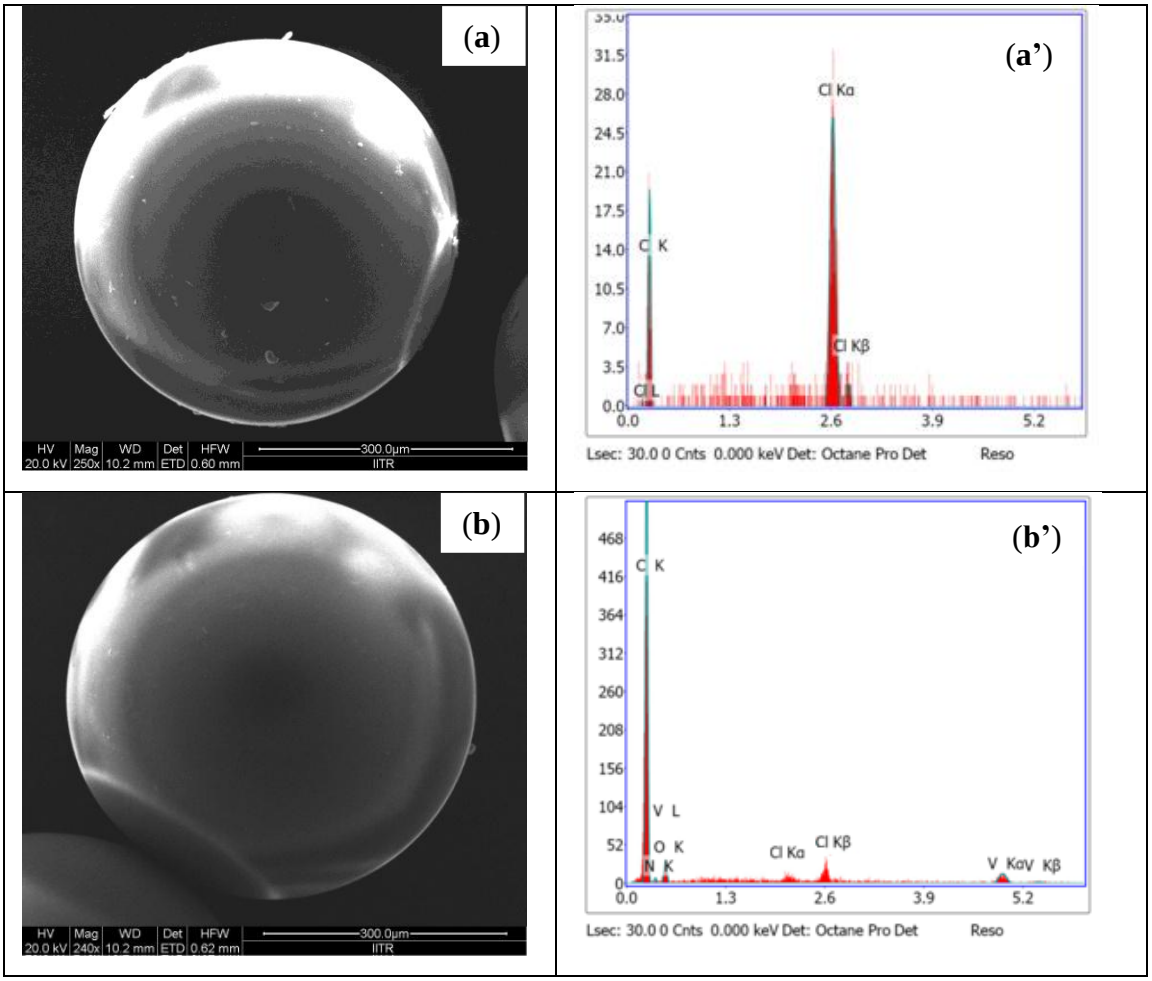

Figure 5.7. Field emission scanning electron micrographs of PS-Cl (**a**) and PS-[$V^{IV}O$(sal-dahp)] (**b**) and the energy dispersive x-ray analysis graphs of PS-Cl (**a'**) and PS-[$V^{IV}O$(sal-dahp)] (**b'**).

5.3.7. Atomic force microscopy (AFM) study

The change in morphology of PS-Cl after anchoring of complex was also studied by measuring surface roughness using AFM; Figure 5.8. The surface roughness and mean height for PS-Cl were observed to be 7.28006 nm and 72.8304 nm, respectively. On reacting PS-Cl with complex [$V^{IV}O$(Hsal-dahp)(dmso)], the surface roughness and mean height decreased to 1.91519 nm and 13.8057 nm, respectively. This shows that the complex has been anchored in the pores of beads thereby reducing the porosity. However, after 4^{th} cycle of oxidation reaction study the surface roughness and mean height increased slightly to 2.44583 nm and 18.0639 nm, respectively due to some morphological changes but it is quite less than that of PS-Cl, indicating that complex is

still anchored to the PS-Cl. This is in agreement with the fact that no leaching was observed even after 4th cycle of oxidation reaction.

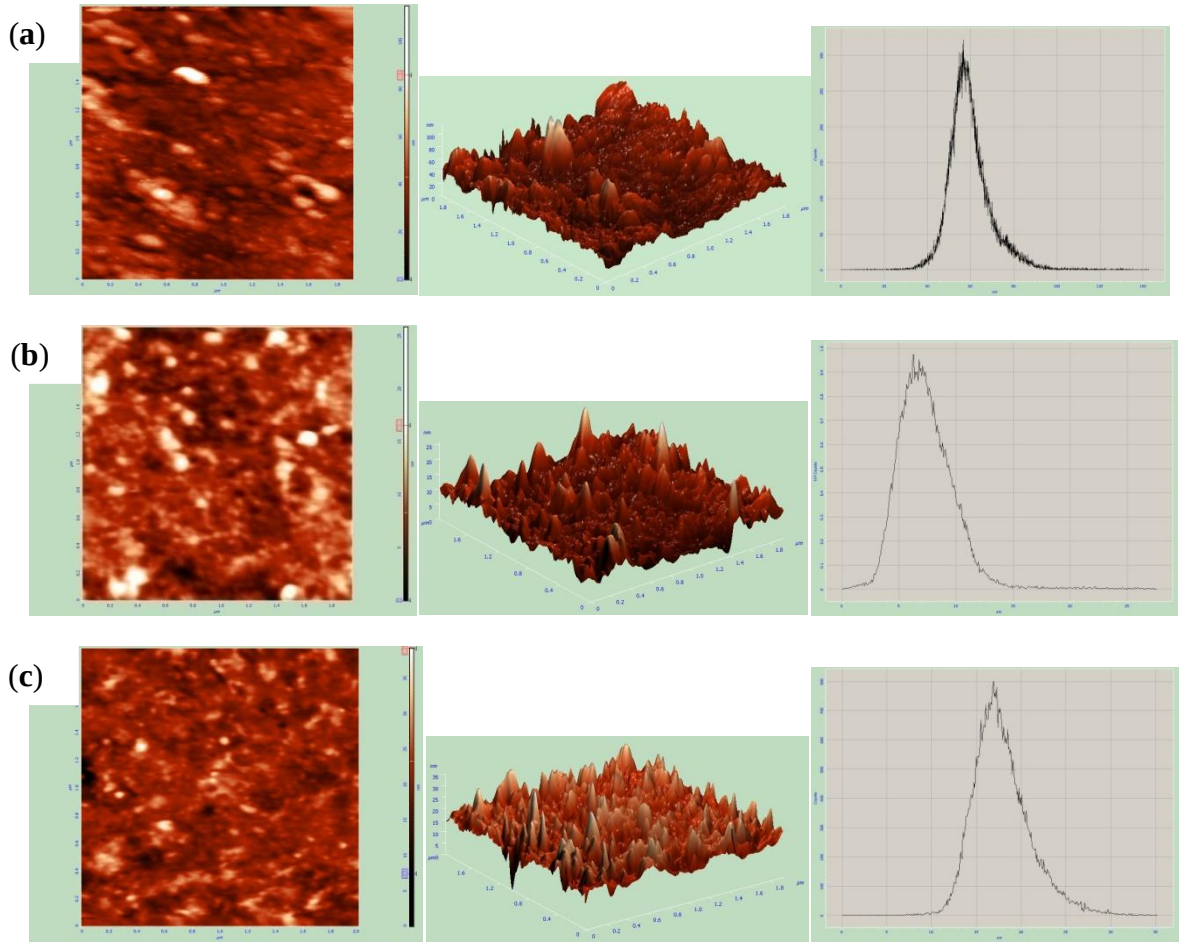

Figure 5.8. AFM images (left), 3d-views (middle) and respective histograms (right) of PS-Cl (**a**),PS-[$V^{IV}O$(sal-dahp)] (**b**) and PS-[$V^{IV}O$(sal-dahp)] after use (**c**). Scanning area 2×2 µM.

5.3.8. Peroxidase mimetic activity of polymer supported complex

We have investigated the peroxidase mimetic activity of polymer supported complex PS–[$V^{IV}O$(sal-dahp)] (**5.2**) by using the typical peroxidase substrate pyrogallol [180] in the presence of H_2O_2. It is capable to catalyze the chromogenic reaction, i.e. oxidation of pyrogallol, which was monitored using a UV-visible spectrophotometer.

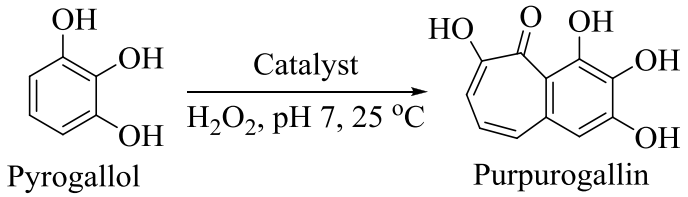

Scheme 5.3. Peroxidase like oxidation of pyrogallol to purpurogallin catalyzed by PS–[$V^{IV}O$(sal-dahp)] (**5.2**).

To start with a preliminary experiment was carried out considering (i) 1 mL of 0.25×10^{-1} M pyrogallol, (ii) 1 mL of 0.25×10^{-1} M pyrogallol in 3 mL of phosphate buffer of pH 7 and 1 mL of 0.25×10^{-1} M solution of 30% H_2O_2 (0.00315 g, 0.025 mmol) and (iii) 1 mL of 0.25×10^{-1} M pyrogallol in 3 mL phosphate buffer of pH 7, 1 mL of 0.25×10^{-1} M solution of 30% H_2O_2 (0.00315 g, 0.025 mmol) and different amounts of previously swelled catalyst and monitoring them by UV-visible spectrophotometer after 2 min of their preparations. The transparent pyrogallol has no absorption while it turns yellow [181] in the presence of buffer solution and H_2O_2 and shows a very weak absorption at *ca.* 420 nm. Solution of set (iii) gradually changes to pink and then to reddish-brown along with the sharpening of 420 nm band in the presence of catalyst indicating that pyrogallol can be oxidized by H_2O_2 in the absence as well as in the presence of catalyst both but the extent of oxidation is different in two cases. Further, slight variations in colour along with different intensity of absorption at 420 nm could also be observed for solutions having different amount of catalyst; Figure 5.9. The characteristic new band at 420 nm is due to the formation of purpurogallin which is absent in pyrogallol [182, 183]. The monitoring of the successive increment in the absorbance of the new band at 420 nm for one of the sets having 1 mL of 0.25×10^{-1} M pyrogallol in 3 mL phosphate buffer of pH 7, 1 mL of 0.25×10^{-1} M solution of 30% H_2O_2 (0.00315 g, 0.025 mmol) and catalyst (0.007 g) was continued with time. The reaction attained the maximum measurable absorbance in 2 h; Figure 5.10. Therefore, various parameters such as different amounts of oxidant and catalyst and pH of the reaction medium have been optimized to conclude the best suited reaction conditions for the maximum oxidation of pyrogallol.

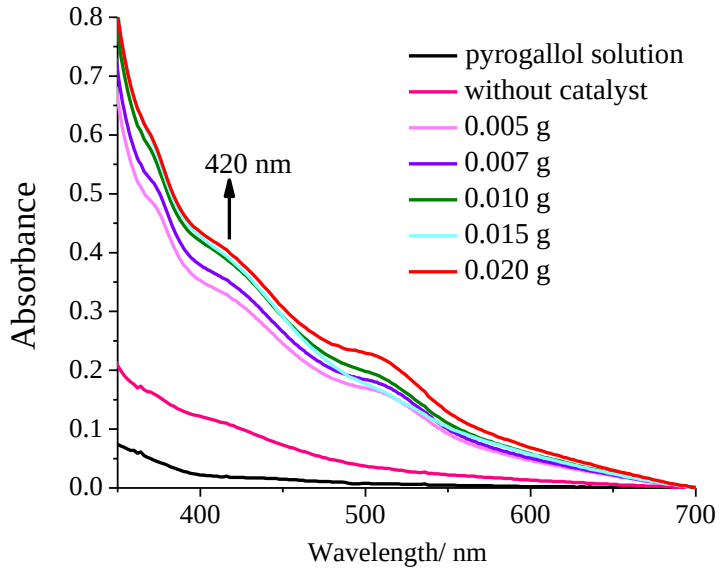

Figure 5.9. Spectra of different solutions of pyrogallol obtained within 2 min after the preparation of solutions for set (iii). For experimental detail see text.

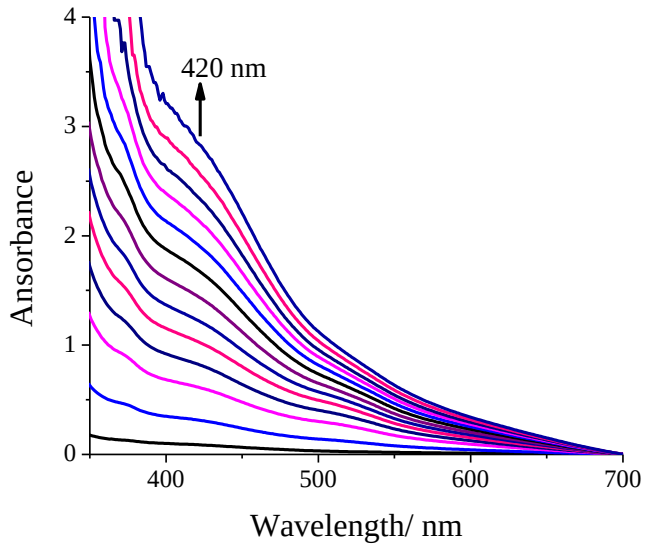

Figure 5.10. Successive increment in the absorbance of the band at 420 nm due to the formation of purpurogallin. Reaction conditions: Pyrogallol solution 1 mL (0.25×10^{-1} M) mixed with 1 mL of 30% H_2O_2 (0.25×10^{-1} M), 3 mL phosphate buffer (pH 7) and catalyst PS-[$V^{IV}O$(sal-dahp)] (0.007 g) at 25 ^oC.

The amount of catalyst was optimized by taking five different amounts of catalyst under the above reaction conditions i.e.1 mL of 0.25×10^{-1} M pyrogallol

(0.00283 g, 0.025 mmol) in 3 mL phosphate buffer of pH 7, 1 mL of 0.25×10^{-1} M solution of 30% H_2O_2 (0.00315 g, 0.025 mmol) and reaction temperature 25 ^oC and the 420 nm band was monitored. Figure 5.11 summarizes the results of the oxidation of pyrogallol using different amounts of catalyst after 2 h of reaction time. It can be concluded from the plot that the peroxidase activity i.e. the oxidation of pyrogallol is quite low in the absence of catalyst. The peroxidase activity increases considerably using 0.005 g of catalyst. Increasing catalyst amount to 0.007 g significantly improved the peroxidase activity. Only a small increase in this activity was observed on further increasing the catalyst amount from 0.007 g to 0.010 g, 0.015 g or 0.020 g. However, the overall reaction time to reach the peroxidase activity similar to the one shown by 0.007 g catalyst was reduced; e.g. the 0.020 g catalyst showed the activity equivalent to 0.007 g catalyst within 1.5 h. Therefore, an amount of 0.007 g of catalyst was considered the best one to optimize other reaction conditions for this activity.

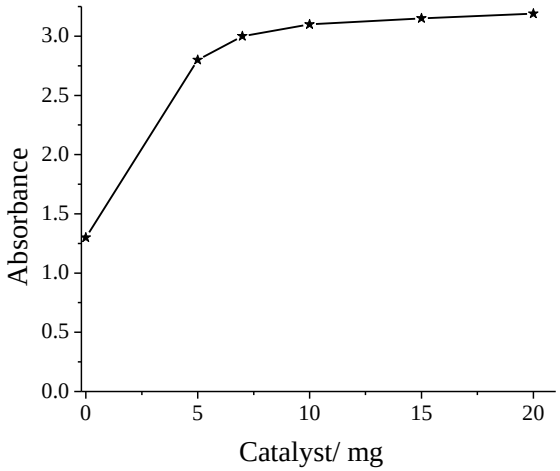

Figure 5.11. Plot of maximum absorbance at 420 nm during peroxidase activity towards pyrogallol measured using different amounts of catalyst. Other reaction conditions: i.e. 1 mL of 0.25×10^{-1} M pyrogallol in 3 mL phosphate buffer of pH 7, 1 mL of 0.25×10^{-1} M solution of 30% H_2O_2 (0.00315 g, 0.025 mmol) and reaction temperature 25 ^oC in 2 h of reaction time.

The dependence of the pyrogallol oxidation on different amount of oxidant i.e. 30% H_2O_2 was also studied. Thus, 1 mL of different concentration of H_2O_2 (see Figure

5.12 for detail) was added to each set having a fix amount of pyrogallol solution (1 mL of 0.25×10^{-1} M) and pH 7 phosphate buffer (3 mL) and reaction was monitored at 25 ^{o}C for 2 h. Figure 5.12 shows the plots of absorbance monitored at λ_{max} = 420 nm at varying concentration of H_2O_2 with time. The catalyst shows good response towards different H_2O_2 concentration and the minimum detectable H_2O_2 concentration found was 0.25×10^{-6} M. This indicates the excellent efficiency of catalyst PS-[V^{IV}O(sal-dahp)] in least H_2O_2 amount detection in biological systems.

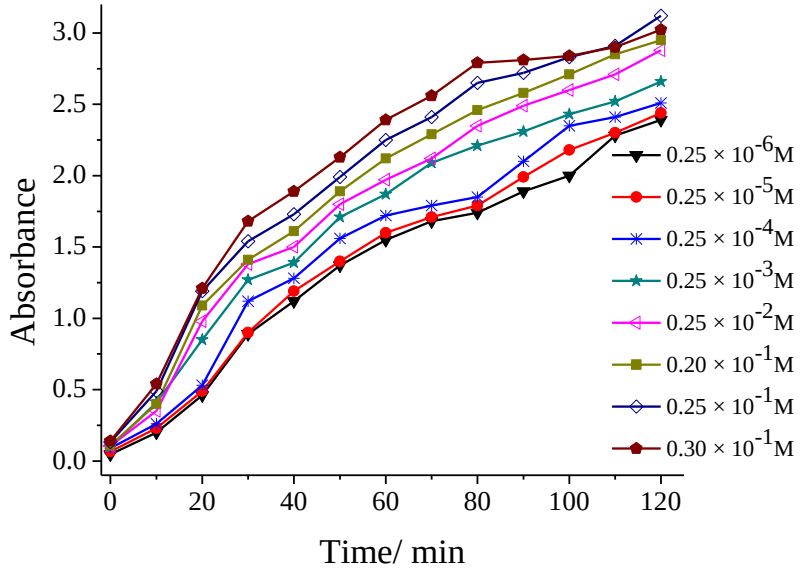

Figure 5.12. The variation of absorbance of a 1 mL (0.25×10^{-1}M) pyrogallol solution with time for different concentration of H_2O_2 solutions in a 3 mL (pH 7) phosphate buffer solution in the presence of catalyst PS-[V^{IV}O(sal-dahp)] (0.007 g) at 25 ^{o}C.

The peroxidase activity i.e. oxidation of pyrogallol using above catalyst was also studied in the buffer solutions of five different pHs. The maximum measurable absorbance at λ_{max} = 420 nm, independent of time, is shown in Figure 5.13. The reaction rate was fastest in pH 8 buffer and the 420 nm band gained the maximum measurable absorbance within 20 min of reaction time. Peroxidase activity was comparatively slower in pH 7 buffer but the 420 nm band attained the same absorbance in 2 h as of pH 8 buffer. In pH 9 buffer, the reaction rate became extremely slow and maximum absorbance of 0.25 at λ_{max} = 420 nm could only be obtained. Same observations were

found in acidic buffers of pHs 5 and 6. The activity was slowest in pH 5 buffer. In spite of being maximum activity at pH 8, we considered pH 7 as optimal pH for our catalyst as this pH is physiologically ideal and also environmentally similar to natural peroxidase in biological systems. No leaching of metal complex was observed from polymer support at different pHs making it versatile for different reaction environments.

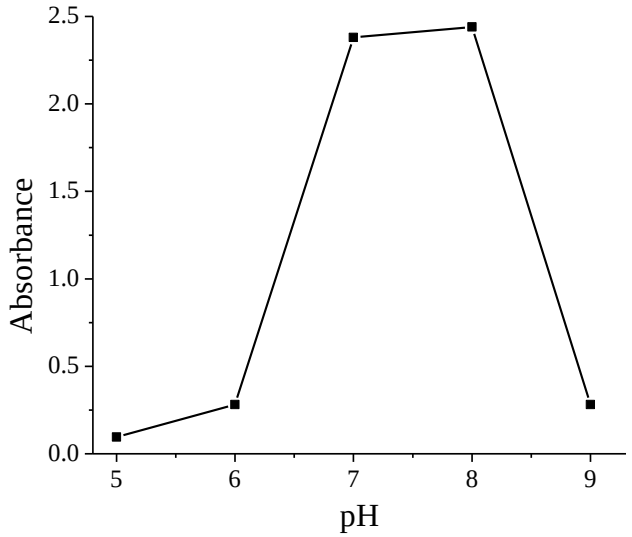

Figure 5.13. Plots showing maximum absorbance at λ_{max} = 420 nm by catalyst at different pHs of buffer solutions (3 mL). Other reaction conditions: pyrogallol solution (1 mL, 0.25×10^{-1}M), PS-[$V^{IV}O$(sal-dahp)] (0.007 g), 30% H_2O_2 (1 mL, 0.25×10^{-6}M) and reaction temp. (25 ^oC).

Thus, the optimized reaction conditions for the maximum oxidation of 1 mL of 0.25×10^{-1} M pyrogallol using catalyst PS-[$V^{IV}O$(sal-dahp)] as concluded above are: catalyst amount (0.007 g), 30% H_2O_2 (1 mL, 0.25×10^{-6} M), pH 7 buffer (3 mL) and reaction temp. (25 ^oC). Catalyst **5.2** is recyclable also up to 4th cycle after washing with acetonitrile and drying and exhibits almost similar activity. Thus, a good catalytic activity of supported catalyst at pH 7 in aqueous medium under above reaction conditions also suggests a possible peroxidase mimicking activity of the above in biological conditions and can also be employed to an environment friendly greener heterogeneous catalytic process.

In order to confirm the identity of the oxidation product of pyrogallol, the spectra of 0.05 mL (0.25×10^{-1} M) pyrogallol solution mixed with 0.007 g of catalyst PS-[$V^{IV}O$(sal-dahp)] and 0.05 mL H_2O_2 solution (0.25×10^{-6} M) in 3 mL phosphate buffer solution (pH 7) were recorded at 25 ^oC in full wavelength range (i.e. from 200 to 700 nm) at every 10 min interval. Gradually four new bands at 295, 315, 420 and 508 nm generated with an increase in their intensities; Figure 5.14. These bands are the characteristic bands of oxidation product of pyrogallol i.e. purpurogallin [182,183]. After 120 minutes no change in intensity of these bands suggests the completion of the reaction within this time for the catalyst PS-[$V^{IV}O$(sal-dahp)] under above specified conditions. Moreover, the final spectrum of this reaction is identical with the spectrum of chemically synthesized purpurogallin [183] supporting the product identity.

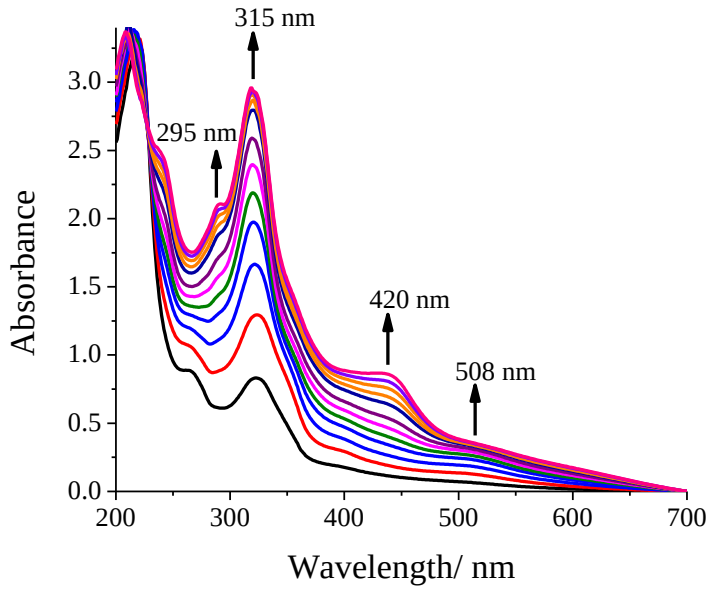

Figure 5.14. Spectral changes obtained during catalytic oxidation of pyrogallol to purpurogallin. Spectra were recorded at every 10 min interval after mixing 0.05 mL (0.25×10^{-1} M) pyrogallol solution, 0.007 g of catalyst PS-[$V^{IV}O$(sal-dahp)], 0.05 mL H_2O_2 solution (0.25×10^{-6} M) in 3 mL phosphate buffer at temp. 25 ^oC.

5.3.9. Reactivity of [$V^{IV}O$(Hsal-dahp)(dmso)] towards H_2O_2 and possible reaction mechanism

The reactivity of [$V^{IV}O$(Hsal-dahp)(dmso)] towards H_2O_2 was studied by UV-vis absorption spectroscopy. The spectral changes in the absorption spectra during the drop

wise addition of a solution prepared from one drop of 30 % H_2O_2 dissolved in 5 ml of MeOH to 35 ml of *ca.* 0.57 × 10^{-4} M solution of [$V^{IV}O$(Hsal-dahp)(dmso)] (**5.1**) in MeOH are shown in Figure 5.15. The band appearing at 361 nm slowly disappeared with a decrease in intensity. Simultaneously two new bands generated at 310 and 398 nm along with the formation of two isosbestic points centered at 340 and 395 nm. The intensity of band at 270 nm increased continuously and finally disappeared while the intensity of 232 nm band continuously increased with a shift to 253 nm.

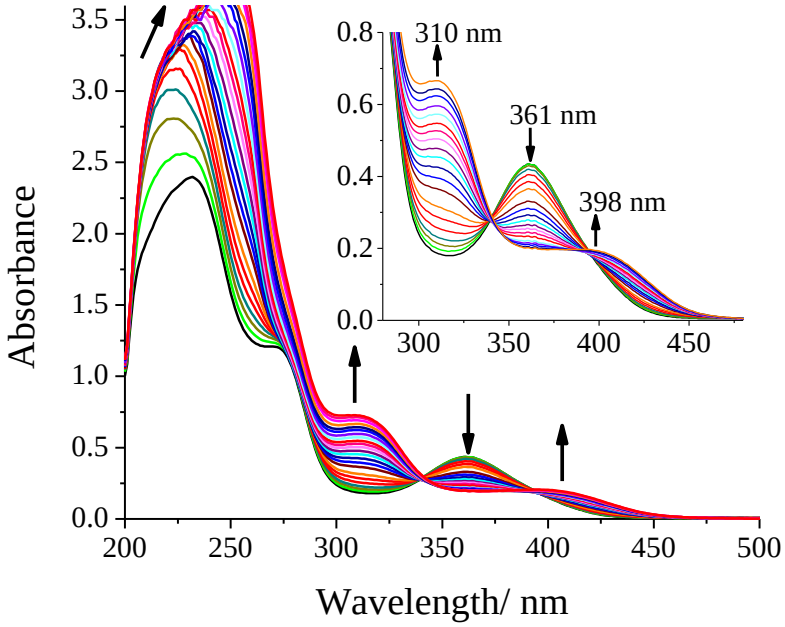

Figure 5.15. Spectral changes obtained during the titration of stepwise additions of a solution prepared from one drop of 30 % H_2O_2 dissolved in 5 ml of MeOH to 35 ml of *ca.* 0.57 × 10^{-4} M solution of [$V^{IV}O$(Hsal-dahp)(dmso)] in MeOH. In set provides expanded view covering 280 – 480 nm region.

Spectral changes in the visible region are observable only in its concentrate solution. Thus, drop wise addition of a solution prepared from one drop of 30 % H_2O_2 dissolved in 5 ml of DMF to 5 ml of *ca.* 1.75 × 10^{-3} M solution of [$V^{IV}O$(Hsal-dahp)(dmso)] in DMF resulted in the slow but complete disappearance of both d-d bands at 488 and 748 nm; Figure 5.16. These spectral changes indicate the oxidation of V(IV) center to V(V) and plausible generation of oxidoperoxidovanadium(V) species [$V^{V}O(O_2)$(Hsal-dahp)(dmso)]$^{-}$. Now addition of 3 drops of 0.25×10^{-1} M pyrogallol

solution to the above mixture resulted in the appearance of both d – d bands (Figure 5.16) confirming of the regeneration of original oxidovanadium(IV) complex.

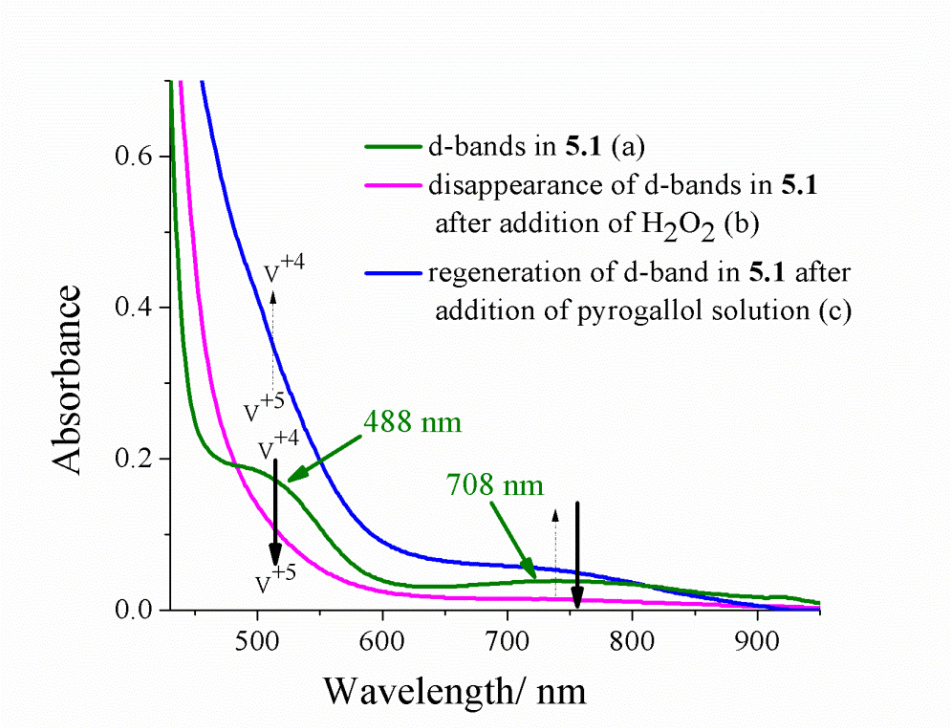

Figure 5.16. Electronic spectrum of (a): [$V^{IV}O$(sal-dahp)(dmso)] (**5.1**) in DMF, (b): **5.1** after addition of H_2O_2 solution and (c): **5.1** after adding pyrogallol solution to (b). For details of concentration of reagents refer to the text.

During peroxidase activity the vanadium center is in contact with either H_2O_2 followed by pyrogallol or vise-versa. Therefore, we have also studied the reactivity of [$V^{IV}O$(sal-dahp)(dmso)] (**5.1**) with H_2O_2 in the presence of pyrogallol. The observed changes are shown in Figure 5.17. Here, concentration of **5.1** in acetonitrile was selected in such a way that its d – d band at 748 is not visible while 488 band is clearly visible. Thus drop wise addition of a 0.25×10^{-1} M pyrogallol solution in acetonitrile to a 13 mL 0.27×10^{-3} M solution of **1** in acetonitrile resulted in the generation of a new band at *ca.* 670 nm. Simultaneously, the intensity of 488 nm band gradually decreased and finally disappeared showing the oxidation of V^{+4} to V^{+5} and possible coordination of pyrogallol to the vanadium(V) center. At this stage addition of a drop wise solution of H_2O_2 (one drop portion of aqueous 30% H_2O_2 in 5 mL acetonitrile) to the above mixture slowly regenerates the d – d band at 488 nm along with the flattening of newly

generated *ca.*670 nm band (Figure 5.17). These changes indicate the detachment of pyrogallol from vanadium center followed by its oxidation to purpurogallin after addition of H_2O_2 and regeneration of V^{+4} species. Complete flatness of *ca.* 700 nm band in final spectrum is not expected as purpurogallin weakly absorbs in this region (see Figure 5.14). These observations suggest that sequential addition of substrate and oxidant do not play any specific role and the transfer of oxygen to pyrogallol takes place from peroxidovanadium(V) species. Further, metal center in catalyst restores its oxidation state after catalytic reaction.

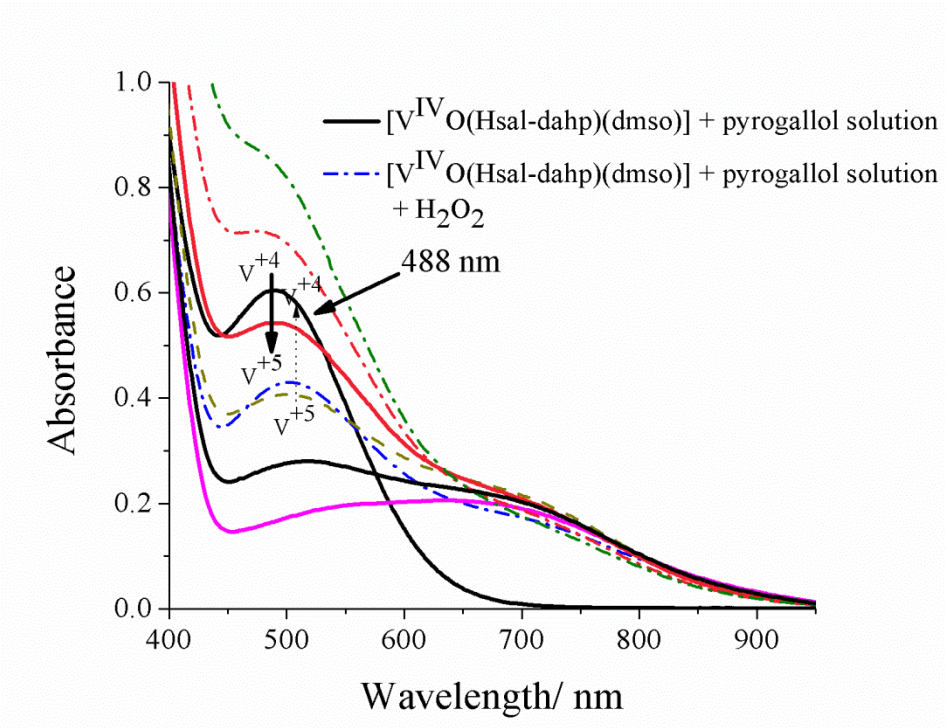

Figure 5.17. Electronic spectra of **5.1** showing changes in 488 nm band after addition of pyrogallol solution (solid lines) and spectral changes after addition of H_2O_2 solution to the mixture of **5.1** and pyrogallol in acetonitrile (dashed lines). For details of concentration of reagents refer to the text.

5.4. Conclusions

Mononuclear complex [V^{IV}O(Hsal-dahp)(dmso)] has been prepared and structurally characterized. Its polymer supported catalyst PS-[V^{IV}O(sal-dahp)] has been prepared by interacting mononuclear [VO^{IV}(Hsal-dahp)(dmso)] with chloromethylated polystyrene cross-linked with 5% divinylbenzene in DMF. The supported complex has

successfully been applied for the peroxidase mimicking activity in aqueous medium. The oxidation of pyrogallol to purpurogallin has been achieved under mild reaction conditions at pH 7 buffer solution. It has been confirmed that sequential addition of substrate and oxidant do not play any specific role during catalytic reaction and the transfer of oxygen to pyrogallol takes place from peroxidovanadium(V) species. Metal center in catalyst restores its oxidation state after catalytic reaction. Catalyst PS-[$V^{IV}O$(sal-dahp)] has good stability over wide pH range. Its good activity at pH 7 and recyclability without considerable decrease in activity suggest it as future catalyst for greener application in industry.

References

1. L. Canali and D. C. Sherrington, "Utilisation of homogeneous and supported chiral metal(salen) complexes in asymmetric catalysis", *Chem. Soc. Rev.,* **28** (1999) 85 – 93.

2. M. Maneiro, M. R. Bermejo, M. I. Fernández, E. Gómez-Fórneas, A. M. González-Noya and A. M. Tyryshkin, "A new type of manganese-Schiff base complex, catalysts for the disproportionation of hydrogen peroxide as peroxidase mimics", *New J. Chem.,* **27** (2003) 727 – 733.

3. H. Zhang, Y. Zhang and C. Li, "Asymmetric epoxidation of unfunctionalized olefins catalyzed by Mn(salen) axially immobilized onto insoluble polymers", *Tetrahedron: Asym.*, **16** (2005) 2417 – 2423.

4. M. Moghadam, S. Tangestaninejad, V. Mirkhani, I. Mohammadpoor-Baltork and H. Kargar, "Mild and efficient oxidation of alcohols with sodium periodate catalyzed by polystyrene-bound Mn(III)porphyrin", *Bioorg. Med. Chem.,* **13** (2005) 2901 – 2905.

5. M. R. Maurya, P. Saini, C. Haldar and F. Avecilla, "Synthesis, characterisation and catalytic activities of manganese (III) complexes of pyridoxal-based ONNO donor tetradenatate ligands", *Polyhedron,* **31** (2012) 710–720.

6. M. R. Maurya, P. Saini, C. Haldar and F. Avecilla, "Mn (III) complexes of monoprotic tridentate ONN donor 2-[2-(1H-(benzo[d]imidazol-2-yl)ethylimino)methyl]phenol as functional mimic of haloperoxidase", *Polyhedron*, **46** (2012) 33 – 40.

7. V. Conte and B. Floris, "Vanadium and molybdenum peroxides: synthesis and catalytic activity in oxidation reactions", *Dalton Trans.*, **40** (2011) 1419–1436.

8. R. D. Chakravarthy, K. Suresh, V. Ramkumar and D. K. Chand, "New chiral molybdenum complex catalyzed sulfide oxidation with hydrogen peroxide", *Inorg. Chim. Acta*, **376** (2011) 57–63.

9. R. D. Chakravarthy and D. K. Chand, "Synthesis, structure and applications of [cis-dioxomolybdenum(VI)-(ONO)] type complexes", *J. Chem. Sci.*, **123** (2011) 187–199.

10. R. D. Chakravarthy, V. Ramkumar and D. K. Chand, "A molybdenum based meallomicellar catalyst for controlled and selective sulfoxidation reactions in aqueous medium", *Green Chem.*, **16** (2014) 2190–2196.

11. M. Bagherzadeh, R. Latifi, L. Tahsini, V. Amani, A. Ellern and L. K. Woo, "Synthesis, characterization and crystal structure of a dioxomolybdenum(VI) complexe with a N,O type bidentate Schiff base ligand as a catalyst for homogeneous oxidation of olefins", *Polyhedron*, **28** (2009) 2517–2521.

12. J. Pisk, B. Prugovečki, D. Matković-Čalogović, R. Poli, D. Agustin and V. Vrdoljak, "Charged dioxomolybdenum(VI) complexes with pyridoxal thiosemicarbazone ligands as molybdenum(V) precursors in oxygen atom transfer process and epoxidation (pre)catalysts", *Polyhedron*, **33** (2012) 441–449.

13. K. C. Gupta and A. K. Sutar, "Catalytic activities of Schiff base transition metal complexes", *Coord. Chem. Rev.*, **252** (2008) 1420–1450.

14. M. Bagherzadeh, M. Aminia, H. Parastar, M. Jalali-Heravi, A. Ellern and L.K. Woo, "Synthesis, X-ray structure and oxidation catalysis of a oxido-peroxido molybdenum(VI) complex with tridentate shiff base ligand", *Inorg. Chem. Commun.*, **20** (2012) 86 – 89.

15. S. Singhal, S. L. Jain and B. Sain, "Alumina-supported molybdenum(VI) oxide: An efficient and recyclable heterogeneous catalyst for regioselective ring opening of epoxides with thiols, acetic anhydride, and alcohols under solvent-free conditions", *Chem. Lett.*, **37 (**2008) 620 – 621.

16. F. Saleem, G. K. Rao, G. Mukherjee and A. K. Singh, "Half sandwich ruthenium(II) complexes of click generated 1,2,3-triazole based organo-sulfur/selenium ligands: structural and donor site dependent catalytic oxidation and transfer hydrogenation aspects", *Organometallics*, **32** (2013) 3595 – 3603.

17. G. K. Rao, A. Kumar, S. Kumar, U. B. Dupare and A. K. Singh, "Palladacycles of thioethers catalyzing Suzuki Miyaura C –C coupling: generation and catalytic activity of nanoparticles", *Organometallics*, **32** (2013) 2452 –2458.

18. H. Joshi, K. N. Sharma, A. K. Sharma, O. Prakash and A. K. Singh, "Grahine oxide grafted with Pd17Se15 nano particles generated from single source precursor as recyclable and efficient catalyst for C-O coupling in O-arylation at room temperature", *Chem. Commun.*, **49** (2013) 7483 – 7485.

19. M. Weyand, H. J. Hecht, M. Kiess, M. F. Liaud, H. Vilter and D. Schomburg, "X-ray structure determination of a vanadium-dependent haloperoxidase from Ascophyllum nodosum at 2.0 A resolution", *J. Mol. Biol.*, **293** (1999) 595–611.

20. J. N. Carter-Franklin, J. D. Parrish, R. A. Tchirret-Guth, R. D. Little and A. Butler, "Vanadium haloperoxidase-catalyzed bromination and cyclization of terpenes", *J. Am. Chem. Soc.*, **125** (2003) 3688–3689.

21. A. Butler, "Mechanistic considerations of the vanadium haloperoxidases", *Coord. Chem. Rev.,* **187** (1999) 17–35.

22. A. Butler in "Bioinorganic Catalysis", ed. J. Reedijk, E. Bouwman, Marcel Dekker, New York, 2nd edn, 1999, ch. 5.

23. M. J. Clague, N. N. Keder and A. Butler, "Biomimics of vanadium bromoperoxidase: vanadium (V)-schiff base catalyzed oxidation of bromide by hydrogen peroxide", *Inorg. Chem.,* **32** (1993) 4754–4761.

24. V. Conte, F. Di Furia and G. Licini, "Liquid phase oxidation reactions by peroxides in the presence of vanadium complexes", *Appl. Catal. A: Gen.,* **157 (**1997) 335 – 361.

25. A. G. J. Ligtenbarg, R. Hage and B. L. Feringa, "Catalytic oxidations by vanadium complexes", *Coord. Chem. Rev.,* **237 (**2003) 89 – 101.

26. C. Bolm, "Vanadium-catalyzed asymmetric oxidations", *Coord. Chem. Rev.,* **237 (**2003) 245 – 256.

27. M. R. Maurya, A. Kumar, M. Ebel and D. Rehder, "Synthesis, characterization, reactivity, and catalytic potential of model vanadium(IV,V) complexes with benzimidazole-derived ONN donor ligands", *Inorg. Chem.*, **45** (2006) 5924 – 5937.

28. P.Adão, M. R. Maurya, U. Kumar, F. Avecilla, R. T. Henriques, M. L. Kuznetsov, J. Cost Pessoa, and I. Correia, "Vanadium-salen and -salan complexes: Characterization and application in oxygen transfer Reaction", *Pure Appl. Chem.*, **81** (2009) 1279–1296.

29. P. Adão, J. Costa Pessoa, R. T. Henriques, M. L. Kuznetsov, F. Avecilla, M. R. Maurya, U. Kumar and I. Correia, "Synthesis, characterization and application of vanadium-salan complexes in oxygen transfer reactions", *Inorg. Chem.*, **48** (2009) 3542–3561

30. M. V. Kirillova, M. L. Kuznetsov, V. B. Romakh, L. S. Shul'pin, J. J. R. F. da

Silva, A. J. L. Pombeiro and G. B. Shul'pin, "Mechanism of oxidations with H_2O_2 catalyzed by vanadate anion or oxovanadium(V) triethanolaminate (vanadatrane) in combination with pyrazine-2-carboxylic acid (PCA): Kinetic and DFT studies", *J. Catal.*, **267** (2009) 140-157.

31. R. R. Fernandes, J. Lasri, M. F. C. G. da Silva, J. A. L. da Silva, J. J. R. F. da Silva and A. J. L. Pombeiro, "Mild alkane C–H and O–H oxidations catalyzed by mixed-N,S copper, iron and vanadium systems", *Appl. Catal. A: Gen.*, **402** (2011) *110-120.*

32. V. Conte, A. Coletti, B. Floris, G. Licini and C. Zonta, "Mechanistic aspects of vanadium catalyzed oxidations with peroxides", *Coord. Chem. Rev.*, **255** (2011) 2165-2177.

33. J. A. L. da Silva, J. J. R. Fraústo da Silva and A. J. L. Pombeiro, "Oxovanadium complexes in catalytic oxidations", *Coord. Chem. Rev.*, **255** (2011) 2232-2248.

34. M. Kirihara, "Aerobic oxidation of organic compounds catalyzed by vanadium compounds", *Coord. Chem. Rev.*, **255** (2011) 2281-2302.

35. J-Q. Wu and Y.-S. Li, "Well-defined vanadium complexes as the catalysts for olefin polymerization", *Coord. Chem. Rev.*, **255** (2011) 2303 – 2314

36. G. Licini, V. Conte, A. Coletti, M. Mba and C. Zonta, "Recent advances in vanadium catalyzed oxygen transfer reactions", *Coord. Chem. Rev.*, **255** (2011) 2345-2357.

37. S. akizawa, F. A. Arteaga, Y. Yoshida, J. Kodera, Y. Nagata and H. Sasai, "Vanadium-catalyzed enantioselective Friedel–Crafts-type reactions", *Dalton Trans.*, 42 (2013) 11787-11790 .

38. M. Sutradhar, N. V. Shvydkiy, M. C. G. da Silva, M. V. Kirillova, Y. N. Kozlov, A. J. L. Pombeiro and G. B. Shul'pin, "A new binuclear oxovanadium(V) complex as a catalyst in combination with pyrazine carboxylic acid (PCA) for efficient alkane oxygenation by H_2O_2"**,** *Dalton Trans.***, 42 (**2013) 11791-11803

39. (a) T. Hirao, "Selective synthetic methods using vanadium-mediated redox reactions", *Pure Appl. Chem.*, **77** (2005) 1539 – 1557. (b) T. Hirao, "Oxidovanadium(V)-induced oxidative transformations of main-group organometallics", *Coord. Chem. Rev.*, **237** (2003) 271 – 279.

40. S. L. Jain and B. Sain, "An efficient approach for immobilizing the oxo-vanadium schiff base onto polymer supports using staudinger ligation", *Adv. Synth. Catal.*, **350 (**2008) 1479 – 1483.

41. D. Rehder, Bioinorganic Vanadium Chemistry, John Wiley & Sons, New York, 2008.

42. K. Soai, M. Watanable and A. Yamamoto, "Enantioselective addition of dialkylzinc to aldehyde using heterogeneous chiral catalysts immobilized on alumina and silica gel", *J. Org. Chem.*, **55 (**1990) 4832 – 4835.

43. P. Barbaro, C. Bianchini, V. D. Santro, A. Meli, S. Moneti, R. Psaro, A. Scaffidi, L. Sordelli and F. Vizza, "Hydrogenation of arenes over silica-supported catalysts that combine a grafted rhodium complex and paladium nanoparticles: Evidence for substrate activation on $Rh_{single\text{-}site}$–Pd_{metal} moieties", *J. Am. Chem. Soc.*, **128 (**2006) 7065 – 7076.

44. H. G. Alt, P. Schertl and A. Köppl, "Polymerization of ethylene with metallocene/methylaluminoxane catalysts supported on polysiloxane microgels and silica", *J. Organomet. Chem*., **568** (1998) 263 – 269.

45. T. Maschmeyer, F. Rey, G. Sankar and J. M. Thomas, "Heterogeneous catalysts obtained by grafting metallocene complexes onto mesoporous silica", *Nature*, **378** (1995) 159 – 162.

46. T. Joseph, S. S. Deshpande, S. B. Halligudi, A. Vinu, S. Ernst and M. Hartmann, "Hydrogenation of olefins over hydridochlorocarbonyltris(triphenylphosphine) ruthenium(II) complex immobilized on MCM-41 and SBA-15", *J. Mol. Catal. A: Chem.*, **206** (2003) 13 – 21.

47. T. Joseph and S. B. Halligudi, "Oxyfunctionalization of limonene using vanadium complex anchored on functionalized SBA-15", *J. Mol. Catal. A: Chem.*, **229** (2005) 241 – 247.

48. S. L. Jain, B. S. Rana, B. Singh, A. K. Sinha, A. Bhaumik, M. Nandi and B. Sain, "An improved high yielding immobilization of vanadium Schiff base complexes on mesoporous silica *via* azide–alkyne cycloaddition for the oxidation of sulfides", *Green Chem.*, **12** (2010) 374–377.

49. R. Arshady, G. W. Kenner and A. Ledwith, "The introduction of chloromethyl groups into styrene-based polymers, 1. Synthesis of 4-chloromethylstyrene and 4-

methoxymethylstyrene and their co-polymerizations with styrene", *Makromol. Chem.*, **177** (1976) 2911 – 2918.

50. R. B. Merrifield, "Solid phase peptide synthesis: The synthesis of a tetrapeptide", *J. Am. Chem. Soc.*, **85** (1963) 2149 – 2154.

51. S. Mohanraj and W. T. Ford, "Phase-transfer-catalyzed chlorination of poly(p-methylstyrene)", *Macromolecules*, **19** (1986) 2470 – 2472.

52. K. C. Gupta, A. K. Sutar and C.-C. Lin, "Polymer-supported Schiff base complexes in oxidation reactions", *Coord. Chem. Rev.*, **253** (2009) 1926–1946.

53. M. R. Maurya and J. Costa Pessoa, "Polymer-bound metal complexes as catalysts: Synthesis, characterization, reactivity and catalytic activity in E-H bond activation", *J. Organometal. Chem.*, **696** (2011) 244–254.

54. M. R. Maurya, A. Kumar and J. Costa Pessoa, "Vanadium complexes immobilized on solid supports and their use as catalysts for oxidation and functionalization of alkanes and alkenes", *Coord. Chem. Rev.*, **255** (2011) 2315-2344.

55. M. R. Maurya, "Catalytic applications of polymer-supported molybdenum complexes in organic transformations", *Curr. Org. Chem.*, **16** (2012) 73–88.

56. A. Syamal and M. M. Singh, "Syntheses of polystyrene-supported chelating resin containing the Schiff base derived from 3-formylsalicylic acid and *o*-hydroxybenzylamine and its copper(II), nickel(II), iron(III), zinc(II) cadmium(II), zirconium(IV), molybdenum(V and VI) and uranium(VI) complexes", *Indian J. Chem.*, **31A** (1992) 110 – 115.

57. A. Syamal and M. M. Singh, "Novel polystyrene-anchored copper(II), nickel(II), cobalt(II), iron(III), zinc(II), cadmium(II), zirconium(IV), molybdenum(V), molybdenum(VI) and uranium(VI) complexes of the chelating resin containing the Schiff base derived from salicylaldehyde and 1-amino-2-naphthol-4-sulfonic acid", *React. Polym.*, **21** (1993) 149 – 158.

58. Y. Wang, Y. Chang, R. Wang and F. Zha, "Preparation and catalytic oxidation by polymer supported 4-(2-pyridylazo)resorcinol-metal complexes". *J. Mol. Catal. A: Chem.*, **159** (2000), 31 – 35.

59. M. R. Maurya, "Structural models of vanadate-dependent haloperoxidases, their reactivity, immobilization on polymer support and catalytic activities", *J. Chem.*

Sci., **123** (2011) 215–228.

60. M. R. Maurya, M. Kumar and S. Sikarwar, "Polymer-anchored oxoperoxo complexes of vanadium(V), molybdenum(VI) and tungsten(VI) as catalyst for the oxidation of phenol and styrene using hydrogen peroxide as oxidant", *React. Funct. Polym.*, **66** (2006) 808 – 818.

61. M. R. Maurya and S. Sikarwar, "Oxidation of phenol and hydroquinone catalysed by copper(II) and oxovanadium(IV) complexes of N,N′-bis(salicyledene)diethylenetriamine (H_2saldien) covalently bonded to chloromethylated polystyrene", *J. Mol. Catal. A: Chem.*, **263** (2006) 175 – 185.

62. M. R. Maurya and S. Sikarwar, "Oxovanadium(IV) complex of β-alanine derived ligand immobilized on polystyrene for the oxidation of various organic substrates", *Catal. Commun.*, **8** (2007) 2017-2024.

63. L. Canali, D. C. Sherrington and H. Deleuze, "Synthesis of resins with pendently-bound chiral manganese-salen complexes and use as heterogeneous asymmetric alkene epoxidation catalysts", *React. Funct. Polym.*, **40** (1999) 155 – 168.

64. M. R. Maurya, M. Kumar, A. Kumar and J Costa Pessoa, "Oxidation of *p*-chlorotoluene and cyclohexene catalysed by polymer-anchored oxovanadium(IV) and copper(II) complexes of amino acid derived tridentate ligands", *Dalton Trans.*, (2008) 4220–4232.

65. R. Ando, T. Yagyu and M. Maeda, "Characterization of oxovanadium(IV)-Schiff-base complexes and those bound on resin, and their use in sulfide oxidation", *Inorg. Chim. Acta*, **357** (2004) 2237 – 2244.

66. X.-Q. Yu, J.-S. Huang, W.-Y. Yu and C.-M. Che, "Polymer-supported ruthenium porphyrins: Versatile and robust epoxidation catalysts with unusual selectivity", *J. Am. Chem. Soc.*, **122** (2000) 5337 – 5342.

67. F. Minutolo, D. Pini and P. Salvadori, "Polymer-bound chiral (salen) Mn (III) complex as heterogeneous catalyst in rapid and clean enantioselectiveepoxidation of unfunctionalised olefins", *Tetrahedron Lett.*, **37** (1996) 3375 – 3378.

68. G. Grivani, S. Tangestaninejad, M. H. Habibi and V. Mirkhani, "Epoxidation of alkenes by a highly reusable and efficient polymer-supported molybdenum carbonyl catalyst", *Catal. Commun.*, **6** (2005) 375 – 378.

69. M. R. Maurya, M. Kumar and A. Arya, "Model dioxovanadium(V) complexes through direct immobilization on polymersupport, their characterization and catalytic activities", *Catal. Commun.,* **10** (2008) 187–191.

70. M. M. Miller, D. C. Sherrington and S. Simpson, "Alkene epoxidations catalyzed by molybdenum(VI) supported on imidazole-containing polymers. Part 3. Epoxidation of oct-1-ene and propene", *J. Chem. Soc. Perkin Trans.*, **2** (1994) 2091 – 2096.

71. D. C. Sherrington and S. Simpson, "Polymer-supported Mo alkene epoxidation catalysts", *React. Polym.*, **19** (1993) 13 – 25.

72. L. Canali, D. C. Sherrington and H. Deleuze, "Synthesis of resins with pendently-bound chiral manganese-salen complexes and use as heterogeneous asymmetric alkene epoxidation catalysts", *React. Funct. Polym.*, **40** (1999) 155 – 168.

73. L. Canali, E. Cowan, C. L. Gibson, D. C. Sherrington and H. Deleuze, "Remarkable matrix effect in polymer-supported Jacobsen's alkene epoxidation catalysts", *Chem. Commun.,* **23** (1998) 2561 – 2562.

74. M. M. Miller and D. C. Sherrington, "Alkene epoxidations catalyzed by Mo(VI) supported on imidazole-containing polymers", *J. Catal.*, **152** (1995) 368 – 376.

75. S. M. Islam, P. Mondal, K. Tuhina, A. S. Roy, D. Hossain and S. Mondal, "Synthesis, characterization and catalytic activity of polymer anchored transition metal complexes toward oxidation reactions", *Trans. Met. Chem.,* **35** (2010) 891–901.

76. M. R. Maurya, A. Arya, A. Kumar and J. Costa Pessoa, "Polystyrene bound oxidovanadium(IV) and dioxidovanadium(V) complexes of histamine derived ligand for the oxidation of methyl phenyl sulfide, diphenyl sulfide and benzoin", *Dalton trans.*, (2009) 2185–2195.

77. M. R. Maurya, M. Kumar and U. Kumar, "Polymer-anchored vanadium, molybdenum and copper complexes of bidantate ligand as catalyst for the liquid phase oxidation of organic substance", *J. Mol. Catal. A: Chem.*, **273** (2007) 133-143.

78. A. Barbarini, R. Maggi, M. Muratori, G. Sartori and R. Sartorio, "Enantioselective sulfoxidation catalyzed by polymer-supported chiral Schiff base-$VO(acac)_2$ complexes", *Tetrahedron: Asym.*, **15** (2004) 2467 – 2473.

79. R. S. Walmsley, N. Torto, S. Chigome and Z.R. Tshentu, "Towards the development of fiber-based oxidovanadium(IV) catalysts for the oxidation of thioanisole", *Catal. Lett.*, **142** (2012) 243–250.

80. M. R. Maurya, A. Arya, A. Kumar, M. L. Kuznetsov, F. Avecilla and J. Costa Pessoa, "Polymer-bound oxidovanadium(IV) and dioxidovanadium(V) complexes as catalysts for the oxidative desulfurization of model fuel diesel", *Inorg. Chem.*, **49** (2010) 6586–6600.

81. G. Zampella, P. Fantucci, V. L. Pecorao and L. De Gioia, "Reactivity of peroxo forms of the vanadium haloperoxidases cofactor. A DFT investigation", *J. Am. Chem. Soc*., **127** (2005) 953 – 960.

82. T. S. Smith II and V. L. Pecoraro, "Oxidation of organic sulfides by vanadium haloperoxidase model complexes", *Inorg. Chem*., **41** (2002) 6754 –6760.

83. S. M. Islam, A. S. Roy, P. Mondal and N. Salam, "Synthesis, catalytic oxidation and oxidative bromination reaction of a reusable polymer anchored oxovanadium(IV) complex", *J. Mol. Catal. A: Chem.*, **358** (2012) 38–48.

84. S. M. Islam, R. A. Molla, A. S. Roy, K. Ghosh, N. Salam, M. A. Iqubal, K. Tuhina, "Aerobic oxidation and oxidative bromination in aqueous medium using polymer anchored oxovanadium complex", *J. Orgn. Chem.*, **761** (2014) 169-178.

85. V. Hulea and E. Dumitriu, "Styrene oxidation with H_2O_2 over Ti-containing molecular sieves with MFI, BEA and MCM-41 topologies", *Appl. Catal. A: Gen.*, **277** (2004) 99–106.

86. M. R. Maurya, S. Sikarwar and P. Manikandan, "Oxovanadium(IV) complex of 2-(α-hydroxyethyl)benzimidazole covalently bonded to chloromethylated polystyrene for oxidation of benzoin", *Appl. Catal. A: Gen*., **315** (2006) 74 – 82.

87. M. R. Maurya, U. Kumar and P. Manikandan, "Polymer supported vanadium and molybdenum complexes as potential catalysts for the oxidation and oxidative bromination of organic substrates", *Dalton. Trans*, (2006) 3561-3575.

88. S. Suresh, S. Skaria and S. Ponrathnam, "Polymer-supported vanadium salt as a catalyst for the oxidation of phenols", *Synth.Commun.*, **26** (1996) 2113 – 2117.

89. R. Pathak and G. N. Rao, "Oxidation of 2,6-di-*tert*-butylphenol with polymer-anchored molybdenyl and vanadyl complexes", *J. Mol. Catal. A: Chem.,* **130** (1998) 215 – 220.

90. M. R. Maurya, A. Arya, U. Kumar, A. Kumar, F. Avecilla and J. Costa Pessoa, "Polymer-bound oxidovanadium(IV) and dioxidovanadium(V) complexes: synthesis, characterization and catalytic application for the hydroamination of styrene and vinyl pyridine", *Dalton Trans.*, (2009) 9555–9566.

91. M. R. Maurya, U. Kumar, I. Correia, P. Adão and J. Costa Pessoa, "Polymer bound oxidovanadium(IV) complex of L-cysteine derived ligand for the oxidative amination of styrene", *Eur. J. Inorg. Chem*., (2008) 577 - 587.

92. M. R. Maurya, M. Kumar, A. Kumar and J Costa Pessoa, "Oxidation of *p*-chlorotoluene and cyclohexene catalysed by polymer-anchored oxovanadium(IV) and copper(II) complexes of amino acid derived tridentate ligands", *Dalton Trans.*, (2008) 4220–4232.

93. M. R. Maurya, A. Arya, P. Adão and J. Costa Pessoa, "Immobilization of oxovanadium(IV), dioxomolybdenum(VI) and copper(II) complexes on polymer for the liquid phase oxidation of styrene, cyclohexene and ethylbenzene", *Appl. Catal. A: Gen*., **351** (2008) 239–252.

94. M. R. Maurya, A. A. Khan, A. Azam, A. Kumar, S. Ranjan, N. Mondal and J. Costa Pessoa, "Dinuclear oxidovanadium(IV) and dioxidovanadium(V) complexes of 5,5'-methylenebis(dibasic tridentate) ligands: synthesis, spectral characterisation, reactivity, and catalytic and antiamoebic activities", *Eur. J. Inorg. Chem.*, (2009) 5377–5390.

95. M. R. Maurya, A. A. Khan, A. Azam, S. Ranjan, N. Mondal, A. Kumar, F. Avecilla and J. Costa Pessoa, "Vanadium complexes having $[V^{IV}O]^{2+}$ and $[V^{V}O_2]^{+}$ cores with binucleating dibasic tetradentate ligands: Synthesis, characterization, catalytic and antiamoebic activities", *Dalton Trans*., **39** (2010) 1345–1360.

96. M. R. Maurya, C. Haldar, A. A. Khan, A. Azam, A. Salahuddin, A. Kumar and J. Costa Pessoa, "Synthesis, characterization, catalytic and antiamoebic activity of vanadium complexes of binucleating bis(dibasic tridentate ONS donor) ligand systems", *Eur. J. Inorg. Chem*., (2012) 2560–2577.

97. M. Pagano, B. Demoro, J. Toloza, L. Boiani, M. González, H. Cerecetto, C. Olea Azar, E. Norambuena, D. Gambino and L. Otero, "Effect of ruthenium

complexation on trypanosidal activity of 5-nitrofuryl containing thiosemicarbazones", *Eur. J. Med. Chem.,* **44** (2009) 4937 – 4943.

98. M. Vieites, P. Smircich, L. Guggeri, E. Marchán, A. Gómez-Barrio, M. Navarro, B. Garat and D. Gambino, "Synthesis and characterization of a pyridine-2-thiol N-oxide gold(I) complex with potent antiproliferative effect against Trypanosoma cruzi and Leishmania sp. Insight into its mechanism of action", *J. Inorg. Biochem.*, **103** (2009) 1300 – 130.

99. B. Demoro, F. Caruso, M. Rossi, D. Benítez, M. Gonzalez, H. Cerecetto, B. Parajón-Costa, J. Castiglioni, M. Gallizi, R. Docampo, L. Otero and D. Gambino, "Risedronate metal complexes potentially active against chagas disease", *J. Inorg. Biochem.,* **104** (2010)1252 – 1258.

100. D. Gambino, "Potentiality of vanadium compounds as anti-parasitic agents", *Coord. Chem. Rev.,* **255** (2011) 2193–2203.

101. *Vanadium compounds: Chemistry, biochemistry and therapeutic applications,* ed. V. L. Pecoraro, C. Slebodnick, B. Hamstra, D. C. Crans and A. S. Tracy, ACS Symposium Series 1998, Ch. 12;

102. H. Sakurai, Y. Kojima, Y. Yoshikawa, K. Kawabe and H. Yasui, "Antidiabetic vanadium(IV) and zinc(II) complexes", *Coord. Chem. Rev*., **226** (2002) 187–198.

103. D. Rehder, J. Costa Pessoa, C. F. G. C. Geraldes, M. M. C. A. Castro, T. Kabanos, T. Kiss, B. Meier, G. Micera, L. Pettersson, M. Rangel, A. Salifoglou, I. Turel and D. Wang, "In vitro study of the insulin-mimetic behaviour of vanadium(IV),V) co-ordination compounds", *J. Biol. Inorg. Chem*., **7** (2002) 384–396.

104. D. Rehder, "Biological and medicinal aspects of vanadium", *Inorg. Chem. Commun.*, **6** (2003) 604–617.

105. A. Messerschmidt and R. Wever, "X-ray structure of a vanadium-containing enzyme: Chloroperoxidase from the fungus Curvularia inaequalis", *Proc. Natl. Acad. Sci. U.S.A.*, **93** (1996) 392–396.

106. M. I. Isupov, A. R. Dalby, A. Brindley, Y. Izumi, T. Tanabe, G. N. Murshudov and J. A. Littlechild, "Crystal structure of vanadium dependent bromoperoxidase from Corallina officinalis", *J. Mol. Biol.,* **299** (2000) 1035–1049.

107. M. R. Maurya, "Development of the coordination chemistry of vanadium through

bis(acetylacetonato)oxovanadium(IV): Synthesis, reactivity and structural aspects", *Coord. Chem. Rev*., **237** (2003) 163–181.

108. M. R. Maurya, S. Agarwal, C. Bader and D. Rehder, "Dioxovanadium(V) complexes of ONO donor ligands derived from pyridoxal and hydrazides: Models of vanadate-dependent haloperoxidases", *Eur. J. Inorg. Chem.*, (2005)147–157.

109. M. R. Maurya, C. Haldar, A. Kumar, M. L. Kuznetsov, F. Avecilla and J. Costa Pessoa, "Vanadium complexes having $[VO]^{2+}$, $[VO]^{3+}$ and $[VO_2]^{+}$ cores with hydrazones of 2,6-diformyl-4-methylphenol: Synthesis, characterization, reactivity, and catalytic potential", *Dalton Trans.*, **42** (2013) 11941-11962.

110. G. Grivani, S. Tangestaninejad, M. H. Habibi, V. Mirkhani and M. Moghadam, "Epoxidation of alkenes by a readily prepared and highly active and reusable heterogeneous molybdenum-based catalyst", *Appl. Catal. A: Gen.*, **299** (2006) 131–136.

111. R. A. Rowe and M. M. Jones, "Vanadium (IV) oxy(acetylacetonate)", *Inorg. Synth.*, **5** (1957) 113–116.

112. A. Rockenbauer and L. Korecz, "Automatic computer simulations of ESR spectra", *Appl. Magn. Reson.*, **10** (1996) 29–43.

113. G. M. Sheldrick, SHELXL-97: An Integrated System for Solving and Refining Crystal Structures from Diffraction Data (Revision 5.1); University of Göttingen, Germany, 1997.

114. H. Kelm and H.-J. Krüger, "A Superoxovanadium(V) Complex Linking the Peroxide and Dioxygen Chemistry of Vanadium", *Angew. Chem. Int. Ed.*, **40** (2001) 2344 –2348.

115. M. Kaliva, C. Gabriel, C. P. Raptopoulou, A. Terzis, G. Voyiatzis, M. Zervou, C. Mateescu and A. Salifoglou, "A unique dinuclear mixed V(V) oxo-peroxo complex in the structural speciation of the ternary V(V)-peroxo-citrate System. Potential mechanistic and structural insight into the aqueous synthetic chemistry of dinuclear V(V)-citratespecies with H_2O_2", *Inorg. Chem.*, 50 (2011) 11423–11436.

116. C. R. Waidmann, A. G. DiPasquale, J. M. Mayer, "Synthesis and reactivity of Oxo-Peroxo-Vanadium(V) Bypyridine compounds", *Inorg. Chem.*, **49** (2010) 2383–239.

117. S. Basu, S. Halder, I. Pal, S. Samanta, P. Karmakar, M. G. B. Drew and S. Bhattacharya, "1-(2′-pyridylazo)-2-naphtholate complexes of ruthenium: Synthesis, characterization and DNA binding properties", *Polyhedron*, **27** (2008) 2943–2951.

118. M. R. Maurya, S. Khurana, W. Zhang and D. Rehder, "Biomimetic oxo-, dioxo- and oxo-peroxo-hydrazonato - vanadium(IV/V) complexes", *J. Chem Soc., Dalton Trans.,* (2002) 3015–3023

119. K. Wüthrich, "E.S.R. (electron spin resonance) investigation of VO^{2+} complex compounds in aqueous solution. II", *Helv. Chim. Acta*, **48** (1965) 1012–1017.

120. N. D. Chasteen, in: J. Reuben (Ed.), "Biological Magnetic Resonance", Plenum, New York, p. 53 (1981).

121. E. Garriba, G. Micera and D. Sanna, "The solution structure of bis(acetylacetonato)oxovanadium(IV)", *Inorg. Chim. Acta*, **359** (2006) 4470–4476.

122. D. Rehder, C. Weidemann, A. Duch and W. Priebsch, "Vanadium-51 shielding in vanadium(V) complexes: a reference scale for vanadium binding sites in biomolecules", *Inorg. Chem.*, **27** (1988) 584–587.

123. V. Conte and B. Floris, "Vanadium catalyzed oxidation with hydrogen peroxide", *Inorg. Chim. Acta.*, **363** (2010) 1935–1946.

124. T. Moriuchi, M. Yamaguchi, K. Kikushima and T. Hirao, "An efficient vanadium-catalyzed bromination reaction", *Tetrahedron Lett.*, **48** (2007) 2667–2670.

125. M. R. Maurya, P. Saini, A. Kumar and J. Costa Pessoa, "Oxidovanadium(IV) complexes of tetradentate ligands encapsulated in zeolite-Y as catalysts for oxidation of styrene, cyclohexene and methyl phenyl sulphide", *Eur. J. Inorg. Chem.,* (2011) 4846–4861.

126. V. Conte, F. Di Furia and S. Moro, "Studies directed toward the prediction of the oxidative reactivity of vanadium peroxo complexes in water. Correlations between the nature of the ligands and ^{51}V-NMR chemical shifts", *J. Mol.Catal. A: Chem.*, **104** (1995) 159–169.

127. G. J. Colpas, B. J. Hamstra, J. W. Kampf and V. L. Pecoraro, "Functional models for vanadium haloperoxidase: Reactivity and mechanism of halide oxidation", *J. Am. Chem. Soc.*, **118** (1996) 3469–3478.

128. C. J. Schneider, J. E. Penner-Hahn and V. L. Pecoraro, "Elucidating the Protonation Site of Vanadium Peroxide Complexes and the Implications for Biomimetic Catalysis", *J. Am. Chem. Soc.*, **130**, (2008) 2712–2713.

129. S. Rana, R. Haque, G. Santosh and D. Maiti, "Decarbonylative halogenation by a vanadium complex", *Inorg. Chem.*, **52** (2013) 2927–2932.

130. M. R. Maurya, U. Kumar and P. Manikandan, "Synthesis and characterisation of polymer-anchored oxidovanadium(IV) complexes and their use for the oxidation of styrene and cumene", *Eur. J. Inorg. Chem.* (2007) 2303–2314.

131. A. Butler, M. J. Clague and G. E. Meister, **"**Vanadium peroxide complexes", *Chem. Rev.*, **94** (1994) 625–638.

132. D. C. Crans, A. D. Keramidas, S. S. Amin, O. P. Anderson and S. M. Miller, "Six-coordinated vanadium(IV) and (V) complexes of benzimidazole and pyridyl containing ligands", *J. Chem. Soc., Dalton Tans.*, (1997) 2799–2812.

133. M. R. Maurya, S. Agarwal, M. Abid, A. Azam C. Bader, M. Ebel and D. Rehder, "Synthesis, characterization, reactivity and in vitro antiamoebic activity of hydrazone based oxidovanadium(IV), oxidovanadium(V) and μ–oxidobis{oxidovanadium(V)} complexes", *Dalton Trans.*, (2006) 937–947.

134. Wynberg and H. J. Kooreman, "The mechanism of the Hinsberg Thiophene ring synthesis[1,2]", *J. Am. Chem. Soc.*, **87** (1965) 1739–1742.

135. W. W. Paudler and J. M. Barton, "The synthesis of 1,2,4-triazine", *J. Org. Chem.*, **31** (1966) 1720–1722.

136. W. R. Dunnavant and F. L. James, "Molecular rearrangements. I. The base-catalyzed condensation of benzil with urea", *J. Am. Chem. Soc.*, **78** (1956) 2740–2743.

137. S. Tangestaninejad, M. H. Habibi, V. Mirkhani and G. Grivani, "Simple preparation of some reusable and efficient polymer–supported tungsten carbonyl catalysts and clean epoxidation of *cis*-cyclooctene in the presence of H_2O_2", *J. Mol. Catal. A: Chem.*, **255** (2006) 249–253.

138. A. W. Addison, T. N. Rao, J. Reedijk, J. Rijn and G. C. Verschoor, "Synthesis, structure and spectroscopic properties of copper(II) compounds containing nitrogen–sulphur donor ligands; the crystal and molecular structure of aqua[1,7-

bis(*N*-methylbenzimidazole-2′-yl)-2,6-dithiaheptane]copper(II) perchlorate", *J. Chem. Soc., Dalton Trans.,* (1984) 1349–1356.

139. (a) M. R. Maurya, A. Kumar, A. R. Bhat, A. Azam, C. Bader, and D. Rehder, "Dioxido– and oxidovanadium(V) complexes of thiohydrazone ONS donor ligands: Synthesis, characterization, reactivity, and antiamoebic activity", *Inorg. Chem*., **45** (2006) 1260–1269; (b) M. R. Maurya, A. Kumar, M. Abid and A. Azam, "Dioxidovanadium(V) and l–oxido bis[oxidovanadium(V)] complexes containing thiosemicarbazone based ONS donor set and their antiamoebic activity", *Inorg. Chim. Acta*, **359** (2006) 2439–2447.

140. J. Costa Pessoa, M. J. Calhorda, I. Cavaco, I. Correia, M. T. Duarte, V. Felix, R. T. Henriques, M. F. M. Piedade and I. Tomaz, "Molecular modelling studies of N-salicylideneamino acidato complexes of oxovanadium(IV), molecular and crystal structure of a new dinuclear LOV^{IV}–O–$V^{V}OL$ mixed valence complex", *J. Chem. Soc. Dalton Trans.*, (2002) 4407–4415.
141. M. R. Maurya, S. Khurana, W. Zhang and D. Rehder, "Vanadium(IV/V) complexes containing $[VO]^{2+}$, $[VO]^{3+}$, $[VO_2]^{+}$ and $[VO(O_2)]$+ cores with ligands derived from 2-acetylpyridine and S-benzyl- or S-methyldithiocarbazate", *Eur. J. Inorg. Chem.,* (2002) 1749–1760.

142. M. R. Maurya, S. Agarwal, C. Bader, M. Ebel and D. Rehder, "Synthesis, characterisation and catalytic potential of hydrazonatovanadium(V) model complexes with $[VO]^{3+}$ and $[VO_2]^{+}$ cores", *Dalton Trans.,* (2005) 537–544.

143. O. W. Howarth, "Vanadium-51 NMR", *Progr. Magn. Reson. Spectrosc.*, **22**(5) (1990) 453–485.

144. D. Rehder, *Transition Metal Nuclear Magnetic Resonance* (Ed.: P. S. Pregosin), Elsevier, New York, p. 1, 1991.

145. (a) M. Aureliano and R. M. C. Gandara, "Decavanadate effects in biological systems", *J. Inorg. Biochem.,* **99** (2005) 979–985; (b) M. Aureliano, T. Tiago, R. M. C. Gandara, A. Sousa, A. Moderno, M. Kaliva, A. Salifoglou, R. O. Duarte and J. J. G. Moura, "Interactions of vanadium(V) –citrate complexes with the sarcoplasmic reticulum calcium pump", *J. Inorg. Biochem.,* **99** (2005) 2355–2361.

146. B. J. Hamstra, G. J. Colpas and V. L. Pecoraro, **"**Reactivity of dioxovanadium(V) complexes with hydrogen peroxide: Implications for vanadium haloperoxidase", *Inorg. Chem.,* **37** (1998) 949–955.

147. G. Zampilla, P. Fantucci, V. L. Pecoraro, L. De Gioia, "Reactivity of peroxo forms of the vanadium haloperoxidase cofactor. A DFT investigation", *J. Am. Chem. Soc.*, **127** (2005) 953–960.

148. C. R. Cornman, J. Kampf, M. S. Lah and V. L. Pecoraro, "Modeling vanadium bromoperoxidase: Synthesis, structure, and spectral properties of vanadium(IV) complexes with coordinated imidazole", *Inorg. Chem.*, **31** (1992) 2035–2043.

149. L. J. Calviou, J. M. Arber, D. Collison, C. D. Garner and W. Clegg, "A structural model for vanadyl-histidine interactions: structure determination of [VO(1-vinylimidazole)$_4$Cl]Cl by a combination of X-ray crystallography and X-ray absorption spectroscopy", *J. Chem. Soc., Chem. Commun.* (1992) 654–656.

150. A. D. Keramidas, S. M. Miller, O. P. Anderson and D. C. Crans, "Vanadium(V) hydroxylamido complexes: Solid state and solution properties", *J. Am. Chem. Soc.*, **119** (1997) 8901–8915.

151. V. Conte, O. Bortolini, M. Carraro and S. Moro, "Models for the active site of vanadium–dependent haloperoxidases: Insight into the solution structure of peroxo vanadium compounds", *J. Inorg. Biochem.*, **80** (2000) 41–49.

152. O. Bortolini, M. Carrano, V. Conte and S. Moro, "Vanadium–peroxidase–mimicking systems: Direct evidence of a hypobromite–like vanadium intermediate", *Eur. J. Inorg. Chem.*, (2003) 42–46.

153. G. B. Gill, in: G. Pattenden (Ed.), Comprehensive Organic Synthesis, Vol. 3, Pergamon Press, New York, 1991, pp. 821–838.

154. M Weiss and M. Appel, "The catalytic oxidation of benzoin to benzil", *J. Am. Chem. Soc.*, **70** (1948) 3666–3667.

155. W-Y Sun, N. Ueyama and A. Nakamura, "Air oxidation of *p*–substituted benzoin to corresponding benzil catalyzed by Fe(II)–cysteine peptide complexes", *Tetrahedron*, **48** (1992) 1557–1566.

156. M. R. Maurya, M. Bisht, A. Kumar, M. L. Kuznetsov, F. Avecilla and J. Costa Pessoa, "Synthesis, characterization, reactivity and catalytic activity of oxidovanadium(IV), oxidovanadium(V) and dioxidovanadium(V) complexes of benzimidazole modified ligands", *Dalton Trans.*, **40** (2011) 6968–6983.

157. M. R. Maurya, M. Bisht and F. Avecilla, "Synthesis, characterization and catalytic

activities of vanadium complexes containing ONN donor ligand derived from 2-aminoethylpyridine", *J. Mol. Catal. A: Chem.*, **344** (2011) 18–27.

158. X. Li, M. S. Lah, V. L. Pecoraro, "Vanadium complexes of the tridentate schiff base ligand of N-salicylidine-N′-(2-hydroxyethyl)ethylenediamine: acid-base and redox conversion between vanadium(IV) and vanadium(V) imino phenolates", *Inorg. Chem*, **27** (1988) 4657–4664.

159. L. M. Mokry, C. J. Carrano, "Steric control of vanadium(V) coordination geometry: a mononuclear structural model for transition-state-analog RNase inhibitors", *Inorg. Chem.*, **32** (1993) 6119–6121.

160. G. Asgedom, A. Sreedhara, J. Kivikoski, E. Kolehmainen, C. P. Rao, "Structure, characterization and photoreactivity of monomeric dioxovanadium(V) Schiff-base complexes of trigonal-bipyramidal geometry", *J. Chem. Soc., Dalton Trans.*, (1996) 93–97.

161. V. D. Deflon, D. M. de Oliveira, G. F. de Sousa, A. A. Batista, L. R. Dinelli and E. E. Castellano, "Oxovanadium(IV,V) complexes with 2-acetylpyridine-2-furanoylhydrazone (Hapf) as ligand. X-ray crystal structure of $[VO_2(apf)]$ and $[V_2O_2(\mu\text{-}O)_2(apf)_2]$", *Z. Anorg. Allg. Chem.*, **628** (2002) 1140–1144.

162. M. Kuriakose, M. R. P. Kurup and E. Suresh, "Synthesis, spectroscopic studies and crystal structures of two new vanadium complexes of 2-benzoylpyridine containing hydrazone ligands", *Polyhedron*, **26** (2007) 2713–2718.

163. N. A. Mangalam, S. Sivakumar, SR Sheeja, M. R. P. Kurup, E. RT Tiekink, "Chemistry of molecular and supramolecular structures of vanadium(IV) and dioxygen-bridged V(V) complexes incorporating tridentate hydrazone ligands", *Inorg. Chim. Acta*, **362** (2009) 4191–4197.

164. M. Kuriakose, M. R. P. Kurup and E. Suresh, "Spectral characterization and crystal structure of 2-benzoylpyridine nicotinoyl hydrazone", *Spectrochim. Acta A*, **66** (2007) 353–358.

165. I. Correia, J. Costa Pessoa, M. T. Duarte, R. T. Henriques, M. F. M. da Piedade, L. F. Veiros, T. Jakusch, T. Kiss, I. Dornyei, M. M. C. A. Castro, C. F. G. C. Geraldes and F. Avecilla, "N,N′-ethylenebis (pyridoxylideneiminato) and N,N′-ethylenebis(pyridoxylaminato): Synthesis, characterization, potentiometric, spectroscopic and DFT studies of their vanadium(IV) and vanadium(V) complexes", *Chem. Eur. J.*, **10** (2004) 2301–2317.

166. W. Plass, "Magneto-structural correlations in dinuclear d^1–d^1 complexes: Structure and magnetochemistry of two ferromagnetically coupled V(IV) dimmers", *Angew. Chem., Int. Ed. Engl.*, **35** (1996) 627–631.

167. F. Avecilla, P. Adão, I. Correia and J. Costa Pessoa, "Influence of polydentate ligands in the structure of dinuclear vanadium compounds", *Pure Appl. Chem.*, **81** (2009) 1297–1311.

168. L. Zheng, P. Zheng, Z. Sun, Y. Bai, J. Wang and X. Guo., "Production of vanillin from waste residue of rice bran oil by *Aspergillus niger* and *Pycnoporus cinnabarinus*", *Bioresour. Technol.*, **98** (2007) 1115–1119.

169. R. Seshadri, A. S. Lamm, A. Khare and J. P. N. Rosazza, "Oxidation of isoeugenol by *Nocardia iowensis", Enzyme and Microbial Technology*, **43** (2008) 486–494.

170. D. Hua, C. Ma, S. Lin, L. Song, Z. Deng, Z. Maomy, Z. Zhang, B. Yu and P. Xu, "Biotransformation of isoeugenol to vanillin by a newly isolated *Bacillus pumilus* strain: Identification of major metabolites", *Journal of Biotechnology*, **130** (2007) 463–470.

171. V. Augugliaro, G. Camera-Roda, V. Loddo, G. Palmisano, L. Palmisano, F. Parrino and M. A. Puma, "Synthesis of vanillin in water by TiO_2 photocatalysis", *Appl. Catal. B: Environ.*, **111– 112** (2012) 555– 561.

172. E. V. Gusevskaya, L. Menini, L. A. Parreira, R. A. Mesquita, Y. N. Kozlov, G. B. Shul'pin, "Oxidation of isoeugenol to vanillin by the "H_2O_2–vanadate–pyrazine-2-carboxylic acid" reagent", *J. Mol. Catal. A: Chem.*, **363–364** (2012) 140–147.

173. H.B. ten Brink, H. L. Dekker, H. E. Schoemaker and R. Wever, "Oxidation reactions catalyzed by vanadium chloroperoxidase from *Curvularia inaequalis*", *J. Inorg. Bio.*, **80** (2000) 91–98.

174. R. André, F. Natálio, M. Humanes, J. Leppin, K. Heinze, R. Wever, H. – C. Schröder, W. E. G. Müller, and W. Tremel, "V_2O_5 nanowires with an intrinsic peroxidase-like activity", *Adv. Funct. Mater.*, **2** (2011) 501–509.

175. A. E. Anderson, M. P. Weberski, Jr. and C. C. McLauchlan, "Phosph(on/in)ate-bridged vanadium(IV) dimers: Synthesis and characterization", *Inorg. Chem.*, **51** (2012) 8719-8728.

176. X. Riart-Ferrer, A. E. Anderson, B. M. Nelson, F. Haoand and C.C. McLauchlan, "Organo-Phosph(on/in)ate-Bridged Dimers of Vanadium(IV) Complexes with the Kläui Ligand: Synthesis and Characterization", *Eur. J. Inorg. Chem.* (2012) 4585–4592.

177. M. L. Tarlton, A. E. Anderson, M. P. Weberski Jr., X. Riart-Ferrer, B. M. Nelson and C. C. McLauchlan, "Synthesis, characterization, and electrochemical properties of l-oxalate bridged vanadium(III) and (IV) dimers incorporating the Kläui ligand, $pP^{OR}Co$ (R = Me,Et)", *Inorg. Chim. Acta* , **420** (2014) 159–165.

178. K. I. Smith, L. L. Borer and M. M. Olmstead "Vanadium(IV) and Vanadium(V) Complexes of Salicyladimine Ligands", *Inorg. Chem.*, 42 (2003) 7410–7415.

179. M. R. Maurya, M. Bisht, N. Chaudhary, F. Avecilla, U. Kumar and H. – F. Hsu, "Synthesis, structural characterization, encapsulation in zeolite Y and catalytic activity of an oxidovanadium(V) complex with a tribasic pentadentate ligand", *Polyhedron*, **54**, (2013) 180 – 188.

180. 17. D. Feng, Z. – Y. Gu, J. – R. Li, H. – L. Jiang, Z. Wei and H. – C. Zhou, "Zirconium-Metalloporphyrin PCN-222: Mesoporous Metal–Organic Frameworks with Ultrahigh Stability as Biomimetic Catalysts", *Angew. Chem.*, **51** (2012) 10307–10310.

181. P. C. Pandey and A. K. Pandey, "Electrochemical sensing of dopamine and pyrogallol on mixed analogue of Prussian blue nanoparticles modified electrodes – Role of transition metal on the electrocatalysis and peroxidase mimetic activity", *Elect. Acta*, **109** (2013) 536–545.

182. N. Puvvada, P. K. Panigrahi, D. Mandal and A. Pathak, "Shape dependent peroxidase mimetic activity towards oxidation of pyrogallol by H_2O_2", *RSC. Advances*, **2** (2012) 3270–3273.

183. H. Tauber, "Oxidation of pyrogallol to purpurogallin by crystalline catalase", *J. Biol. Chem.*, **205** (1953) 395–400.

*****

Summary and Conclusions

Synthesis of new polymer-supported vanadium complexes, their characterization and catalytic potentials for various organic transformations have been reported in the present thesis. To achieve the goal polymer-supported vanadium complexes, PS–im[$V^{V}O_2$(pan)] [Hpan = 1-(2-pyridylazo)-2-naphthol], PS-im[$V^{V}O_2$(acpy-bhz)] (Hacpy-bhz = Schiff based derived from acetylpyridine and benzoylhydrazide), PS-im[$V^{V}O_2$(acpy-inh)] (Hacpy-inh = Schiff based derived from acetylpyridine and isonicotinoyl hydrazide), PS-im[$V^{V}O_2$(acpy-nah] (Hacpy-nah = Schiff based derived from acetylpyridine and nicotinoyl hydrazide), PS–im[$V^{V}O_2$(bzpy-inh)] (Hbzpy-inh = Schiff based derived from benzylpyridine and isonicotinoyl hydrazide) and PS–im[$V^{V}O_2$(bzpy-tch)] (Hbzpy-tch = Schiff based derived from benzylpyridine and thiophene-2-carbyxylic acid hydrazide), have been isolated by direct reaction of imidazolomethylpolystyrene cross-linked with 5% divinylbenzene with the corresponding neat dioxidovanadium(V) complexes. Some of the known neat dioxidovanadium(V) complexes were synthesized by literature procedures while new ones were prepared by reacting [$V^{IV}O(acac)_2$] with the corresponding ligands followed by aerial oxidation. All the complexes are characterized by various spectroscopic techniques (IR, electronic, NMR (^{1}H and ^{51}V), and electron paramagnetic resonance (EPR)), thermal, AFM, field-emission scanning electron micrographs (FE–SEM) as well as energy dispersive X-ray (EDX) studies. New Non-supported complexes have also been characterized by single crystal X-ray.

The polymer-grafted complex PS–im[$V^{V}O_2$(pan)] has been used for the oxidative bromination of styrene, salicylaldehyde and *trans*–stilbene. Under the optimized reaction conditions, styrene gave a maximum of 99 % conversion after 2 h of reaction with the main products having a selectivity order of: 1-phenylethane-1,2-diol (75 %) > 2-bromo-1-phenylethane-1-ol (20 %) > 1,2-dibromo-1-phenylethane (1.2 %). Oxidative bromination of salicylaldehyde gave three products with the selectivity order: 5-bromosalicylaldehyde > 2,4,6-tribromophenol > 3,5-dibromosalicylaldehyde. A maximum of 91 % conversion of *trans*–stilbene has been obtained in 2 h of reaction time where selectivity of the obtained reaction products follows the order: 2,3-diphenyloxirane (*trans*–stilbene oxide) > 1,2-dibromo-1,2-diphenylethane > 2-bromo-1,2-diphenylethanol. Catalytic activity of non-

polymer supported complex [{$V^{V}O(pan)\}_2(\mu\text{-}O)_2$] gives lower conversion than that of the polymer-supported one.

Polymer-supported complexes, PS-im[$V^{V}O_2$(acpy-bhz)], PS-im[$V^{V}O_2$(acpy-inh)] and PS-im[$V^{V}O_2$(acpy-nah)] as well as corresponding neat ones, [$V^{V}O_2$(acpy-bhz)], [$V^{V}O_2$(acpy-inh)] and [$V^{V}O_2$(acpy-nah)] have been used as catalyst precursors for the oxidative bromination of styrene and *trans*-stilbene using 30 % aqueous H_2O_2 as an oxidant, the compounds acting as functional models of vanadium dependent haloperoxidases. 1-Phenylethane-1,2-diol, 2-bromo-1-phenylethane-1-ol (bromohydrin) and 1,2-dibromo-1-phenylethane are the reaction products of styrene after 1 h of reaction, while those of *trans*-stilbene are: 2,3-diphenyloxirane (trans-stilbene oxide), 2-bromo-1,2-diphenylethanol and 1,2-dibromo-1,2-diphenylethane. These compounds also catalyze the oxidation of benzoin by peroxide to give benzil, methylbenzoate, benzoic acid and benzaldehyde-dimethylacetal. All these supported catalysts are stable and do not leach during the catalytic reactions. They are recyclable as well. All of these also show better catalytic results over their corresponding neat analogues.

In the last chapter peroxidase mimicking property of polymer-supported complex PS-[$V^{IV}O$(sal-dahp)] (H_3sal-dahp = Schiff base derived from salicylaldehyde and 1,3-diamino-2-hydroxypropane) at pH 7 in aqueous medium has been described. The monomeric complex [$V^{IV}O$(Hsal-dahp)(dmso)] used to immobilize on polymer support has also been characterized by single crystal X-ray confirming the coordination of two phenolic oxygen and two imine nitrogen atoms of the ligand to the vanadium center while hydroxyl group of the ligand does not participate in coordination. The polymer-supported complex has been successfully used for the peroxidase-like oxidation of pyrogallol at pH 7.0. The plausible intermediate species formed during peroxidase mimicking activity has been established in solution by electronic spectroscopy. Stability of polymeric supported complex in a wide range of pHs, its easy separation from the reaction medium and reusability without considerable decrease in activity makes it useful in terms of its greener application in industry.

The achievements presented in this study contribute significantly to our knowledge and may have future industrial applications.